

A new *in vitro* model to study mitochondria in Parkinson's Disease

Inauguraldissertation

zur

Erlangung der Würde eines Doktors der Philosophie

vorgelegt der

Philosophisch-Naturwissenschaftlichen Fakultät

der Universität Basel

von

Lara Sironi

Basel, 2022

Originaldokument gespeichert auf dem Dokumentenserver der Universität Basel

edoc.unibas.ch

Genehmigt von der Philosophisch-Naturwissenschaftlichen
Fakultät auf Antrag von

Fakultätsverantwortlicher: Prof. Christoph Handschin

Dissertationsleiter: Prof. Dr. Stephan Frank

Koreferent: Prof. Dr. Frank Edlich

Basel, den 22.03.2022

The Dean of Faculty

Prof. Dr. Marcel Mayor

Index

1. INTRODUCTION.....	1
1.1 Mitochondria	1
1.1.1 Structure.....	1
1.1.2 Dynamics	3
1.1.2.1 Mitochondrial Fission.....	4
1.1.2.2 Mitochondrial Fusion	7
1.1.2.3 Cristae structure and remodeling	10
1.1.3 Mitochondrial dynamics in cellular functions	10
1.1.3.1 Apoptosis.....	10
1.1.3.2 Mitochondrial quality control	11
1.1.3.2.1 The ubiquitin proteasome system (UPS).....	13
1.1.3.2.2 The AAA+-type ATPase p97	14
Intracellular roles of p97	15
P97 adapter proteins and cofactors	16
UBXD1	17
SAKS1	18
1.1.4 Mitochondrial interactions with other organelles	18
1.1.4.1 Mitochondria-associated membranes (MAMs)	19
1.1.4.2 Mitochondria-Lysosome membrane contact sites.....	20
1.1.4.3 Mitochondria-Peroxisome contact sites	21
1.1.4.4 Mitochondria bound to Lipid Droplets	22
1.1.5 Mitochondrial motility.....	22
1.1.6 Mitochondria and neurodegeneration	23
1.1.6.1 Parkinson’s Disease	24
1.1.6.2 Autosomal dominant optic atrophy	25
1.1.6.3 Charcot-Marie-Tooth Disease.....	26
1.1.7 Dysfunction of p97 and neurodegeneration.....	27
2. MATERIAL AND METHODS	29
2.1 Materials	29
2.1.1 Equipment	29
2.1.2 Reagents	29

2.1.3 Antibodies.....	31
2.1.4 Composition of Buffers and Media.....	31
2YT medium.....	31
SOB media.....	31
Transformation buffer 1 (TFB 1).....	32
Transformation buffer 2 (TFB 2).....	32
2.1.5 Enzymes and Nucleic Acids.....	32
2.1.6 Oligonucleotides.....	33
2.1.7 Plasmids.....	33
2.2 Methods.....	35
2.2.1 Molecular Biological Methods.....	35
2.2.1.1 Bacterial Strains.....	35
2.2.1.2 Preparation of chemically competent <i>E.coli</i>	35
2.2.1.3 Polymerase chain reaction (PCR).....	35
2.2.1.4 DNA digestion.....	36
2.2.1.5 DNA ligation.....	37
2.2.1.6 DNA transformation into chemically competent <i>E. coli</i>	37
2.2.1.7 DNA plasmid isolation.....	37
2.2.1.8 Agarose gel electrophoresis.....	38
2.2.1.9 Yeast two-hybrid.....	38
2.2.1.10 RNA extraction.....	38
2.2.1.11 Reverse transcription of RNA to cDNA.....	38
2.2.1.12 Droplet digital PCR (ddPCR).....	39
2.2.2 Biochemical Methods.....	39
2.2.2.1 Preparation of cell lysates.....	39
2.2.2.2 Measurement of protein content.....	39
2.2.2.3 SDS page.....	40
2.2.2.4 Western blotting.....	40
2.2.2.5 Extraction of genomic DNA.....	40
2.2.3 Cell Biology Methods.....	41
2.2.3.1 Cell culture.....	41
2.2.3.2 Transfection of mammalian cells.....	41
2.2.3.3 Immunohistochemistry (IHC).....	42

3. RESULTS	43
3.1 Opa1 PROJECT.....	43
3.1.1 Generation of a double transgenic mouse model	43
3.1.1.1 A53T α -synuclein transgenic line M83.....	43
3.1.1.2 <i>Opa1</i> ^{ts} mouse line.....	44
3.1.2 Generation of stable cell lines	47
3.1.3 Characterization of stable cell lines.....	62
3.2 p97 PROJECT	70
Mutation in p97 causing IBMPFD might impact interaction with its cofactor UBXD1	70
4. DISCUSSION	75
4.1 Opa1 PROJECT.....	75
4.1.1 Generation of a double transgenic mouse model	75
4.1.1.1 A53T α -synuclein transgenic line M83.....	75
4.1.1.2 <i>Opa1</i> ^{ts} mouse line.....	76
4.1.2 Generation of stable cell lines	77
4.1.3 Characterization of stable cell lines.....	79
4.1.4 Conclusions and future perspectives.....	81
4.2 p97 project	82
Mutation in p97 causing IBMPFD might impact interaction with its cofactor UBXD1	82
5. APPENDIX	84
5.1 List of Figures	84
5.2 List of Tables.....	86
6. REFERENCES	87
7. REVIEW	122
8. ACKNOWLEDGEMENTS	145

1. Introduction

1.1 Mitochondria

The origin of mitochondria dates back to over 1.5 billion years ago, when an α -proteobacterium was engulfed by a eukaryotic progenitor, starting a process of endosymbiosis [1]: whereas mitochondria supplied the host eukaryotic progenitor with metabolites and energy, their replication and morphology largely came under control of the host. Most of the mitochondrial genetic material was transferred to the nucleus, leaving a circular chromosome of 16 kilobases within the organelle, coding for a total of 37 genes: 13 for protein subunits of the respiratory chain, 22 for mitochondria-specific transfer RNA (tRNAs) and 2 for ribosomal RNAs (rRNAs) [2]. The remaining about 1500 proteins that constitute the mitochondrial proteome are nuclear-encoded and post-translationally imported and sorted into the four mitochondrial sub-compartments: the outer mitochondrial membrane (OMM), the inner mitochondrial membrane (IMM), the intermembrane space (IMS) and the matrix [3]. Since the discovery of the Krebs cycle in the 1950s, mitochondria have traditionally been regarded as the “powerhouses” of the cell, due to their association with cellular bioenergetics. The identification of their important contributions to apoptotic cell death in the 1990s [4] paved the way to the idea that mitochondria have a role in cell signalling, as they are implicated in several complex cellular processes, from autophagy [5] to stem cell differentiation [6] and regulation of immune responses [7].

1.1.1 Structure

Mitochondria are surrounded by two membranes, characterized by different composition and function: the OMM and the IMM.

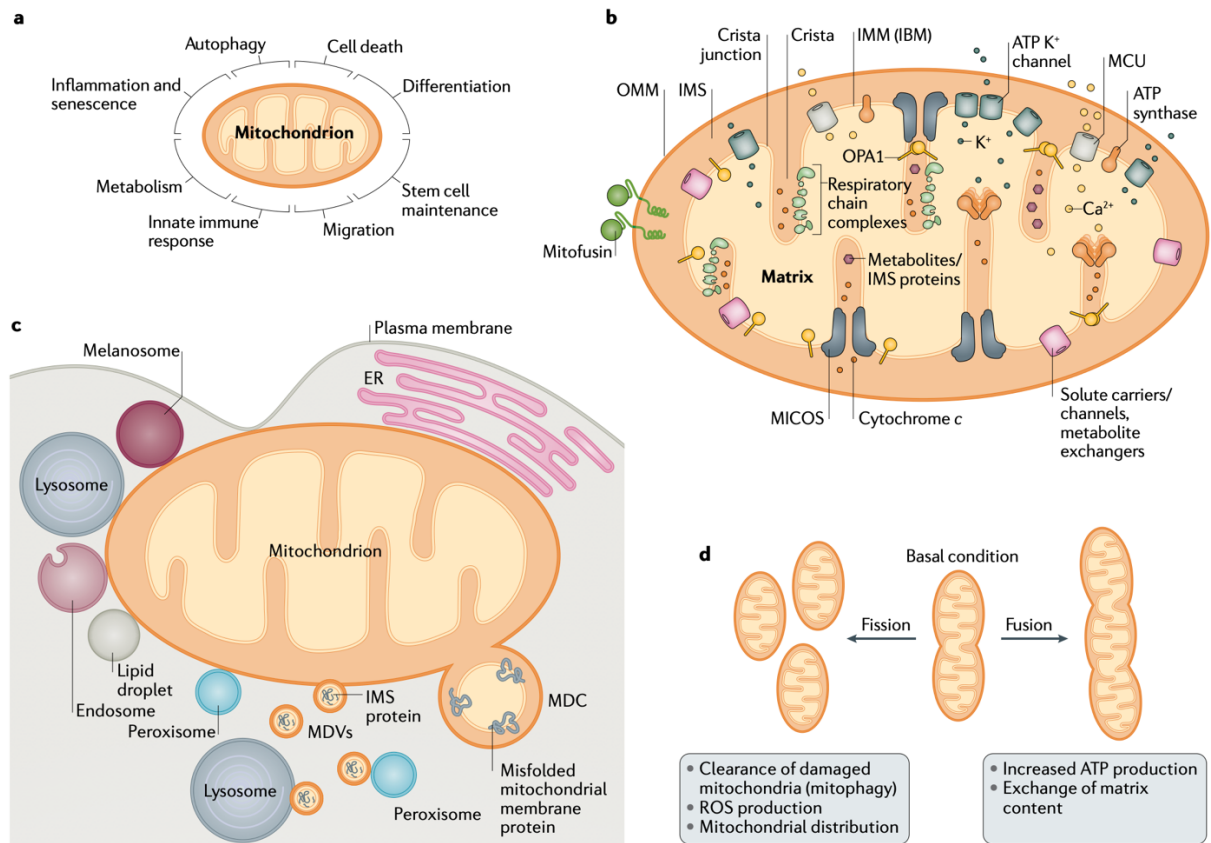
The OMM acts as a barrier with low selectivity for solutes, metabolites and larger molecules ($\leq \sim 5000$ Da), but also acts as a platform for signalling pathways that are decoded and transmitted into mitochondria. The OMM is also important for interorganellar communication, by the establishment of membrane contact sites with other subcellular compartments, such as the endoplasmic reticulum (ER), lysosomes, peroxisomes, lipid droplets and the plasma membrane.

The IMM marks the limits of the mitochondrial lumen, called matrix, and can be subdivided into three specialised zones: the inner boundary membrane (IBM), the cristae junctions (CJs) and the cristae.

The IBM runs parallel to the OMM and contains proteins for the correct assembly and localization of IMM proteins [8] as well as the translocase inner membrane (TIM) for shuttling proteins into the matrix space [9].

The cristae are bag-like structures protruding into the mitochondrial matrix, hosting the oxidative phosphorylation (OXPHOS) system. The OXPHOS system is composed of protein complexes that couple the oxidation of reducing equivalents (NADH and FADH₂) to the pumping of protons across the IMM (also known as electron transport chain (ETC)), generating an electrochemical proton gradient used by ATP synthase to synthesize ATP. According to the “plasticity model”, OXPHOS complexes, located at both sides of the cristae, can be present as both single complexes and supercomplexes (SCs) of different composition (complex I+III, I+III+IV and III+IV) [10], allowing a more efficient transport of electrons. In contrast, ATP synthase is found at the cristae edge as monomer or dimer [11].

Mitochondrial cristae are connected to the IBM via narrow tubular segments of rather uniform diameter of 20-40 nm [12, 13], known as CJs. These CJs create two distinct mitochondrial subcompartments: the intermembrane space (IMS) between the OMM and the IBM, and the intracristal space (ICS). Thus, CJs compartmentalize cristae content (i.e. metabolites, protons and ADP) into the IMS. The formation and maintenance of the CJs are under the control of a large oligomeric complex termed mitochondrial contact site and cristae organizing system, MICOS [14]. The MICOS complex is localized at the IMM and comprises eight components: Mic60, Mic10, Mic19, Mic25, Mic23, Mic27, Mic13 and Mic14. This complex, together with the sorting and assembly machinery (SAM) complex and the interacting protein DnaJC11, forms the mitochondrial intermembrane space bridging complex (MIB), a large protein complex spanning both the IMM and the OMM [15].



Nature Reviews Molecular Cell Biology

Figure 1.1 Mitochondrial structure and function.

a Mitochondrial function. Mitochondria are implicated in several cellular processes. **b** Mitochondrial structure. Mitochondria are surrounded by a double-membrane system, OMM and IMM, enclosing the IMS. The IMM protrudes into the mitochondrial matrix to form invaginations called cristae, hosting the respiratory chain complexes. CJs, under the control of MICOS complex, reduce the release of ICS content into the IMS. **c** Mitochondrial membrane contact sites. Mitochondria are recognized as signalling platforms, and they interact with other organelles, such as endoplasmic reticulum, lysosomes, lipid droplets, and peroxisomes to convey signals and exchange substrates. **d** Mitochondrial shape. Mitochondria display a wide range of morphologies. Whereas fragmented mitochondria produce more ROS and are efficiently removed by mitophagy, mitochondrial fragmentation also enables an even distribution of the organelles to daughter cells during cell division. Mitochondrial fusion favours the exchange of matrix content and increases ATP production efficiency. (Figure from Giacomello et al., 2020 [16]).

1.1.2 Dynamics

Mitochondria are highly dynamic organelles, displaying a wide range of morphologies, from single isolated organelles to large interconnected networks [17].

The term “mitochondrial dynamics” was coined to describe the processes of mitochondrial fission and fusion and of cristae remodeling, which all provide the mitochondrial network with the flexibility to adapt to the metabolic and biosynthetic demands of the cell. A family of large GTPases known as dynamin-related proteins (DRPs) controls mitochondrial dynamics,

due to their ability to remodel biological membranes through self-assembly and GTP hydrolysis.

The main effector of mitochondrial fission is Dynamin-related protein 1 (Drp1), while Mitofusins 1 and 2 (Mfn1, Mfn2) and Optic atrophy 1 (OPA1) mediate mitochondrial fusion of the OMM and IMM, respectively. Drp1 is also the main mediator of peroxisomal fragmentation [18].

1.1.2.1 Mitochondrial Fission

Mitochondrial fission is the process through which a single mitochondrial tubule undergoes constriction to generate two daughter mitochondria, and the main mediator is Drp1.

Structural studies revealed that Drp1 has four functional domains: at the N-terminus a GTPase domain holding the enzymatic activity; a middle domain; a variable domain harbouring sites of posttranslational modification; and at the C-terminus a GTPase effector domain interacting with the GTPase domain. Drp1 dimerization is mediated by the GTPase effector domain and the middle domain through their α -helix-containing stalk domains [19, 20].

Electron microscopy (EM) and tomography have shown that the ER is required for the initial step of mitochondrial division. Indeed, ER tubules, besides purely making contact with mitochondria, also wrap around these organelles [21] to mark future sites of mitochondrial fission. This process is spatially coupled to sites of mtDNA replication [22], thereby allowing proper mtDNA distribution between newly generated daughter mitochondria. This ER wrapping step of mitochondrial pre-constriction is required to decrease the mitochondrial diameter from approximately 300-500 nm to 150 nm [21] in order for Drp1 recruitment and oligomerization to proceed. Furthermore, ER-bound inverted-formin 2 (IFN2) [23] and the mitochondrial anchored formin-binding Spire1C [24] cooperate at these contact sites to regulate the assembly of actin which is required for mitochondrial constriction, followed by myosin IIA recruitment [25]. Drp1 is subsequently recruited to the OMM through adaptor proteins, the tail-anchored proteins mitochondrial fission factor (Mff) [26] and mitochondrial dynamics proteins 49 and 51 (MiD49 and MiD51) [27, 28]. Of note, Fis1 seems to be dispensable for the mitochondrial fission reaction under basal conditions [28].

Multiple posttranslational modifications can regulate Drp1 fission capacity: phosphorylation, S-nitrosylation, ubiquitylation and SUMOylation [29, 30].

Phosphorylation may occur at two serine residues in the GTPase effector domain. Protein kinase A (PKA) phosphorylates Drp1 on Ser637 in presence of high levels of cyclic adenosine monophosphate (cAMP) resulting in the inhibition of fission activity likely through changes in the association between the GED and GTP-binding/middle domains [31]. Mitochondrial elongation following PKA-mediated Drp1 phosphorylation can protect mitochondria from autophagosomal degradation during nutrient deprivation [5] and prevent cell death [31, 32]. Other kinases can phosphorylate Drp1 and modulate mitochondrial morphology, including Rho-associated coiled coil-containing protein kinase 1 (ROCK1) [33] and glycogen synthase kinase 3 β (GSK3B) [34, 35]. Conversely, the calcium-dependent phosphatase calcineurin can target Drp1 phosphorylation at Ser637 to enhance Drp1 fission activity [36].

Cdk1/CyclinB kinase phosphorylates Drp1 at Ser616 exerting the opposite effect of Ser637 phosphorylation, stimulating its oligomerization and triggering mitochondrial fission to enable even mitochondrial distribution to daughter cells during mitosis [37].

Other kinases can also phosphorylate Drp1 at this residue: protein kinase C (PKC) [38] and the Ca²⁺-/calmodulin-dependent kinase II (CaMKII) [39, 40] during cell death, and ERK-1/2 during cancer cell invasion [41, 42] and reprogramming [42].

While it was also reported that Drp1 can undergo S-nitrosylation on a conserved cysteine residue in the GTPase effector domain [43, 44], thereby leading to increased mitochondrial fission, this mode of regulation is still controversially discussed [45].

Drp1 function can also be modulated through ubiquitylation via the activity of the RING-finger ubiquitin E3 ligase MARCH5/MITOL [46] and Parkin [47], but it is not yet confirmed whether Drp1 is a direct target of Parkin [48] or if there are alternative mechanisms linking Parkin activity and mitochondrial morphology [49].

Finally, the conjugation of small ubiquitin-like modifier (SUMO) to Drp1 leads to a more stable association of Drp1 with the OMM [50, 51]. In this context, SUMO1, Ubc9 and mitochondrial-anchored protein ligase (MAPL, also known as MULAN) have all been implicated in Drp1 SUMOylation [50, 52, 53]. The family of seven conserved cysteine proteases (Sentrin proteases [SenPs]) catalyse protein deSUMOylation [54]. SenP5 has been identified as a protease that cleaves SUMOylated mitochondrial substrates, including Drp1,

playing a specific role at the G2/M transition [55]. Of note, MAPL-mediated SUMOylation and the following Drp1 stabilisation have recently been implicated as a mechanism downstream of Bax/Bak activation promoting apoptosis, stabilising ER-mitochondria contacts, and generating mitochondrial constriction and cytochrome c release [56].

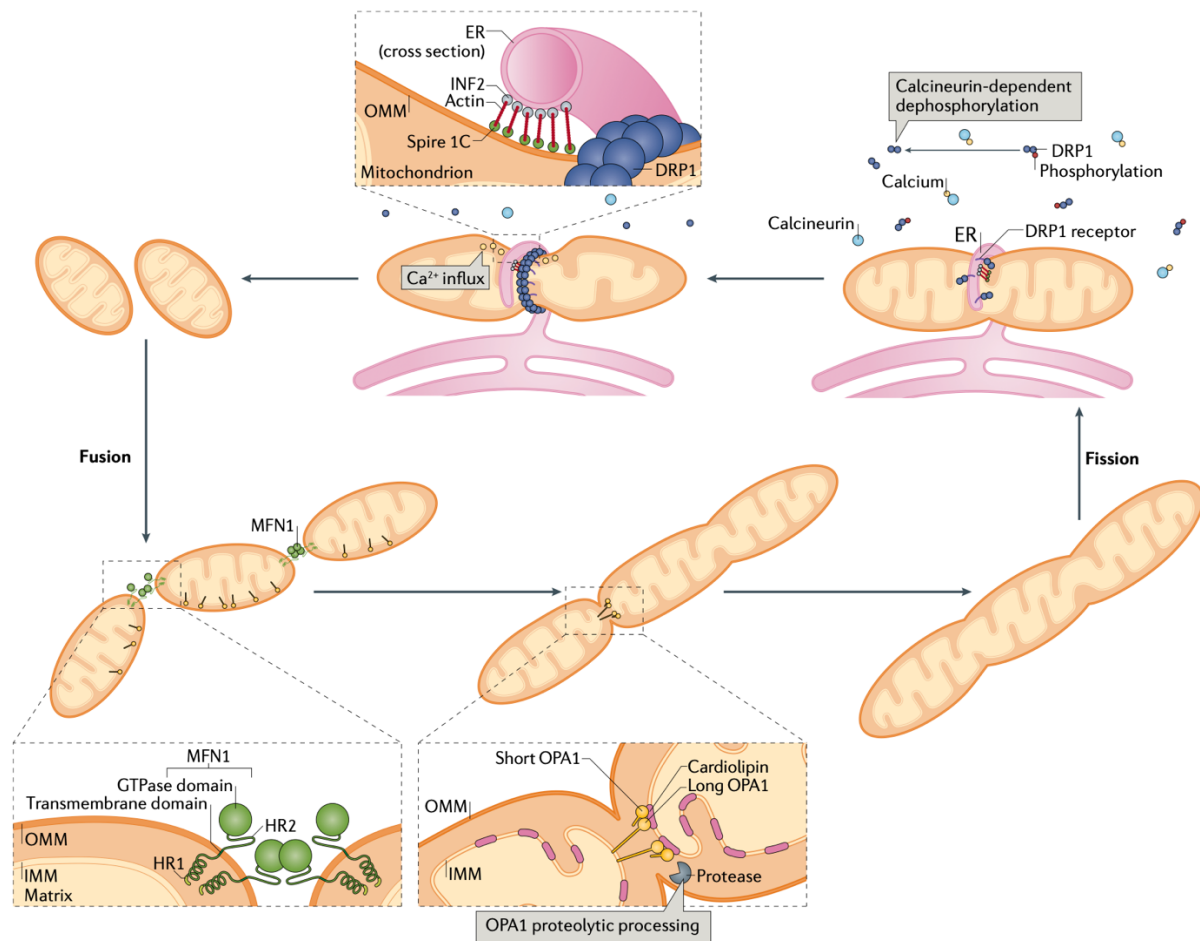
In addition, post-translational modifications can also regulate Drp1 receptors. Indeed, MFF can be targeted by the cellular energy sensor AMP-activated protein kinase (AMPK) upon mitochondrial dysfunction and a decrease in the cytosolic ATP/AMP ratio. AMPK-mediated phosphorylation of MFF enhances Drp1 recruitment, facilitating mitochondrial fission and elimination of defective portions of the mitochondrial network [57].

Finally, MiD49 ubiquitylation by MARCH5/MITOL leads to its proteasomal degradation, thereby preventing mitochondrial fragmentation and protecting cells from stress-induced apoptosis [58].

After the recruitment to the OMM, Drp1 oligomerizes in a ring-like structure that wraps around ER-marked mitochondrial tubules, and GTP-hydrolysis leads to a conformational change, enhancing pre-existing mitochondrial constriction. Recently, the ubiquitously expressed classical dynamin-2 (Dyn2) has been found to have a direct role in mitochondrial division, downstream of Drp1 constriction. Indeed, Drp1-mediated constriction promotes Dyn2 recruitment, which mediates the final separation of the mitochondrial membrane to complete mitochondrial division [59].

A mechanism for IMM constriction and division has been proposed recently, occurring at ER-mitochondria contacts sites in a Ca^{2+} -dependent manner. The constriction and division of the IMM may be induced upon stimulation of ER Ca^{2+} release to mitochondria, independently of OMM-constriction and prior to Drp1 recruitment [60, 61]. In human osteosarcoma cells, this mechanism has been attributed to INF2-mediated actin polymerization, which stimulates mitochondria-ER contacts and mitochondrial calcium uptake [60], while in neurons this mechanism prominently involves OPA1 processing [61]. Following Ca^{2+} entry into mitochondria, a drop in mitochondrial membrane potential leads to activation of the IMM peptidase OMA1, which processes the IMM protein OPA1 into short (s) forms (s-OPA1). Accumulation of s-OPA1 disrupts the ability of the MICOS complex to stabilise the tethering

between OMM and IMM, leading to the untethering of the IMM and its possible constriction [61].



Nature Reviews Molecular Cell Biology

Figure 1.2 Mitochondrial fission and fusion.

Fission and fusion regulate mitochondrial morphology and function to respond to cellular demands. Fission takes place at sites where ER wraps around mitochondria upon calcineurin-dependent Drp1 dephosphorylation and mitochondrial recruitment. Fusion of the OMM requires the association of two MFN1 molecules in trans followed by GTP hydrolysis. The fusion-competent protein of the IMM is OPA1. Long OPA1 isoforms undergo proteolytic processing to yield fusion-competent short OPA1 isoforms. (Figure from Giacomello et al., 2020 [16]).

1.1.2.2 Mitochondrial Fusion

The process of mitochondrial fusion, in which two mitochondria merge into a larger organelle, is crucial for the maintenance of a homogeneous and healthy mitochondrial network, allowing mixing of membranes and contents and reducing organelle-to-organelle variability [2].

Three distinct steps characterize mitochondrial fusion: first, two mitochondria are tethered in *trans*; the distance between the two docking membranes reduces due to increasing contact

surface area [62], and finally, GTP hydrolysis induces conformational changes to allow fusion of the adjacent OMMs [63, 64].

The fusion process is regulated by three dynamin-like GTPases: Mitofusin 1 (Mfn1) and Mitofusin 2 (Mfn2) at the level of the OMM, and Optic Atrophy 1 (Opa1) located in the IMM [65].

Mfn1 and Mfn2 mediate OMM fusion. Both proteins can establish homo- and heterotypic complexes leading to mitochondrial fusion, with heterotypic complexes showing greater efficacy [66]. Mfn1 and Mfn2 share a high degree of homology and a similar structural organization [67]: they both possess an N-terminal GTPase domain required for fusion activity, a transmembrane domain necessary for OMM insertion, and two predicted heptad repeats that are presumed to mediate tethering between adjacent mitochondria [68]. Nevertheless, Mfn1 and Mfn2 serve different functions: together with Opa1, Mfn1 is a core component of the fusion reaction, while Mfn2 is thought to stabilize the interactions between mitochondria, in addition to participating in juxtaposition of mitochondria the ER [63, 65, 69]. Furthermore, Mfn2 has a role in regulating mitochondrial axonal transport through interaction with the Miro/Milton complex [70].

The conserved dynamin-like GTPase Opa1 is the key mediator of the IMM fusion process. It is encoded by a single gene containing 30 exons. In humans, eight mRNA variants exist as a result of alternative splicing of exons 4, 4b and 5b [71], with exons 4b and 5b being specific for vertebrates [72]. The eight variants are ubiquitously expressed, although at levels which considerably vary among different tissues. This suggests fine regulation of alternative splicing, probably providing cellular flexibility to respond to different metabolic and stress conditions that may perturb mitochondrial homeostasis.

OPA1 protein harbours a mitochondrial targeting sequence (MTS) at the N-terminus, followed by a transmembrane domain (TM) embedded in the IMM and a coiled-coil domain. There are three highly conserved dynamin regions: the GTPase domain, the middle domain and the GTPase effector domain (GED) at the C-terminus [73]. The OPA1 precursor protein is imported through OMM and IMM translocases, upon which the MTS is cleaved by Mitochondrial Processing Peptidase (MPP) to generate OPA1 long forms (l-OPA1). These long forms can then be further processed to produce s-OPA1, which is soluble in the IMS [74]. Two

1.1.2.3 Cristae structure and remodeling

Changes in number, length, width, or tightness of cristae and cristae junctions are referred to as "cristae remodeling", and occur in response to multiple stimuli in the cell, including oxygen deprivation (hypoxia), glucose depletion, increased reactive oxygen species (ROS) or other toxicity, requiring mitochondrial adaptation [68]. Exposure of the cell to a non-glycolytic substrate such as galactose leads to an increase in cristae number, accompanied by higher levels of respiratory chain proteins and supercomplexes, boosting the activity of OXPHOS [83, 84, 85]. A decrease in cristae width is observed during starvation, supporting respiratory chain supercomplex assembly and ATPase dimerization and activity [5, 83]. A reduction in cristae width upon cell death stimuli decreases the release of apoptotic molecules [86, 87] until the cellular stress becomes detrimental and apoptosis is induced. The key player of cristae remodelling is Opa1, independently of its role during IMM fusion [68]. Indeed, ablation or knockdown of the gene in mammals and yeast results in aberrant cristae morphology [86, 88, 89], whereas overexpression of Opa1 leads to increased cristae numbers and reduced cristae width [83, 90]. Cristae structure maintenance and intercristae membrane tethering are mediated by l-OPA1 oligomers along the length of the cristae membrane [68]. Whereas experiments in YME1L/OMA1 double-knockout mice demonstrated that s-OPA1 is not necessary for the steady-state maintenance of cristae morphology [76], s-OPA1 may play a role by connecting two membrane-bound l-OPA1 molecules, acting like a "staple", thereby increasing OPA1 oligomerization between apposing cristae membranes [16, 68]. The consequence of l-OPA1 cleavage is a disruption in cristae structure and widening of cristae junctions, with the release of proteins such as cytochrome *c* otherwise sequestered within the cristae [68].

1.1.3 Mitochondrial dynamics in cellular functions

1.1.3.1 Apoptosis

Apoptosis is a programmed form of cell death, essential for the removal of damaged or harmful cells for the greater good of the organism [91]. It can be triggered by either extrinsic or intrinsic signals and is immunologically silent [92]. Upon a death stimulus, pro-apoptotic pore-forming proteins BAX and BAK translocate to discrete mitochondrial foci, colocalizing with DRP1 and MFN2, promoting DRP1 stabilization on mitochondria and initiating

apoptotic mitochondrial fragmentation [51, 93]. OMM permeabilization and cristae remodelling, with the widening of cristae junctions, leads to the release of cytochrome *c* from the intracristae space into the cytosol; this process involves I-OPA1 cleavage directly by proapoptotic, truncated Bid [94] or by stress-activated Presenilins-Associated Rhomboid-Like (PARL) protein [86, 87]. In the cytosol, cytochrome *c* interacts with Apoptotic protease activating factor-1 (Apaf-1) and caspase 9 to form the apoptosome and initiate the apoptotic cascade [95]. The activity of diverse kinases phosphorylating both mitofusins, such as the mitogen-activated protein kinase cascade member extracellular signal-regulated kinase (ERK) and the stress-induced JUN amino-terminal kinase (JNK), has been linked with inhibition of mitochondrial fusion during the apoptotic process [16].

Mitochondrial fission is an important step in the apoptotic cascade. Cells deficient in mitochondrial fission show increased resistance to apoptosis [96]; FIS1-knockout, MFN1-overexpressing cells [97, 98, 99] or MAPL-KO cells [56] present a similar phenotype. In contrast, mitochondrial fragmentation following excessive fission or decreased fusion leads to cellular sensitization toward apoptotic stimuli [99, 100].

1.1.3.2 Mitochondrial quality control

One of the major causes of mitochondrial dysfunction is oxidative stress. Antioxidant activity is the first line of defence to prevent direct damage caused by ROS to mitochondrial components and involves mitochondrial proteases degrading unfolded and oxidised proteins inside the matrix and the intermembrane space [101].

Mitochondrial surface proteins can also be removed in response to cellular signals [102]: after ubiquitination, oxidised OMM proteins are retrotranslocated to the cytosol and delivered to the proteasome via the AAA+ ATPase p97 [103, 104] through a process termed OMMAD (outer mitochondrial membrane-associated degradation) [105].

Mitophagy is a specialised form of autophagy dedicated to the removal and recycling of dysfunctional mitochondria, to guarantee the mitochondrial network's integrity and functionality. Physiologically, this mechanism underlies the degradation of mitochondria during erythrocyte maturation, as well as the removal of sperm-derived mitochondria in fertilised oocytes, the latter being the correlate of the maternal mtDNA inheritance [106].

In mammals, two major mitophagic pathways can be distinguished based on their dependency on the ubiquitin ligase Parkin. Parkin-dependent mitophagy removes damaged or dysfunctional mitochondria through the combined action of the PTEN induced putative kinase 1 (PINK1) and of the E3 ubiquitin ligase Parkin. PINK1 is normally targeted to the mitochondria, imported, and can be cleaved by the matrix processing peptidases and PARL [107, 108], and released from the import channel into the cytosol to be degraded through the N-end rule proteolytic pathway [109, 110, 111]. The import machinery becomes inactivated upon mitochondrial depolarization, and PINK1 is eventually trapped within the import channel or nearby anchored to the OMM [108, 110]. PINK1 kinase domain is then exposed to the cytosol where it phosphorylates ubiquitin and Parkin, leading to Parkin-dependent ubiquitination of OMM proteins, to allow their mitophagic degradation [112].

Different protein regulators drive the tagging and recognition of mitochondria in the PINK1/Parkin independent pathway, such as BCL2 Interacting Protein 3 Like (BNIP3L) [113], FUN14 Domain Containing 1 (FUNDC1) [114], or Autophagy And Beclin 1 Regulator 1 (AMBRA1) [115]. Mitophagy efficiency relies on the formation of the autophagosome to selectively engulf damaged organelles without affecting the entire mitochondrial network. Indeed, mitochondrial fragmentation is observed prior to mitophagy. In fact, not only post-translational modifications such as SUMOylation modulate the pro-fission protein Drp1, but also selective ubiquitin-dependent degradation of proteins involved in fusion and transport of the organelles such as Mfn2 or Miro promote mitophagy [116]. Proteomic studies have shown that the turnover rate of IMM proteins is comparable to the turnover of whole mitochondria through mitophagy [117]. As OMM and mitochondrial matrix proteins redistribute much faster via fusion and fission events throughout the mitochondrial network compared to IMM proteins [118], degradation of IMM proteins may mostly be achieved via mitophagy.

Mitochondrial-derived vesicles (MDVs) are vesicles derived from mitochondrial membrane containing selective protein cargoes, which can include mitochondrial outer and inner membrane as well as matrix content [119, 120, 121]. MDVs are likely another level of mitochondrial quality control, at an early stage of ROS production, to eject damaged proteins and avoid organelle failure [122]. Their size is relatively uniform, between 70 and 150 nm, and

their generation does not require the mitochondrial fission machinery [119, 120, 121]. Once generated, MDVs undergo either fusion with lysosomes [120], or peroxisomes [119].

Cargoes destined for degradation in lysosomes are enriched with oxidised proteins, following mitochondrial stress [121], and their generation requires protein kinase PINK1 and the cytosolic ubiquitin E3 ligase Parkin [122]. Therefore, it has been speculated that the PINK1-Parkin mitophagic mechanism applies to MDVs formation, but at a more localised level [123]. Local oxidative damage or complex assembly defects could interfere with the import process, causing protein misfolding and aggregation at the import site. Imported PINK1 can then accumulate within the import channel and phosphorylate ubiquitin and Parkin, leading to Parkin recruitment and activation [124, 125]. Saturation of matrix chaperones or localised cardiolipin oxidation could lead to failure of the inner membrane import channel. Therefore, cardiolipin could locally become oxidised and alter membrane curvature [126], helping initiate the outward bending of the membrane [123]. The final step is the formation of a vesicle and its release from mitochondria.

The purpose of MDVs delivered to peroxisomes is currently unclear [127]. Only one protein, MAPL, has so far been identified in vesicles destined to peroxisomes [119].

1.1.3.2.1 The ubiquitin proteasome system (UPS)

Controlling the degradation of misfolded or unfolded proteins to prevent cellular damage, the UPS is one of the principal pathways for cellular protein homeostasis [128].

Processing by the UPS depends on the covalent tagging of substrate proteins with the 76 amino acid-short protein modifier ubiquitin (Ub). In the first step of this process, E1 ubiquitin-activating enzyme binds individual ubiquitin molecules in an ATP-dependent manner, to then transfer the activated ubiquitin to an E2 ubiquitin-conjugating enzyme. An E3 enzyme or ubiquitin ligase binds both the E2-ubiquitin complex and a substrate protein to facilitate the bond formation between the C-terminal glycine of ubiquitin and the lysine residue on the substrate [129, 130, 131]. The ubiquitination substrate can either be a target protein or any of the seven lysine residues of ubiquitin itself, leading to poly-ubiquitin chains formation [132]. There is only one ubiquitin-activating enzyme in the human genome, in contrast to some 50 E2 and hundreds of E3 enzymes [133], allowing multiple combinations of E1, E2 and E3 enzymes to promote substrate specificity of ubiquitination [134]. Following ubiquitination,

proteins are recognized by the 26S proteasome and degraded into short peptides, which are further degraded by cytoplasmic peptidases into their component amino acids [135].

The 26S proteasome is a multimeric complex composed of two different subcomplexes, the 19S cap complex and the 20S proteolytic core [136]. The 19S cap is responsible for recognizing ubiquitinated substrates, removing and recycling their ubiquitin chains by deubiquitinating enzymes, regulating access to the 20S core [137, 138]. Bound proteins are then unfolded and sent into the 20S proteolytic core for sequential cleavage into small peptides [139, 140]. Proteasome activity and function are regulated by chaperones and cofactors, which manage subcellular localization and substrate specificity [141, 142].

The removal of ubiquitin chains is promoted by deubiquitinases (DUBs), which hydrolyze all types of polyubiquitin chains [143] to replenish the cellular pool of free ubiquitin. Additionally, DUBs can reverse ubiquitin signaling by removal of ubiquitin chains from post-translationally modified proteins thereby preventing proteasomal degradation [131].

1.1.3.2.2 The AAA+-type ATPase p97

P97, also known as valosin-containing protein (VCP), is a hexameric ATPase associated with a variety of cellular activities (AAA ATPase) [144]. It is conserved from yeast to man and essential for cellular homeostasis.

Each subunit exhibits a regulatory N-terminal domain, essential for substrate binding, and two ATPase domains: the D1 domain required for hexameric assembly, and the D2 domain responsible for overall ATPase activity [145, 146].

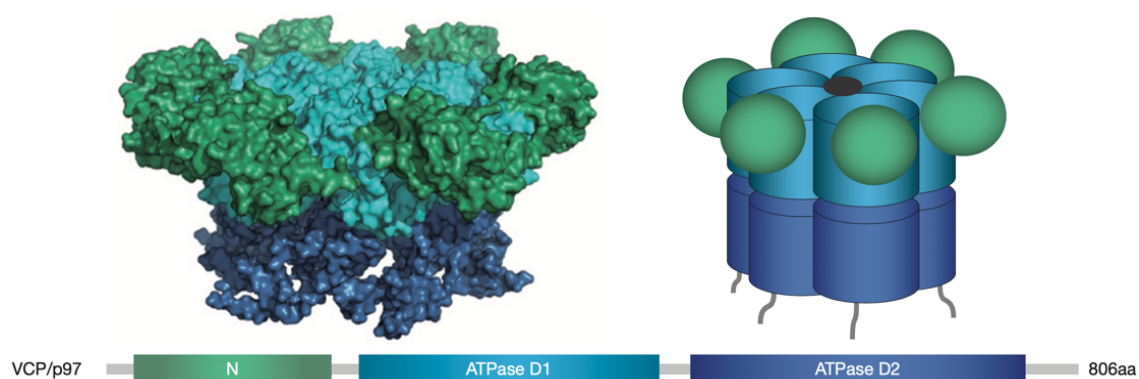


Figure 1.4 p97 protein structure.
(Meyer et al., 2012 [147]).

Nature Cell Biology

P97 is essential for ATP-driven protein unfolding, directed by ubiquitin and assisted by diverse cofactor proteins [144]. Hence, p97 is able to extract proteins from membranes, unfold proteins for proteasomal degradation, or segregate proteins from binding partners for downstream activity, with a critical role in the ubiquitin proteasome system [148, 149, 150].

Intracellular roles of p97

P97 has a well-established role in ER-associated degradation (ERAD) [151, 152], whereby both luminal and membrane-bound misfolded proteins are retrotranslocated from the ER to the cytosol. During this process, the substrate protein is recruited from the ER lumen to the ER membrane, to be ubiquitinated by specialised ER membrane-anchored E3 ubiquitin ligases. On the ER membrane, p97 cofactors recruit p97 [153], which pulls substrate proteins out of the membrane through ATP hydrolysis [154]. After extraction, cofactors may further process these proteins, for example by removal of sugars from glycoproteins [155], by ubiquitin chain elongation [156] or ubiquitin removal by DUBs [157]. Finally, the substrate is degraded by the proteasome, whereas deubiquitination by DUBs can redirect some substrates from proteasomal degradation [158].

P97 can also play a role in a positive feedback loop where an E4 ubiquitin chain elongation factor is recruited to poly-ubiquitinate oligo-ubiquitinated substrates prior to proteasomal degradation [159]. The subsequent transfer of ubiquitinated substrate proteins to the proteasome is also regulated by p97 cofactors: whereas UFD2 and RAD23 promote the transfer of ubiquitinated substrates to the proteasome [159], while UFD3 diverts substrates from proteasomal degradation [160]. P97 also supports the unfolding of its substrates, thereby promoting proteasomal processing [161, 162].

Inhibition of p97 leads to the accumulation of ubiquitin conjugates in the cytosol [163, 164], in addition to eliciting the unfolded protein response [165], which can trigger ER stress-induced apoptosis.

On the mitochondrial level, P97 extracts ubiquitinated proteins from the OMM through a process called mitochondria-associated degradation (MAD) [104, 166, 167]. In particular, p97 takes part in the degradation of two OMM proteins, the anti-apoptotic factor Mcl1 and the fusion protein Mfn1 [104]: p97 binds ubiquitinated OMM proteins and transports them to the cytosol for degradation. In mammalian cells binding and extraction of ubiquitinated Mfn1 by

p97 prevents fusion of damaged mitochondria, facilitating their removal through mitophagy [103, 168].

In the cytosol, p97 facilitates the degradation of unassembled protein complex components in collaboration with the ubiquitin ligase HUWE1 [169] and counteracts protein aggregation. Even when p97 is localised on cytosolic protein aggregates [170], a disaggregase activity similar to the AAA ATPases Hsp104 in yeast or ClpB in bacteria has not been demonstrated so far [171].

In the nucleus, p97 exerts a regulatory role at the level of chromatin and helps to maintain genome stability and function. Following their ubiquitination, p97 mediates segregation of proteins such kinase Aurora B at the end of mitosis, replication licensing factor Cdt1, stalled RNA polymerase II, and several DNA repair factors [172].

P97 adapter proteins and cofactors

A variety of p97-interacting proteins has been identified, which either function as adaptors, linking p97 to a specific substrate or subcellular compartment, or act as cofactors to aid in substrate processing. Sequence analyses identified conserved protein-protein interaction motives, such as the ubiquitin regulatory X (UBX) motif [173], the VCP interacting motif (VIM) [174], VCP-binding motif (VBM) [175] and the SHP box domain [176]. The vast majority of interacting proteins such as Ufd1, Npl4, p47, ataxin3, and FAF1, bind to the p97 N-terminal domain [177] via their UBX, UBX-L, VIM, VBM or SHP motifs. A smaller group of proteins binds to the C-terminus domain of p97 via peptide N-glycosidase/ubiquitin-associated (PUB) (PNGase/UBA- or UBX-containing proteins) and PUL (PLAA, Ufd3p and Lub1p) domains [178].

The largest family of p97 cofactors identified in the human genome are proteins containing the UBX domain, which is structurally homologous to ubiquitin [179]. Proteins of this family can be further classified into two groups according to their domain composition: UBA-UBX and UBX-only proteins. p47, UBXD7, UBXD8, FAF1, and SAKS1 carry a ubiquitin-associated (UBA) domain at their N-terminus in addition to the UBX domain, enabling them to bind ubiquitinated substrates [180] and function as ubiquitin-receptors in the ubiquitin-proteasome pathway.

Members of the UBX-only group (UBXD1, UBXD2, UBXD3, UBXD4, UBXD5, ASPL, p37, VCIP135 and YOD1) lack the UBA domain and thus the ability to bind ubiquitinated substrates [181].

P97 non-UBX domain-containing cofactors can be classified into two subgroups, adapters and accessory proteins. P97 adapters are required for substrate binding, and the two best studied, nuclear protein localization 4 (Npl4) and ubiquitin fusion degradation 1 (Ufd1), form a heterodimer that binds p97 in a 1:1 ratio [182]. Npl4-Ufd1 heterodimers function as recruiting factors that bind to ubiquitinated substrates at the ER membrane and link the conformational change of p97 upon ATP hydrolysis to substrate translocation into the cytosol [155, 163, 183, 184].

P97 accessory proteins or substrate-processing cofactors use p97 as a docking site to perform a specific enzymatic function on the substrate already associated with p97. Examples of accessory proteins include the deglycosylase PNGase I, the E3 ubiquitin ligases Hrd1, gp78, and Ufd2, as well as the deubiquitinase Ataxin-3.

UBXD1

Human UBX domain protein 1 (UBXD1) has been shown to be a stable protein localized to the nucleus, cytosol, and centrosomes in HeLa cells [185]. UBXD1 is involved in vesicle [186] and endolysosomal trafficking [187, 188], in autophagic removal of damaged lysosomes [189], and in OMMAD [190].

From the N- to the C-terminus, UBXD1 harbours a VIM domain, a PUB domain, as well as a UBX domain. Its interaction with p97 differs from that of other UBX domain-containing proteins, as it involves the VIM and PUB, but not the UBX domain [191]. Interestingly, UBXD1 lacks a clear ubiquitin-binding domain, and it is one of a few adapters that can bind to both the N- and C-terminal domains of p97.

Recently, it was shown that UBXD1 is a mitochondrial recruitment factor for p97, connecting the ubiquitin-proteasome system to Parkin-dependent mitophagy. Under mitophagic conditions, UBXD1 localises to mitochondria due to its UBX domain, and p97 is then recruited to mitochondria via interaction with the VIM and PUB domains without the need for additional factors or signals, supporting a pro-mitophagic role for UBXD1 [192]. Due to p97 mutations, this interaction between UBXD1 and p97 is impaired in inclusion body myopathy

associated with Paget's disease of the bone and frontotemporal dementia (IBMPFD) and ALS [188].

SAKS1

The p97 cofactor SAKS1 (stress-activated protein kinase substrate 1) [193] colocalizes with ubiquitin. It is involved in ubiquitin-proteasome functions [194] via its UBA and UBX domains, which bind ubiquitin and p97, respectively [193]. P97 and SAKS1 co-immunoprecipitate, suggesting that p97 might be directed to polyubiquitinated proteins by SAKS1. SAKS1 was also found to selectively prevent the degradation of ERAD substrates without perturbing cytosolic proteasomal substrates [195]. Furthermore, SAKS1 protects polyubiquitin chains from deubiquitination, thus modulating p97-mediated protein degradation [196].

SAKS1, in complex with p97, is required for the recognition of selected ubiquitylated BAG6 (BCL2-associated athanogene 6) chaperone complex clients [197] prior to their degradation by the proteasome. The degradation of these substrates is crucial, as they could accumulate and overwhelm chaperone systems, leading to inappropriate interactions with cytosolic components, and ultimately to aggregation. Loss of SAKS1 sensitises cells to proteotoxic (in particular ER) stress [198].

Moreover, p97 cofactor SAKS1 has been recently identified as a novel regulator of mitophagic initiation. In this context, SAKS1 has been found to translocate along with p97 to mitochondria upon mitochondrial depolarization. Furthermore, SAKS1 appears to modulate the dynamics of mitochondria - Parkin interaction. Loss of SAKS1 negatively impacts on mitochondrial morphology, ATP generation and ER-mitochondrial contacts, in addition to interfering with the removal of MFN2 from mitochondria, leading to formation of para-mitochondrial MFN2 blobs [199].

1.1.4 Mitochondrial interactions with other organelles

Membrane-confined organelles generate dedicated microenvironments, which enable eukaryotic cells to compartmentalize specialized biochemical reactions at specific cellular locations, like protein degradation, lipid breakdown, or ATP production. Cellular homeostasis is maintained by inter-organelle communication, either through physical contact

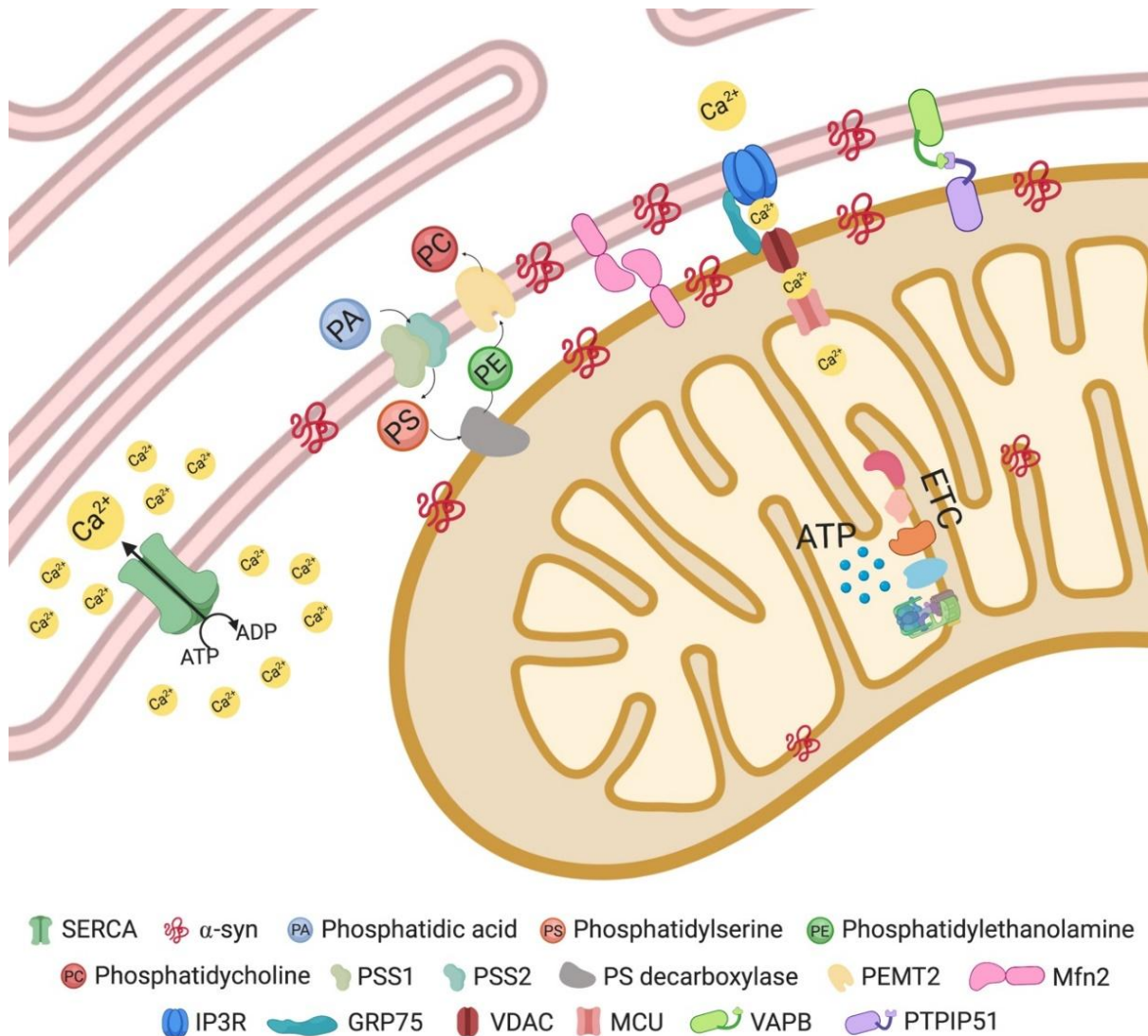
or through transfer of specific metabolites. Many cellular processes, such as signaling, regulation of calcium homeostasis, lipid metabolism, and organelle localization and dynamics rely on membrane contact sites (MCSs), a fast and efficient way to exchange molecules and information [200, 201]. MCSs are defined as regions in which membranes of different organelles are kept in close proximity by dedicated tethering machineries [202]. Of note, the two organelles at MCSs never fuse their membranes, and in most cases the distance between the opposing membranes ranges from 10 to 30 nm, although a distance up to 300 nm has been described [203]. MCSs exist between either identical (homotypic) or different (heterotypic) organelles [202].

Recent guidelines define MCSs by the presence of protein-lipid or protein-protein interactions mediating tethering forces among two membranes in the absence of fusion intermediates or of fused membranes; a defined lipidome and proteome of MCSs is necessary to fulfil the above-mentioned definitions [202].

Mitochondria are now recognized as key signaling platforms [204, 205], and their interaction with other organelles is required to exchange substrates and transmit signals for metabolism regulation, intracellular signaling, and cell maintenance [206].

1.1.4.1 Mitochondria-associated membranes (MAMs)

To date, the regions of close apposition between ER and mitochondria are the best-studied type of membrane contact sites, and they were first described by Bernhard in 1956 [207] and later by Copeland and Dalton using electron microscopy [208]. ER-mitochondria contact sites play crucial roles in lipid metabolism and calcium homeostasis, thus regulating essential processes such as mitochondrial morphology [21, 209], reactive oxygen species (ROS)-induced cell stress [210], autophagy [211], and apoptosis [212]. It has been found that MAM-localized functions are significantly up-regulated not only in cellular and animal models of Alzheimer's disease (AD) but also in AD patient-derived cells [213].



Cells, MDPI

Figure 1.5 Mitochondria–ER contact site and main resident proteins.
(Sironi et al., 2020 [214]).

review [214]

2. Mitochondria-associated membranes (MAMs)

1.1.4.2 Mitochondria-Lysosome membrane contact sites

Similar to mitochondria, lysosomes are highly dynamic organelles responsible for the turnover of cellular components, including proteins and lipids, via hydrolytic enzymes stored in the lysosomal lumen. These organelles also act as iron and calcium stores, and in addition mediate cell death signaling upon lysosomal membrane permeabilization [215].

Mitochondria–lysosome contact sites have been imaged in various cellular models [216, 217, 218, 219, 220, 221]. Lysosomes, together with mitochondria, are critical for the maintenance of

cellular homeostasis, as dysfunction of both organelles is functionally and genetically linked to several human diseases, such as Parkinson's disease, Huntington's disease, Gaucher disease and Niemann-Pick A/B disease. [222, 223, 224, 225].

review [214]

3. Mitochondria-Lysosome Membrane Contact Sites

1.1.4.3 Mitochondria-Peroxisome contact sites

Peroxisomes are ubiquitous and dynamic single membrane-bound organelles and show similar to mitochondria an oxidative type of metabolism. These organelles are essential for human health and development as they fulfil important functions in hydrogen peroxide and lipid metabolism [226]. Additionally, they act as important intracellular platforms for redox-, lipid-, inflammatory-, and innate immunity signaling [227, 228]. Peroxisomes closely cooperate with other organelles, including mitochondria, the ER, and lipid droplets to fulfil their functions [229].

Peroxisomes and mitochondria engage in a close functional interplay [18, 229], perhaps best illustrated by their metabolic cooperation in fatty acid β -oxidation to maintain lipid homeostasis [230], in addition to anti-viral signaling and defence [231, 232]. Moreover, sharing a redox-sensitive relationship [233], peroxisomes and mitochondria contribute to cellular ROS homeostasis. Both organelles also share key components of their division machinery [234], [18], including the large dynamin-like/related GTPase DLP1/Drp1 and its membrane adaptor proteins Fis1 (fission factor 1) and Mff (mitochondrial fission factor), which recruit cytosolic DLP1 to both peroxisomal and mitochondrial constriction sites [235]. Among the mechanisms of communication between mitochondria and peroxisomes there are diffusion processes, for example via the channel-forming peroxisomal membrane protein PXMP2, physical contact sites, and vesicular transport through MDVs interacting and fusing with peroxisomes [119, 123, 236, 237]. However, evidence for a peroxisome - to - mitochondria vesicular transport path is still absent.

The degree of contact between these organelles dynamically changes depending on the cell type and physiological circumstances.

Currently, one peroxisome-mitochondria tethering complex has been identified in mammals, involving the peroxisomal import receptor PEX5, the mitochondrial import receptor subunit TOMM20, and the either peroxisomal- or mitochondrial-targeting protein ACBD2/ECI2 isoform A (acyl-coenzyme A-binding domain 2/ enoyl- CoA- δ isomerase 2), with a function in basal and hormone-stimulated steroid formation [238].

1.1.4.4 Mitochondria bound to Lipid Droplets

Mitochondria associated with lipid droplets (LDs) were first observed in 1959 [239] and reported in a variety of tissue types and cell culture models. A recent report showed that mitochondria bound to LDs, named peridroplet mitochondria (PDM), are more elongated than free mitochondria, and have reduced motility as well as distinct proteome and metabolic capabilities [240].

The LD-coating protein PLIN5 was confirmed to localize to mitochondria-LD contact sites by super-resolution microscopy [241], although the mechanisms by which it promotes the interaction between these organelles remain to be elucidated; of note, a postulated OMM protein that associates with PLIN5 has yet to be discovered. It has also been proposed that mitochondrial-LD tethering could involve mechanisms other than protein-protein interactions, such as membrane-membrane interactions [242].

The tethering complex MFN2-PLIN1 was identified in brown adipose tissue (BAT) following treatment with an adrenergic agonist [243]. In addition, biotin-labeling experiments performed under conditions of glucose deprivation revealed interactions between the mitochondrial protein ACSL1 (acyl-CoA synthase long chain family member 1) and SNAP23 and VAMP4 on LDs [244].

1.1.5 Mitochondrial motility

Mitochondria not only continuously change their morphology, but also actively localize to different subcellular areas in order to fulfil their functions. This notion is particularly evident in neuronal cells which have high bioenergetic demands at pre- and post-synaptic terminals and show extensive transport of mitochondrial subunits along their axons. Moreover, mitochondria close to synapses are crucial for local Ca²⁺ buffering [245].

Mitochondrial transport over long distances occurs along microtubule tracks, with the support of motor proteins [245], and live-cell imaging in neuronal axons has deciphered mechanisms of both anterograde and retrograde transport [246].

Anterograde transport is driven by the KIF5 family of kinesins, holding an ATPase motor domain at the N-terminus and a C-terminal cargo-binding domain [247], while retrograde transport depends on dynein, in association with dynactin [248].

The association of mitochondria to both motor complexes is achieved via adaptor proteins and OMM proteins. In mammals, the adaptor proteins TRAK1 and TRAK2, homologous to *Drosophila* Milton, bridge the OMM proteins Miro1 and Miro2 and the molecular motors [249]. In particular, TRAK1 can interact with both kinesin and dynein, whereas TRAK2 binds mainly the dynein/dynactin complex [245]. Other adaptor proteins have been identified, including syntabulin, linking mitochondria to kinesin motors [250, 251], and FEZ1, mediating mitochondrial anterograde transport during *in vitro* neurite outgrowth upon NGF induction [252]. The complexes formed by OMM proteins, adaptor proteins and molecular motors guarantee mitochondrial trafficking and regulate their distribution in response to changes in neuronal activity. Upon high synaptic activity, the sustained Ca^{2+} entry is sensed by Miro1 and Miro2, causing the inactivation of the MIRO/TRAK/molecular motor complexes, leading to mitochondrial arrest at active synapses [245]. Additionally, the mitochondria-docking protein syntaphilin immobilizes mitochondria in axons during sustained neuronal activity [253].

Miro proteins also have a role in regulating mitochondrial morphology following Ca^{2+} increases: whereas Miro favours fusion by inhibiting Drp1 activity at resting Ca^{2+} concentrations, Drp1-dependent fragmentation is initiated upon rising Ca^{2+} levels [254]. Moreover, it was shown that neuronal Drp1 ablation alters synaptic mitochondrial distribution *in vivo* [255, 256].

1.1.6 Mitochondria and neurodegeneration

Neurodegenerative diseases are a group of heterogeneous disorders, the majority of which are primarily sporadic, but in rare cases they can be inherited. Nevertheless, the phenotypes of sporadic and familial forms are often indistinguishable, suggesting common underlying mechanisms [257]. The study of hereditary forms suggested that not only defects in

mitochondrial respiration but also in mitochondrial dynamics could contribute to the pathogenesis of many of the most common neurodegenerative disorders, through perturbed mitochondrial trafficking, mitochondrial quality control and communication with other organelles. Neurons are particularly sensitive to mitochondrial dysfunction, due to their high energy demand, and due to their complex morphology [258]. Several *in vitro* models of neurodegenerative diseases including autosomal dominant optic atrophy (ADOA), Alzheimer's disease (AD), and Parkinson's disease (PD) revealed a fragmented mitochondrial network [258, 259, 260, 261, 262].

Moreover, pathogenic mutations identified in genes with a key role in mitochondrial morphology resulted in primarily neurodegenerative disease, indicating that mitochondrial dynamics is a crucial process in brain tissue [223].

1.1.6.1 Parkinson's Disease

Parkinson's disease (PD), the most common movement neurodegenerative disorder, is a complex multifactorial disease with an incidence ranging from 5 up to >35 per 100,000 population [263]. Clinically, it is characterised by motor symptoms such as bradykinesia, resting tremor, muscle rigidity, and postural instability, which may be accompanied by depression, sleep disorders, anosmia, and, with disease progression, dementia. The neuropathological hallmarks of the disease include a progressive loss of dopaminergic neurons in the substantia nigra (SN) pars compacta that project to the striatum, and the presence of α -synuclein (α -syn) positive neuronal inclusions known as Lewy bodies (LB) and Lewy neurites (LN) [264].

Familial and sporadic PD forms share common clinical, pathological, and biochemical characteristics. Although many aspects of PD pathogenesis remain elusive, dysregulation of various fundamental physiological processes has been implicated, including impairment of the ubiquitin-proteasome pathway, mitochondrial dysfunction, oxidative stress, and neuroinflammation.

Both environmental and genetic factors converge in the complex molecular pathophysiology of Parkinson's disease, with mitochondrial dysfunction playing a major role [265, 266, 267, 268]. Several lines of evidence obtained from studies of familial forms of PD, patient tissue samples, and various *in vitro/in vivo* models point to a prominent involvement of

dysregulated mitochondrial crosstalk with other organelles in addition to impaired mitochondrial quality control pathways.

Review [214]

2.1. MAMs in Parkinson's Disease

2.1.1. α -synuclein

2.1.2. Parkin and PINK1

2.1.3. DJ-1

2.1.4. LRRK2

3. Mitochondria-Lysosomes contact sites in Parkinson's Disease

3.1. VPS35

3.2. ATP13A2

3.3. LRRK2

1.1.6.2 Autosomal dominant optic atrophy

The most common inherited optic nerve disorder is Dominant Optic Atrophy (DOA), characterized by the loss of retinal ganglion cells and consequent optic nerve degeneration and blindness [223]. Missense mutations or premature termination within the *OPA1* gene, with a consequent loss of function, cause more than half of the cases [269]. The transmission of the disease is autosomal dominant due to the effect of haploinsufficiency, with one copy of the *OPA1* gene being insufficient to handle the cell requirements. Most of the missense variants are localized to the GTPase domain (exons 8–16) [270].

Interestingly, the phenotype often almost exclusively affects the eye, although *OPA1* expression is ubiquitous. Syndromic forms, known as DOAplus, are reported in up to 20% of *OPA1* mutation carriers [271, 272, 273, 274, 275], which may show variable signs of myopathy, peripheral neuropathy, ataxia, encephalopathy, sensorineural hearing loss, and chronic progressive external ophthalmoplegia as clinical features [276].

Recently, bi-allelic *OPA1* mutations were associated with Behr syndrome, a syndromic disease characterized by early-onset optic atrophy, spasticity, spinocerebellar ataxia, peripheral neuropathy, gastrointestinal dysmotility, and intellectual disability [277].

In addition, rare associations of heterozygous or bi-allelic *OPA1* mutations have been reported in patients affected by a multiple sclerosis-like syndrome [278], optic atrophy and spastic para-paresis [275], severe syndromic cardiomyopathy associated with myopathy and encephalopathy [279], syndromic parkinsonism and dementia [280, 281], and Behr-like syndrome with metabolic stroke [282], reflecting a remarkable clinical diversity of *OPA1*-linked phenotypes.

Beyond *OPA1*, mutations in twelve other genes are associated with DOA, the majority of which encode proteins linked to mitochondrial function.

WFS1 mutations cause an autosomal recessive neurodegenerative disorder primarily associated with optic atrophy and diabetes, and frequently also featuring hearing loss, renal deficits and mental disease, known as Wolfram syndrome [283]. Remarkably, the protein product of *WFS1*, Wolframin, is an ER membrane glycoprotein enriched at MAMs with a role in Ca^{2+} homeostasis [284, 285]. Mutations in *WFS1* gene have been reported in families with DOA and neuro-sensorial deafness [286, 287, 288, 289], in Wolfram-like syndrome with variable expression of glucose intolerance [290, 291], as a cause of autosomal dominant inherited deafness [292, 293], and in recessive isolated optic atrophy [287].

In addition, autosomal recessive 3-methylglutaconic aciduria type III (or Costeff syndrome) is due to mutations in the *OPA3* gene, which encodes a mitochondrial inner membrane protein of still unknown function [294]. Clinically, this syndrome is characterised by optic atrophy, spasticity, and movement disorders [295, 296].

Optic atrophy associated with extraocular features, such as cataract, sensorineural hearing loss, peripheral neuropathy, ataxia and areflexia, has been described in several families with dominant *OPA3* mutations [297, 298, 299, 300, 301].

1.1.6.3 Charcot-Marie-Tooth Disease

Charcot-Marie-Tooth Disease (CMT) is a genetically and phenotypically heterogeneous group of inherited peripheral neuropathies [302] characterized by progressive degeneration of peripheral nerves. CMT can be classified depending on whether the pathological process is predominantly axonal (CMT2), with axonal loss and without demyelinating lesions, or demyelinating (CMT1), with reduced nerve-conduction velocities and segmental de- and

remyelination [303]. Irrespective of the aetiology, the degenerative processes clinically result in muscle weakness and sensory loss, with variations in age of onset and rate of clinical progression, which depend on the genetic cause [304, 305].

CMT2A is a severe autosomal dominant form of CMT, identified in families with *MFN2* mutations [306]. The majority of patients develop a severe peripheral neuropathy, which in some cases can be complicated by subacute visual failure and optic atrophy [307].

Loss-of-function mutations in ganglioside-induced differentiation-associated protein 1 (*GDAP1*), involved in mitochondrial fission, cause another form of CMT, CMT4A [308, 309], which features both demyelination and axonal pathology [310, 311]. Studies in *GDAP1*-KO mice showed disrupted calcium homeostasis and store-operated calcium release in peripheral neurons [312].

1.1.7 Dysfunction of p97 and neurodegeneration

P97 has a crucial role in maintaining cellular proteostasis, and it is therefore not unexpected that mutations in the gene encoding p97 lead to a multisystem degenerative disorder known as inclusion body myopathy associated with Paget disease of the bone and frontotemporal dementia (IBMPFD). This rare disease is characterized by muscle weakness, which may lead to difficulty breathing and heart failure due to the involvement of cardiac and respiratory muscles. Besides affecting muscles, IBMPFD also manifests itself in the bone, resulting in chronic pain, as well as in the brain, leading to frontotemporal dementia.

P97 mutations can result in ubiquitin-positive intracellular inclusion in skeletal muscles, bone and brain, which were shown to contain TAR DNA binding protein 43 (TDP43), β -amyloid, and phosphorylated tau protein, also present in other neurodegenerative diseases [313, 314, 315].

Most of disease-associated mutations are found in the interface region between the N- and D1-domain, and they do not appear to alter the protein oligomerization; however, some mutations enhance the basal hydrolysis of ATP of p97 [316, 317]. Disease-associated mutations could also affect p97 interaction with some cofactors [318], leading to impairment of a subset of p97 functions rather than a global loss-of-function. Altered p97-UBXD1 interaction affects ubiquitin-dependent membrane sorting at endosomes and degradation in lysosomes, suggesting a role of this pathway in IBMPFD, which probably involves weakened substrate

recognition. Specifically, the interaction of p97-UBXD1 with the main component of caveolae, caveolin-1 (CAV1), is affected [188]. Whereas UBXD1 is required for the endolysosomal trafficking of ubiquitinated CAV1, CAV1 is destined for degradation after being modified with mono-ubiquitin. Accumulation of CAV1-positive endolysosomes and reduced levels of the muscle-specific caveolin CAV3 at the sarcolemmal membrane of skeletal muscle have been seen in mice and patients with pathogenic p97 mutations [319].

Interestingly, a novel heterozygous missense p97 mutation (c.828 A>T, exon 6), in the evolutionary highly conserved linker domain, was described in 3 generations of a Swiss family in 2012 [320]. This new mutation leads to a change from isoleucine to phenylalanine at position 206 (I206F). Affected family members suffered from late-onset progressive muscle weakness, with both acute and chronic muscle denervation, fiber size variation and focal rimmed vacuoles. Immunohistochemistry revealed perivascular and endomysial inflammatory infiltrates. Brain autopsy of one of the affected family members revealed moderate frontotemporal cortical atrophy, and multiple dystrophic neurites positive for ubiquitin and TDP-43 in the neocortex and CA1 region of the hippocampus, a pattern corresponding to TDP-43 positive frontotemporal lobar degeneration type 4 [321]. In none of the patients symptoms indicative of Paget disease of the bone were reported [320].

2. Material and Methods

2.1 Materials

2.1.1 Equipment

Equipment	Manufacturer
BC43 microscope	Olympus
BioWizard Golden Line biosafety Cabinet	Kojair
C1000 Touch Thermal Cycler with 96-Deep Well Reaction Module	Bio-Rad
Countess II	Thermo Fisher Scientific
Fusion FX	Vilber
HM 355S Automatic Microtome	Thermo Fisher Scientific
Labofuge 400R	Heraeus Instruments
NanoDrop TM 2000	Thermo Fisher Scientific
PowerPac TM Basic Power Supply	Bio-Rad
PX1 PCR Plate Sealer	Bio-Rad
QX200 Droplet Generator	Bio-Rad
QX200 Droplet Reader	Bio-Rad
Seahorse XF HS Mini Analyzer	Agilent
SimpliAMP TM Thermal Cycler	Thermo Fisher Scientific
SubAqua Pro Unstirred Water Bath	Grant Instruments
TES 99 Paraffin Embedding Center	Medite
Thermomixer	Eppendorf
Tissue processor TPC15	Medite
TProfessional TRIO Thermocycler	Analytik Jena
Trans-Blot Turbo Transfer System	Bio-Rad
Varioskan™ LUX multimode microplate reader	Thermo Fisher Scientific
Water Bath	Memmert

Table 2.1: Equipment used during this study.

2.1.2 Reagents

Item	Order Number	Supplier
Agarose	2267.4	Carl Roth
Ampicillin sodium salt	K0291	Carl Roth
Aureobasidin A	630466	Sigma-Aldrich
BCA protein assay kit	23225	Thermo Fisher Scientific
Cell scraper	99002	TPP
CellTiter-Glo Luminescent cell viability assay	G7571	Promega

Material and Methods

Countess Cell counting chamber slides	C10283	Invitrogen
ddPCR Supermix for Probes (No dUTP)	1863023	Bio-Rad
DG8 Cartridges	1864008	Bio-Rad
DG8 Gaskets	1863009	Bio-Rad
DMEM high glucose (1X)	41965062	Gibco
DPBS (1X)	14190-094	Gibco
Droplet Generation Oil	1863005	Bio-Rad
Ethidium Bromide	1410433	Bio-Rad
FBS Tet system approved	16876796	Fisher Scientific
Fetal Bovine Serum (FBS) Heat Inactivated	S181H-500	Biowest
FuGENE® 6	E2691	Promega
GelRed Nucleic Acid Stain	41003	Biotium
Gene Pulser Cuvettes	165-2086	Bio-Rad
GenElute Mammalian Genomic DNA Miniprep Kit	G1N70-1KT	Sigma-Aldrich
Glycerol	3783.1	Carl Roth
Glycine	3790.3	Carl Roth
HeLa cell line		LGC Standards
Histidine		Sigma-Aldrich
HistoGel	HG-4000-012	Thermo Fisher Scientific
Hygromycin B	10687010	Thermo Fisher Scientific
K12 ER2925 <i>E. coli</i>	E4109	NEB (Bioconcept)
L-Glutamine (200mM)	2503032	Thermo Fisher Scientific
LB-broth	X968.3	Carl Roth
Leucine	L8912	Sigma-Aldrich
Lipofectamine 3000	L3000008	Thermo Fisher Scientific
Matchmaker Gold Y2H System	630489	Clontech Laboratories
NucleoSpin Gel/PCR Clean-Up	740609.25	Macherey-Nagel
NucleoSpin Plasmid	470588.25	Macherey-Nagel
NuPAGE 4-12% Bis Tris, 1.5 mm, Mini Protein Gel, 15-well	NP00336	Invitrogen
NuPAGE LDS Sample Buffer (4X)	NP007	Invitrogen
NuPAGE MOPS SDS Running Buffer (20X)	NP0001	Novex by LifeTechnologies
NuPAGE Sample Reducing Agent (10X)	NP0009	Life Technologies
NuPAGE TM MOPS SDS Running Buffer (20X)	NP0001	Thermo Fisher Scientific
Opti-MEM Reduced Serum Medium	31985070	Thermo Fisher Scientific
Pierce BCA Protein Assay kit	23227	Thermo Fisher Scientific
Pierce TM ECL Western Blotting Substrate	32209	Thermo Fisher Scientific
Pierce TM RIPA buffer	89901	Thermo Fisher Scientific
Precision Plus Protein Dual Color Standards	161-0374	Bio-Rad
Rneasy Mini Kit (50)	74104	Qiagen
Sodium pyruvate solution	S8636	Sigma-Aldrich

Stbl3 Chemically Competent <i>E. coli</i>	C737303	Thermo Fisher Scientific
SureBlock	SB232010	Lubio Science
SuperScript™ VILO™ cDNA Synthesis Kit	11754050	Thermo Fisher Scientific
TBS Buffer 20X	28358	Thermo Fisher Scientific
Tetracycline hydrochloride	HP63.1	Carl Roth
Tissue-Tek® Uni-Cassette® Stacked Cassettes White	8170	Sakura
Trans-Blot Turbo Midi Nitrocellulose Transfer Pack	1704159	Bio-Rad
Trypsin-EDTA PBS 1:250 w/o Ca/Mg with Phenol Red	5-51FOO-H	BioConcept
Tween 20	P9416-100ML	Sigma-Aldrich

Table 2.2: Reagents used during this study.

2.1.3 Antibodies

Name	Order number	Vendor	Usage
rabbit anti-alpha-synuclein	ab138501	Abcam	1:10000 WB
mouse anti-GAPDH	sc-32233	Santa Cruz	1:6000 WB
rabbit anti-OPA1	80471	Cell Signaling	1:1000 WB

Table 2.3: Antibodies used during this work.

WB = western blotting

2.1.4 Composition of Buffers and Media

2YT medium

NaCl 10 g/l
 yeast extract 10 g/l
 peptone 12 g/l
 MgSO₄ 20 mM
 KCl 10 mM

MgSO₄ and KCl were added from sterile 1 M stock solutions after autoclaving.

SOB media

peptone 2 % (w/v)
 yeast extract 0.5 % (w/v)
 NaCl 10 mM
 KCl 2.5 mM
 MgCl₂ 10 mM
 MgSO₄ 10 mM

Transformation buffer 1 (TFB 1)

MnCl₂ 30 mM
 RbCl 100 mM
 CaCl₂ 10 mM
 glycerol 15 % (v/v)
 pH 5.8

Transformation buffer 2 (TFB 2)

MOPS 10 mM
 RbCl 10 mM
 CaCl₂ 75 mM
 glycerol 15 % (v/v)
 pH 6.8

2.1.5 Enzymes and Nucleic Acids

Name	Order number	Vendor
<i>AgeI</i>	R0552	New England Biolabs (NEB)
<i>ApaI</i>	R0114	New England Biolabs (NEB)
<i>BamHI</i>	R0136	New England Biolabs (NEB)
<i>BclI</i> -HF	R3160	New England Biolabs (NEB)
<i>BglII</i>	R0144	New England Biolabs (NEB)
<i>ClaI</i>	R0197	New England Biolabs (NEB)
<i>EcoRV</i>	R0195	New England Biolabs (NEB)
<i>EcoRV</i> -HF	R3195	New England Biolabs (NEB)
<i>HindIII</i>	R0104	New England Biolabs (NEB)
<i>HpaI</i>	R0105	New England Biolabs (NEB)
<i>KpnI</i>	R0142	New England Biolabs (NEB)
<i>NdeI</i>	R0131	New England Biolabs (NEB)
<i>NotI</i>	R0189	New England Biolabs (NEB)
<i>NotI</i> -HF	R3189	New England Biolabs (NEB)
<i>NruI</i>	R0192	New England Biolabs (NEB)
<i>NruI</i> -HF	R3192	New England Biolabs (NEB)
<i>SpeI</i>	R0133	New England Biolabs (NEB)
<i>XhoI</i>	R0146	New England Biolabs (NEB)
DNA Polymerase I, Large (Klenow) Fragment	M0210	New England Biolabs (NEB)
Phusion Polymerase	M0530	New England Biolabs (NEB)
T4 DNA ligase	M0202	New England Biolabs (NEB)

Table 2.4: DNA modifying enzymes used during this study.

2.1.6 Oligonucleotides

Name	Sequence
OAN2670	AGATGACATATGAAGAAATTCCTTCAGGAGTTCAAGG
OAN2671	AGATGAGGATCCTTACTTCCTCAGGGTGGCCCCAG
OAN2691	AGATGACATATGGCTTCTGGAGCCGA
OAN2692	AGATGAATCGATGAAGATGATAGCAGGAGC
OAN2953	AGATGAGCGGCCGCATGTGGCGACTACGTCCG
OAN2954	AGATGAGGGCCCTCAAGCGTAATCTGGAACATCGTATG
OAN2884	CCTTGAGCTCTACTGGCTTCTGCGCC
OAN2886	CCCTAGAGGATCCCCGGGTACCAAG
OAN2889	GCTGCCTCAAAGGGCTTGCCAAC
OAN2890	GCAGTCACCCACAGTTGGAGGAG
OAN3029	ATTCTCCGCCCATGGCTGAC
OAN3030	ATCTTTGTAGAAACCATCGGCGCAGC
OAN3031	CGAGATCCGTGGTCGCGAAGTTG
OAN3032	AGCCATCTGTTGTTGCCCCCTCC
OAN3323	CCGCCAGAACACAGGTAAGTGCC
OAN3324	TACGTAAAGGAAGGTTTGTTCAGAGAAGAGAAC
OAN3325	GCTGAAGATGGTGAGAAGAAGATTAATTAATTGC
OAN3352	CTAGAGCCCCAGCTGGTCTTTC
Opa1 primer forward	CCCAAGAGGATCTGGGGAGA
hOpa1 primer reverse	ATAGGGCCACATGGTGAGGA
hOpa1 probe	TGACACGTTCTCCAGTTAAGGTGACT
hGAPDH primer forward	CAGCAATGCCTCCTGCACC
hGAPDH primer reverse	TGGACTGTGGTCATGAGTCC
hGAPDH probe	CCCCCTGGCCAAGGTCATCCA

Table 2.5: Oligonucleotides used during this study (All purchased from Sigma-Aldrich).

2.1.7 Plasmids

Name	Description	Vector	Insert
pAN2103		pBluescript SK (+)	
pAN2861	YFP-UBXD1	EYFP-C1	pAN2741 *OAN 2020/2021
pAN3090	pGBTK7 with UBXD1 wt (bait for Y2H)	pGBTK7 *NdeI, BamHI	PCR pAN2861 OAN2398/9 *NdeI, BamHI
pAN3102	pGADT7 with p97 wt (prey for Y2H)	pAN3089*EcoRI, PmlI	pAN1502*EcoRI, PmlI
pAN3266	α -synuclein WT	pEGFP-C1	addgene #40822
pAN3267	α -synuclein A53T	pEGFP-C1	addgene #40823
pAN3303	Gal4BD-UBXD11-133 (VIM/N-Term)	p3090 *NdeI, BamHI	PCR on pAN2861 with OAN2670/1

Material and Methods

pAN3304	GAL4AD-p97 (on fixed wt)	pAN3102 *NdeI/ClaI	BioCat - p97_noClaI_fixed wt
pAN3305	GAL4AD-p97R155H (on fixed wt)	pAN3102 *NdeI/ClaI	BioCat - p97R155H
pAN3306	GAL4AD-p97I206F (on fixed wt)	pAN3102 *NdeI/ClaI	BioCat - p97I206F
pAN3310	Gene synthesized at Biocat	pUC57	p97 WT
pAN3311	Gene synthesized at Biocat	pUC57	p97 R155H
pAN3312	Gene synthesized at Biocat	pUC57	p97 I206F
pAN3414	vector of Invitrogen Flp-InT-REX system	pcDNA5/FRT/TO	Invitrogen Flp-InT-REX system
pAN3415	vector of Invitrogen Flp-InT-REX system	pcDNA6/TR	Invitrogen Flp-InT-REX system
pAN3417	pcDNA6/TR derivative with EF1a promoter instead of CMV	pAN3415- pcDNA6/TR*SpeI/SacI	PCR on pAN2045 OAN2852/3 *SpeI/SacI
pAN3418	AAVS1 donor with EF1a- rabbit-b-globin intron - TetR - synthetic pA - PSV40-FRT-ATG-Gluc-SV40pA for generation of stable cell lines	pAN3413*MluI-HF, AgeI	PCR on pAN3417 OAN2854/51*MluI-HF, AgeI
pAN3419	pBluescript with <i>ApaI-SacII</i> fragment of pAN3414 - pcDNA5/FRT/TO	pBluescript_skplus* <i>ApaI, SacII</i>	pAN3414* <i>ApaI, SacII</i>
pAN3420	pBluescript with <i>ApaI-SacII</i> fragment of pAN3414 - pcDNA5/FRT/TO and inserted ATG for hygromycin gene; add <i>NdeI</i> site for control digest upstream ATG	pAN3419* <i>XbaI, AatII</i>	annealed oligos OAN2855/56
pAN3421	modified pcDNA5/FRT/TO with additional ATG for hygromycin gene; low copy!	pAN3414* <i>ApaI, SacII</i>	pAN3420 * <i>ApaI, SacII</i>
pAN3463	pcDNA3.1- with human OPA1 variant 1	pcDNA3.1- * <i>XhoI/BamHI</i>	hOPA1v1 retroviral plasmid from Scorano * <i>XhoI/BamHI</i>
pAN3469	Tet-Inducible WT α -synuclein	pcDNA5/FRT/TO * <i>XhoI/ApaI</i>	pAN3266 * <i>XhoI/ApaI</i>
pAN3470	Tet-Inducible A53T α -synuclein	pcDNA5/FRT/TO * <i>XhoI/ApaI</i>	pAN3267 * <i>XhoI/ApaI</i>
pAN3502	WT α -synuclein - SV40pA - EF1 α	pUC57-BsaI-Free	Biocat gene synthesis
pAN3503	A53T α -synuclein - SV40pA - EF1 α	pUC57-BsaI-Free	Biocat gene synthesis
pAN3507	WT α -synuclein - SV40pA - EF1 α in modified pcDNA5/FRT/TO for integration into FRT site	pAN3421 * <i>KpnI/NotI</i>	pAN3502 * <i>KpnI/NotI</i>
pAN3516	WT α -synuclein - SV40pA - EF1 α - hOPA1v1 in modified pcDNA5/FRT/TO for integration into FRT site	pAN3507 * <i>XhoI/BclI</i>	pAN3463 * <i>XhoI/BamHI</i>
pAN3517	A53T α -synuclein - SV40pA - EF1 α - hOPA1v1 in modified pcDNA5/FRT/TO for integration into FRT site	pAN3508 * <i>XhoI/BclI</i>	pAN3463 * <i>XhoI/BamHI</i>
pAN3518	EF1 α -hOPA1v1 in modified pcDNA5/FTR/TO for integration into FRT site	pAN3516 * <i>NruI-HF/BamHI</i> +KlenowFill	religation blunt end
pcDNA 3.1 (-)		Thermo Fisher Scientific	
pcDNA5/FRT/TO		Thermo Fisher Scientific	
pGADT7	GAL4AD	Matchmaker (Clontech)	
pGBKT7	Gal4BD	Matchmaker (Clontech)	

Table 2.6: Plasmids used in this study.

2.2 Methods

2.2.1 Molecular Biological Methods

2.2.1.1 Bacterial Strains

The *Escherichia coli* (*E. coli*) strains DH5 α and *dam*⁻/*dcm*⁻ *E. coli* K12 ER2925 were used for cloning as well as amplification of plasmid DNA. Both strains were grown in Luria-Bertani media (LB) [322] and on LB agar plates supplemented with the appropriate antibiotic for selection. *E. coli* strain Stbl3 was used for amplification of viral vector DNA. Antibiotics used were ampicillin (100 μ g/ml) or kanamycin (50 μ g/ml).

2.2.1.2 Preparation of chemically competent *E.coli*

DH5 α or *dam*⁻/*dcm*⁻ *E. coli* strains 6 ml were grown overnight following inoculation in 2YT medium. This culture was diluted 1:100 in 10 ml 2YT medium and grown to OD₆₀₀ = 0.5. This new culture was diluted 1:100 in 100 ml 2YT medium, grown again until OD₆₀₀ = 0.5 and then chilled for 10 minutes in an ice-water bath. Bacteria were spun down in a pre-cooled centrifuge at 2000 g and 4 °C for 7 minutes. The pellet was resuspended in ice-cold transformation buffer 1 and chilled in an ice-water bath for 10 minutes. Bacteria were again spun down in a pre-cooled centrifuge at 2000 g and 4 °C for 7 minutes, and the pellet was resuspended in 2 ml of ice-cold transformation buffer 2. The bacterial suspension was aliquoted on dry ice in 50 μ l aliquots and immediately stored at -80 °C.

2.2.1.3 Polymerase chain reaction (PCR)

Polymerase chain reaction is a method to exponentially amplify a defined segment of double-stranded DNA using a thermo-stable DNA-polymerase [323].

Component	PCR 1	PCR 2	PCR 3	PCR 4
Template (< 250 ng)	1 µL	1 µL	1 µL	1 µL
Oligonucleotide 1 (10 µM)	2,5 µL	2,5 µL	2,5 µL	2,5 µL
Oligonucleotide 2 (10 µM)	2,5 µL	2,5 µL	2,5 µL	2,5 µL
dNTPs (2 mM each)	5 µL	5 µL	5 µL	5 µL
5X Phusion HF buffer	10 µL	10 µL	-	-
5X Phusion GC buffer	-	-	10 µL	10 µL
DMSO	-	1,5 µL	-	1,5 µL
Phusion polymerase	0,5 µL	0,5 µL	0,5 µL	0,5 µL
Water up to 50 µL	up to 50 µL	up to 50 µL	up to 50 µL	up to 50 µL

Table 2.7: Pipetting scheme to optimise DNA amplification using high fidelity Phusion polymerase (NEB).

Four different conditions were tested to then select the condition with the most optimal DNA amplification.

	temperature	time
1X	98°C	30 s
35X	98°C	10 s
	annealing	30 s
	72°C	15-30 s/kb
1X	72°C	10 min
1X	10°C	∞

Table 2.8: Temperature and time profile for amplification using high fidelity Phusion polymerase.

The annealing temperature was chosen based on the recommendation of the web-based NEB tm calculator (<https://tmcalculator.neb.com>). For DNA cloning purposes, PCR amplified DNA was separated from free oligonucleotides through agarose gel electrophoresis and purified using NucleoSpin Gel and PCR Clean-Up according to the manufacturer's recommendations.

2.2.1.4 DNA digestion

For cloning purposes, restriction enzymes were used to treat plasmid DNA. Between 0.5 and 5 µg of plasmid DNA was treated with 1 to 10 U of restriction enzyme for at least 1 h at the manufacturer recommended temperature and buffer conditions. DNA obtained following PCR amplification was digested overnight to improve digestion at the 5' and 3' ends. Double

digestion using two or more restriction enzymes were performed according to the manufacturer's instructions whenever possible and where indicated. Digested DNA was purified using agarose gel electrophoresis ([2.2.1.8](#)) followed by Machery and Nagel's NucleoSpin Gel and PCR Clean-Up kit.

2.2.1.5 DNA ligation

DNA ligation reactions were prepared by mixing vector DNA and insert DNA fragments, obtained by DNA digestion of plasmid DNA ([2.1.7](#)) or PCR products ([2.2.1.3](#)), at a 1:3 ratio, with 1 μ l of T4 DNA ligase and 2 μ l of the appropriate buffer (NEB) in a total reaction volume of 20 μ l were added. The ligation mix was incubated at room temperature overnight, and used for transformation into DH5 α or *dam*⁻/*dcm*⁻ *E. coli* ([2.2.1.6](#)).

2.2.1.6 DNA transformation into chemically competent *E. coli*

Competent DH5 α or *dam*⁻/*dcm*⁻ *E. coli* were thawed on ice. 3 μ l of DNA ligation mix ([2.2.1.5](#)) was added to 40 μ l of competent bacteria and incubated for 10 minutes on ice. Heat shock was carried out by incubating the reaction mix for 45 seconds at 42 °C and shaken at 600 rpm in a thermomixer, immediately followed by cooling for 2 minutes on ice. The transformed bacteria were resuspended in 900 μ l SOC medium and shaken at 600 rpm and 37 °C in a Thermomixer for 1 h. An aliquot of the transformation mix was spread on LB plates containing an appropriate antibiotic and incubated at 37 °C overnight.

2.2.1.7 DNA plasmid isolation

After DNA transformation, several *E.coli* clones grown on LB plates were picked for verification. Each clone was used to inoculate 5 ml of LB medium containing the appropriate antibiotic and incubated overnight at 37 °C and 250 rpm. Plasmid DNA isolation was performed using Machery-Nagel's NucleoSpin Plasmid kit. DNA was then digested ([2.2.1.4](#)) using appropriate restriction enzymes, and agarose gel electrophoresis ([2.2.1.8](#)) was performed to select correct clones. Sequence analysis (Microsynth, Basel, CH) was used to verify the correct clones.

2.2.1.8 Agarose gel electrophoresis

Agarose gels were prepared from agarose (0,8 to 2% w/v) diluted in 50 ml TAE buffer supplemented with 0.5 µg/ml ethidium bromide. Plasmid DNA was mixed with DNA loading dye, and gel electrophoresis was carried out at 85 V for 45 minutes. NucleoSpin Gel and PCR Clean-Up kit (Machery-Nagel) was used according to manufacturer's recommendations for DNA fragments purification.

2.2.1.9 Yeast two-hybrid

In a Matchmaker GAL4-based two-hybrid assay, a bait protein is expressed as a fusion to the Gal4 DNA-binding domain (DNA-BD), while libraries of prey proteins are expressed as fusions to the Gal4 activation domain. The interaction of two proteins or polypeptides of interest leads to the reconstitution of a functional transcription factor (Fig. 3.25) in genetically modified yeast strains, in which the transcription of a reporter gene results in a specific phenotype, usually growth on a selective medium or change in the colour of the yeast colonies [324]. A downstream analysis was used to quantify the effects of point mutations on the strength of interaction. The Gal-responsive LacZ gene (b-galactosidase) integrated in Y187 yeast strain was employed as a reporter for quantitative studies of protein-protein interactions because it is strongly expressed in this strain.

2.2.1.10 RNA extraction

RNA extraction from cell pellets was performed using RNeasy Mini Kit (Qiagen) according to manufacturer's guidelines, followed by RNA quantification (NanoDrop™ 2000, Thermo Fisher Scientific).

2.2.1.11 Reverse transcription of RNA to cDNA

Reverse transcription of extracted RNA was performed using SuperScript™ IV VILO Master Mix (Thermo Fisher) according to manufacturer's guidelines, and 1,5 µg RNA as input for the reaction. Then, SimpliAMP™ Thermal Cycler (Thermo Fisher) was used as follows: 25°C for 10 min, 42°C for 60 min, 85°C for 5 min, and 4°C thereafter. Samples were then stored at -20°C until further processed.

2.2.1.12 Droplet digital PCR (ddPCR)

For ddPCR, the human OPA1 and human GAPDH primer/probe mixes were prepared as follows: forward primer FAM or HEX (100 μ M) 9 μ l, reverse primer FAM or HEX (100 μ M) 9 μ l, probe (100 μ M) 2,5 μ l, and 79,5 μ l ddH₂O. Then, 1 μ l of cDNA templates at three different dilutions (1:50, 1:100 and 1:200) was added to a 20- μ l reaction mixture containing 10 μ l Bio-Rad 2x digital PCR supermix for probes (No dUTP), 1 μ l of hOPA1 FAM primer/probe mix, 1 μ l of hGAPDH HEX primer/probe mix, and 8 μ l of nuclease-free water.

For droplet generation, a Bio-Rad cartridge was inserted into the cartridge holder, loaded with droplet generator oil (70 μ l) and PCR reactions, covered with Bio-Rad gasket and placed in the QX200 Droplet generator. The droplets volume (around 40 μ l) was transferred from the cartridge to a twin.tec semi-skirted 96-well PCR plate, then sealed with an easy pierce heating sealing foil (Thermo Fisher) using the PX1 PCR plate sealer. The PCR reaction was performed in the C1000 Touch Thermal Cycler as follows: 95°C for 10 min followed by 40 cycles 94°C for 30 seconds and 60°C for 1 minute, then 98°C for 10 minutes, and 4°C thereafter. The plate is thus placed in the QX200 Droplet Reader for signal detection. For each sample, the reaction was performed in triplicate, and Bio-Rad QuantaSoft software was used to manually set the amplitude threshold.

2.2.2 Biochemical Methods

2.2.2.1 Preparation of cell lysates

Cells were harvested and cell pellets were stored on ice for immediate use or at -80 °C for several days. For lysis, pellets were resuspended in RIPA buffer supplemented with protease and phosphatase inhibitor cocktail and incubated on ice for 45 minutes. Samples were then centrifuged at 14000 g and 4°C for 15 minutes. Supernatants were collected and stored on ice for immediate use or at -80 °C for several days.

2.2.2.2 Measurement of protein content

Pierce BCA protein assay kit (Thermo Fisher Scientific) was used to measure protein content of cell lysates (add reference) according to manufacturer's recommendations. Cell lysate supernatants were diluted in ddH₂O (1:5 ratio). 10 μ l of diluted samples and eight BCA reference solutions were added in triplicate to a 96 well plate. 100 μ l of BCA Working Reagent

was added to each well, followed by incubation at 37 °C for 30 minutes. Absorption at 562 nm was then measured with the Varioskan™ LUX multimode microplate reader (Thermo Fisher Scientific) to calculate protein content of the sample.

2.2.2.3 SDS page

Sodium dodecyl sulfate polyacrylamide gel electrophoresis (SDS-PAGE) method is used to separate proteins on an acrylamide gel according to their size. Samples were loaded onto precast polyacrylamide gels (NuPAGE™ 4 to 12%, Bis-Tris, 1.5 mm, 15-well, Thermo Fisher Scientific) and were separated at 90 V for 120 minutes in NuPAGE™ MOPS SDS Running Buffer.

2.2.2.4 Western blotting

Western blotting is a method to transfer proteins from an SDS-PAGE gel to a nitrocellulose membrane for antibody-based detection. Protein transfer or blotting was performed on a Trans-Blot Turbo Transfer System (Bio-Rad). After blotting, nitrocellulose membranes were blocked in 1X TBS, 0.1% Tween® 20 (TBS-T) containing 3 % (w/v) SureBlock (Lubio Science) for 1 h to reduce nonspecific antibody binding. Primary antibody (Table 2.3) was added to the membranes in TBS-T or TBS-T 5% w/v BSA and incubated with gentle shaking at 4 °C overnight. After three washes in TBS-T, secondary HRP-coupled antibody diluted in TBS-T was added to the membrane and incubated with gentle shaking for 2 h, after which the membrane was washed three times with TBS-T. Proteins were detected using a chemiluminescent substrate.

2.2.2.5 Extraction of genomic DNA

Genomic DNA was extracted from cells using the GenElute Mammalian Genomic DNA Miniprep kit (Sigma-Aldrich) according to the manufacturer's recommendations.

2.2.3 Cell Biology Methods

2.2.3.1 Cell culture

All cell lines were grown in a humidified incubator at 5% CO₂ and 37°C. Cell lines without inducible genes were maintained in DMEM (Dulbecco's modified Eagle's media) supplemented with 10% FBS, 2 mM L-glutamine, and 1 mM sodium pyruvate, whereas cell lines harbouring tetracycline-inducible genes were maintained in the same medium but supplemented with 10% Tet system approved FBS. Cells were passaged after reaching 80-90% confluency by removing growth medium, washing once with PBS and incubating with Trypsin/EDTA at 37°C for 5 minutes. Trypsin/EDTA was inactivated by adding medium in 1:1 ratio. The solution was transferred in a 15 mL falcon tube centrifuged at 1300 rcf for 5 min. The cell pellet was resuspended in fresh medium. Cells were distributed into new tissue culture containers as required. For single cell cloning experiments, cells were grown in 96 well tissue culture plates. For western blot and immunohistochemistry experiments, cells were grown in tissue culture dishes. To select cells with integration of the construct of interest, HeLa cells were treated with 150 µg/ml Hygromycin B. Cells were treated with 1 µg/ml Tetracycline to stimulate expression of tetracyclin-inducible genes.

2.2.3.2 Transfection of mammalian cells

For integrative vector transfection, cells were transfected with FuGENE® 6 (Promega). Cells were grown in 6 well tissue culture plates. After 24 h at approximately 60% confluency, cells were transfected as follows. 6 µl FuGENE® 6 was added to 100 µl Opti-MEM in an Eppendorf Safe-Lock tube while minimising direct contact of FuGENE® 6 to plastic surfaces. After incubation at room temperature for 5 minutes, 2 µg of plasmid DNA was added to the solution, which was incubated for another 15 minutes at room temperature. Finally, the solution was added dropwise to the cells. 24 h after transfection, growth medium was replaced with fresh tetracycline-free growth medium.

Transient transfection of plasmids was done using Lipofectamine™ 3000 (Thermo Fisher Scientific). Cells were seeded in a tissue culture dish and grown for 24h before transfection. 6 µg of plasmid DNA (pOG44/pAN3XXX ratio; 9:1) were added to Opti-MEM® medium together with the lipofectamine reagents following manufacturer's recommendations. After

24 h the medium was exchanged. Cells were grown for an additional 24 h before hygromycin addition to select cells harbouring expression plasmids integration.

2.2.3.3 Immunohistochemistry (IHC)

Cells were harvested in p100 dishes and fixed with 4% paraformaldehyde (PFA) for 15 minutes at room temperature (RT). Cells were collected with a cell scraper, washed in PBS, and spun at 1200 rcf for 5 min to obtain cell pellets. Histogel (Thermo Fisher) was melted in a microwave and used to resuspend the cell pellets (80 μ l). Histogel drops with resuspended cells were dried on parafilm for 1 hr and transferred in a uni-cassette system for tissue processing (Tissue Processor TPC15 Medite). Each sample was embedded in paraffin (Tes 99 Paraffin embedding Center Medite), sections were obtained with an automatic microtome (HM 355S Thermo Fisher) and stained with mouse anti-alpha-synuclein antibody. Images of stained sections were acquired with the Olympus BC43 microscope and analyzed using Ilastik software.

3. Results

3.1 Opa1 PROJECT

3.1.1 Generation of a double transgenic mouse model

The aim of this project was to create a double transgenic mouse model that overproduces the inner mitochondrial membrane protein Opa1 along with the mutated human α -synuclein^{A53T} mutation. The question we intended to answer was whether mild overexpression of *OPA1* would rescue, at least partially, the mitochondrial phenotype provoked by mutant α -synuclein A53T. To this end, we crossed *Opa1*^{tg} [83] with *B6;C3-Tg(Prnp-SNCA*^{A53T})83Vle/J* mice [325], the latter also known in the literature as A53T α -synuclein transgenic line M83.

3.1.1.1 A53T α -synuclein transgenic line M83

For genotyping the A53T α -synuclein transgenic line M83, southern blot or qPCR-based methods are established as standard PCR is not able to discriminate between homozygous and heterozygous animals. As there is no clear qPCR Δ Ct threshold established for discrimination, the transgene genotype is usually determined by comparing Δ Ct values of unknown samples against known homozygous and heterozygous controls. Furthermore, the exact number of copies of the transgene is not known for either homozygous or heterozygous animals.

To investigate the genotype of heterozygous mice purchased from Jackson Laboratory, Sybr green real-time PCR was performed. Human A53T α -synuclein plasmid (Addgene, 40823) was used to establish a standard curve by serial dilution, to then compare the results of DNA samples obtained from heterozygous mice.

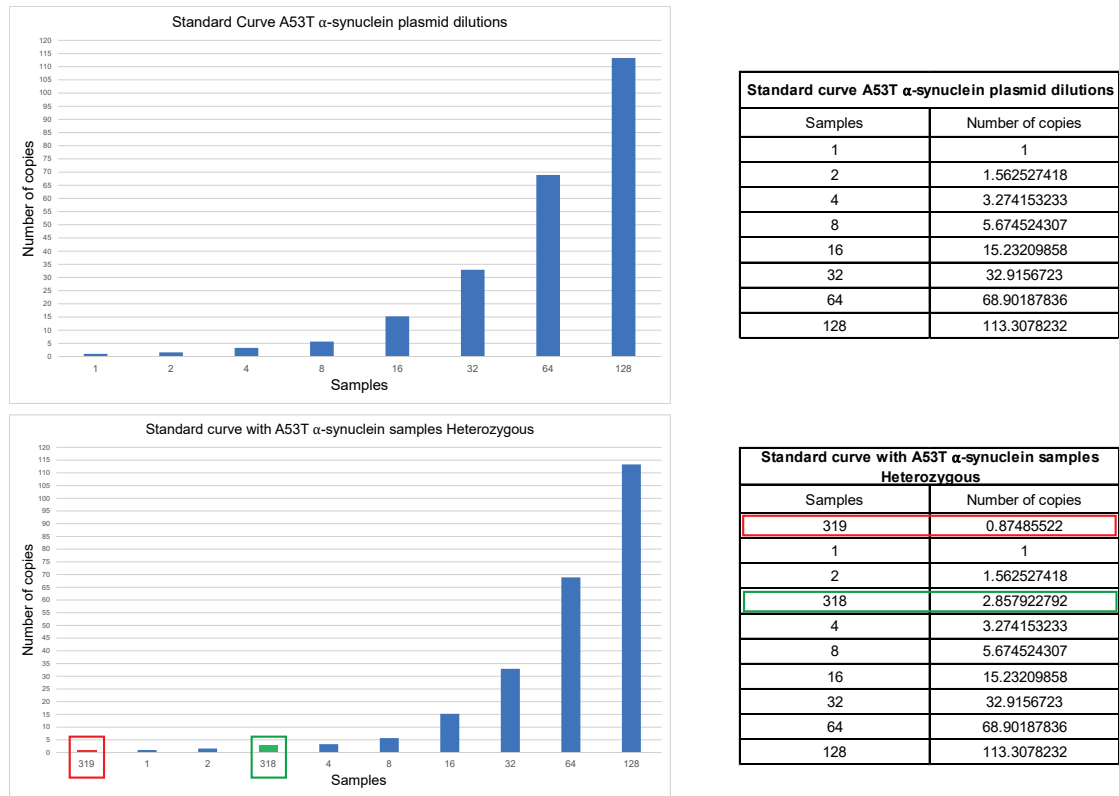


Figure 3.1 Analysis of Sybr green real-time PCR of A53T α -synuclein heterozygous mice.

Sybr Green real-time PCR revealed that heterozygous mice had one (mouse 319) and three (mouse 318) copies of A53T α -synuclein transgene, respectively (Fig. 3.1).

3.1.1.2 *Opa1*^{tg} mouse line

The *Opa1*^{tg} mouse line was re-derived from animal sperm at the Centre for Transgenic Models (CTM) of Basel. After line re-derivation, DNA extracted from tail tissue was PCR amplified to define animal genotype.

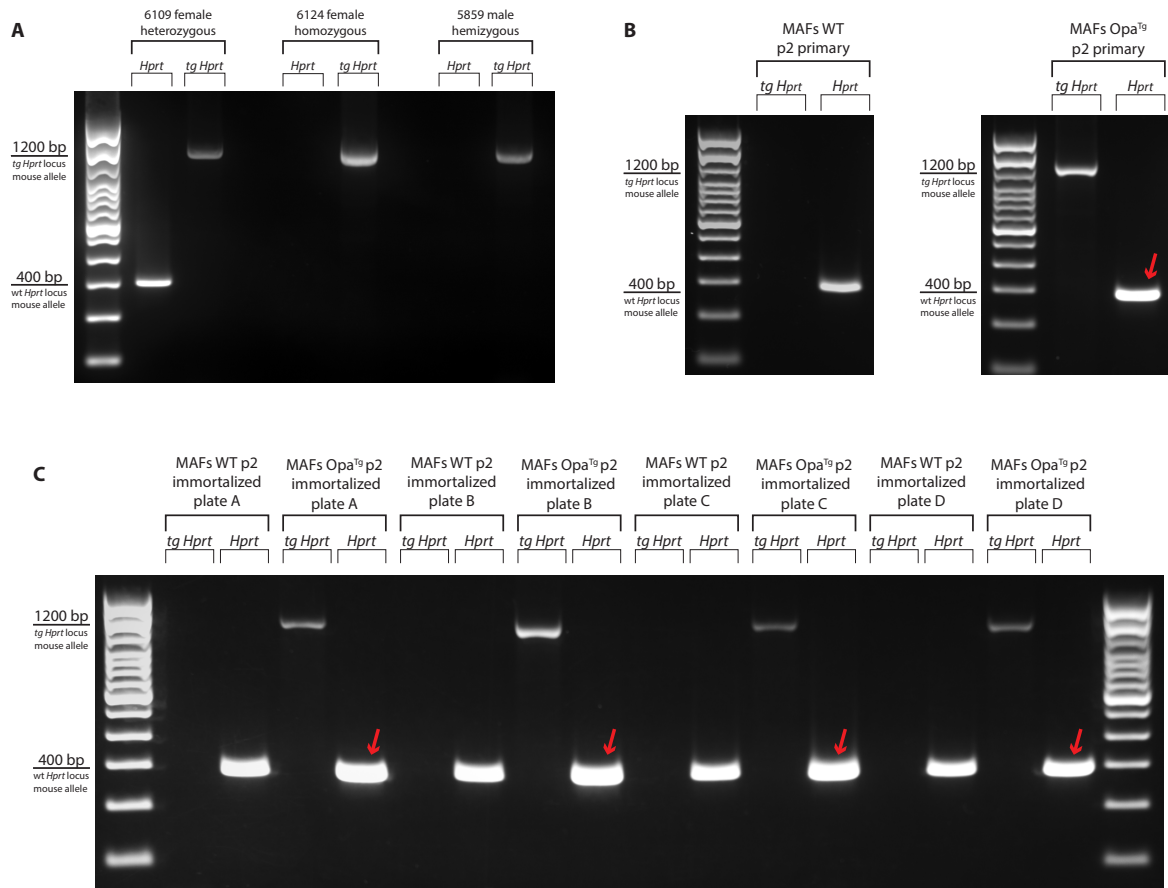


Figure 3.2 PCR analysis of *Opa1^{tg}* mice and derived MAFs.

A. Representative PCR analysis of female heterozygous, female homozygous and male hemizygous *Opa1^{tg}* mice. **B.** Representative PCR analysis of primary wt and *Opa1^{tg}* MAFs from diaphragm of 7-week-old C57BL6/J male mice. **C.** Representative PCR analysis of immortalized wt and *Opa1^{tg}* MAFs from diaphragm of 7-week-old C57BL6/J male mice. Red arrows: unexpected 400bp band in *Opa1^{tg}* MAFs

Female heterozygous animals showed the wt *Hprt* locus mouse allele at 400 bp, and the tg *Hprt* locus mouse allele at 1200 bp; the tg *Hprt* locus mouse allele at 1200 bp is exclusively present in female homozygous animals, as well as in male hemizygous animals (Fig. 3.2A). Fibroblasts were isolated from the diaphragm of wt and hemizygous *Opa1^{tg}* 7-week-old C57BL6/J male mice (MAFs) and immortalized, with the aim of transfecting them with wt and A53T α -synuclein and thus generating stable cell lines for further experiments.

PCR analysis was performed on primary and immortalized wt and *Opa1^{tg}* MAFs. While primary (Fig. 3.2B, left picture) and immortalized (Fig. 3.2C) wt MAFs showed a single 400 bp band corresponding to the wt *Hprt* locus mouse allele, primary (Fig. 3.2B, right picture) and immortalized (Fig. 3.2C) *Opa1^{tg}* MAFs unexpectedly displayed the 400 bp band of wt *Hprt* locus mouse allele in addition to the 1200 bp band of the tg *Hprt* locus mouse allele, as if there would be a mixed population of cells.

To investigate whether the unexpected PCR pattern was solely concerning the diaphragm tissue used to prepare primary MAFs, PCR analysis was performed on DNA extracted from five different tissues including brain, diaphragm, liver, muscle and tail of two animals per genotype as determined by PCR analysis of tail tissue.

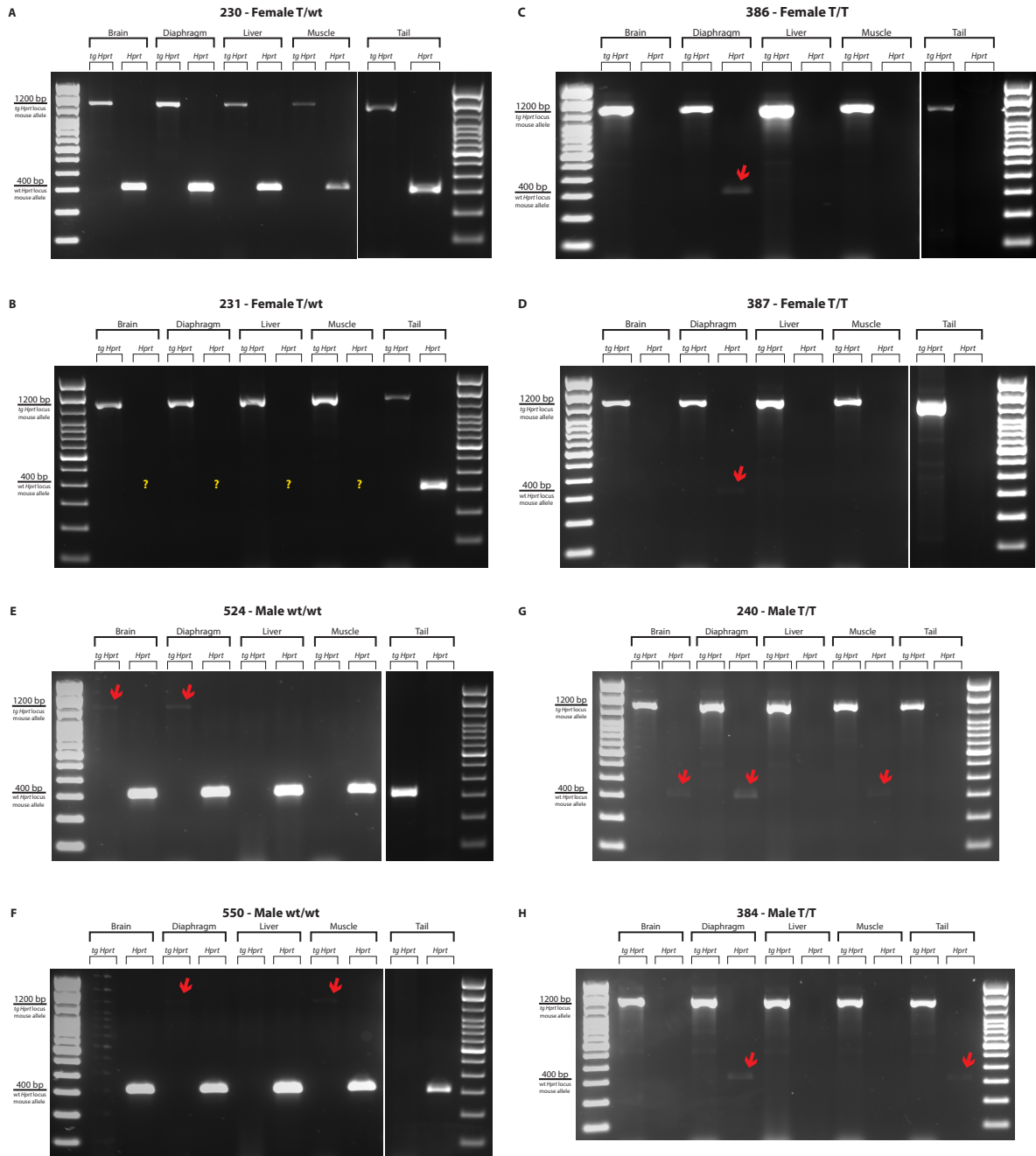


Figure 3.3 PCR analysis of brain, diaphragm, liver, muscle, and tail tissues of two animals per genotype. **A, B.** Female heterozygous. **C, D.** Female homozygous. **E, F.** Male wild type. **G, H.** Male hemizygous. Red arrows: unexpected band; yellow question marks: missing band.

The results showed that out of eight animals examined, only one mouse, 230-Female T/wt (Fig. 3.3A), exhibited the same genotype in all tissues analysed, while the remaining seven

mice showed aberrant PCR patterns (red arrows = unexpected band, yellow question marks = missing band) among the analysed tissues (Fig. 3.3B-H). Interestingly, the genotype of the diaphragm displayed a different pattern in seven out of eight animals analysed.

Based on the performed genotyping analyses, and taking into account the available literature, we came to the conclusion that the planned generation of an *Opa1* \times *A53T* α -synuclein double transgenic mouse model that was suitable for studying relevant disease aspects was impossible within the time frame of a PhD thesis, as this would have required e.g. extensive back-breeding due to the different genetic backgrounds of the mouse strains.

3.1.2 Generation of stable cell lines

To overcome the unexpected genotypic problems in the MAFs isolated from *Opa1*^{ts} mice, we chose an alternative strategy by creating an *in vitro* model to test whether mild OPA1 overexpression would rescue the mitochondrial impairment caused by A53T mutant α -synuclein. Our new approach to generating respective stable cell lines took advantage of the genomic safe harbour (GSH) adeno-associated virus site 1 (AAVS1) for targeted gene delivery and integration subsequent to the introduction of DNA double-strand breaks (DSBs) and homologous recombination (HR). GSH sites are regions within the human genome, into which genetic material can be integrated without adverse effects on the host cell or organism. GSHs thereby allow regulated transgene expression. The GSH AAVS1 site on human chromosome 19, also known as *PPP1R2C* locus, has an open chromatin structure and is transcription-competent [326].

To achieve targeted human *OPA* as well as α -synuclein (wt and A53T mutant) gene delivery and integration we combined the GeneCopoeia Genome-TALER™ human AAVS1 Safe Harbor Gene Knock-in System with the ThermoFisher Flp-In™ T-REx™ System, with some modifications. For easy orientation, an overview of the pursued strategy is provided by Figure 3.4.

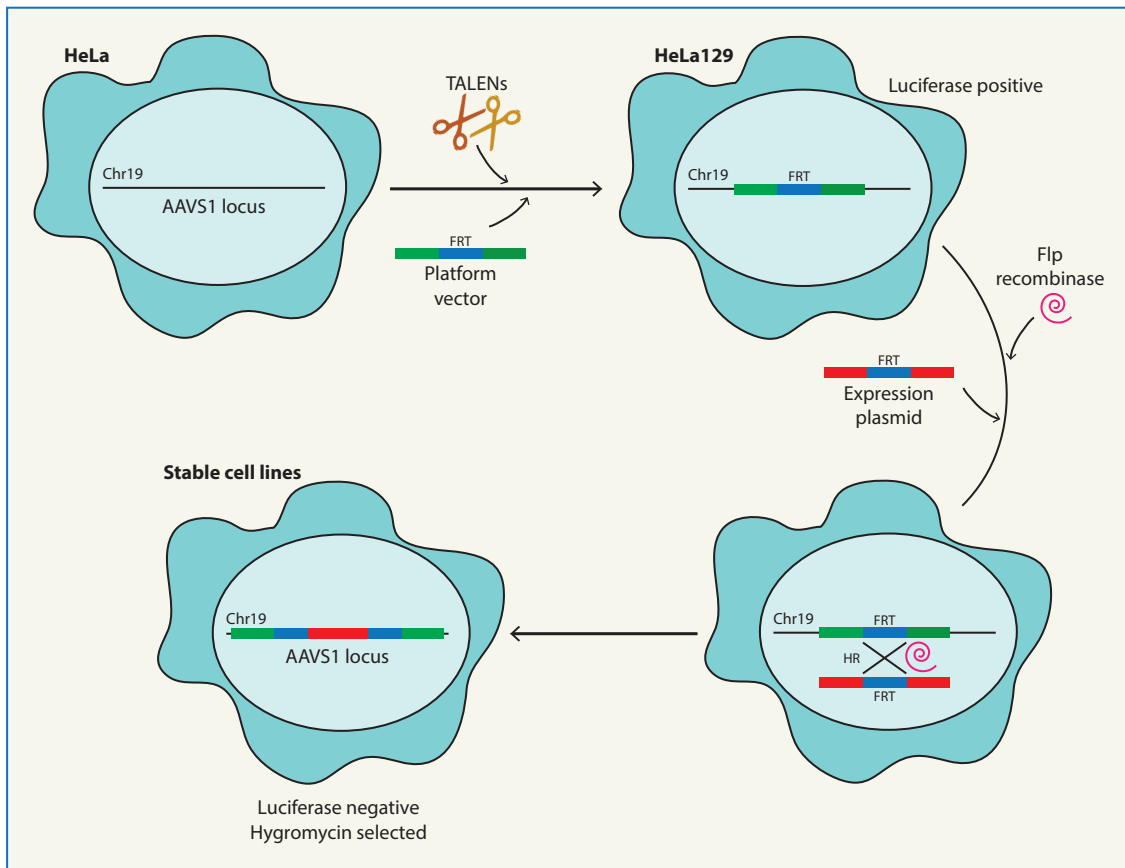


Figure 3.4 Graphic overview of the strategy for generation of stable cell lines.

HeLa cells are co-transfected with specific TALENs generating double-strand breaks (DSBs) within the AAVS1 site on chromosome 19 for the integration of a platform vector holding an FRT site by HR due to presence of AAVS1 homology arms. Cells with successful integration of the platform vector can be selected after single cloning as they are luciferase positive. A second transfection step allows then the integration of an expression plasmid holding an FRT site by HR via Flp recombinase mediation into the platform. The obtained stable expression cells are luciferase negative and hygromycin resistant.

Chr19: chromosome 19; AAVS1: adeno-associated virus site 1; TALENs: transcription activator-like effector nucleases; FRT: Flp recombination target; Flp: flippase; HR: homologous recombination.

The GeneCopoeia Genome-TALER™ human AAVS1 Safe Harbor Gene Knock-in System can generate DSBs in the AAVS1 locus mediated by a pair of AAVS1-specific TALENs (AAVS1-left and AAVS1-right TALEN¹). This generation of DSBs thus stimulates HR as DNA repair mechanism, and allows the integration of a gene, selection marker or other genetic elements of interest from a donor plasmid cotransfected with AAVS1-specific TALENs into the safe harbour site (Fig. 3.5).

¹ TALENs (transcription activator-like effector nucleases) are restriction enzymes that can be engineered to bind and cut specific DNA locations. Therefore they can be used to edit genomes by inducing double-strand breaks, but are now increasingly replaced by CRISPR-Cas technology [348].

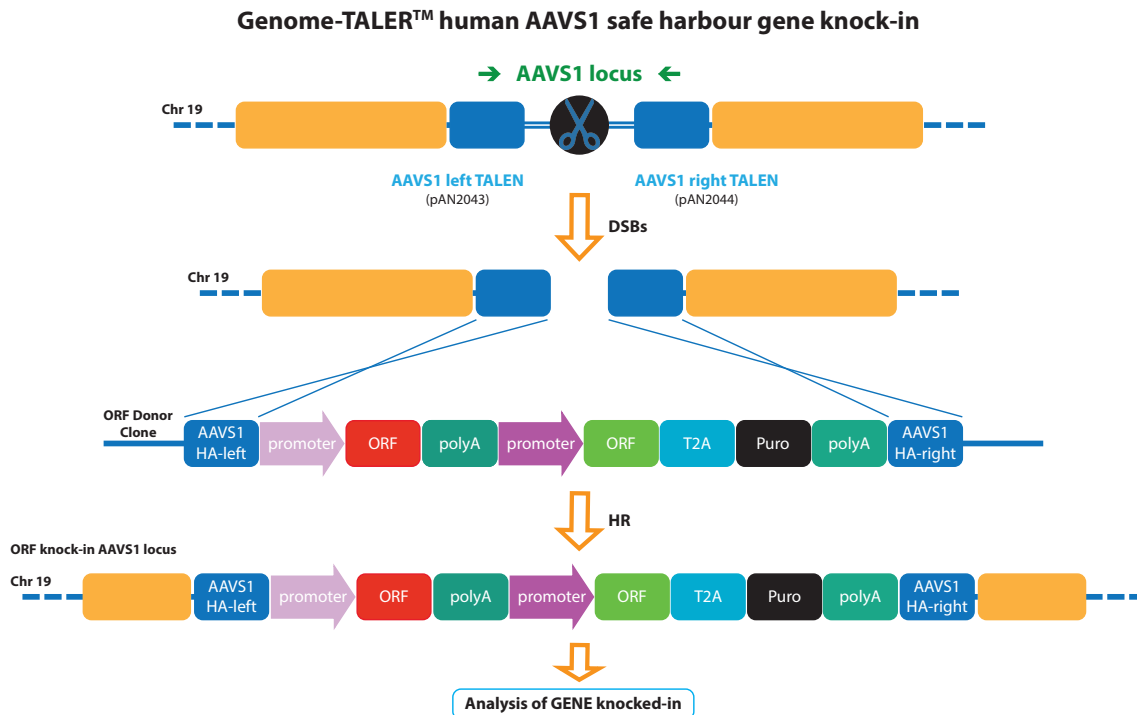


Figure 3.5 Genome-TALER™ human AAVS1 Safe Harbor Gene Knock-in System.

AAVS1 HA-left: AAVS1 homology arm left; AAVS1 HA-right: AAVS1 homology arm right; ORF: open reading frame; polyA: polyadenylation site; T2A: 2A self-cleaving peptide; Puro: puromycin resistance. (modified from Genome-TALER™ Human AAVS1 Safe Harbor Gene Knock-in User Manual)

The ThermoFisher Flp-In™ T-REx™ System requires two steps to generate stable, inducible mammalian expression cell lines. The first step consists of transfection and random independent integration of two plasmids: the pFRT/lacZeo target site vector and the pcDNA6/TR plasmid. The result is a host cell line containing a single integrated FRT site, expressing the lacZ-Zeocin™ fusion gene and the Tet repressor under the control of the human CMV promoter. In a second step, the pOG44 plasmid and the pcDNA5/FRT/TO expression vector carrying the gene of interest are cotransfected into the host cell line. The pOG44 plasmid contains the flippase (Flp) recombinase gene, which mediates an HR event between the FRT site integrated into the genome and the FRT site of the pcDNA5/FRT/TO plasmid, resulting in the integration of the pcDNA5/FRT/TO construct into the genome. The obtained stable expression cell line can then be selected for the following phenotypes: hygromycin resistance, blasticidin resistance, Zeocin™ sensitivity and lack of beta-galactosidase activity.

Once stable integration is obtained, expression of the protein of interest can be induced by the addition of tetracycline (Fig. 3.6).

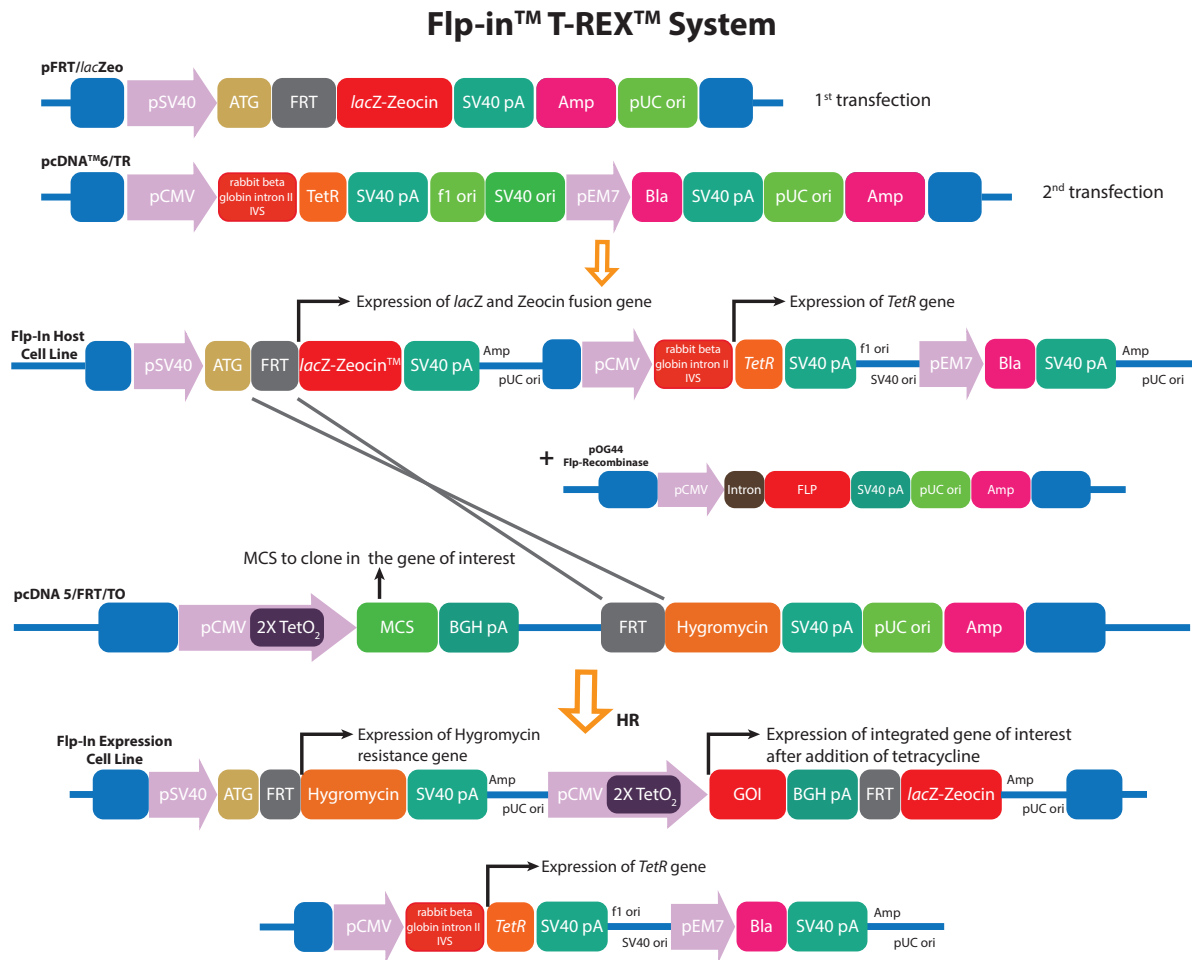


Figure 3.6 Flp-In™ T-REx™ System.

pSV40: SV40 early promoter; *FRT*: Flp recombination target; *lacZ-Zeocin™*: LacZ (beta-galactosidase) ORF, Zeocin™ resistance gene; *SV40 pA*: SV40 early polyadenylation signal; *Amp*: ampicillin resistance gene; *pUC ori*: plasmid origin of replication; *pCMV*: cytomegalovirus promoter; *TetR*: tetracycline repressor gene; *f1 ori*: f1 origin; *SV40 ori*: SV40 promoter and origin; *pEM-7*: EM-7 promoter; *Bla*: blasticidin resistance gene; *Intron*: synthetic intron; *Flp*: flippase; *SV40pA*: SV40 early polyadenylation signal; *2X TetO₂*: tetracycline operator sequences; *MCS*: multiple cloning site; *BGH pA*: bovine growth hormone polyadenylation site; *Hygromycin*: hygromycin resistance gene; *GOI*: gene of interest.

The targeted gene delivery and integration approach to generate stable cell lines requires two steps. The first step involves the use of AAVS1-specific TALENs to generate DSBs in the AAVS1 locus of chromosome 19 of the host cell line, to then allow the integration of a donor plasmid, called platform vector, by HR due to the presence of AAVS1 homology arms (Fig. 3.7).

In addition to the AAVS1 homology arms, the platform vector (pAN3418) is composed of the following elements:

- elongation factor 1 α promoter (*pEF1 α*);

- rabbit beta-globin intron II (IVS), which enhances *TetR* gene expression;
- tetracycline repressor gene (*TetR*). TetR binds to *tet* operator sequences, thereby repressing transcription of the gene of interest in the absence of tetracycline;
- synthetic polyadenylation signal (synthetic pA);
- SV40 early promoter (pSV40);
- FRT (Flp recombination target) site, as binding site for Flp recombinase;
- *Gaussia* luciferase (Gluc) gene, a reporter gene isolated from the marine copepod *Gaussia princeps*, naturally secreted from mammalian cells;

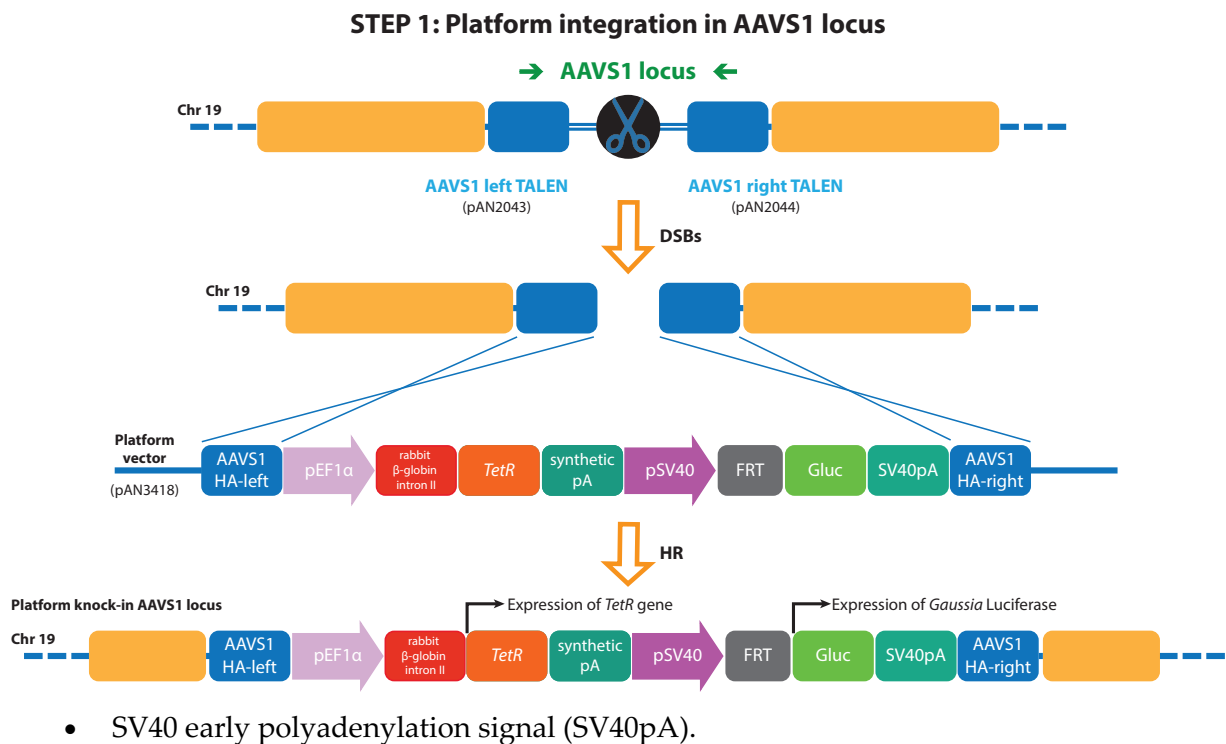


Figure 3.7 Step1: platform integration in HeLa AAVS1 locus.

AAVS1 HA-left: AAVS1 homology arm left; AAVS1 HA-right: AAVS1 homology arm right; pEF1 α : EF1 α promoter; *TetR*: tetracycline repressor gene; synthetic pA: synthetic polyadenylation signal; pSV40: SV40 early promoter; FRT: Flp recombination target; Gluc: *Gaussia* Luciferase gene; SV40pA: SV40 early polyadenylation signal.

For our experiments, HeLa cells were chosen (limitations of this choice discussed on page 77). HeLa cells were seeded at an amount of 5×10^4 cells/well of a 6-well plate and grown for 24 hours in a humidified incubator at 37°C with 5% CO₂. Cells were transfected using FuGENE[®]6 Transfection Reagent at a FuGENE[®]6/DNA ratio of 3:1, and a total DNA amount of 2 μ g (0.5 μ g for pAN2043 (left TALEN), 0.5 μ g for pAN2044 (right TALEN) and 1.0 μ g for pAN3418 (platform vector)). The day after transfection, Luciferase assay was performed using the

Pierce™ Gaussia Luciferase Glow Assay kit following the standard protocol for a 96-well plate. HeLa WT and HeLa WT transfected with GFP were used as controls (Fig. 3.8A).

A

HeLa WT	HeLa WT + GFP	HeLa + pAN3418
1054	1198	25805

B

HeLa pAN3418 single clones		
Clone 19	Clone 31	Clone 129
1373	4753	3219

Figure 3.8 Luciferase assay.

A. Luciferase signal 24 hours after transfection. B. Luciferase signal of positive single clones.

Transfected HeLa cells were then single cloned in a 96-well plate at a density of 1.5 cells/well in 200 μ l tetracycline free (tet-free) growth medium and kept for two weeks in a humidified incubator at 37°C with 5% CO₂. Thereafter, Luciferase assay was performed again to evaluate integration of the platform vector (pAN3418) in single clones. Three out of 222 clones occurred to be luciferase positive: clones 19, 31, and 129 (Fig. 3.8B). Positive clones were transferred into 6-well plates in tet-free growth medium, and luciferase signal was assayed again to confirm stable platform vector integration (data not shown).

The three positive clones were also controlled for the absence of mycoplasma contamination. To this end, 100 μ l of growth medium was collected from each clone, boiled for 5 minutes at 95°C and centrifuged at 13000 rpm for 5 seconds to discard any debris. The supernatant was collected and analyzed by PCR for the presence of 16S rRNA mycoplasma sequence. None of the clones were contaminated by mycoplasma (Fig. 3.9).

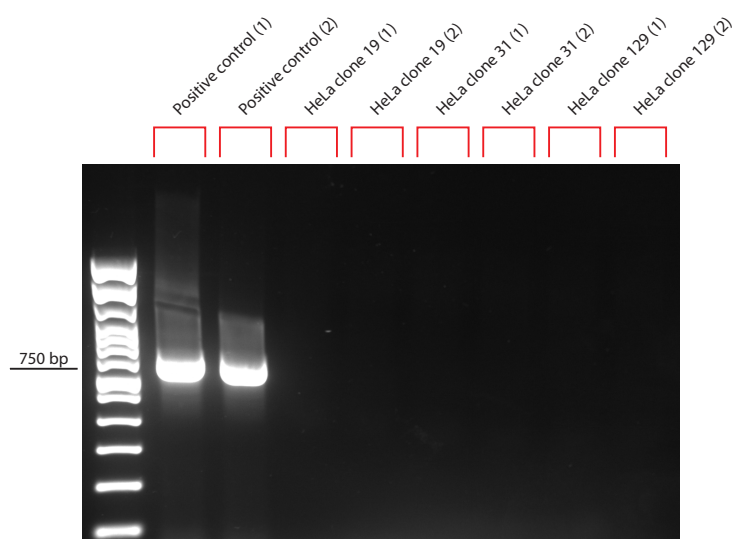


Figure 3.9 PCR analysis for mycoplasma contamination.

Each sample was run in duplicates: lane 1 and 2 positive control, showing a band at 750 bp; lane 3 and 4 HeLa clone 19; lane 5 and 6 HeLa clone 31; lane 7 and 8 HeLa clone 129. Primers: GPO-1 (5'

ACTCCTACGGGAGGCAGCAGTA 3'), MGSO (5' TGCACCATCTGTCCTCTGTAAACCTC 3'). PCR thermocycler program: 94°C for 3 min, 35 cycles at 94°C for 1 min, 58°C for 1 min and 30 s, 72°C for 1 min and 30 s, and 72°C for 10 min. (Agarose 1,5% and TAE 1X, loading purple dye 6X, TrackIT 100 bp DNA ladder Invitrogen)

Genomic DNA isolated from each clone using the GeneElute™ Mammalian Genomic DNA Miniprep Kit was PCR-analysed to check platform vector integration into the AAVS1 site. (Fig. 3.10A).

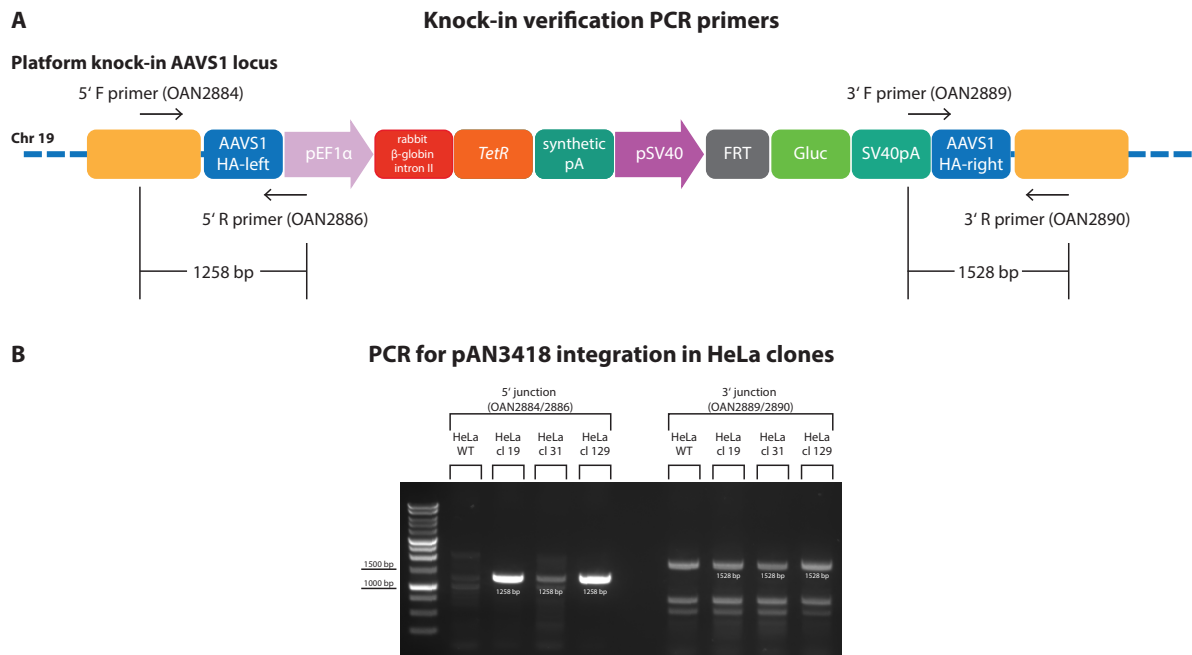


Figure 3.10 Platform knock-in integration.

A. Knock-in verification primer pairs. Primers for 5' junction amplification and 3' junction amplification to verify integration of pAN3418. **B. PCR analysis for integration of pAN3418 in HeLa clones.** Primers for 5' junction amplification: OAN2884 (CTTTGAGCTCTACTGGCTTCTGCGCC) and OAN2886 (CCCTAGAGGATCCCCGGGTACCAAG), expected PCR product 1258 bp. Primers for 3' junction amplification: OAN2889 (GCTGCCTCAAAGGGCTTGCCAAC) and OAN2890 (GCAGTCACCCCACAGTTGGAGGAG), expected PCR product 1528 bp. PCR thermocycler program for 5' and 3' junction amplification: 98°C for 30 s, 35 cycles at 98°C for 10 s, 69°C for 30 s, 72°C for 30 s, and 72°C for 10 min. (Agarose 0,8% and TAE 1X, loading purple dye 6X, BenchTop 1 kb DNA ladder Promega).

As shown in Fig. 3.10B, all three clones integrated the platform vector pAN3418 into the AAVS1 safe harbour locus.

To determine the clone most suitable for subsequent experimentation, proliferation of the three HeLa pAN3418 clones was evaluated using the CellTiter-Glo® 2.0 Assay; this assay determines the number of viable cells in culture by quantitating the amount of ATP present. The same number of cells (5×10^3 /well) was seeded for each clone in 6 wells of a 96-well plate, and one 96-well plate was prepared for each of five time points (Fig. 3.11).

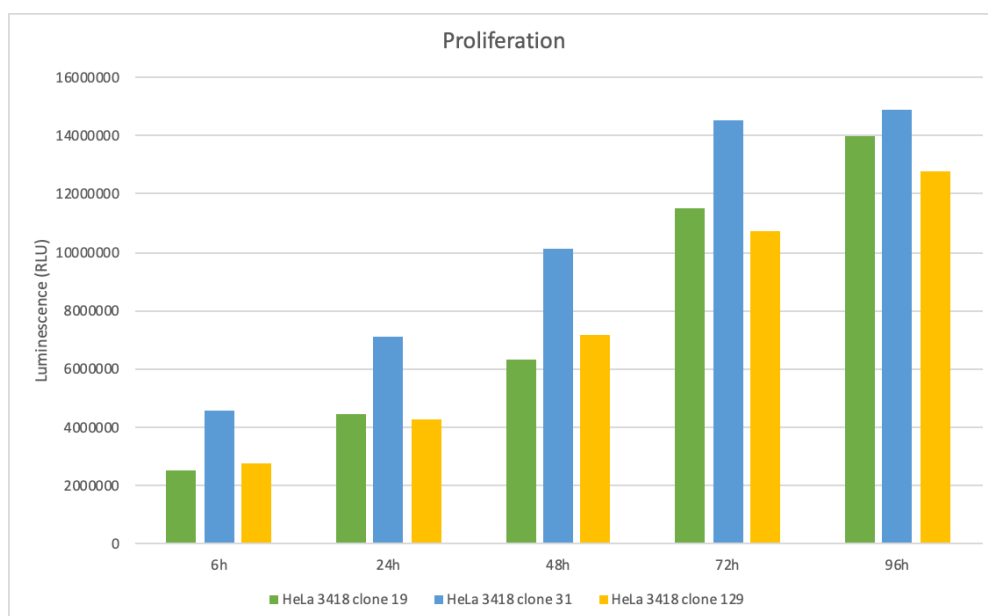


Figure 3.11 CellTiter-Glo® 2.0 Assay.

Evaluation of HeLa clones proliferation. 5×10^3 cells/well seeded for each clone. CellTiter-Glo was performed 6h, 24h, 48h, 72h and 96h after cell seeding.

As can be appreciated in Fig. 10, clone 31 grew too fast, reaching a plateau condition between 72 and 96h, and was thus excluded. Clone 129 showed a more linear growth when compared to clone 19, and was therefore selected for further experiments.

Before proceeding with the targeted gene delivery and integration step, CellTiter-Glo® 2.0 Assay was performed to establish the hygromycin concentration required to select cells with integrated construct. HeLa129 cells were seeded at an amount of 1×10^4 /well into two 96-well plates using 100 μ l of growth medium, 6 wells per condition, and grown in a humidified incubator at 37°C with 5% CO₂. After 48 hours, growth medium was replaced with 100 μ l of hygromycin-supplemented growth medium. Hygromycin B (Invitrogen) concentrations of 50, 100, 150, 200, 300, 400 and 500 μ g/ml were tested. Cell death was measured using the CellTiter-Glo® 2.0 Assay (Fig. 3.12).

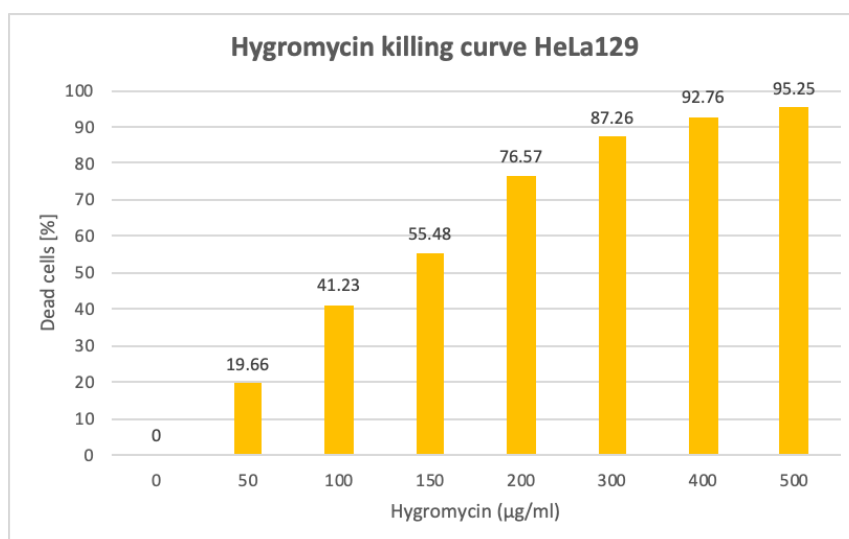


Fig. 3.12 Hygromycin killing curve HeLa129.

CellTiter-Glo® 2.0 Assay to evaluate hygromycin concentration to be used to select cells with integrated construct after the second step of transfection.

As the hygromycin concentration to select cells with construct integration should be the one killing between 70 to 80% of the cell population, 200 µg/ml hygromycin was selected for later use.

The second step of our targeted gene delivery and integration approach required cotransfection of pOG44 plasmid, constitutively expressing Flp recombinase, together with the expression vector carrying our genes of interest for integration in the platform located in the AAVS1 site of HeLa clone 129. The expression vector used was the same as the Flp-In™ T-REx™ System, that is the pcDNA5/FRT/TO plasmid, whose multiple cloning site (MCS) was used to clone in our genes of interest (Fig. 3.13).

The expression vector (pcDNA5/FRT/TO) is composed of the following elements:

- cytomegalovirus promoter (pCMV);
- tetracycline operator sequences (2X TetO₂);
- multiple cloning site (MCS), to clone in the inducible gene of interest;
- bovine growth hormone polyadenylation site (BGHpA);
- FRT (Flp recombination target) site, as binding site for Flp recombinase;
- hygromycin resistance gene;
- SV40 early polyadenylation signal (SV40pA);
- plasmid origin of replication (pUC ori);
- ampicillin resistance gene (*Amp*).

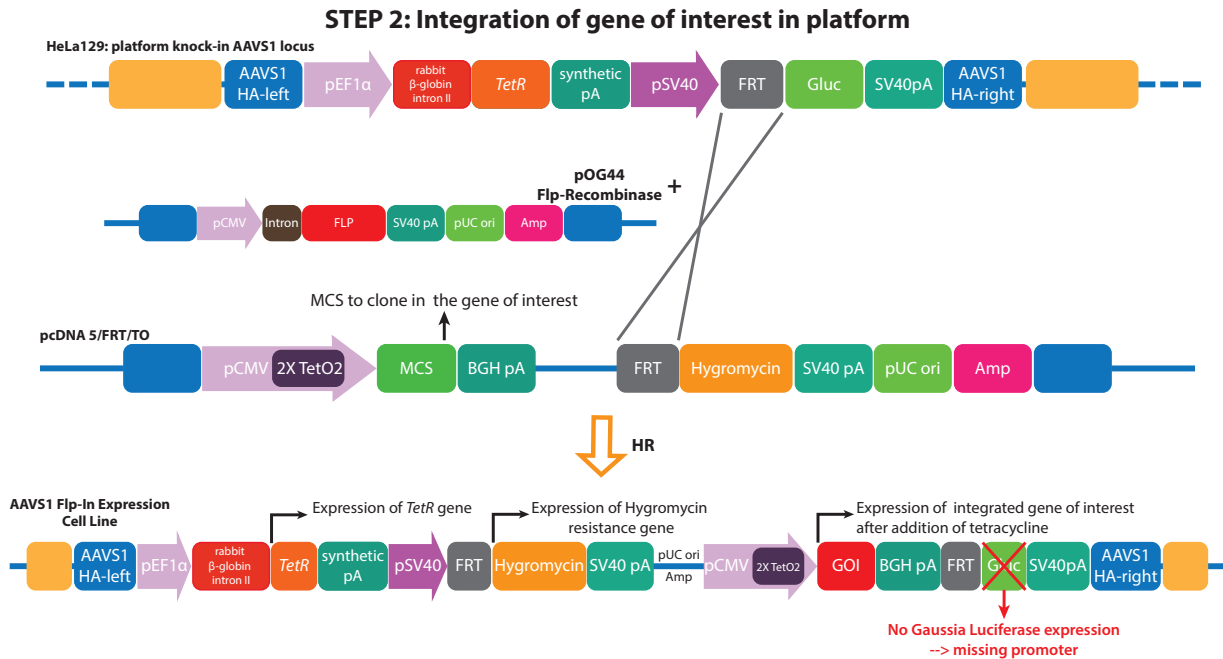


Fig. 3.13 Step2: integration of pcDNA5/FRT/TO plasmid with genes of interest in HeLa129.

AAVS1 HA-left: AAVS1 homology arm left; pEF1α: EF1α promoter; *TetR*: tetracycline repressor gene; synthetic pA: synthetic polyadenylation signal; pSV40: SV40 early promoter; FRT: Flp recombination target; *Gluc*: *Gaussia* Luciferase gene; SV40pA: SV40 early polyadenylation signal; AAVS1 HA-right: AAVS1 homology arm right; pCMV: cytomegalovirus promoter; Flp: flippase; pUC ori: plasmid origin of replication; Amp: ampicillin resistance gene; 2X TetO: tetracycline operator sequences; MCS: multiple cloning site; BGH pA: bovine growth hormone polyadenylation site; Hygromycin: hygromycin resistance gene; GOI: gene of interest.

Once the expressing vector is integrated, hygromycin can be added to the growth medium to select only the cells where HR and integration took place. These cells do no longer express *Gaussia* luciferase gene (*Gluc*) as correct integration separates the promoter from the *Gluc* open reading frame. Expression of the gene of interest can be triggered by addition of tetracycline. The intent of this approach was to generate an *in vitro* model that would recapitulate features of the two single mouse models (*Opa1*^{tg}; α -synuclein^{A53T} ^{tg}) as well as the planned double transgenic mouse (3.1.1). Therefore, respective plasmids were designed, cloned, and cotransfected into HeLa129 cells together with Flp recombinase (pOG44), giving rise to stable cell lines after HR (Fig. 3.14).

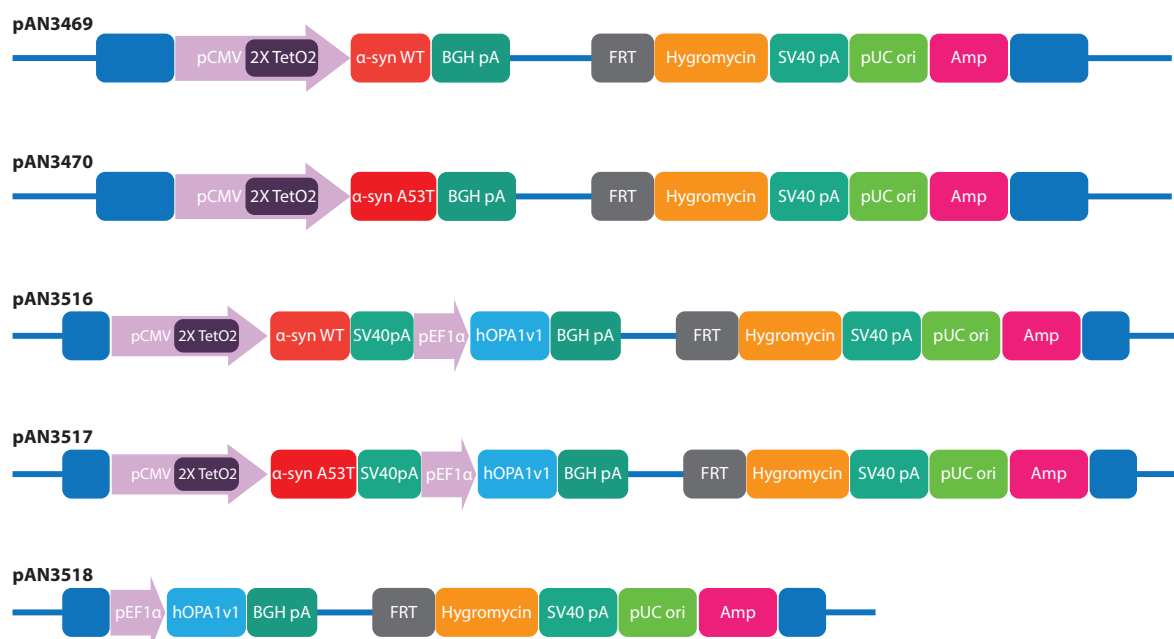


Fig. 3.14 Plasmids for the second step of targeted gene delivery and integration.

Overview of plasmids designed and cloned for the generation of stable cell lines. pAN3469: tetracycline-inducible human wild type α -synuclein. pAN3470: tetracycline-inducible human A53T α -synuclein. pAN3516: tetracycline-inducible human wild type α -synuclein and human *OPA1* variant 1 under the EF1 α promoter. pAN3517: tetracycline-inducible human A53T α -synuclein and human *OPA1* variant 1 under the EF1 α promoter. pAN3518: human *OPA1* variant 1 under the EF1 α promoter.

As a form of hereditary, early-onset Parkinson disease is known to be caused by duplication or triplication of the *SNCA* gene, human wild-type α -synuclein was also cloned into the pcDNA5/FRT/TO plasmid.

Thus, five plasmids were generated starting from pcDNA5/FRT/TO plasmid:

- pAN3469: tetracycline-inducible human wild type α -synuclein with FRT site;
- pAN3470: tetracycline-inducible human A53T α -synuclein with FRT site;
- pAN3516: tetracycline-inducible human wild type α -synuclein and human *OPA1* variant 1 under the EF1 α promoter with FRT site;
- pAN3517: tetracycline-inducible human A53T α -synuclein and human *OPA1* variant 1 under the EF1 α promoter with FRT site;
- pAN3518: human *OPA1* variant 1 under the EF1 α promoter.

Name	Description	Vector	Insert
pAN3266	EGFP/WT α -synuclein	pEGFP-C1	Addgene #40822
pAN3267	EGFP/A53T α -synuclein	pEGFP-C1	Addgene #40823
pAN3414	vector of Invitrogen Flp-InT-REX system	pcDNA5/FRT/TO	Invitrogen Flp-InT-REX system

Results

pAN3415	vector of Invitrogen Flp-InT-REX system	pcDNA6/TR	Invitrogen Flp-InT-REX system
pAN3417	pcDNA6/TR derivative with EF1 α promoter	pAN3415- pcDNA6/TR* <i>SpeI/SacI</i>	PCR on pAN2045 OAN2852/3 * <i>SpeI/SacI</i>
pAN3418	AAVS1 donor with EF1 α /rabbit-b-globin intron/TetR/synthetic pA/pSV40/FRT/ATG/Gluc/SV40pA for generation of stable cell lines	pAN3413* <i>MluI</i> -HF, <i>AgeI</i>	PCR on pAN3417 OAN2854/51* <i>MluI</i> -HF, <i>AgeI</i>
pAN3419	pBluescript with <i>ApaI</i> - <i>SacII</i> fragment of pAN3414 - pcDNA5/FRT/TO	pBluescript_skplus* <i>ApaI</i> , <i>SacII</i>	pAN3414* <i>ApaI</i> , <i>SacII</i>
pAN3420	pBluescript with <i>ApaI</i> - <i>SacII</i> fragment of pAN3414 - pcDNA5/FRT/TO and inserted ATG for hygromycin gene; add <i>NdeI</i> site for control digest upstream ATG	pAN3419* <i>XbaI</i> , <i>AatII</i>	annealed oligos OAN2855/56
pAN3421	modified pcDNA5/FRT/TO with additional ATG for hygromycin gene; low copy!	pAN3414* <i>ApaI</i> , <i>SacII</i>	pAN3420 * <i>ApaI</i> , <i>SacII</i>
pAN3469	Tet-Inducible WT α -synuclein	pcDNA5/FRT/TO * <i>XhoI/ApaI</i>	pAN3266 * <i>XhoI/ApaI</i>
pAN3470	Tet-Inducible A53T α -synuclein	pcDNA5/FRT/TO * <i>XhoI/ApaI</i>	pAN3267 * <i>XhoI/ApaI</i>
pAN3502	WT α -synuclein/SV40pA/EF1 α	pUC57- <i>BsaI</i> -Free	Biocat gene synthesis
pAN3503	A53T α -synuclein/SV40pA/EF1 α	pUC57- <i>BsaI</i> -Free	Biocat gene synthesis
pAN3507	WT α -synuclein/SV40pA/EF1 α in modified pcDNA5/FRT/TO for integration into FRT site	pAN3421 * <i>KpnI/NotI</i>	pAN3502 * <i>KpnI/NotI</i>
pAN3463	pcDNA3.1- with human OPA1 variant 1	pcDNA3.1- * <i>XhoI/BamHI</i>	hOPA1v1 retroviral plasmid from Scorrano * <i>XhoI/BamHI</i>
pAN3516	WT α -synuclein/SV40pA/EF1 α /hOPA1v1 in modified pcDNA5/FRT/TO for integration into FRT site	pAN3507 * <i>XhoI/BclII</i>	pAN3463 * <i>XhoI/BamHI</i>
pAN3517	A53T α -synuclein/SV40pA/EF1 α /hOPA1v1 in modified pcDNA5/FRT/TO for integration into FRT site	pAN3508 * <i>XhoI/BclII</i>	pAN3463 * <i>XhoI/BamHI</i>
pAN3518	EF1 α /hOPA1v1 in modified pcDNA5/FTR/TO for integration into FRT site	pAN3516 * <i>NruI</i> - HF/BamHI+KlenowFill	religation blunt end

Table 3.1. Plasmids used for cloning the five expression plasmids.

HeLa129 cells were seeded at an amount of 1×10^6 cells in a p100 dish and grown in tet-free growth medium for 24 hours in a humidified incubator at 37°C with 5% CO₂. Cells were co-transfected using Lipofectamine™ 3000 at a pOG44/pAN3469 ratio of 9:1, and a total DNA amount of 6 μ g (i.e., 5.4 μ g for pOG44, 0.6 μ g for pAN3469). The day after transfection, growth medium was changed and supplemented with 200 μ g/ml hygromycin for seven days (Fig. 3.12) to select cells with successful integration. However, this selection scheme was too toxic for cells additionally stressed by the co-transfection procedure, we repeated this experiment at a reduced hygromycin concentration of 150 μ g/ml. After seven days of hygromycin exposure, cells were grown in a p100 dish with growth medium supplemented with 50 μ g/ml

hygromycin. Once confluent, 2×10^6 cells were collected for genomic DNA isolation using the GeneElute™ Mammalian Genomic DNA Miniprep Kit.

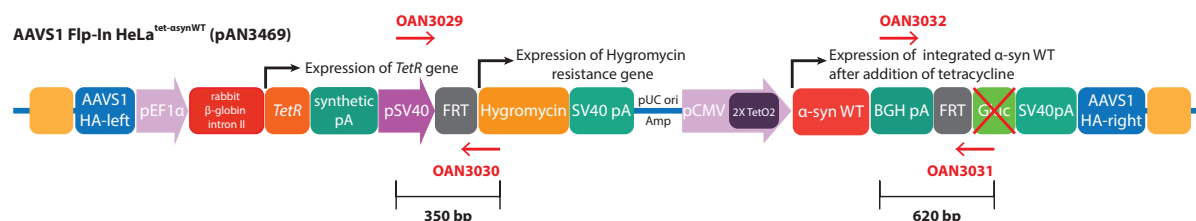


Fig. 3.15 Expression plasmid knock-in verification primer pairs.

Design of primer pairs to verify integration of the expression plasmid pAN3469 in the AAVS1 knock-in platform.

By subsequent PCR analysis we verified integration of the expression vector in the AAVS1 knock-in platform. Whereas primer pair OAN3029/OAN3030 was used to amplify the region between the SV40 early promoter and the hygromycin gene, primer pair OAN3031/OAN3032 amplified the region between the BGH polyadenylation site and the *Gaussia Luciferase* gene (Fig. 3.15). This design allowed verifying expression vector integration in all the five stable cell lines.

The PCR reaction setup was performed following the next scheme, to establish the best PCR reaction condition:

OAN3029/3030: expected PCR product 350bp

Component	Volume to use	1	2	3	4	Master mix 4,5x
H ₂ O up to 50 µL		29 µL	27,5 µL	29 µL	27,5 µL	-- --
5X Phusion HF buffer		10 µL	10 µL	-- --	-- --	-- --
5X Phusion GC buffer		-- --	-- --	10 µL	10 µL	-- --
2 mM dNTPs	5 µL					22,5 µL
10 µM OAN3029	2,5 µL					11,25 µL
10 µM OAN3030	2,5 µL					11,25 µL
Template: genomic DNA, not diluted	1 µL					-- --
DMSO (optional)	(1,5 µl)	-- --	1,5 µl	-- --	1,5 µl	-- --
Phusion polymerase	0.5 µL					2,25 µl
master mix		11 µl	11 µl	11 µl	11 µl	

OAN3031/3032: expected PCR product 620bp

Component	Volume to use	1	2	3	4	Master mix 4,5x
H ₂ O up to 50 µL		29 µL	27,5 µL	29 µL	27,5 µL	-- --
5X Phusion HF buffer		10 µL	10 µL	-- --	-- --	-- --
5X Phusion GC buffer		-- --	-- --	10 µL	10 µL	-- --
2 mM dNTPs	5 µL					22,5 µL
10 µM OAN3031	2,5 µL					11,25 µL
10 µM OAN3032	2,5 µL					11,25 µL
Template: genomic DNA, not diluted	1 µL					-- --
DMSO (optional)	(1,5 µl)	-- --	1,5 µl	-- --	1,5 µl	-- --
Phusion polymerase	0.5 µL					2,25 µl
master mix		11 µl	11 µl	11 µl	11 µl	

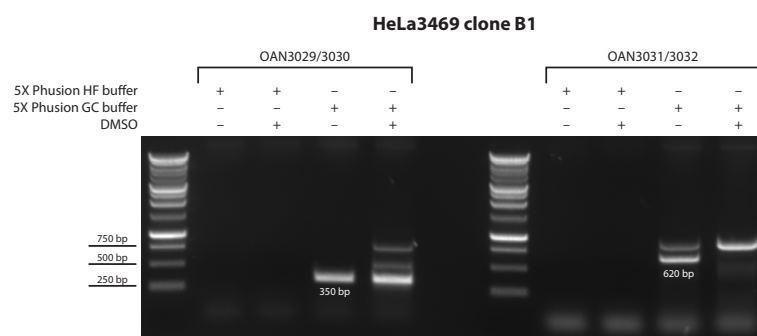


Fig. 3.16 PCR reaction setup analysis for integration of expression plasmid pAN3469 in HeLa129.

Primers for 5' junction amplification: OAN3029 (ATTCTCCGCCCATGGCTGAC) and OAN3030 (ATCTTTGTAGAAACCATCGGCGCAGC), expected PCR product 350 bp. Primers for 3' junction amplification: OAN3031 (CGAGATCCGTGGTCGCGAAGTTG) and OAN3032 (AGCCATCTGTTGTTTGCCCCCTCC), expected PCR product 620 bp. PCR thermocycler program for 5' and 3' junction amplification: 98°C for 30 s, 35 cycles at 98°C for 10 s, 67°C for 30 s, 72°C for 30 s, and 72°C for 10 min. (Agarose 1% and TAE 1X, loading purple dye 6X, BenchTop 1 kb DNA ladder Promega).

Clone B1 of HeLa3469 proved to have integrated the expression vector pAN3469 into the AAVS1 knock-in platform (Fig. 3.16), and the line was renamed HeLa^{tet- α syn^{WT}} clone B1.

The cell seeding and transfection protocol applied for the integration of the expression plasmid pAN3469 were used for the other four expression plasmids. Cells were then grown in growth medium supplemented with 150 µg/ml hygromycin for seven days, and once confluent, 2×10^6 cells were collected to isolate genomic DNA as described. PCR analysis was then performed using the same conditions as for the HeLa^{tet- α syn^{WT}} clone B1.

Results

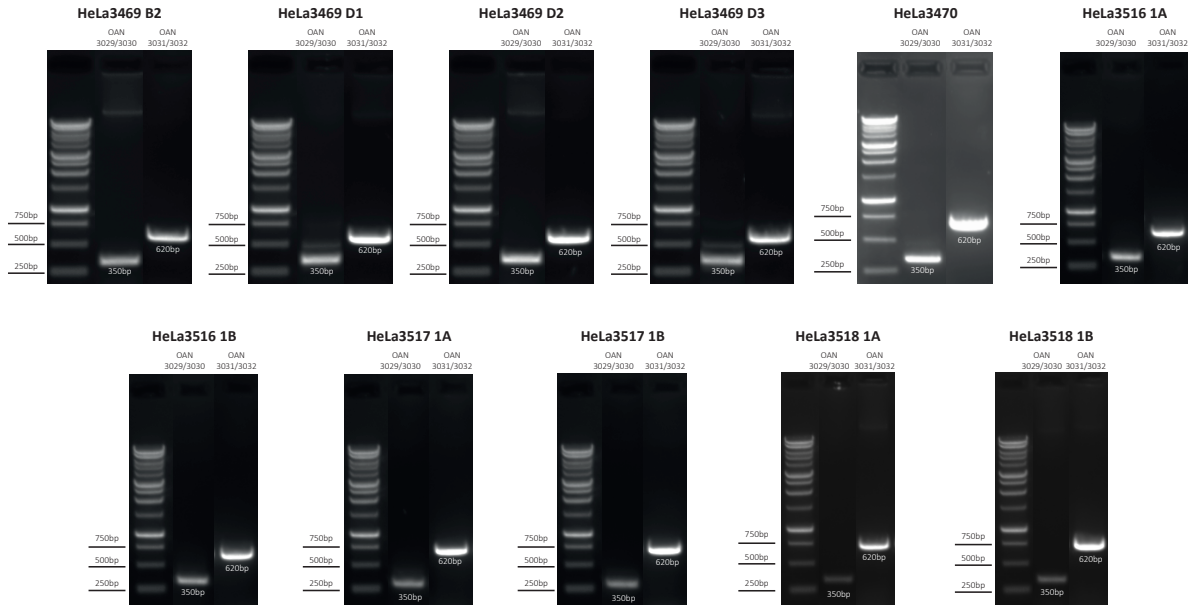


Fig. 3.17 PCR analysis for integration of expression plasmids pAN3470, pAN3516, pAN3517 and pAN3518 in HeLa129.

Primers for 5' junction amplification: OAN3029 (ATTCTCCGCCCATGGCTGAC) and OAN3030 (ATCTTTGTAGAAACCATCGGCGCAGC), expected PCR product 350 bp. Primers for 3' junction amplification: OAN3031 (CGAGATCCGTGGTCGCGAAGTTG) and OAN3032 (AGCCATCTGTTGTTGCCCTCC), expected PCR product 620 bp. PCR thermocycler program for 5' and 3' junction amplification: 98°C for 30 s, 35 cycles at 98°C for 10 s, 67°C for 30 s, 72°C for 30 s, and 72°C for 10 min. (Agarose 1% and TAE 1X, loading purple dye 6X, BenchTop 1 kb DNA ladder Promega).

Integration of the other four expression plasmids into the AAVS1 knock-in platform was successful (Fig. 3.17), and clones were renamed as follows (Fig. 3.18):

- HeLa^{tet- α synA53T}: HeLa129 with integrated pAN3470
- HeLa^{tet- α synWT/Opa1}: HeLa129 with integrated pAN3516
- HeLa^{tet- α synA53T/Opa1}: HeLa129 with integrated pAN3517
- HeLa^{Opa1}: HeLa129 with integrated pAN3518

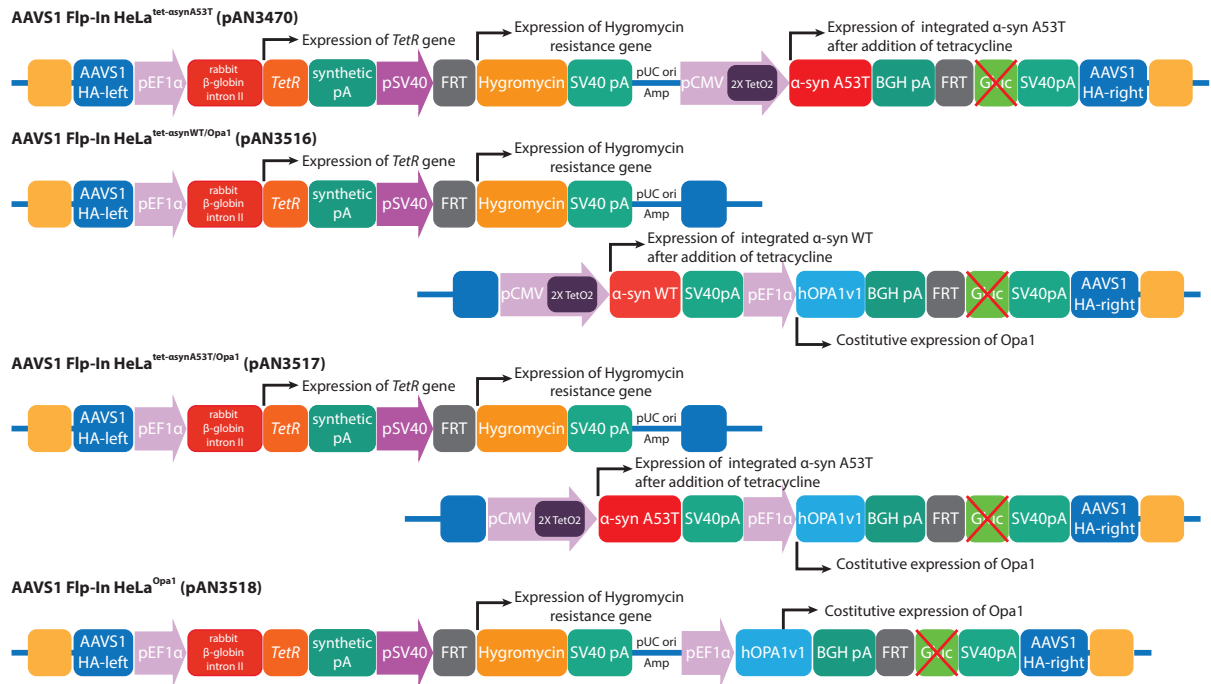


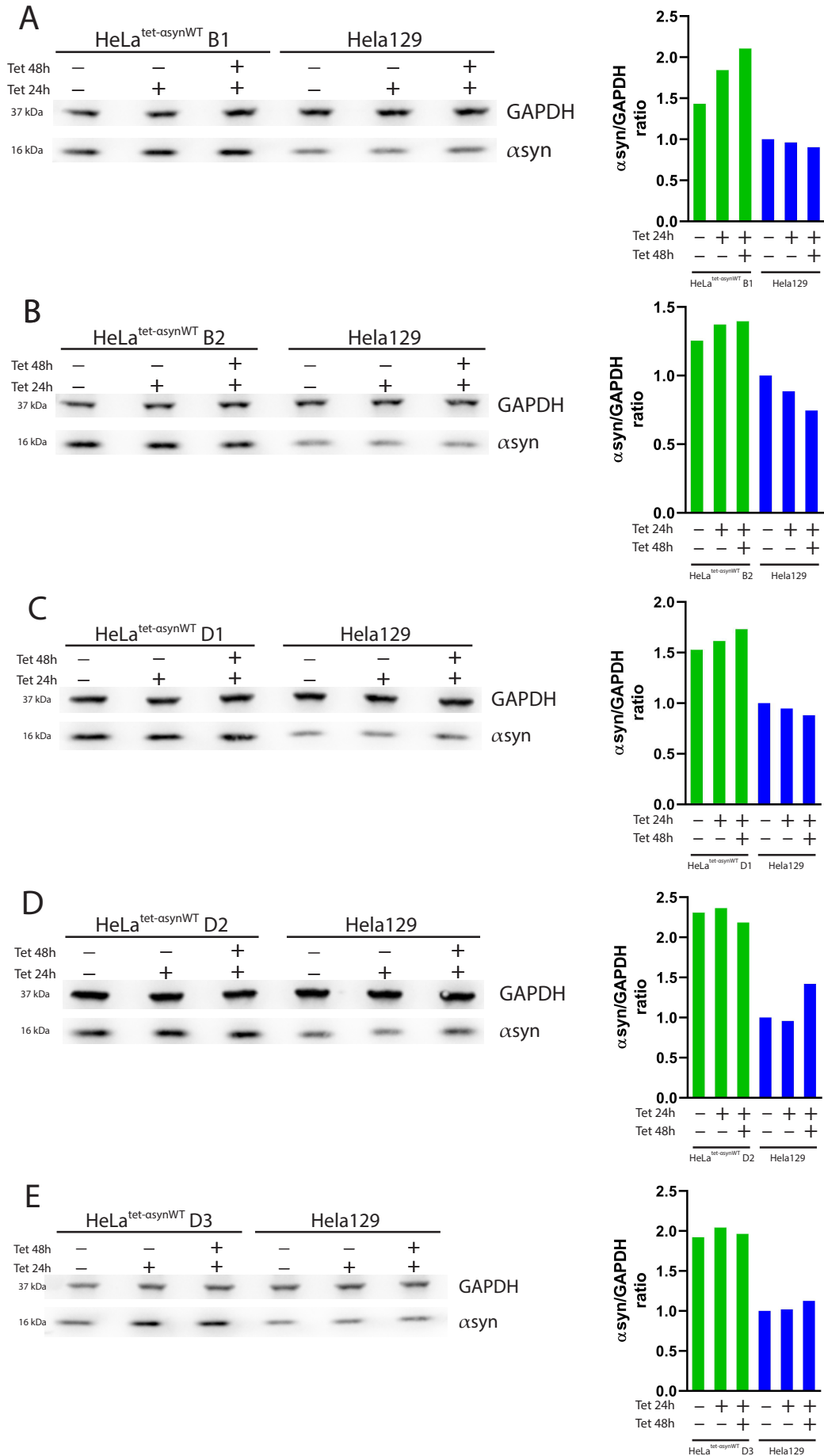
Fig. 3.18 AAVS1 Flp-In stable cell lines.

Overview of the AAVS1 site after integration of the single expression plasmids. HeLa^{tet-αsynA53T}: AAVS1 knock-in tetracycline-inducible human A53T α -synuclein. HeLa^{tet-αsynWT/Opa1}: AAVS1 knock-in tetracycline-inducible human wild type α -synuclein with stable overexpression of OPA1. HeLa^{tet-αsynA53T/Opa1}: AAVS1 knock-in tetracycline-inducible human A53T α -synuclein with stable overexpression of OPA1. HeLa^{Opa1}: stable overexpression of OPA1.

Cells with verified integration of the expression plasmids were grown in medium supplemented with 50 μ g/ml hygromycin to maintain a mild selection condition.

3.1.3 Characterization of stable cell lines

In the next step, we set out to verify the overexpression of inducible genes (human wild type α -synuclein; human A53T α -synuclein) after tetracycline addition, and to check the stable overproduction of human OPA1. Cells of each cell line were seeded at an amount of 1×10^6 /p100 into p100 dishes with tetracycline-free growth medium as follows: one p100 dish with untreated cells, and two p100 dishes with cells induced with tetracycline (1 μ g/ml) for 24 and 48 hours, respectively. Cell lines without inducible genes, i.e. HeLa129 and HeLa^{Opa1}, received an identical treatment to control for any possible toxic effects or impacts on protein expression. Each sample was analysed by Western blot. HeLa129 were used in all SDS PAGE experiments as control to evaluate protein expression in stable cell lines (Fig. 3.19).



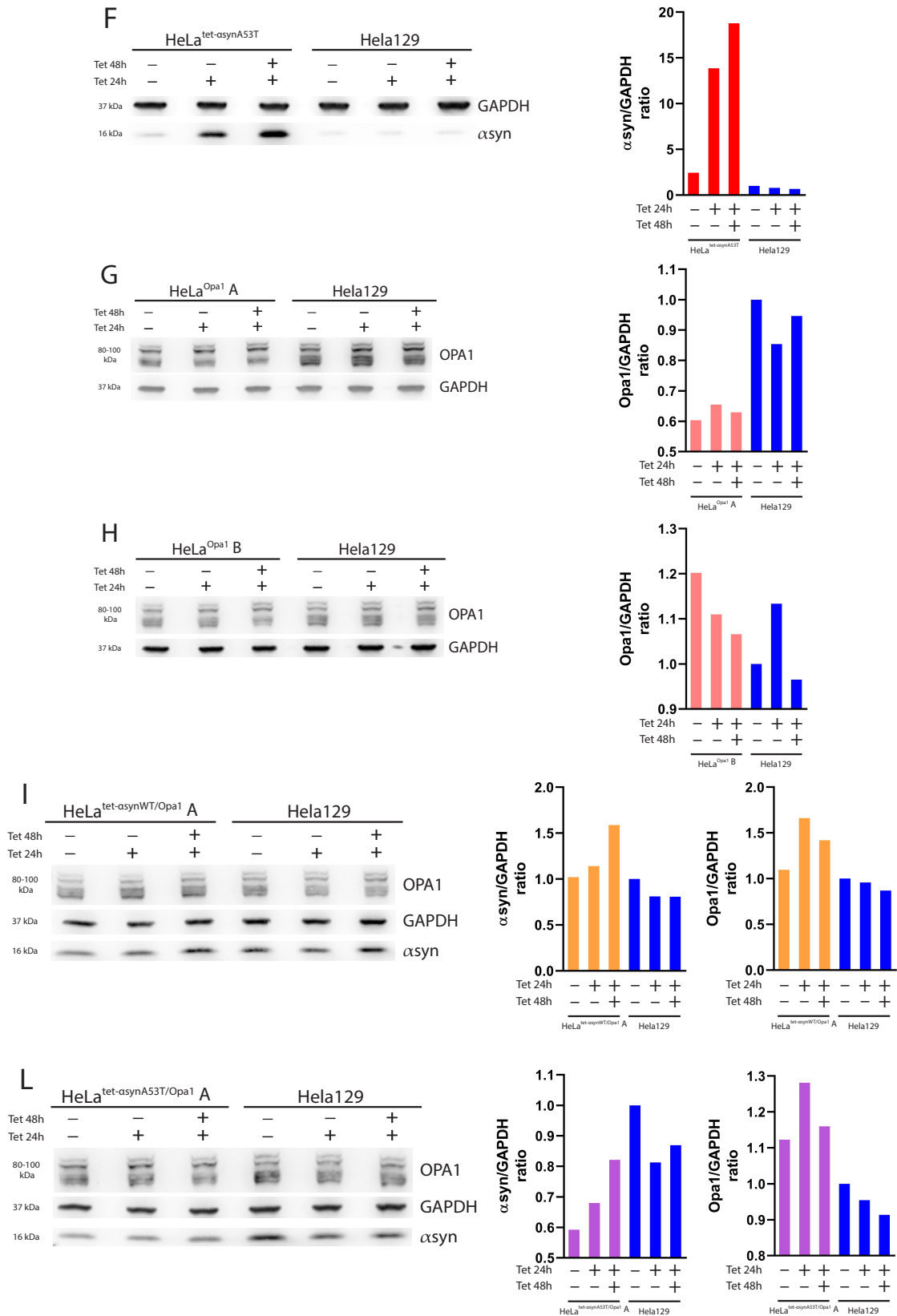


Fig. 3.19 Evaluation of α -synuclein and Opa1 expression levels in AAVS1 Flp-In stable cell lines.

Representative western blot (left side) and related quantification (right side) of each stable cell line. A. HeLa^{tet- α synWT} clone B1. B. HeLa^{tet- α synWT} clone B2. C. HeLa^{tet- α synWT} clone D1. D. HeLa^{tet- α synWT} clone D2. E. HeLa^{tet- α synWT} clone D3. F. HeLa^{tet- α synA53T}. G. HeLa^{Opa1} clone A. H. HeLa^{Opa1} clone B. I. HeLa^{tet- α synWT/Opa1}. L. HeLa^{tet- α synA53T/Opa1}. HeLa129 cells were used as a control. Whole cell lysates were analyzed by western blotting using anti- α syn (Abcam 138501,

1:10000 in 5% low-fat milk TBST), anti-OPA1 (Cell Signaling D6U6N, 1:1000 in TBST 5% BSA), and anti-GAPDH antibodies (Santa Cruz 32233, 1:1000 in TBST). Secondary antibodies: Goat anti-Mouse IgG (H+L) Cross-Adsorbed Secondary Antibody, HRP (ThermoFisher A16072); Goat anti-Rabbit IgG (H+L) Cross-Adsorbed Secondary Antibody, HRP (ThermoFisher A16104). Vilber Fusion FX and Fusion FX software for acquisition and quantification (average of three technical replicates).

As semi-quantitative technique, Western blotting allows only relative comparisons between protein expression levels. Therefore, we additionally applied immunohistochemistry to verify α -synuclein overexpression. Due to the strong induction of A53T mutant α -synuclein, HeLa^{tet- α synA53T} line was used. Cells were seeded at an amount of 1×10^6 /p100 in three p100 dishes following the same scheme used for Western blot analysis: one p100 dish with untreated cells, and two p100 dishes containing cells induced with tetracycline (1 μ g/ml) for 24 and 48 hours, respectively. Cells of each condition were collected, washed in PBS, resuspended in 4% PFA and incubated one hour at room temperature for fixation. Each sample was then resuspended in HistoGel (Thermo Scientific HG-4000-012) and paraffin-embedded. Histological sections were stained with anti- α -synuclein antibody according to the standard protocol. Images were acquired for each sample using an Olympus BC43 microscope (10X and 20X magnification), and analysed with Ilastik software to assess the percentage of α -synuclein expressing cells over the total number of cells (Fig. 3.20).

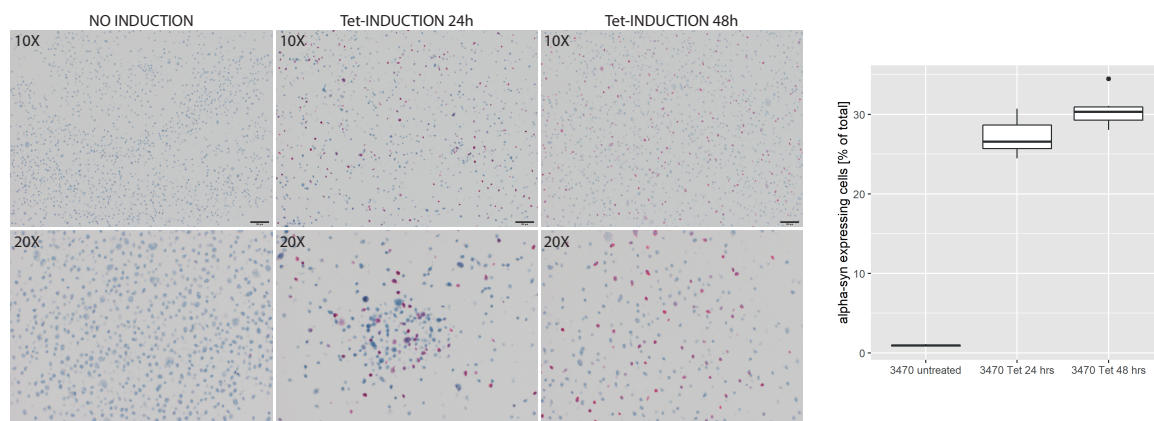


Fig. 3.20 α -synuclein overexpression in HeLa^{tet- α synA53T}.

Representative micrographs showing α -synuclein staining in uninduced, 24 hours tet-induced and 48 hours tet-induced HeLa^{tet- α synA53T}. Ilastik analysis of expressing cells: six images (10X magnification) analysed for each condition. Statistics: t-test one way ANOVA. * denotes p-values < 0.05, *** p-values < 0.001.

Ilastik analysis revealed that 30% of HeLa^{tet- α synA53T} cells overexpressed A53T α -synuclein at 48 hours after tetracycline-induction. Considering that hygromycin selection was conducted right after transfection of the expression plasmid without any single clone passage, it was expected to have a mixture of stably transfected cells and cells without integration of the

expression plasmids. For this reason, cells of each cell line underwent an additional hygromycin selection step (150 $\mu\text{g}/\text{ml}$) to remove as many cells lacking expression plasmid integration as possible. Cells were collected (2×10^6 cells for each cell line) to isolate genomic DNA and continued integration of the expression plasmids was verified by PCR as described before.

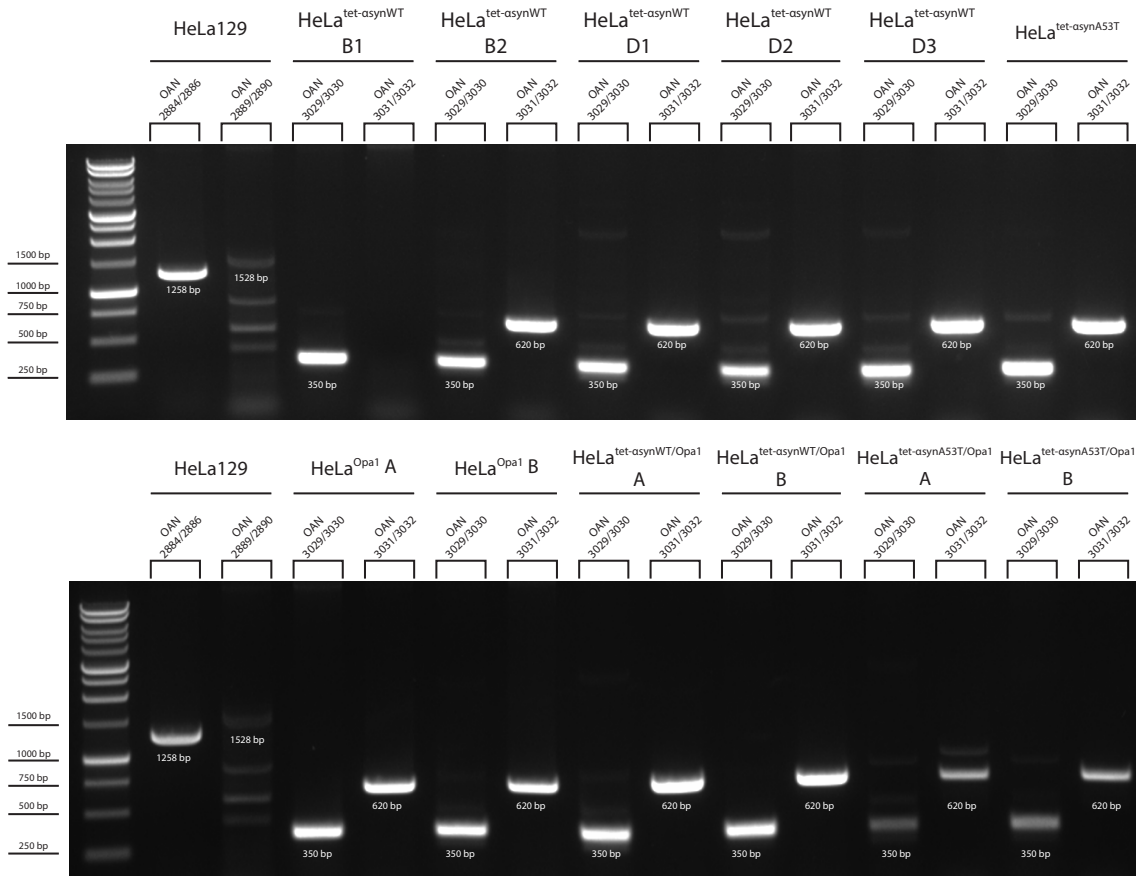


Fig. 3.21 PCR analysis for integration of expression plasmids after second hygromycin selection.

HeLa129. Primers for 5' junction amplification: OAN2884 (CTTTGAGCTCTACTGGCTTCTGCGCC) and OAN2886 (CCCTAGAGGATCCCCGGGTACCAAG), expected PCR product 1258 bp. Primers for 3' junction amplification: OAN2889 (GCTGCCTCAAAGGGCTTGCCAAC) and OAN2890 (GCAGTACCCCCACAGTTGGAGGAG), expected PCR product 1528 bp. PCR thermocycler program for 5' and 3' junction amplification: 98°C for 30 s, 35 cycles at 98°C for 10 s, 69°C for 30 s, 72°C for 30 s, and 72°C for 10 min.

Stable cell lines. Primers for 5' junction amplification: OAN3029 (ATTCTCCGCCCATGGCTGAC) and OAN3030 (ATCTTTGTAGAAACCATCGGCGCAGC), expected PCR product 350 bp. Primers for 3' junction amplification: OAN3031 (CGAGATCCGTGGTTCGCGAAGTTG) and OAN3032 (AGCCATCTGTTGTTTGGCCCTCC), expected PCR product 620 bp. PCR thermocycler program for 5' and 3' junction amplification: 98°C for 30 s, 35 cycles at 98°C for 10 s, 67°C for 30 s, 72°C for 30 s, and 72°C for 10 min. (Agarose 1% and TAE 1X, loading purple dye 6X, BenchTop 1 kb DNA ladder Promega).

Except for HeLa^{tet- α synWT} clone B1, all other stable lines showed expression plasmid integration (Fig. 3.21). As for HeLa^{tet- α synWT} additional four clones were available, we decided not to use clone B1 anymore.

As it was not possible to apply immunohistochemistry to verify OPA1 overexpression due to lack of a suitable anti-Opa1 antibody, we decided to use droplet digital PCR to evaluate Opa1 expression levels in those cell lines harbouring integration of the *OPA1* construct. Cells were collected (1×10^6 for each cell line) and QIAGEN RNeasy mini kit was used to purify RNA. Reverse transcription of extracted RNA was performed using SuperScript™ IV VILO Master Mix. Each cDNA sample was diluted 1:200 prior to addition to the human *OPA1* and human *GAPDH* primer/probe PCR mix. For each sample, the reaction was performed in triplicate. Following droplets generation, PCR reaction was performed in a C1000 Touch Thermal Cycler, and signal detection was accomplished using the QX200 Droplet Reader. Bio-Rad QuantaSoft software was used to manually set the amplitude threshold and to analyse the data. HeLa129 were used as control.

Samples	Number of copies
HeLa ^{Opa1} 1A	0.734
HeLa ^{Opa1} 1B	0.774
HeLa ^{tet-αsynWT/Opa1} 1A	0.833
HeLa ^{tet-αsynWT/Opa1} 1B	1.479
HeLa ^{tet-αsynA53T/Opa1} 1A	1.037
HeLa ^{tet-αsynA53T/Opa1} 1B	0.938

Table 3.2 ddPCR results. Number of copies of Opa1 in stable cell lines with integrated Opa1 construct.

ddPCR data analysis revealed that only HeLa^{tet- α synWT/Opa1} clone 1B showed ~ 1,5 fold overexpression of OPA1 (Table 3.2) compared to the control cell line (HeLa129). The other cell lines with *OPA1* construct integration did not show any Opa1 overexpression.

As one cell line out of six displayed Opa1 overexpression, we decided to verify the integrity of both the EF1 α promoter and the *OPA1* gene in these cell lines by PCR. HeLa129 were used as control.

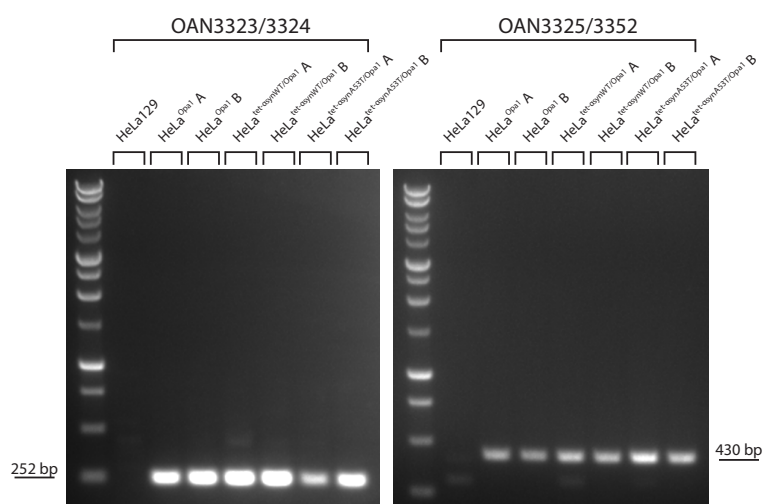


Fig. 3.22 PCR analysis for integrity of EF1 α promoter and Opa1 gene in stable cell lines with integrated Opa1 construct.

Primers for amplification between EF1 α promoter and Opa1: OAN3323 (CCGCCAGAACACAGGTAAGTGCC) and OAN3324 (TACGTAAAGGAAGGTTTGTCTAGAGAAGAGAAC), expected PCR product 252 bp. Primers for amplification between the final part of Opa1 construct and the FRT site: OAN3325 (GCTGAAGATGGTGAGAAGAAGATTAATTGC) and OAN3352 (CTAGAGCCCCAGCTGGTTCTTTC), expected PCR product 430 bp. PCR thermocycler program: 98°C for 30 s, 35 cycles at 98°C for 10 s, 67°C for 30 s, 72°C for 30 s, and 72°C for 10 min.

(Agarose 1% and TAE 1X, loading purple dye 6X, BenchTop 1 kb DNA ladder Promega).

Except for the control HeLa129 line, all the stable cell lines exhibited intact EF1 α promoter and *OPA1* construct (Fig. 3.22)

Following the additional hygromycin selection step, immunohistochemistry was applied to all stable cell lines to verify α -synuclein expression levels. Cells were seeded, treated, collected, fixed and paraffin-embedded as previously described. Histological sections were stained with anti- α -synuclein antibody according to the standard protocol and images were acquired using an Olympus BC43 microscope. Ilastik software was employed to analyse the acquired pictures and assess the percentage of α -synuclein expressing cells over the total number of cells. HeLa129 were used as control.

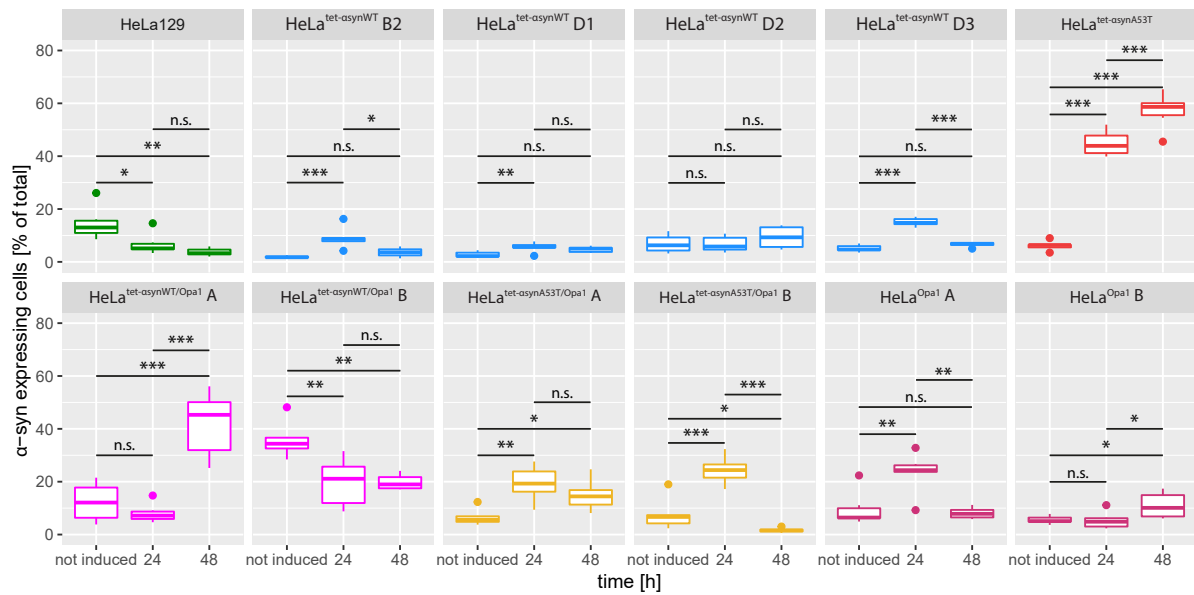


Fig. 3.23 α -synuclein immunohistochemistry.

Ilastik analysis of α -synuclein stained uninduced, 24 hours tet-induced and 48 hours tet-induced cells: six images (10X magnification) analysed for each condition. Statistics: t-test one way ANOVA.

* denotes p-values < 0.05, ** p-values < 0.01, *** p-values < 0.001, n.s. - no significant difference.

Ilastik analysis revealed that almost 60% of HeLa^{tet- α synA53T} cells overexpressed A53T α -synuclein at 48 hours after tetracycline-induction following the additional hygromycin selection procedure. As expected, this result points out that sequential steps of hygromycin treatment are required to remove cells lacking expression plasmid integration, thereby to obtain a more homogeneous cell population. Concerning HeLa^{tet- α synWT} cells, none of the clones showed a significant overexpression of wt α -synuclein after 48 hours of tetracycline-induction, despite the expression plasmid integration. The two clones of HeLa^{tet- α synWT/Opa1} showed opposite results: clone A displayed a significant overexpression of wt α -synuclein 48 hours after tetracycline-induction, while clone B showed a reduction of wt α -synuclein expression at the same time point, compared to non-induced cells. Regarding HeLa^{tet- α synA53T/Opa1} cells, A53T α -synuclein is significantly overexpressed at 24 hours after tetracycline-induction compared to non-induced cells, but then expression decreases at 48 hours after tetracycline-induction. Lastly, a moderate overexpression of α -synuclein is shown 24 hours after tetracycline-induction in HeLa^{Opa1} clone A, while HeLa^{Opa1} clone B cells display a light overexpression 48 hours after tetracycline-induction, even though α -synuclein is not present in the integrated expression plasmids.

3.2 p97 PROJECT

Mutation in p97 causing IBMPFD might impact interaction with its cofactor UBXD1

The AAA-ATPase valosin containing protein p97/VCP is the central component of the retrotranslocation machinery, which enables the proteasomal degradation of misfolded proteins at different subcellular locations, thereby preventing proteotoxic cell stress. The p97 protein is therefore regarded as a cofactor-guided, multifunctional protein important for the degradation of ubiquitinated client proteins.

In 2013, the Frank lab (Basel) was involved in the identification of a novel heterozygous missense mutation in the *p97* gene in a Swiss family with hereditary inclusion body myopathy and dementia [320]. Three brothers (III 1-3) independently presented with varying degrees of muscular weakness (Fig. 3.24 D). Patient III 2, a half brother of patient III 1, declined follow-up after the first evaluation. Muscle biopsies of all three patients revealed similar features: variation of fiber size, centralised nuclei, and focal perivascular and endomysial lymphocytic infiltrates of varying degrees (Fig. 3.24 A), interpreted as inclusion-body myositis. Brain autopsy of patient III 1 revealed a moderate frontotemporal cortical atrophy (Fig. 1B), and immunostaining of the neocortex and hippocampal CA1 region revealed numerous dystrophic neurites positive for ubiquitin and TDP43 (Fig. 3.24 C). Genomic sequencing of the *VCP* gene (*p97*) of the three brothers disclosed a novel heterozygous missense mutation c.828 A>T in exon 6 (Fig. 3.24 E), leading to a change from isoleucine to phenylalanine at position 206 (I206F) within the conserved linker domain of p97 protein. Furthermore, skeletal muscle tissue analysed by electron microscopy displayed altered mitochondrial morphology (swollen mitochondria) and ultrastructure (paracrystalline inclusions) (Fig. 3.24 F).

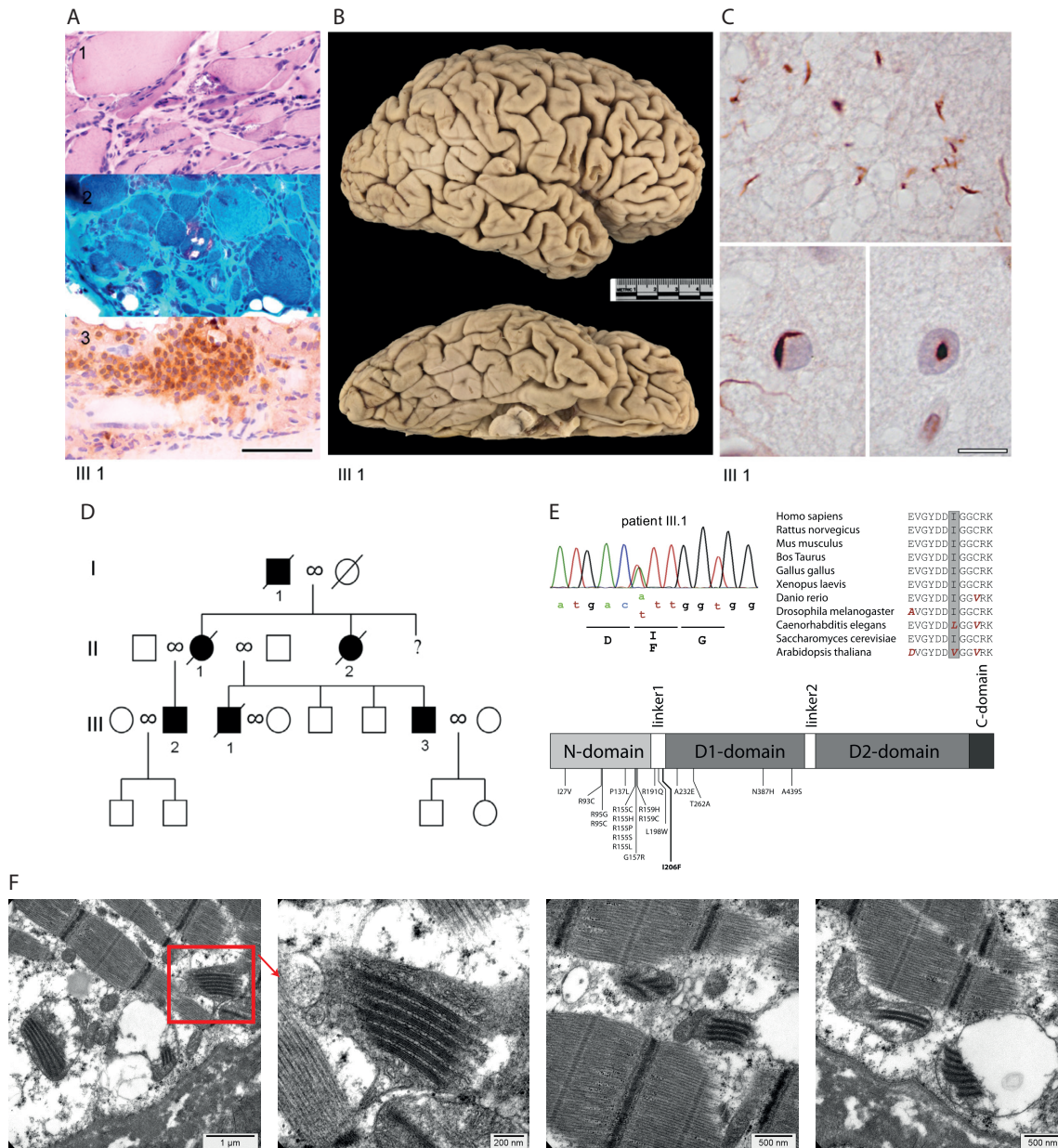


Fig. 3.24 Novel p97 missense mutation.

A. Skeletal muscle biopsy of patient III 1: H&E (1) and Gömöri trichrome (2) staining showing muscle fibers with rimmed vacuoles; anti-CD3 staining (brown colour) with hematoxylin counter-staining (3) highlighting a focal endomysial T cell inflammatory infiltrate. Scale bar 100 μ m. **B.** Brain macroscopic aspect: comparison between normal brain (top part) and patient III 1 brain (lower part) showing frontotemporal cortical atrophy of brain of III 1. **C.** Neocortex and hippocampal CA1 region immunostaining demonstrating dystrophic neurites (top image), and nuclear inclusions (lower images) positive for ubiquitin and TDP-43, respectively. 100x magnification, scale bar 10 μ m. **D.** Family tree with three generations of affected individuals. **E.** Sequencing chromatogram of patient III 1 genomic DNA showing the dominant negative allelic A>T missense mutation in exon 6, leading to amino acid exchange I206F (top left image). Multispecies alignment of the amino acid sequence in the I206F region (top right image). The novel missense mutation is located between the N-terminal domain and the first of the two ATPase domains (D1-domain) within the linker 1 region (lower image). **F.** Electron microscopy images of skeletal muscle of patient III 1 revealing paracrystalline mitochondrial inclusions. (Figure 1A-E from [320])

p97 is assisted by diverse cofactors for the recognition and processing of its substrates. One of these cofactors is the UBXD1/UBXN6/UBXDC2 protein, which targets p97 to perform its

Serial dilutions of yeast strains containing GAL4BD-UBXD1 VIM domain as bait and GAL4AD fused with the three different p97 as preys or GAL4AD vector as prey control on media selective for interaction (QDOX and QDOXA) revealed growth of strains containing GAL4BD-UBXD1 VIM domain and each of the three different p97 preys, while no growth was detected for yeast strains containing pGBKT7 (empty vector) bait or pGADT7 (empty vector) prey, as shown in Figure 3.26.

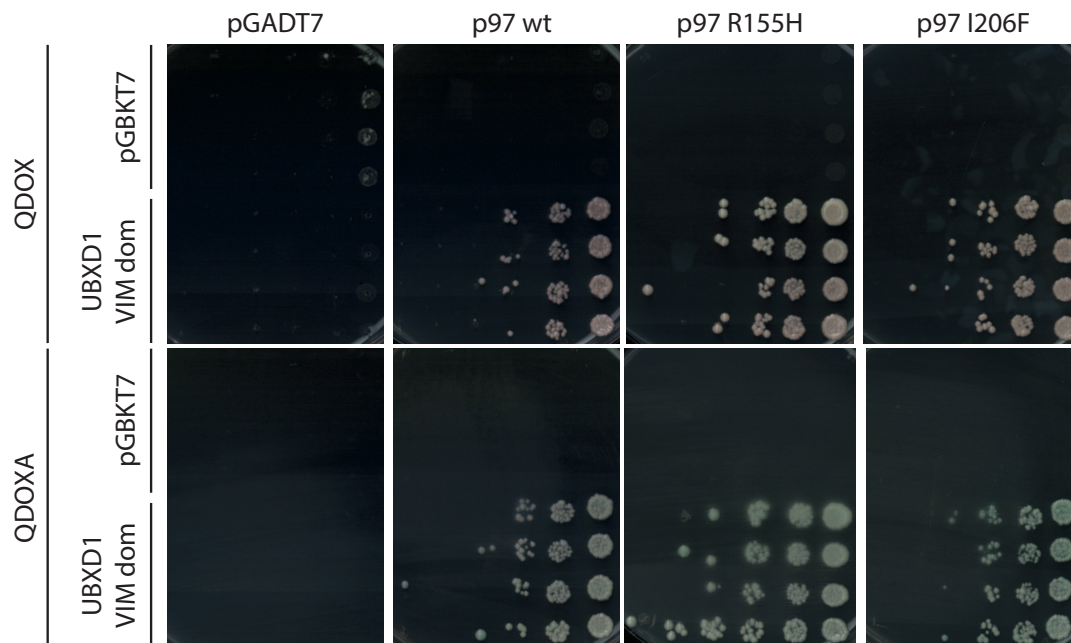


Fig. 3.26 Physical interaction of UBXD1-VIM domain with three isoforms of p97.

Cells of yeast strain Y2HGGold were transformed with expression constructs for fusion protein between the GAL4 DNA binding domain and UBXD1-VIM domain, and the GAL4 activation domain and three isoforms of p97 (p97 wt, p97 R155H, p97 I206F). Transformation with pGBKT7 (empty vector with GAL4 DNA binding domain) or pGADT7 (empty vector with GAL4 activation domain) served as control. Yeast strains were serially diluted onto plates selecting for yeast two-hybrid interaction (QDOX and QDOXA).

As all three p97 variants (wild-type; R155H; I206F) interacted with the VIM domain of UBXD1, we had to set out to quantify the strength of the interaction by an α -galactosidase quantitative assay. This sensitive colorimetric method detects and quantifies the yeast α -galactosidase activity by measuring the rate of hydrolysis of a chromogenic substrate, p-nitrophenyl- α -D-galactoside (PNP- α -Gal). As shown in Figure 3.27, the two disease-associated p97 mutants displayed a stronger interaction with UBXD1 as compared to wild-type p97.

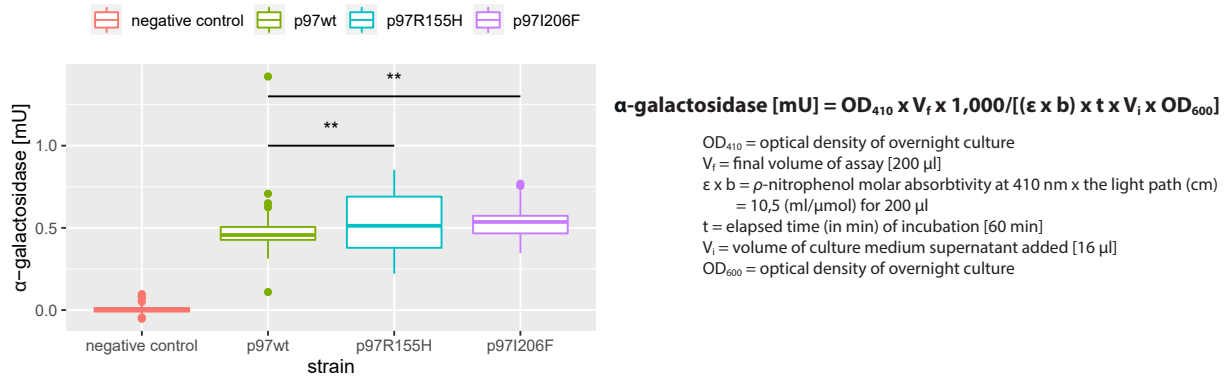


Fig. 3.27 α-galactosidase quantitative assay.

Strength of yeast two-hybrid interaction between the VIM domain of UBXD1 and p97 wild-type or the two disease-relevant p97 mutants was quantified using a para-nitrophenyl-α-galactoside assay. The graph shows the average of two independent experiments with three technical replicates each. Error bars represent standard deviation (SD). Statistical significance was assessed by ANOVA pairwise comparison followed by Student's t-test using false discovery rate (FDR) correction to account for multiple comparisons. ** denotes p-values < 0.01.

As can be appreciated, differences, although statistically significant, were too small to justify further characterization of the interaction between UBXD1 and newly identified mutant p97.

4. Discussion

4.1 Opa1 PROJECT

4.1.1 Generation of a double transgenic mouse model

Parkinson's disease (PD) is a pathogenically complex multifactorial disease and the most common neurodegenerative movement disorder [263]. Several lines of evidence, obtained from studies of familial forms of PD, patient samples, and *in vitro/in vivo* models, underline a major role of mitochondrial dysfunction, impaired mitochondrial quality control, and dysregulated mitochondrial crosstalk with other organelles .

This project aimed to understand whether moderate overexpression of the inner mitochondrial membrane OPA1 would rescue the mitochondrial dysfunction caused by A53T mutant α -synuclein. The underlying rationale for this work was based on the fact that mild overexpression of OPA1 was recently demonstrated to improve the motor performance in addition to biochemical and molecular phenotypes of two mouse models of mitochondrial disease [328]; of note, in mice, mild OPA1 overexpression is compatible with normal development, fertility and lifespan [83]. Therefore, our intention was to cross the *Opa1*^{tg} mouse with the A53T α -synuclein transgenic line M83 model [325] to analyse the mitochondrial phenotype in the double transgenic mouse.

4.1.1.1 A53T α -synuclein transgenic line M83

The PD mouse model expressing the A53T mutant human α -synuclein was generated by the group of Virginia M. Lee in 2002 [325] by microinjection of the MoPrP.Xho expression vector harboring the A53T mutant human α -synuclein into C57Bl/C3H mouse eggs. Potential founders were identified by Southern blot analysis of the isolated genomic DNA with a ³²P-labeled oligonucleotide-primed α -synuclein DNA probe. As standard PCR is not able to discriminate between homozygous and heterozygous animals, genotype evaluation is currently achieved by Southern blot and qPCR. However, as no clear qPCR Δ Ct threshold has been established for discrimination, the transgene genotype is usually determined by comparing Δ Ct values of unknown samples against known homozygous and heterozygous controls. Furthermore, the exact transgene copy numbers are not known for either homozygous or heterozygous animals, which represented a significant limitation for the

establishment of genotypically defined animal groups after crossing the two mouse models, as double transgenic mice would not have the same number of copies of A53T mutant human α -synuclein. Indeed, sybr green real-time PCR performed on heterozygous mice purchased from Jackson Laboratory revealed varying α -synuclein transgene copy numbers (Fig. 3.1). In addition, the Jackson Laboratory also reported a high incidence of nonproductive matings in homozygous mice. Moreover, the A53T α -synuclein transgenic line M83 model has a different genetic background (C3H) compared to the *Opa1*^{tg} mouse (Sv129). This would have implied several passages of back-crossing to achieve an identical genetic background in the double transgenic model.

Even if abnormal α -synuclein inclusions of homozygous mice resemble human pathological inclusions of patients with the A53T mutation known as Lewy bodies with regard to their immunological, histological, biochemical and ultrastructural properties, the anatomical distribution of these lesions in A53T mouse brains does not recapitulate the situation in human PD. Infact, tyrosine hydroxylase (TH)-expressing neurons of the substantia nigra do not show the same selective vulnerability as in humans, possibly due to a lack of neuromelanin generation. Additionally, intrinsic protective mechanisms counteracting oxidative damage could prevent this population of neurons from pathological α -synuclein inclusion formation.

4.1.1.2 *Opa1*^{tg} mouse line

The *Opa1*^{tg} mouse was developed by the research group of Luca Scorrano in 2013 [83] by targeting mouse variant 1 *Opa1* under the human beta-actin promoter in the murine X chromosome *Hprt* region via homologous recombination in BPES embryonic stem cells, thus avoiding toxically high *Opa1* levels and consequent mitochondrial fragmentation [65]. Mice were viable and fertile, with moderate (~1.5 increase) and ubiquitous overproduction of *Opa1*. Mitochondria turned out to be slightly elongated, with tighter cristae as well as with increased respiratory chain supercomplex (RCS) assembly and respiratory function.

As the generation of the double transgenic mouse despite our best efforts was not feasible, we decided to switch to an *in vitro* model to address our aim of research. Therefore, to benefit from the moderate *Opa1* overexpression already achieved with the *Opa1*^{tg} mouse, we proceeded with the isolation and immortalization of fibroblasts from the diaphragm of wt and

hemizygous *Opa1*^{tg} 7-week-old C57BL6/J male mice (MAFs), as described in Cogliati et al. [83]. Our intent was to later stably transfect wt and *Opa1*^{tg} MAFs with wt and mutated α -synuclein to create an appropriate cellular model to address our research question. Following PCR analysis, primary (Fig. 3.2 B, right picture) and immortalized (Fig. 3.2 C) *Opa1*^{tg} MAFs displayed an unexpected molecular pattern, showing not only the 1200 bp band of the tg *Hprt* locus mouse allele but also the 400b bp band of the wt *Hprt* locus mouse allele, as if the analysed DNA belonged to a mixed population of cells. PCR analysis performed on five different tissues (brain, diaphragm, liver, muscle and tail) confirmed an aberrant PCR pattern among the different tissues in seven out of eight mice (Fig. 3.3). While the exact reasons for this aberrant genotyping remains unclear, our observations point to a mosaicism in these mice. In conclusion, mouse-derived fibroblasts could not be used for our aim of research.

4.1.2 Generation of stable cell lines

Genomic safe harbors (GSHs) are regions of the human genome able of accommodating genetic material and allowing transgene expression without adverse effects on the host cell or organism. Thus, a GSH must not alter cellular functions or predispose cells to malignant transformation [326]. Among the few candidate genomic safe harbors, the adeno-associated virus site 1 (AAVS1) has been successfully targeted. AAVS1 is located within the *protein phosphatase 1, regulatory (inhibitor) subunit 12C (PPP1R12C)* gene on chromosome 19, characterised by an open chromatin conformation and a transcription-competent environment [329]. It is considered a “safe harbor” for transgene integration into the human genome as no known adverse effects have been observed following disruption of the *PPP1R12C* gene locus [330]. For this reason, we decided to use AAVS1 for targeted gene delivery and integration of our genes of interest to generate stable cell lines. Our approach is based on the combination of two existing systems, with some modifications: the GeneCopoeia Genome-TALER™ human AAVS1 Safe Harbor Gene Knock-in System combined with the ThermoFisher Flp-In™ T-REx™ System. As described in Fig. 3.4, we used the GeneCopoeia Genome-TALER™ system to generate DSBs in the AAVS1 locus through specific TALENs, thus stimulating HR and allowing the integration of a platform vector due to the presence of AAVS1 homology arms (Fig. 3.7). HeLa cells were used as cellular model for the application of our targeted gene delivery strategy. We were aware that this cell line, derived from human

cervical cancer [331], did not represent the optimal model to study neurodegenerative disorders such as Parkinson's disease. Indeed, our initial choice was the neuroblastoma SH-SY5Y cell lineage, a widely used *in vitro* model for PD even though its properties do not classify this lineage as dopaminergic [332]. Nevertheless, most of the genes and pathways dysregulated in PD pathogenesis are intact in these cells [333]. Neuroblastoma SH-SY5Y cells followed the same protocol applied to HeLa cells for the transfection and integration of the platform vector within the AAVS1 locus, as well as the process of single cloning in 96 well plates and the Luciferase assay. However, as several attempts were unsuccessful (i.e. no luciferase-positive SH-SY5Y clones could be obtained), we decided to proceed with HeLa cells, with which three luciferase-positive clones were obtained (Fig. 3.8 B). While not of neuronal origin, HeLa cells nonetheless are a widely employed model to study basic mechanisms of mitochondrial quality control. After excluding mycoplasma contamination (Fig. 3.9) and assessing pAN3418 platform vector integration by PCR analysis (Fig. 3.10 B), proliferation of the three luciferase-positive clones was evaluated to determine the clone best suitable for further experimentation. Clone 129 was selected, as it showed a more linear growth compared to clones 19 and 31 (Fig. 3.11).

The second step of our targeted gene delivery and integration approach is based on the ThermoFisher Flp-In™ T-REx™ System. Therefore, Flp-In™ T-REx™ System expression plasmid pcDNA5/FRT/TO, modified after insertion of our genes of interest, was cotransfected with Flp recombinase (pOG44 plasmid) to be integrated into the knock-in platform of HeLa129 following HR. The inserted genes of interest are human *OPA1* variant 1 and human A53T α -synuclein with the aim of recapitulating *in vitro* the characteristics of the two mouse models as well as what would have been the double transgenic mouse. Human *OPA1* variant 1 was chosen among the eight isoforms expressed in humans because it generates both long (l)- and short (s)-*OPA1* forms through alternative splicing. *OPA1* variant 1 is characterised by exon 4b deficiency and incomplete cleavage at the S1 site, just as variants 2, 4 and 7. Indeed, variants containing exon 4 are required for maintaining a fused mitochondrial network [72]. Conversely, the region encoded by exon 4b is present in the other four variants (3, 5, 6 and 8), leading to complete cleavage at the S1 site, generating s-*OPA1* forms only [334]. Of note, the *OPA1* l/s isoform dysbalance towards s-forms inhibits mitochondrial fusion, leads to network

fragmentation and activates mitochondrial quality control processes to remove fragmented and depolarized mitochondria through mitophagy [335], [336].

Additionally, we decided to clone human wild-type α -synuclein into the pcDNA5/FRT/TO plasmid, as a familial form of (inherited) PD is known to be caused by duplication [337], [338] or triplication [339] of the *SNCA* gene (coding for α -synuclein), leading to increased formation of toxic aggregates and widespread neuronal damage [340]. Both wild-type and mutated α -synuclein were cloned next to a tetracycline-inducible promoter to evaluate the effects of their overexpression at different time points, while constitutive expression of human *OPA1* variant 1 was obtained using the EF1 α promoter. Five plasmids were designed, cloned and cotransfected into HeLa129 cells to generate the corresponding stable cell lines, and integration was verified by PCR analysis upon hygromycin selection (Figs. 3.16 and 3.17).

4.1.3 Characterization of stable cell lines

The characterization of the newly generated AAVS1 Flp-in stable cell lines started with evaluation of α -synuclein and Opa1 expression levels by Western blot (Fig. 3.19 A-L). All five HeLa^{tet- α synWT} clones displayed α -synuclein overexpression following tetracycline-induction compared to the control cell line (HeLa129), with clone D2 (Fig. 3.19 D) displaying the highest α -synuclein expression levels at 24 hours after tetracycline-induction. However, clone B1 presented a more linear increase of protein expression over time upon tetracycline-induction (Fig. 3.19 A).

The two HeLa^{Opa1} clones showed opposite changes in OPA1 expression levels, with clone A displaying lower OPA1 expression as compared to the control cell line, while clone B showed decreased OPA1 expression following tetracycline treatment.

As for HeLa^{tet- α synWT/Opa1} and HeLa^{tet- α synA53T/Opa1}, only one clone for each cell line was analysed by Western blotting (WB), revealing substantial variability in expression levels, which was also true for HeLa^{Opa1} and HeLa^{tet- α synWT} clones.

Quite the opposite, HeLa^{tet- α synA53T} showed a strong and reproducible α -synuclein band in all the WB membranes analysed, with high levels of mutant protein at 48 hours of tetracycline-induction (Fig. 3.19 F). Indeed, this α -synuclein mutant is more prone to aggregate formation and subsequent adoption of a β -sheet conformation [341], which could explain the early disease onset of the α -synuclein A53T mutation-linked form of PD [342]. Among the known

consequences of α -synuclein aggregation there are inhibition of the ubiquitin proteasome system (UPS) and impaired autophagy-lysosomal pathway (ALP) function [343], [344], suggesting possible failure of protein degradation machineries.

In order to verify the strong α -synuclein overexpression, immunohistochemistry was applied to HeLa^{tet- α synA53T}, revealing that 30% of the cell population overexpressed mutant α -synuclein following 48 hours of tetracycline-induction (Fig. 3.20). Due to the lower hygromycin concentration used to avoid massive cell death while selecting cells with expression plasmid integration, it was expected to still have cells without any expression plasmid integration. Therefore, prior to applying immunohistochemistry to the other stable cell lines, an additional hygromycin selection step was performed, followed by PCR to verify persistent integration of the expression plasmids. As shown in Fig. 3.21, all the stable cell lines retained the expression plasmid integration, except for HeLa^{tet- α synWT} clone B1, which was discontinued even though it showed a linear increase in protein expression following tetracycline-induction and prior to additional hygromycin selection (as judged by Western blotting).

The evaluation of *OPA1* expression levels in cell lines harboring integration of the *OPA1* construct was performed with droplet digital PCR as no good anti-OPA1 antibodies for immunohistochemistry are commercially available. The analysis revealed that only one out of six cell lines, HeLa^{tet- α synWT/Opa1} clone 1B, displayed *OPA1* overexpression (Table 3.2). Therefore, we performed PCR analysis in all the stable lines with *OPA1* integration to evaluate if both EF1 α promoter and *OPA1* construct were still intact after the repeated selection steps. All samples displayed intact EF1 α promoters and *OPA1* constructs (Fig. 3.22). Further experiments are needed to understand the absence of OPA1 overexpression even though promoter and gene constructs are intact in all the stable lines as well as in the starting plasmid vector where they were cloned in.

Immunohistochemistry for α -synuclein was repeated after the additional hygromycin selection procedure to verify levels of protein expression in all the stable cell lines. As expected, a higher percentage of HeLa^{tet- α synA53T} cells (~ 60%) overexpressed A53T α -synuclein at 48 hours after tetracycline-induction (Fig. 3.23), compared to the first immunohistochemistry staining. Indeed, with several selection passages, it is possible to reduce the number of cells lacking expression plasmid integration, and to thereby obtain a more homogeneous cell population for further experimentation.

Further evaluations are necessary for the other stable cell lines as none of the HeLa^{tet- α synWT} clones showed robust wild-type α -synuclein overexpression, not even at 48 hours after tetracycline-induction, while the two HeLa^{tet- α synWT/Opa1} clones showed opposite results, with clone B displaying reduced expression following tetracycline induction. HeLa^{tet- α synA53T/Opa1} cells showed an increase in mutant α -synuclein overexpression at 24 hours after tetracycline-induction, followed by a significant decrease at 48 hours only in clone B. It is not possible yet to speculate that this decrease at 48 hours is a consequence of OPA1 overexpression, as the droplet digital PCR analysis was applied to cells in basal conditions, that is without any induction of α -synuclein overexpression, and OPA1 expression levels at 48 hours after tetracycline-induction were not analysed.

Finally, HeLa^{Opa1} clone A showed moderate overexpression of α -synuclein at 24 hours after tetracycline-induction even though the α -synuclein construct is not present in the integrated expression plasmid, as well as clone B which showed slight overexpression at 48 hours after tetracycline-induction. This could be due to unspecific α -synuclein staining of spaces between the cells (images not shown), and also along the edges of histological sections.

4.1.4 Conclusions and future perspectives

The generation of stable cell lines by combining the GeneCopoeia Genome-TALER™ human AAVS1 Safe Harbor Gene Knock-in System with the ThermoFisher Flp-In™ T-REx™ System (Fig. 3.4) was successful with regard to integration of the expression plasmids. Regarding the expression of our proteins of interest, the inducible system worked in HeLa cells with integration of A53T α -synuclein, while the other stable cell lines (i.e. HeLa^{tet- α synWT}, HeLa^{tet- α synWT/Opa1}, HeLa^{tet- α synA53T/Opa1}) did not show any significant expression. Further experimentation is needed to exclude whether the problem is due to chromatin structure, even if the AAVS1 locus is characterised by an open chromatin conformation and a transcription-competent environment.

The generation of these stable cell lines was pursued with the aim of recapitulating *in vitro* the mitochondrial phenotype of the two single mouse models (*Opa1*^{tg}; *α -synuclein*^{A53T tg}) as well as what would have been the double transgenic mouse, with a focus on mitochondrial morphology, mitochondrial ultrastructure, mitochondrial respiration and mitochondrial crosstalk with other organelles, which occur to be compromised in Parkinson's disease.

4.2 p97 project

Mutation in p97 causing IBMPFD might impact interaction with its cofactor UBXD1

P97 is a multifunctional protein with a central role in the ubiquitin dependent protein degradation pathway [149], in addition to being required for the full capacity of the lysosomal and autophagic systems [345, 346]. The best-studied function of p97 is in endoplasmic reticulum (ER)-associated degradation (ERAD), where p97 retrotranslocates misfolded ubiquitinated proteins from the ER to the cytosol for degradation [347]. P97 is also important at the mitochondrial level where it extracts ubiquitin-modified proteins from the mitochondrial outer membrane in a process termed outer mitochondrial membrane-associated degradation (OMMAD), preserving mitochondrial integrity and thus cellular homeostasis [167]. Moreover, p97 has a direct function in mitophagy and lysophagy, i.e. affects the selective macroautophagy of mitochondria and lysosomes, respectively [103], [189].

The new heterozygous missense mutation within the conserved linker domain of p97 protein was identified in a Swiss family with hereditary inclusion body myopathy and dementia in 2013 [320]. Altered mitochondrial morphology and ultrastructure (Fig. 3.24 F) were discovered by electron microscopy analysis of skeletal tissue of patient III-1. Since p97 is a cofactor-guided protein and considering that UBXD1 cofactor promotes p97 recruitment following recognition of depolarized mitochondria undergoing Parkin-dependent mitophagy [192], we performed a yeast two-hybrid assay to evaluate whether the novel p97 missense mutation would compromise the interaction with the UBXD1 cofactor.

Since it was reported that the UBXD1 VIM domain is sufficient to bind p97 and promote mitochondrial recruitment [191, 192], the UBXD1 VIM domain was fused to the GAL4 DNA-BD and used as bait protein. Instead, the GAL AD was fused with three different preys: the N-terminal domain of wild-type p97; the N-terminal domain of the most common disease-related mutant p97, R155H; and the N-terminal domain of p97 newly identified missense mutation, I206F (Fig. 3.25). The p97 N-terminus was used as prey because UBXD1 interaction takes place at this region of the p97 protein [191].

Serial dilutions on plates selecting for yeast two-hybrid interaction assessed the interaction of all the three p97 variants with the VIM domain of UBXD1 (Fig. 3.26). Strength interaction quantification by α -galactosidase assays showed only very marginal, although statistically

significant differences between the newly identified p97 mutant and the wild-type form (Fig. 3.27); therefore no further characterization was pursued.

The VIM domain is not the only UBXD1 domain interacting with the N-terminal of p97. UBXD1 PUB domain is also capable of binding and recruiting p97 to mitochondria under mitophagic conditions [192]. Indeed, UBXD1 binds p97 in two regions, at the C-terminus via the PUB domain, and the N-domain with the VIM interaction motif [191]. Hence, it would be of interest to understand if the presence of both UBXD1 domains would give a different result following yeast two-hybrid and α -galactosidase assay experiments.

Moreover, a variety of p97-interacting proteins, functioning as adaptors or cofactors has been identified: their competition for p97 binding regulates the activity of this AAA-ATPase, linking the protein to a specific subcellular compartment or substrate, or helping the substrate processing. Considering the mitochondrial inclusions encountered in the analysed patient's skeletal muscle tissue upon electron microscopy analysis (Fig. 3.24 F), the UBXD1 cofactor was selected among the others to be used in the yeast two-hybrid assay due to its involvement in the mitophagic process [192]. Another p97-interacting protein, SAKS1/UBXN1, was recently identified as a novel regulator of mitophagic initiation in addition to its involvement in ubiquitin-proteasome functions. Loss of SAKS1/UBXN1 was found to interfere with the removal of mitofusin 2 (MFN2) from mitochondria by causing para-mitochondrial MFN2 blob formation [199]. Therefore, it would also be of interest to analyse if the newly discovered p97 mutant would affect the interaction with the SAKS1/UBXN1 cofactor as well, and how this will impact on p97 mitochondrial recruitment under mitophagic conditions.

5. Appendix

5.1 List of Figures

Figure 1.1 Mitochondrial structure and function.	3
Figure 1.2 Mitochondrial fission and fusion.	7
Figure 1.3 Opa1 protein structure and proteolytic cleavage sites.....	9
Figure 1.4 p97 protein structure.	14
Figure 1.5 Mitochondria–ER contact site and main resident proteins.	20
Figure 3.1 Analysis of Sybr green real-time PCR of A53T α -synuclein heterozygous mice...	44
Figure 3.2 PCR analysis of <i>Opa1</i> ^{tg} mice and derived MAFs.....	45
Figure 3.3 PCR analysis of brain, diaphragm, liver, muscle, and tail tissues of two animals per genotype.	46
Figure 3.4 Graphic overview of the strategy for generation of stable cell lines.....	48
Figure 3.5 Genome-TALER™ human AAVS1 Safe Harbor Gene Knock-in System.....	49
Figure 3.6 Flp-In™ T-REx™ System.	50
Figure 3.7 Step1: platform integration in HeLa AAVS1 locus.....	51
Figure 3.8 Luciferase assay.	52
Figure 3.9 PCR analysis for mycoplasma contamination.....	52
Figure 3.10 Platform knock-in integration.....	53
Figure 3.11 CellTiter-Glo® 2.0 Assay.	54
Evaluation of HeLa clones proliferation. 5x10 ³ cells/well seeded for each clone. CellTiter-Glo was performed 6h, 24h, 48h, 72h and 96h after cell seeding.....	54
Fig. 3.12 Hygromycin killing curve HeLa129.	55
Fig. 3.13 Step2: integration of pcDNA5/FRT/TO plasmid with genes of interest in HeLa129.	56
Fig. 3.14 Plasmids for the second step of targeted gene delivery and integration.	57
Fig. 3.15 Expression plasmid knock-in verification primer pairs.	59
Fig. 3.16 PCR reaction setup analysis for integration of expression plasmid pAN3469 in HeLa129.....	60
Fig. 3.17 PCR analysis for integration of expression plasmids pAN3470, pAN3516, pAN3517 and pAN3518 in HeLa129.....	61

Fig. 3.18 AAVS1 Flp-In stable cell lines.	62
Fig. 3.19 Evaluation of α -synuclein and Opa1 expression levels in AAVS1 Flp-In stable cell lines.	64
Fig. 3.20 α -synuclein overexpression in HeLa ^{tet-αsynA53T}	65
Fig. 3.21 PCR analysis for integration of expression plasmids after second hygromycin selection.	66
Fig. 3.22 PCR analysis for integrity of EF1 α promoter and Opa1 gene in stable cell lines with integrated Opa1 construct.....	68
Fig. 3.23 α -synuclein immunohistochemistry.....	69
Fig. 3.24 Novel p97 missense mutation.....	71
Fig. 3.25 Yeast two-hybrid (Y2H) principle.....	72
Fig. 3.26 Physical interaction of UBXD1-VIM domain with three isoforms of p97.....	73
Fig. 3.27 α -galactosidase quantitative assay.....	74

5.2 List of Tables

Table 2.1: Equipment used during this study.	29
Table 2.2: Reagents used during this study.	31
Table 2.3: Antibodies used during this work.	31
Table 2.4: DNA modifying enzymes used during this study.	32
Table 2.5: Oligonucleotides used during this study.	33
Table 2.6: Plasmids used in this study.	34
Table 2.7: Pipetting scheme to optimise DNA amplification using high fidelity Phusion polymerase (NEB).	36
Table 2.8: Temperature and time profile for amplification using high fidelity Phusion polymerase.	36
Table 3.1. Plasmids used for cloning the five expression plasmids.	58
Table 3.2 ddPCR results. Number of copies of Opa1 in stable cell lines with integrated Opa1 construct.	67

6. References

- [1] L. Margulis, "Symbiotic theory of the origin of eukaryotic organelles; criteria for proof," *Symp Soc Exp Biol*, no. 29, pp. 21–38, 1975, Accessed: Feb. 18, 2022. [Online]. Available: <https://pubmed.ncbi.nlm.nih.gov/822529/>
- [2] D. C. Chan, "Mitochondrial Dynamics and Its Involvement in Disease," *Annu Rev Pathol*, vol. 15, pp. 235–259, Jan. 2020, doi: 10.1146/ANNUREV-PATHMECHDIS-012419-032711.
- [3] S. E. Calvo, K. R. Clauser, and V. K. Mootha, "MitoCarta2.0: an updated inventory of mammalian mitochondrial proteins," *Nucleic Acids Res*, vol. 44, no. D1, pp. D1251–D1257, 2016, doi: 10.1093/NAR/GKV1003.
- [4] X. Liu, C. N. Kim, J. Yang, R. Jemmerson, and X. Wang, "Induction of apoptotic program in cell-free extracts: requirement for dATP and cytochrome c," *Cell*, vol. 86, no. 1, pp. 147–157, Jul. 1996, doi: 10.1016/S0092-8674(00)80085-9.
- [5] L. C. Gomes, G. di Benedetto, and L. Scorrano, "During autophagy mitochondria elongate, are spared from degradation and sustain cell viability," *Nat Cell Biol*, vol. 13, no. 5, pp. 589–598, May 2011, doi: 10.1038/NCB2220.
- [6] M. Khacho *et al.*, "Mitochondrial Dynamics Impacts Stem Cell Identity and Fate Decisions by Regulating a Nuclear Transcriptional Program," *Cell Stem Cell*, vol. 19, no. 2, pp. 232–247, Aug. 2016, doi: 10.1016/J.STEM.2016.04.015.
- [7] K. Yasukawa *et al.*, "Mitofusin 2 inhibits mitochondrial antiviral signaling," *Sci Signal*, vol. 2, no. 84, Aug. 2009, doi: 10.1126/SCISIGNAL.2000287.
- [8] J. M. Herrmann and W. Neupert, "Protein insertion into the inner membrane of mitochondria," *IUBMB Life*, vol. 55, no. 4–5, pp. 219–225, Apr. 2003, doi: 10.1080/1521654031000123349.
- [9] N. Pfanner and M. Meijer, "The Tom and Tim machine," *Curr Biol*, vol. 7, no. 2, 1997, doi: 10.1016/S0960-9822(06)00048-0.
- [10] R. Acín-Pérez, P. Fernández-Silva, M. L. Peleato, A. Pérez-Martos, and J. A. Enriquez, "Respiratory active mitochondrial supercomplexes," *Mol Cell*, vol. 32, no. 4, pp. 529–539, Nov. 2008, doi: 10.1016/J.MOLCEL.2008.10.021.

-
- [11] K. M. Davies *et al.*, "Macromolecular organization of ATP synthase and complex I in whole mitochondria," *Proc Natl Acad Sci U S A*, vol. 108, no. 34, pp. 14121–14126, Aug. 2011, doi: 10.1073/PNAS.1103621108/-/DCSUPPLEMENTAL/PNAS.1103621108_SI.PDF.
- [12] A. K. Kondadi *et al.*, "Cristae undergo continuous cycles of membrane remodelling in a MICOS-dependent manner," *EMBO Rep*, vol. 21, no. 3, Mar. 2020, doi: 10.15252/EMBR.201949776.
- [13] C. A. Mannella *et al.*, "Topology of the mitochondrial inner membrane: dynamics and bioenergetic implications," *IUBMB Life*, vol. 52, no. 3–5, pp. 93–100, Sep. 2001, doi: 10.1080/15216540152845885.
- [14] M. Harner *et al.*, "The mitochondrial contact site complex, a determinant of mitochondrial architecture," *EMBO J*, vol. 30, no. 21, pp. 4356–4370, Nov. 2011, doi: 10.1038/EMBOJ.2011.379.
- [15] V. Kozjak-Pavlovic, "The MICOS complex of human mitochondria," *Cell Tissue Res*, vol. 367, no. 1, pp. 83–93, Jan. 2017, doi: 10.1007/S00441-016-2433-7.
- [16] M. Giacomello, A. Pyakurel, C. Glytsou, and L. Scorrano, "The cell biology of mitochondrial membrane dynamics," *Nat Rev Mol Cell Biol*, vol. 21, no. 4, pp. 204–224, Apr. 2020, doi: 10.1038/S41580-020-0210-7.
- [17] T. J. Collins, M. J. Berridge, P. Lipp, and M. D. Bootman, "Mitochondria are morphologically and functionally heterogeneous within cells," *EMBO J*, vol. 21, no. 7, pp. 1616–1627, Apr. 2002, doi: 10.1093/EMBOJ/21.7.1616.
- [18] M. Schrader and Y. Yoon, "Mitochondria and peroxisomes: are the 'big brother' and the 'little sister' closer than assumed?," *Bioessays*, vol. 29, no. 11, pp. 1105–1114, Nov. 2007, doi: 10.1002/BIES.20659.
- [19] K. Faelber *et al.*, "Crystal structure of nucleotide-free dynamin," *Nature*, vol. 477, no. 7366, pp. 556–562, Sep. 2011, doi: 10.1038/NATURE10369.
- [20] M. G. J. Ford, S. Jenni, and J. Nunnari, "The crystal structure of dynamin," *Nature*, vol. 477, no. 7366, pp. 561–566, Sep. 2011, doi: 10.1038/NATURE10441.
- [21] J. R. Friedman, L. L. Lackner, M. West, J. R. DiBenedetto, J. Nunnari, and G. K. Voeltz, "ER tubules mark sites of mitochondrial division," *Science*, vol. 334, no. 6054, pp. 358–362, Oct. 2011, doi: 10.1126/SCIENCE.1207385.

-
- [22] S. C. Lewis, L. F. Uchiyama, and J. Nunnari, "ER-mitochondria contacts couple mtDNA synthesis with mitochondrial division in human cells," *Science*, vol. 353, no. 6296, Jul. 2016, doi: 10.1126/SCIENCE.AAF5549.
- [23] F. Korobova, V. Ramabhadran, and H. N. Higgs, "An actin-dependent step in mitochondrial fission mediated by the ER-associated formin INF2," *Science*, vol. 339, no. 6118, pp. 464–467, Jan. 2013, doi: 10.1126/SCIENCE.1228360.
- [24] U. Manor *et al.*, "A mitochondria-anchored isoform of the actin-nucleating spire protein regulates mitochondrial division," *Elife*, vol. 4, no. AUGUST2015, Aug. 2015, doi: 10.7554/ELIFE.08828.
- [25] F. Korobova, T. J. Gauvin, and H. N. Higgs, "A role for myosin II in mammalian mitochondrial fission," *Curr Biol*, vol. 24, no. 4, pp. 409–414, Feb. 2014, doi: 10.1016/J.CUB.2013.12.032.
- [26] S. Gandre-Babbe and A. M. van der Bliek, "The novel tail-anchored membrane protein Mff controls mitochondrial and peroxisomal fission in mammalian cells," *Mol Biol Cell*, vol. 19, no. 6, pp. 2402–2412, Jun. 2008, doi: 10.1091/MBC.E07-12-1287.
- [27] C. S. Palmer, L. D. Osellame, D. Laine, O. S. Koutsopoulos, A. E. Frazier, and M. T. Ryan, "MiD49 and MiD51, new components of the mitochondrial fission machinery," *EMBO Rep*, vol. 12, no. 6, pp. 565–573, Jun. 2011, doi: 10.1038/EMBOR.2011.54.
- [28] H. Otera *et al.*, "Mff is an essential factor for mitochondrial recruitment of Drp1 during mitochondrial fission in mammalian cells," *J Cell Biol*, vol. 191, no. 6, pp. 1141–1158, Dec. 2010, doi: 10.1083/JCB.201007152.
- [29] T. J. Wilson, A. M. Slupe, and S. Strack, "Cell signaling and mitochondrial dynamics: Implications for neuronal function and neurodegenerative disease," *Neurobiol Dis*, vol. 51, pp. 13–26, Mar. 2013, doi: 10.1016/J.NBD.2012.01.009.
- [30] B. Oettinghaus, M. Licci, L. Scorrano, and S. Frank, "Less than perfect divorces: dysregulated mitochondrial fission and neurodegeneration," *Acta Neuropathol*, vol. 123, no. 2, pp. 189–203, Feb. 2012, doi: 10.1007/S00401-011-0930-Z.
- [31] C. R. Chang and C. Blackstone, "Cyclic AMP-dependent protein kinase phosphorylation of Drp1 regulates its GTPase activity and mitochondrial morphology," *J Biol Chem*, vol. 282, no. 30, pp. 21583–21587, Jul. 2007, doi: 10.1074/JBC.C700083200.

-
- [32] J. T. Cribbs and S. Strack, "Reversible phosphorylation of Drp1 by cyclic AMP-dependent protein kinase and calcineurin regulates mitochondrial fission and cell death," *EMBO Rep*, vol. 8, no. 10, pp. 939–944, Oct. 2007, doi: 10.1038/SJ.EMBOR.7401062.
- [33] W. Wang *et al.*, "Mitochondrial fission triggered by hyperglycemia is mediated by ROCK1 activation in podocytes and endothelial cells," *Cell Metab*, vol. 15, no. 2, pp. 186–200, Feb. 2012, doi: 10.1016/J.CMET.2012.01.009.
- [34] C. H. Chou *et al.*, "GSK3beta-mediated Drp1 phosphorylation induced elongated mitochondrial morphology against oxidative stress," *PLoS One*, vol. 7, no. 11, 2012, doi: 10.1371/JOURNAL.PONE.0049112.
- [35] J. Yan *et al.*, "Blockage of GSK3 β -mediated Drp1 phosphorylation provides neuroprotection in neuronal and mouse models of Alzheimer's disease," *Neurobiol Aging*, vol. 36, no. 1, pp. 211–227, Jan. 2015, doi: 10.1016/J.NEUROBIOLAGING.2014.08.005.
- [36] G. M. Cereghetti *et al.*, "Dephosphorylation by calcineurin regulates translocation of Drp1 to mitochondria," *Proc Natl Acad Sci U S A*, vol. 105, no. 41, pp. 15803–15808, Oct. 2008, doi: 10.1073/PNAS.0808249105.
- [37] N. Taguchi, N. Ishihara, A. Jofuku, T. Oka, and K. Mihara, "Mitotic phosphorylation of dynamin-related GTPase Drp1 participates in mitochondrial fission," *J Biol Chem*, vol. 282, no. 15, pp. 11521–11529, Apr. 2007, doi: 10.1074/JBC.M607279200.
- [38] X. Qi, M. H. Disatnik, N. Shen, R. A. Sobel, and D. Mochly-Rosen, "Aberrant mitochondrial fission in neurons induced by protein kinase C $\{\delta\}$ under oxidative stress conditions in vivo," *Mol Biol Cell*, vol. 22, no. 2, pp. 256–265, Jan. 2011, doi: 10.1091/MBC.E10-06-0551.
- [39] D. I. Kim *et al.*, "A β -Induced Drp1 phosphorylation through Akt activation promotes excessive mitochondrial fission leading to neuronal apoptosis," *Biochim Biophys Acta*, vol. 1863, no. 11, pp. 2820–2834, Nov. 2016, doi: 10.1016/J.BBAMCR.2016.09.003.
- [40] S. Xu *et al.*, "CaMKII induces permeability transition through Drp1 phosphorylation during chronic β -AR stimulation," *Nat Commun*, vol. 7, Oct. 2016, doi: 10.1038/NCOMMS13189.

-
- [41] M. N. Serasinghe *et al.*, "Mitochondrial division is requisite to RAS-induced transformation and targeted by oncogenic MAPK pathway inhibitors," *Mol Cell*, vol. 57, no. 3, pp. 521–536, Feb. 2015, doi: 10.1016/J.MOLCEL.2015.01.003.
- [42] J. A. Kashatus *et al.*, "Erk2 phosphorylation of Drp1 promotes mitochondrial fission and MAPK-driven tumor growth," *Mol Cell*, vol. 57, no. 3, pp. 537–551, Feb. 2015, doi: 10.1016/J.MOLCEL.2015.01.002.
- [43] M. J. Barsoum *et al.*, "Nitric oxide-induced mitochondrial fission is regulated by dynamin-related GTPases in neurons," *EMBO J*, vol. 25, no. 16, pp. 3900–3911, Aug. 2006, doi: 10.1038/SJ.EMBOJ.7601253.
- [44] D. H. Cho *et al.*, "S-nitrosylation of Drp1 mediates beta-amyloid-related mitochondrial fission and neuronal injury," *Science*, vol. 324, no. 5923, pp. 102–105, Apr. 2009, doi: 10.1126/SCIENCE.1171091.
- [45] B. Bossy *et al.*, "S-Nitrosylation of DRP1 does not affect enzymatic activity and is not specific to Alzheimer's disease," *J Alzheimers Dis*, vol. 20 Suppl 2, no. Suppl 2, 2010, doi: 10.3233/JAD-2010-100552.
- [46] M. Karbowski, A. Neutzner, and R. J. Youle, "The mitochondrial E3 ubiquitin ligase MARCH5 is required for Drp1 dependent mitochondrial division," *J Cell Biol*, vol. 178, no. 1, pp. 71–84, Jul. 2007, doi: 10.1083/JCB.200611064.
- [47] H. Wang *et al.*, "Parkin ubiquitinates Drp1 for proteasome-dependent degradation: implication of dysregulated mitochondrial dynamics in Parkinson disease," *J Biol Chem*, vol. 286, no. 13, pp. 11649–11658, Apr. 2011, doi: 10.1074/JBC.M110.144238.
- [48] T. J. Wilson, A. M. Slupe, and S. Strack, "Cell signaling and mitochondrial dynamics: Implications for neuronal function and neurodegenerative disease," *Neurobiol Dis*, vol. 51, pp. 13–26, Mar. 2013, doi: 10.1016/J.NBD.2012.01.009.
- [49] L. Buhlman *et al.*, "Functional interplay between Parkin and Drp1 in mitochondrial fission and clearance," *Biochim Biophys Acta*, vol. 1843, no. 9, pp. 2012–2026, 2014, doi: 10.1016/J.BBAMCR.2014.05.012.
- [50] Z. Harder, R. Zunino, and H. McBride, "Sumo1 conjugates mitochondrial substrates and participates in mitochondrial fission," *Curr Biol*, vol. 14, no. 4, pp. 340–345, Feb. 2004, doi: 10.1016/J.CUB.2004.02.004.

-
- [51] S. Wasiak, R. Zunino, and H. M. McBride, "Bax/Bak promote sumoylation of DRP1 and its stable association with mitochondria during apoptotic cell death," *J Cell Biol*, vol. 177, no. 3, pp. 439–450, May 2007, doi: 10.1083/JCB.200610042.
- [52] E. Braschi, R. Zunino, and H. M. McBride, "MAPL is a new mitochondrial SUMO E3 ligase that regulates mitochondrial fission," *EMBO Rep*, vol. 10, no. 7, pp. 748–754, 2009, doi: 10.1038/EMBOR.2009.86.
- [53] C. Figueroa-Romero *et al.*, "SUMOylation of the mitochondrial fission protein Drp1 occurs at multiple nonconsensus sites within the B domain and is linked to its activity cycle," *FASEB J*, vol. 23, no. 11, pp. 3917–3927, Nov. 2009, doi: 10.1096/FJ.09-136630.
- [54] D. Mukhopadhyay and M. Dasso, "Modification in reverse: the SUMO proteases," *Trends Biochem Sci*, vol. 32, no. 6, pp. 286–295, Jun. 2007, doi: 10.1016/J.TIBS.2007.05.002.
- [55] R. Zunino, A. Schauss, P. Rippstein, M. Andrade-Navarro, and H. M. McBride, "The SUMO protease SENP5 is required to maintain mitochondrial morphology and function," *J Cell Sci*, vol. 120, no. Pt 7, pp. 1178–1188, Apr. 2007, doi: 10.1242/JCS.03418.
- [56] J. Prudent, R. Zunino, A. Sugiura, S. Mattie, G. C. Shore, and H. M. McBride, "MAPL SUMOylation of Drp1 Stabilizes an ER/Mitochondrial Platform Required for Cell Death," *Mol Cell*, vol. 59, no. 6, pp. 941–955, Sep. 2015, doi: 10.1016/J.MOLCEL.2015.08.001.
- [57] E. Q. Toyama *et al.*, "Metabolism. AMP-activated protein kinase mediates mitochondrial fission in response to energy stress," *Science*, vol. 351, no. 6270, pp. 275–281, Jan. 2016, doi: 10.1126/SCIENCE.AAB4138.
- [58] S. Xu *et al.*, "Mitochondrial E3 ubiquitin ligase MARCH5 controls mitochondrial fission and cell sensitivity to stress-induced apoptosis through regulation of MiD49 protein," *Mol Biol Cell*, vol. 27, no. 2, pp. 349–359, Jan. 2016, doi: 10.1091/MBC.E15-09-0678.
- [59] J. E. Lee, L. M. Westrate, H. Wu, C. Page, and G. K. Voeltz, "Multiple dynamin family members collaborate to drive mitochondrial division," *Nature*, vol. 540, no. 7631, pp. 139–143, Dec. 2016, doi: 10.1038/NATURE20555.
- [60] R. Chakrabarti, W. K. Ji, R. v. Stan, J. de J. Sanz, T. A. Ryan, and H. N. Higgs, "INF2-mediated actin polymerization at the ER stimulates mitochondrial calcium uptake, inner membrane constriction, and division," *J Cell Biol*, vol. 217, no. 1, pp. 251–268, Jan. 2018, doi: 10.1083/JCB.201709111.

-
- [61] B. Cho *et al.*, "Constriction of the mitochondrial inner compartment is a priming event for mitochondrial division," *Nat Commun*, vol. 8, no. 1, 2017, doi: 10.1038/NCOMMS15754.
- [62] T. Brandt, L. Cavellini, W. Kühlbrandt, and M. M. Cohen, "A mitofusin-dependent docking ring complex triggers mitochondrial fusion in vitro," *Elife*, vol. 5, no. JUNE2016, Jun. 2016, doi: 10.7554/ELIFE.14618.
- [63] N. Ishihara, Y. Eura, and K. Mihara, "Mitofusin 1 and 2 play distinct roles in mitochondrial fusion reactions via GTPase activity," *J Cell Sci*, vol. 117, no. Pt 26, pp. 6535–6546, Dec. 2004, doi: 10.1242/JCS.01565.
- [64] B. B. Kirschbaum and H. B. Bosmann, "Studies of enzymes involved in glycoprotein synthesis and degradation in diacetylbenzidine nephrosis," *J Med*, vol. 6, no. 1, pp. 97–106, 1975, Accessed: Feb. 18, 2022. [Online]. Available: <https://pubmed.ncbi.nlm.nih.gov/124759/>
- [65] S. Cipolat, O. M. de Brito, B. Dal Zilio, and L. Scorrano, "OPA1 requires mitofusin 1 to promote mitochondrial fusion," *Proc Natl Acad Sci U S A*, vol. 101, no. 45, pp. 15927–15932, Nov. 2004, doi: 10.1073/PNAS.0407043101.
- [66] S. Hoppins *et al.*, "The soluble form of Bax regulates mitochondrial fusion via MFN2 homotypic complexes," *Mol Cell*, vol. 41, no. 2, pp. 150–160, Jan. 2011, doi: 10.1016/J.MOLCEL.2010.11.030.
- [67] M. Rojo, F. Legros, D. Chateau, and A. Lombès, "Membrane topology and mitochondrial targeting of mitofusins, ubiquitous mammalian homologs of the transmembrane GTPase Fzo," *J Cell Sci*, vol. 115, no. Pt 8, pp. 1663–1674, May 2002, doi: 10.1242/JCS.115.8.1663.
- [68] L. Pernas and L. Scorrano, "Mito-Morphosis: Mitochondrial Fusion, Fission, and Cristae Remodeling as Key Mediators of Cellular Function," *Annu Rev Physiol*, vol. 78, pp. 505–531, Feb. 2016, doi: 10.1146/ANNUREV-PHYSIOL-021115-105011.
- [69] O. M. de Brito and L. Scorrano, "Mitofusin 2 tethers endoplasmic reticulum to mitochondria," *Nature*, vol. 456, no. 7222, pp. 605–610, Dec. 2008, doi: 10.1038/NATURE07534.
- [70] A. Misko, S. Jiang, I. Wegorzewska, J. Milbrandt, and R. H. Baloh, "Mitofusin 2 is necessary for transport of axonal mitochondria and interacts with the Miro/Milton

- complex," *J Neurosci*, vol. 30, no. 12, pp. 4232–4240, Mar. 2010, doi: 10.1523/JNEUROSCI.6248-09.2010.
- [71] C. Delettre *et al.*, "Mutation spectrum and splicing variants in the OPA1 gene," *Hum Genet*, vol. 109, no. 6, pp. 584–591, 2001, doi: 10.1007/S00439-001-0633-Y.
- [72] A. Olichon, G. ElAchouri, L. Baricault, C. Delettre, P. Belenguer, and G. Lenaers, "OPA1 alternate splicing uncouples an evolutionary conserved function in mitochondrial fusion from a vertebrate restricted function in apoptosis," *Cell Death Differ*, vol. 14, no. 4, pp. 682–692, Apr. 2007, doi: 10.1038/SJ.CDD.4402048.
- [73] P. Belenguer and L. Pellegrini, "The dynamin GTPase OPA1: more than mitochondria?," *Biochim Biophys Acta*, vol. 1833, no. 1, pp. 176–183, Jan. 2013, doi: 10.1016/J.BBAMCR.2012.08.004.
- [74] T. MacVicar and T. Langer, "OPA1 processing in cell death and disease - the long and short of it," *J Cell Sci*, vol. 129, no. 12, pp. 2297–2306, Jun. 2016, doi: 10.1242/JCS.159186.
- [75] N. Ishihara, Y. Fujita, T. Oka, and K. Mihara, "Regulation of mitochondrial morphology through proteolytic cleavage of OPA1," *EMBO J*, vol. 25, no. 13, pp. 2966–2977, Jul. 2006, doi: 10.1038/SJ.EMBOJ.7601184.
- [76] R. Anand *et al.*, "The i-AAA protease YME1L and OMA1 cleave OPA1 to balance mitochondrial fusion and fission," *J Cell Biol*, vol. 204, no. 6, pp. 919–929, 2014, doi: 10.1083/JCB.201308006.
- [77] S. Ehses *et al.*, "Regulation of OPA1 processing and mitochondrial fusion by m-AAA protease isoenzymes and OMA1," *J Cell Biol*, vol. 187, no. 7, pp. 1023–1036, Dec. 2009, doi: 10.1083/JCB.200906084.
- [78] B. Head, L. Griparic, M. Amiri, S. Gandre-Babbe, and A. M. van der Bliek, "Inducible proteolytic inactivation of OPA1 mediated by the OMA1 protease in mammalian cells," *J Cell Biol*, vol. 187, no. 7, pp. 959–966, Dec. 2009, doi: 10.1083/JCB.200906083.
- [79] M. J. Baker *et al.*, "Stress-induced OMA1 activation and autocatalytic turnover regulate OPA1-dependent mitochondrial dynamics," *EMBO J*, vol. 33, no. 6, pp. 578–593, Mar. 2014, doi: 10.1002/EMBJ.201386474.
- [80] E. Jones *et al.*, "A threshold of transmembrane potential is required for mitochondrial dynamic balance mediated by DRP1 and OMA1," *Cell Mol Life Sci*, vol. 74, no. 7, pp. 1347–1363, Apr. 2017, doi: 10.1007/S00018-016-2421-9.

-
- [81] P. Mishra, V. Carelli, G. Manfredi, and D. C. Chan, "Proteolytic cleavage of Opa1 stimulates mitochondrial inner membrane fusion and couples fusion to oxidative phosphorylation," *Cell Metab*, vol. 19, no. 4, pp. 630–641, Apr. 2014, doi: 10.1016/J.CMET.2014.03.011.
- [82] V. del Dotto, M. Fogazza, V. Carelli, M. Rugolo, and C. Zanna, "Eight human OPA1 isoforms, long and short: What are they for?," *Biochim Biophys Acta Bioenerg*, vol. 1859, no. 4, pp. 263–269, Apr. 2018, doi: 10.1016/J.BBABIO.2018.01.005.
- [83] S. Cogliati *et al.*, "Mitochondrial cristae shape determines respiratory chain supercomplexes assembly and respiratory efficiency," *Cell*, vol. 155, no. 1, pp. 160–171, Sep. 2013, doi: 10.1016/J.CELL.2013.08.032.
- [84] D. A. Patten *et al.*, "OPA1-dependent cristae modulation is essential for cellular adaptation to metabolic demand," *EMBO J*, vol. 33, no. 22, pp. 2676–2691, Nov. 2014, doi: 10.15252/EMBJ.201488349.
- [85] L. C. Gomes and L. Scorrano, "Mitochondrial elongation during autophagy: a stereotypical response to survive in difficult times," *Autophagy*, vol. 7, no. 10, pp. 1251–1253, 2011, doi: 10.4161/AUTO.7.10.16771.
- [86] C. Frezza *et al.*, "OPA1 controls apoptotic cristae remodeling independently from mitochondrial fusion," *Cell*, vol. 126, no. 1, pp. 177–189, Jul. 2006, doi: 10.1016/J.CELL.2006.06.025.
- [87] S. Cipolat *et al.*, "Mitochondrial rhomboid PARL regulates cytochrome c release during apoptosis via OPA1-dependent cristae remodeling," *Cell*, vol. 126, no. 1, pp. 163–175, Jul. 2006, doi: 10.1016/J.CELL.2006.06.021.
- [88] A. Olichon *et al.*, "Loss of OPA1 perturbs the mitochondrial inner membrane structure and integrity, leading to cytochrome c release and apoptosis," *J Biol Chem*, vol. 278, no. 10, pp. 7743–7746, Mar. 2003, doi: 10.1074/JBC.C200677200.
- [89] S. Meeusen *et al.*, "Mitochondrial inner-membrane fusion and crista maintenance requires the dynamin-related GTPase Mgm1," *Cell*, vol. 127, no. 2, pp. 383–395, Oct. 2006, doi: 10.1016/J.CELL.2006.09.021.
- [90] T. Varanita *et al.*, "The OPA1-dependent mitochondrial cristae remodeling pathway controls atrophic, apoptotic, and ischemic tissue damage," *Cell Metab*, vol. 21, no. 6, pp. 834–844, Jun. 2015, doi: 10.1016/J.CMET.2015.05.007.

-
- [91] R. E. Ellis, J. Yuan, and H. R. Horvitz, "Mechanisms and functions of cell death," *Annu Rev Cell Biol*, vol. 7, pp. 663–698, 1991, doi: 10.1146/ANNUREV.CB.07.110191.003311.
- [92] G. Kroemer *et al.*, "Classification of cell death: recommendations of the Nomenclature Committee on Cell Death 2009," *Cell Death Differ*, vol. 16, no. 1, pp. 3–11, 2009, doi: 10.1038/CDD.2008.150.
- [93] A. Antignani and R. J. Youle, "How do Bax and Bak lead to permeabilization of the outer mitochondrial membrane?," *Curr Opin Cell Biol*, vol. 18, no. 6, pp. 685–689, Dec. 2006, doi: 10.1016/J.CEB.2006.10.004.
- [94] L. Scorrano *et al.*, "A distinct pathway remodels mitochondrial cristae and mobilizes cytochrome c during apoptosis," *Dev Cell*, vol. 2, no. 1, pp. 55–67, 2002, doi: 10.1016/S1534-5807(01)00116-2.
- [95] P. Li *et al.*, "Cytochrome c and dATP-dependent formation of Apaf-1/caspase-9 complex initiates an apoptotic protease cascade," *Cell*, vol. 91, no. 4, pp. 479–489, Nov. 1997, doi: 10.1016/S0092-8674(00)80434-1.
- [96] S. Frank *et al.*, "The role of dynamin-related protein 1, a mediator of mitochondrial fission, in apoptosis," *Dev Cell*, vol. 1, no. 4, pp. 515–525, Oct. 2001, doi: 10.1016/S1534-5807(01)00055-7.
- [97] A. Cassidy-Stone *et al.*, "Chemical inhibition of the mitochondrial division dynamin reveals its role in Bax/Bak-dependent mitochondrial outer membrane permeabilization," *Dev Cell*, vol. 14, no. 2, pp. 193–204, Feb. 2008, doi: 10.1016/J.DEVCEL.2007.11.019.
- [98] J. Estaquier and D. Arnoult, "Inhibiting Drp1-mediated mitochondrial fission selectively prevents the release of cytochrome c during apoptosis," *Cell Death Differ*, vol. 14, no. 6, pp. 1086–1094, Jun. 2007, doi: 10.1038/SJ.CDD.4402107.
- [99] Y. J. Lee, S. Y. Jeong, M. Karbowski, C. L. Smith, and R. J. Youle, "Roles of the mammalian mitochondrial fission and fusion mediators Fis1, Drp1, and Opa1 in apoptosis," *Mol Biol Cell*, vol. 15, no. 11, pp. 5001–5011, Nov. 2004, doi: 10.1091/MBC.E04-04-0294.
- [100] G. P. Leboucher *et al.*, "Stress-induced phosphorylation and proteasomal degradation of mitofusin 2 facilitates mitochondrial fragmentation and apoptosis," *Mol Cell*, vol. 47, no. 4, pp. 547–557, Aug. 2012, doi: 10.1016/J.MOLCEL.2012.05.041.

-
- [101] T. Tatsuta and T. Langer, "AAA proteases in mitochondria: diverse functions of membrane-bound proteolytic machines," *Res Microbiol*, vol. 160, no. 9, pp. 711–717, Nov. 2009, doi: 10.1016/J.RESMIC.2009.09.005.
- [102] A. Neutzner, R. J. Youle, and M. Karbowski, "Outer mitochondrial membrane protein degradation by the proteasome," *Novartis Found Symp*, vol. 287, pp. 4–14, 2007, Accessed: Feb. 18, 2022. [Online]. Available: <https://pubmed.ncbi.nlm.nih.gov/18074628/>
- [103] A. Tanaka *et al.*, "Proteasome and p97 mediate mitophagy and degradation of mitofusins induced by Parkin," *J Cell Biol*, vol. 191, no. 7, pp. 1367–1380, Dec. 2010, doi: 10.1083/JCB.201007013.
- [104] S. Xu, G. Peng, Y. Wang, S. Fang, and M. Karbowski, "The AAA-ATPase p97 is essential for outer mitochondrial membrane protein turnover," *Mol Biol Cell*, vol. 22, no. 3, pp. 291–300, Feb. 2011, doi: 10.1091/MBC.E10-09-0748.
- [105] C. Hemion, J. Flammer, and A. Neutzner, "Quality control of oxidatively damaged mitochondrial proteins is mediated by p97 and the proteasome," *Free Radic Biol Med*, vol. 75, pp. 121–128, 2014, doi: 10.1016/J.FREERADBIOMED.2014.07.016.
- [106] G. Ashrafi and T. L. Schwarz, "The pathways of mitophagy for quality control and clearance of mitochondria," *Cell Death Differ*, vol. 20, no. 1, pp. 31–42, Jan. 2013, doi: 10.1038/CDD.2012.81.
- [107] S. M. Jin, M. Lazarou, C. Wang, L. A. Kane, D. P. Narendra, and R. J. Youle, "Mitochondrial membrane potential regulates PINK1 import and proteolytic destabilization by PARL," *J Cell Biol*, vol. 191, no. 5, pp. 933–942, Nov. 2010, doi: 10.1083/JCB.201008084.
- [108] A. W. Greene *et al.*, "Mitochondrial processing peptidase regulates PINK1 processing, import and Parkin recruitment," *EMBO Rep*, vol. 13, no. 4, pp. 378–385, Apr. 2012, doi: 10.1038/EMBOR.2012.14.
- [109] C. Kondapalli *et al.*, "PINK1 is activated by mitochondrial membrane potential depolarization and stimulates Parkin E3 ligase activity by phosphorylating Serine 65," *Open Biol*, vol. 2, no. 5, 2012, doi: 10.1098/RSOB.120080.
- [110] M. Lazarou, S. M. Jin, L. A. Kane, and R. J. Youle, "Role of PINK1 binding to the TOM complex and alternate intracellular membranes in recruitment and activation of the E3

-
- ligase Parkin," *Dev Cell*, vol. 22, no. 2, pp. 320–333, Feb. 2012, doi: 10.1016/J.DEVCEL.2011.12.014.
- [111] K. Yamano and R. J. Youle, "PINK1 is degraded through the N-end rule pathway," *Autophagy*, vol. 9, no. 11, pp. 1758–1769, 2013, doi: 10.4161/AUTO.24633.
- [112] A. Eiyama and K. Okamoto, "PINK1/Parkin-mediated mitophagy in mammalian cells," *Curr Opin Cell Biol*, vol. 33, pp. 95–101, Apr. 2015, doi: 10.1016/J.CEB.2015.01.002.
- [113] H. Sandoval *et al.*, "Essential role for Nix in autophagic maturation of erythroid cells," *Nature*, vol. 454, no. 7201, pp. 232–235, Jul. 2008, doi: 10.1038/NATURE07006.
- [114] L. Liu *et al.*, "Mitochondrial outer-membrane protein FUNDC1 mediates hypoxia-induced mitophagy in mammalian cells," *Nat Cell Biol*, vol. 14, no. 2, pp. 177–185, Feb. 2012, doi: 10.1038/NCB2422.
- [115] F. Strappazzon *et al.*, "AMBRA1 is able to induce mitophagy via LC3 binding, regardless of PARKIN and p62/SQSTM1," *Cell Death Differ*, vol. 22, no. 3, p. 517, 2015, doi: 10.1038/CDD.2014.190.
- [116] S. Campello, F. Strappazzon, and F. Cecconi, "Mitochondrial dismissal in mammals, from protein degradation to mitophagy," *Biochim Biophys Acta*, vol. 1837, no. 4, pp. 451–460, 2014, doi: 10.1016/J.BBABIO.2013.11.010.
- [117] T. Y. Kim *et al.*, "Metabolic labeling reveals proteome dynamics of mouse mitochondria," *Mol Cell Proteomics*, vol. 11, no. 12, pp. 1586–1594, 2012, doi: 10.1074/MCP.M112.021162.
- [118] G. Twig *et al.*, "Fission and selective fusion govern mitochondrial segregation and elimination by autophagy," *EMBO J*, vol. 27, no. 2, pp. 433–446, Jan. 2008, doi: 10.1038/SJ.EMBOJ.7601963.
- [119] M. Neuspiel *et al.*, "Cargo-selected transport from the mitochondria to peroxisomes is mediated by vesicular carriers," *Curr Biol*, vol. 18, no. 2, pp. 102–108, Jan. 2008, doi: 10.1016/J.CUB.2007.12.038.
- [120] V. Soubannier *et al.*, "A vesicular transport pathway shuttles cargo from mitochondria to lysosomes," *Curr Biol*, vol. 22, no. 2, pp. 135–141, Jan. 2012, doi: 10.1016/J.CUB.2011.11.057.
- [121] V. Soubannier, P. Rippstein, B. A. Kaufman, E. A. Shoubridge, and H. M. McBride, "Reconstitution of mitochondria derived vesicle formation demonstrates selective

- enrichment of oxidized cargo," *PLoS One*, vol. 7, no. 12, Dec. 2012, doi: 10.1371/JOURNAL.PONE.0052830.
- [122] G. L. McLelland, V. Soubannier, C. X. Chen, H. M. McBride, and E. A. Fon, "Parkin and PINK1 function in a vesicular trafficking pathway regulating mitochondrial quality control," *EMBO J*, vol. 33, no. 4, pp. 282–295, Feb. 2014, doi: 10.1002/EMBJ.201385902.
- [123] A. Sugiura, G. McLelland, E. A. Fon, and H. M. McBride, "A new pathway for mitochondrial quality control: mitochondrial-derived vesicles," *EMBO J*, vol. 33, no. 19, pp. 2142–2156, Oct. 2014, doi: 10.15252/EMBJ.201488104.
- [124] L. A. Kane *et al.*, "PINK1 phosphorylates ubiquitin to activate Parkin E3 ubiquitin ligase activity," *J Cell Biol*, vol. 205, no. 2, pp. 143–153, 2014, doi: 10.1083/JCB.201402104.
- [125] A. Kazlauskaitė *et al.*, "Parkin is activated by PINK1-dependent phosphorylation of ubiquitin at Ser65," *Biochem J*, vol. 460, no. 1, pp. 127–139, May 2014, doi: 10.1042/BJ20140334.
- [126] S. E. Horvath and G. Daum, "Lipids of mitochondria," *Prog Lipid Res*, vol. 52, no. 4, pp. 590–614, 2013, doi: 10.1016/J.PLIPRES.2013.07.002.
- [127] A. Mohanty and H. M. McBride, "Emerging roles of mitochondria in the evolution, biogenesis, and function of peroxisomes," *Front Physiol*, vol. 4, 2013, doi: 10.3389/FPHYS.2013.00268.
- [128] A. S. Benischke, C. Hemion, J. Flammer, and A. Neutzner, "Proteasome-mediated quality control of S-nitrosylated mitochondrial proteins," *Mitochondrion*, vol. 17, pp. 182–186, 2014, doi: 10.1016/J.MITO.2014.04.001.
- [129] N. Panicker, V. L. Dawson, and T. M. Dawson, "Activation mechanisms of the E3 ubiquitin ligase parkin," *Biochem J*, vol. 474, no. 18, pp. 3075–3086, Sep. 2017, doi: 10.1042/BCJ20170476.
- [130] R. Budhidarmo, Y. Nakatani, and C. L. Day, "RINGs hold the key to ubiquitin transfer," *Trends Biochem Sci*, vol. 37, no. 2, pp. 58–65, Feb. 2012, doi: 10.1016/J.TIBS.2011.11.001.
- [131] Y. T. Kwon and A. Ciechanover, "The Ubiquitin Code in the Ubiquitin-Proteasome System and Autophagy," *Trends Biochem Sci*, vol. 42, no. 11, pp. 873–886, Nov. 2017, doi: 10.1016/J.TIBS.2017.09.002.

-
- [132] H. C. Kim and J. M. Huibregtse, "Polyubiquitination by HECT E3s and the determinants of chain type specificity," *Mol Cell Biol*, vol. 29, no. 12, pp. 3307–3318, Jun. 2009, doi: 10.1128/MCB.00240-09.
- [133] D. E. Spratt, H. Walden, and G. S. Shaw, "RBR E3 ubiquitin ligases: new structures, new insights, new questions," *Biochem J*, vol. 458, no. 3, pp. 421–437, Mar. 2014, doi: 10.1042/BJ20140006.
- [134] D. Chhangani, A. P. Joshi, and A. Mishra, "E3 ubiquitin ligases in protein quality control mechanism," *Mol Neurobiol*, vol. 45, no. 3, pp. 571–585, 2012, doi: 10.1007/S12035-012-8273-X.
- [135] H. J. Meyer and M. Rape, "Enhanced protein degradation by branched ubiquitin chains," *Cell*, vol. 157, no. 4, pp. 910–921, May 2014, doi: 10.1016/J.CELL.2014.03.037.
- [136] D. Voges, P. Zwickl, and W. Baumeister, "The 26S proteasome: a molecular machine designed for controlled proteolysis," *Annu Rev Biochem*, vol. 68, pp. 1015–1068, 1999, doi: 10.1146/ANNUREV.BIOCHEM.68.1.1015.
- [137] R. Rosenzweig, V. Bronner, D. Zhang, D. Fushman, and M. H. Glickman, "Rpn1 and Rpn2 coordinate ubiquitin processing factors at proteasome," *J Biol Chem*, vol. 287, no. 18, pp. 14659–14671, Apr. 2012, doi: 10.1074/JBC.M111.316323.
- [138] E. Koulich, X. Li, and G. N. DeMartino, "Relative structural and functional roles of multiple deubiquitylating proteins associated with mammalian 26S proteasome," *Mol Biol Cell*, vol. 19, no. 3, pp. 1072–1082, Mar. 2008, doi: 10.1091/MBC.E07-10-1040.
- [139] Y. Saeki, A. Toh-E, and H. Yokosawa, "Rapid isolation and characterization of the yeast proteasome regulatory complex," *Biochem Biophys Res Commun*, vol. 273, no. 2, pp. 509–515, Jul. 2000, doi: 10.1006/BBRC.2000.2980.
- [140] B. Ehring, T. H. Meyer, C. Eckerskorn, F. Lottspeich, and R. Tampé, "Effects of major-histocompatibility-complex-encoded subunits on the peptidase and proteolytic activities of human 20S proteasomes. Cleavage of proteins and antigenic peptides," *Eur J Biochem*, vol. 235, no. 1–2, pp. 404–415, 1996, doi: 10.1111/J.1432-1033.1996.00404.X.
- [141] K. U. Kalies, S. Allan, T. Sergeyenko, H. Kröger, and K. Römisch, "The protein translocation channel binds proteasomes to the endoplasmic reticulum membrane," *EMBO J*, vol. 24, no. 13, pp. 2284–2293, Jul. 2005, doi: 10.1038/SJ.EMBOJ.7600731.

-
- [142] W. Ng, T. Sergeyenko, N. Zeng, J. D. Brown, and K. Römisch, "Characterization of the proteasome interaction with the Sec61 channel in the endoplasmic reticulum," *J Cell Sci*, vol. 120, no. Pt 4, pp. 682–691, Feb. 2007, doi: 10.1242/JCS.03351.
- [143] D. Komander, M. J. Clague, and S. Urbé, "Breaking the chains: structure and function of the deubiquitinases," *Nat Rev Mol Cell Biol*, vol. 10, no. 8, pp. 550–563, Aug. 2009, doi: 10.1038/NRM2731.
- [144] J. van den Boom and H. Meyer, "VCP/p97-Mediated Unfolding as a Principle in Protein Homeostasis and Signaling," *Mol Cell*, vol. 69, no. 2, pp. 182–194, Jan. 2018, doi: 10.1016/J.MOLCEL.2017.10.028.
- [145] C. Song, Q. Wang, and C. C. H. Li, "ATPase activity of p97-valosin-containing protein (VCP). D2 mediates the major enzyme activity, and D1 contributes to the heat-induced activity," *J Biol Chem*, vol. 278, no. 6, pp. 3648–3655, Feb. 2003, doi: 10.1074/JBC.M208422200.
- [146] Q. Wang, C. Song, and C. C. H. Li, "Hexamerization of p97-VCP is promoted by ATP binding to the D1 domain and required for ATPase and biological activities," *Biochem Biophys Res Commun*, vol. 300, no. 2, pp. 253–260, Jan. 2003, doi: 10.1016/S0006-291X(02)02840-1.
- [147] H. Meyer, "p97 complexes as signal integration hubs," *BMC Biol*, vol. 10, Jun. 2012, doi: 10.1186/1741-7007-10-48.
- [148] H. Meyer, M. Bug, and S. Bremer, "Emerging functions of the VCP/p97 AAA-ATPase in the ubiquitin system," *Nat Cell Biol*, vol. 14, no. 2, pp. 117–123, Feb. 2012, doi: 10.1038/NCB2407.
- [149] A. Franz, L. Ackermann, and T. Hoppe, "Create and preserve: proteostasis in development and aging is governed by Cdc48/p97/VCP," *Biochim Biophys Acta*, vol. 1843, no. 1, pp. 205–215, Jan. 2014, doi: 10.1016/J.BBAMCR.2013.03.031.
- [150] Y. Ye, W. K. Tang, T. Zhang, and D. Xia, "A Mighty 'Protein Extractor' of the Cell: Structure and Function of the p97/CDC48 ATPase," *Front Mol Biosci*, vol. 4, no. JUN, Jun. 2017, doi: 10.3389/FMOLB.2017.00039.
- [151] C. Wójcik *et al.*, "Valosin-containing protein (p97) is a regulator of endoplasmic reticulum stress and of the degradation of N-end rule and ubiquitin-fusion degradation

- pathway substrates in mammalian cells," *Mol Biol Cell*, vol. 17, no. 11, pp. 4606–4618, Nov. 2006, doi: 10.1091/MBC.E06-05-0432.
- [152] D. H. Wolf and A. Stolz, "The Cdc48 machine in endoplasmic reticulum associated protein degradation," *Biochim Biophys Acta*, vol. 1823, no. 1, pp. 117–124, Jan. 2012, doi: 10.1016/J.BBAMCR.2011.09.002.
- [153] S. S. Vembar and J. L. Brodsky, "One step at a time: endoplasmic reticulum-associated degradation," *Nat Rev Mol Cell Biol*, vol. 9, no. 12, pp. 944–957, Dec. 2008, doi: 10.1038/NRM2546.
- [154] Y. Ye, H. H. Meyer, and T. A. Rapoport, "The AAA ATPase Cdc48/p97 and its partners transport proteins from the ER into the cytosol," *Nature*, vol. 414, no. 6864, pp. 652–656, Dec. 2001, doi: 10.1038/414652A.
- [155] I. Kim *et al.*, "The Png1-Rad23 complex regulates glycoprotein turnover," *J Cell Biol*, vol. 172, no. 2, pp. 211–219, Jan. 2006, doi: 10.1083/JCB.200507149.
- [156] M. Koegl, T. Hoppe, S. Schlenker, H. D. Ulrich, T. U. Mayer, and S. Jentsch, "A novel ubiquitination factor, E4, is involved in multiubiquitin chain assembly," *Cell*, vol. 96, no. 5, pp. 635–644, Mar. 1999, doi: 10.1016/S0092-8674(00)80574-7.
- [157] X. Zhong and R. N. Pittman, "Ataxin-3 binds VCP/p97 and regulates retrotranslocation of ERAD substrates," *Hum Mol Genet*, vol. 15, no. 16, pp. 2409–2420, Aug. 2006, doi: 10.1093/HMG/DDL164.
- [158] E. Tresse *et al.*, "VCP/p97 is essential for maturation of ubiquitin-containing autophagosomes and this function is impaired by mutations that cause IBMPFD," *Autophagy*, vol. 6, no. 2, pp. 217–227, Feb. 2010, doi: 10.4161/AUTO.6.2.11014.
- [159] H. Richly, M. Rape, S. Braun, S. Rumpf, C. Hoegel, and S. Jentsch, "A series of ubiquitin binding factors connects CDC48/p97 to substrate multiubiquitylation and proteasomal targeting," *Cell*, vol. 120, no. 1, pp. 73–84, Jan. 2005, doi: 10.1016/J.CELL.2004.11.013.
- [160] S. Bohm, G. Lamberti, V. Fernandez-Saiz, C. Stapf, and A. Buchberger, "Cellular functions of Ufd2 and Ufd3 in proteasomal protein degradation depend on Cdc48 binding," *Mol Cell Biol*, vol. 31, no. 7, pp. 1528–1539, Apr. 2011, doi: 10.1128/MCB.00962-10.
- [161] L. G. G. C. Verhoef, C. Heinen, A. Selivanova, E. F. Halff, F. A. Salomons, and N. P. Dantuma, "Minimal length requirement for proteasomal degradation of ubiquitin-

- dependent substrates," *FASEB J*, vol. 23, no. 1, pp. 123–133, Jan. 2009, doi: 10.1096/FJ.08-115055.
- [162] C. Song, Q. Wang, C. Song, and T. J. Rogers, "Valosin-containing protein (VCP/p97) is capable of unfolding polyubiquitinated proteins through its ATPase domains," *Biochem Biophys Res Commun*, vol. 463, no. 3, pp. 453–457, Jun. 2015, doi: 10.1016/J.BBRC.2015.05.111.
- [163] Y. Ye, H. H. Meyer, and T. A. Rapoport, "Function of the p97-Ufd1-Npl4 complex in retrotranslocation from the ER to the cytosol: dual recognition of nonubiquitinated polypeptide segments and polyubiquitin chains," *J Cell Biol*, vol. 162, no. 1, pp. 71–84, Jul. 2003, doi: 10.1083/JCB.200302169.
- [164] Q. Wang, A. Li, and Y. Ye, "Inhibition of p97-dependent protein degradation by Eeyarestatin I," *J Biol Chem*, vol. 283, no. 12, pp. 7445–7454, Mar. 2008, doi: 10.1074/JBC.M708347200.
- [165] M. Kothe *et al.*, "Role of p97 AAA-ATPase in the retrotranslocation of the cholera toxin A1 chain, a non-ubiquitinated substrate," *J Biol Chem*, vol. 280, no. 30, pp. 28127–28132, Jul. 2005, doi: 10.1074/JBC.M503138200.
- [166] J. M. Heo *et al.*, "A stress-responsive system for mitochondrial protein degradation," *Mol Cell*, vol. 40, no. 3, pp. 465–480, Nov. 2010, doi: 10.1016/J.MOLCEL.2010.10.021.
- [167] M. Karbowski and R. J. Youle, "Regulating mitochondrial outer membrane proteins by ubiquitination and proteasomal degradation," *Curr Opin Cell Biol*, vol. 23, no. 4, pp. 476–482, Aug. 2011, doi: 10.1016/J.CEB.2011.05.007.
- [168] P. Wild and I. Dikic, "Mitochondria get a Parkin' ticket," *Nat Cell Biol*, vol. 12, no. 2, pp. 104–106, Feb. 2010, doi: 10.1038/NCB0210-104.
- [169] Y. Xu, D. E. Anderson, and Y. Ye, "The HECT domain ubiquitin ligase HUWE1 targets unassembled soluble proteins for degradation," *Cell Discov*, vol. 2, Nov. 2016, doi: 10.1038/CELLDISC.2016.40.
- [170] J. S. Ju, S. E. Miller, P. I. Hanson, and C. C. Weihl, "Impaired protein aggregate handling and clearance underlie the pathogenesis of p97/VCP-associated disease," *J Biol Chem*, vol. 283, no. 44, pp. 30289–30299, Oct. 2008, doi: 10.1074/JBC.M805517200.

-
- [171] S. M. Doyle, O. Genest, and S. Wickner, "Protein rescue from aggregates by powerful molecular chaperone machines," *Nat Rev Mol Cell Biol*, vol. 14, no. 10, pp. 617–629, 2013, doi: 10.1038/NRM3660.
- [172] A. Franz, L. Ackermann, and T. Hoppe, "Ring of Change: CDC48/p97 Drives Protein Dynamics at Chromatin," *Front Genet*, vol. 7, no. MAY, May 2016, doi: 10.3389/FGENE.2016.00073.
- [173] C. Schuberth and A. Buchberger, "UBX domain proteins: major regulators of the AAA ATPase Cdc48/p97," *Cell Mol Life Sci*, vol. 65, no. 15, pp. 2360–2371, Aug. 2008, doi: 10.1007/S00018-008-8072-8.
- [174] C. Stapf, E. Cartwright, M. Bycroft, K. Hofmann, and A. Buchberger, "The general definition of the p97/valosin-containing protein (VCP)-interacting motif (VIM) delineates a new family of p97 cofactors," *J Biol Chem*, vol. 286, no. 44, pp. 38670–38678, Nov. 2011, doi: 10.1074/JBC.M111.274472.
- [175] A. Boeddrich *et al.*, "An arginine/lysine-rich motif is crucial for VCP/p97-mediated modulation of ataxin-3 fibrillogenesis," *EMBO J*, vol. 25, no. 7, pp. 1547–1558, Apr. 2006, doi: 10.1038/SJ.EMBOJ.7601043.
- [176] R. M. Bruderer, C. Bresseur, and H. H. Meyer, "The AAA ATPase p97/VCP interacts with its alternative co-factors, Ufd1-Npl4 and p47, through a common bipartite binding mechanism," *J Biol Chem*, vol. 279, no. 48, pp. 49609–49616, Nov. 2004, doi: 10.1074/JBC.M408695200.
- [177] F. Trusch *et al.*, "The N-terminal Region of the Ubiquitin Regulatory X (UBX) Domain-containing Protein 1 (UBXD1) Modulates Interdomain Communication within the Valosin-containing Protein p97," *J Biol Chem*, vol. 290, no. 49, pp. 29414–29427, Dec. 2015, doi: 10.1074/JBC.M115.680686.
- [178] P. Hänzelmann and H. Schindelin, "The Interplay of Cofactor Interactions and Post-translational Modifications in the Regulation of the AAA+ ATPase p97," *Front Mol Biosci*, vol. 4, no. APR, Apr. 2017, doi: 10.3389/FMOLB.2017.00021.
- [179] A. Buchberger, M. J. Howard, M. Proctor, and M. Bycroft, "The UBX domain: a widespread ubiquitin-like module," *J Mol Biol*, vol. 307, no. 1, pp. 17–24, Mar. 2001, doi: 10.1006/JMBI.2000.4462.

-
- [180] J. H. Hurley, S. Lee, and G. Prag, "Ubiquitin-binding domains," *Biochem J*, vol. 399, no. 3, pp. 361–372, Nov. 2006, doi: 10.1042/BJ20061138.
- [181] G. Alexandru, J. Graumann, G. T. Smith, N. J. Kolawa, R. Fang, and R. J. Deshaies, "UBXD7 binds multiple ubiquitin ligases and implicates p97 in HIF1alpha turnover," *Cell*, vol. 134, no. 5, pp. 804–816, Sep. 2008, doi: 10.1016/J.CELL.2008.06.048.
- [182] H. H. Meyer, J. G. Shorter, J. Seemann, D. Pappin, and G. Warren, "A complex of mammalian ufd1 and npl4 links the AAA-ATPase, p97, to ubiquitin and nuclear transport pathways," *EMBO J*, vol. 19, no. 10, pp. 2181–2192, May 2000, doi: 10.1093/EMBOJ/19.10.2181.
- [183] N. W. Bays, S. K. Wilhovsky, A. Goradia, K. Hodgkiss-Harlow, and R. Y. Hampton, "HRD4/NPL4 is required for the proteasomal processing of ubiquitinated ER proteins," *Mol Biol Cell*, vol. 12, no. 12, pp. 4114–4128, 2001, doi: 10.1091/MBC.12.12.4114.
- [184] S. Raasi and D. H. Wolf, "Ubiquitin receptors and ERAD: a network of pathways to the proteasome," *Semin Cell Dev Biol*, vol. 18, no. 6, pp. 780–791, 2007, doi: 10.1016/J.SEMCDB.2007.09.008.
- [185] L. Madsen *et al.*, "Ubx1 is a novel co-factor of the human p97 ATPase," *Int J Biochem Cell Biol*, vol. 40, no. 12, pp. 2927–2942, 2008, doi: 10.1016/J.BIOCEL.2008.06.008.
- [186] D. S. Haines *et al.*, "Protein interaction profiling of the p97 adaptor UBXD1 points to a role for the complex in modulating ERGIC-53 trafficking," *Mol Cell Proteomics*, vol. 11, no. 6, Jun. 2012, doi: 10.1074/MCP.M111.016444.
- [187] P. Kirchner, M. Bug, and H. Meyer, "Ubiquitination of the N-terminal region of caveolin-1 regulates endosomal sorting by the VCP/p97 AAA-ATPase," *J Biol Chem*, vol. 288, no. 10, pp. 7363–7372, Mar. 2013, doi: 10.1074/JBC.M112.429076.
- [188] D. Ritz *et al.*, "Endolysosomal sorting of ubiquitylated caveolin-1 is regulated by VCP and UBXD1 and impaired by VCP disease mutations," *Nat Cell Biol*, vol. 13, no. 9, pp. 1116–1124, Sep. 2011, doi: 10.1038/NCB2301.
- [189] C. Papadopoulos *et al.*, "VCP/p97 cooperates with YOD1, UBXD1 and PLAA to drive clearance of ruptured lysosomes by autophagy," *EMBO J*, vol. 36, no. 2, pp. 135–150, Jan. 2017, doi: 10.15252/EMBJ.201695148.

-
- [190] X. Guo and X. Qi, "VCP cooperates with UBXD1 to degrade mitochondrial outer membrane protein MCL1 in model of Huntington's disease," *Biochim Biophys Acta Mol Basis Dis*, vol. 1863, no. 2, pp. 552–559, Feb. 2017, doi: 10.1016/J.BBADIS.2016.11.026.
- [191] M. Kern, V. Fernandez-Sáiz, Z. Schäfer, and A. Buchberger, "UBXD1 binds p97 through two independent binding sites," *Biochem Biophys Res Commun*, vol. 380, no. 2, pp. 303–307, Mar. 2009, doi: 10.1016/J.BBRC.2009.01.076.
- [192] A. C. Bento, C. C. Bippes, C. Kohler, C. Hemion, S. Frank, and A. Neutzner, "UBXD1 is a mitochondrial recruitment factor for p97/VCP and promotes mitophagy," *Sci Rep*, vol. 8, no. 1, Dec. 2018, doi: 10.1038/S41598-018-30963-Z.
- [193] H. McNeill, A. Knebel, J. S. C. Arthur, A. Cuenda, and P. Cohen, "A novel UBA and UBX domain protein that binds polyubiquitin and VCP and is a substrate for SAPKs," *Biochem J*, vol. 384, no. Pt 2, pp. 391–400, Dec. 2004, doi: 10.1042/BJ20041498.
- [194] T. Ishibashi *et al.*, "A novel protein specifically interacting with Homer2 regulates ubiquitin-proteasome systems," *J Biochem*, vol. 137, no. 5, pp. 617–623, May 2005, doi: 10.1093/JB/MVI074.
- [195] E. S. Park, Y. J. Yoo, and M. Elangovan, "The opposite role of two UBA-UBX containing proteins, p47 and SAKS1 in the degradation of a single ERAD substrate, α -TCR," *Mol Cell Biochem*, vol. 425, no. 1–2, pp. 37–45, Jan. 2017, doi: 10.1007/S11010-016-2860-5.
- [196] D. P. LaLonde and A. Bretscher, "The UBX protein SAKS1 negatively regulates endoplasmic reticulum-associated degradation and p97-dependent degradation," *J Biol Chem*, vol. 286, no. 6, pp. 4892–4901, Feb. 2011, doi: 10.1074/JBC.M110.158030.
- [197] M. Raman *et al.*, "Systematic proteomics of the VCP-UBXD adaptor network identifies a role for UBXM10 in regulating ciliogenesis," *Nat Cell Biol*, vol. 17, no. 10, pp. 1356–1369, Oct. 2015, doi: 10.1038/NCB3238.
- [198] R. Ganji, S. Mukkavalli, F. Somanji, and M. Raman, "The VCP-UBXM1 Complex Mediates Triage of Ubiquitylated Cytosolic Proteins Bound to the BAG6 Complex," *Mol Cell Biol*, vol. 38, no. 13, Jul. 2018, doi: 10.1128/MCB.00154-18.
- [199] C. Mengus *et al.*, "VCP/p97 cofactor UBXM1/SAKS1 regulates mitophagy by modulating MFN2 removal from mitochondria," *Autophagy*, 2021, doi: 10.1080/15548627.2021.1922982.

-
- [200] S. C. J. Helle, G. Kanfer, K. Kolar, A. Lang, A. H. Michel, and B. Kornmann, "Organization and function of membrane contact sites," *Biochim Biophys Acta*, vol. 1833, no. 11, pp. 2526–2541, Nov. 2013, doi: 10.1016/J.BBAMCR.2013.01.028.
- [201] T. Daniele and M. V. Schiaffino, "Organelle biogenesis and interorganellar connections: Better in contact than in isolation," *Commun Integr Biol*, vol. 7, no. 4, pp. e29587-1-e29587-6, 2014, doi: 10.4161/CIB.29587.
- [202] L. Scorrano *et al.*, "Coming together to define membrane contact sites," *Nat Commun*, vol. 10, no. 1, Dec. 2019, doi: 10.1038/S41467-019-09253-3.
- [203] H. A. Ping, L. M. Kraft, W. T. Chen, A. E. Nilles, and L. L. Lackner, "Num1 anchors mitochondria to the plasma membrane via two domains with different lipid binding specificities," *J Cell Biol*, vol. 213, no. 5, pp. 513–524, 2016, doi: 10.1083/JCB.201511021.
- [204] J. R. Friedman and J. Nunnari, "Mitochondrial form and function," *Nature*, vol. 505, no. 7483, pp. 335–343, 2014, doi: 10.1038/NATURE12985.
- [205] N. S. Chandel, "Evolution of Mitochondria as Signaling Organelles," *Cell Metab*, vol. 22, no. 2, pp. 204–206, Aug. 2015, doi: 10.1016/J.CMET.2015.05.013.
- [206] A. Murley and J. Nunnari, "The Emerging Network of Mitochondria-Organelle Contacts," *Mol Cell*, vol. 61, no. 5, pp. 648–653, Mar. 2016, doi: 10.1016/J.MOLCEL.2016.01.031.
- [207] W. BERNHARD and C. ROUILLER, "Close topographical relationship between mitochondria and ergastoplasm of liver cells in a definite phase of cellular activity," *J Biophys Biochem Cytol*, vol. 2, no. 4 Suppl, pp. 73–78, 1956, doi: 10.1083/JCB.2.4.73.
- [208] D. E. COPELAND and A. J. DALTON, "An association between mitochondria and the endoplasmic reticulum in cells of the pseudobranch gland of a teleost," *J Biophys Biochem Cytol*, vol. 5, no. 3, pp. 393–396, 1959, doi: 10.1083/JCB.5.3.393.
- [209] S. H. Shim *et al.*, "Super-resolution fluorescence imaging of organelles in live cells with photoswitchable membrane probes," *Proc Natl Acad Sci U S A*, vol. 109, no. 35, pp. 13978–13983, Aug. 2012, doi: 10.1073/PNAS.1201882109/-/DCSUPPLEMENTAL/PNAS.1201882109_SI.PDF.
- [210] T. Verfaillie *et al.*, "PERK is required at the ER-mitochondrial contact sites to convey apoptosis after ROS-based ER stress," *Cell Death Differ*, vol. 19, no. 11, pp. 1880–1891, Nov. 2012, doi: 10.1038/CDD.2012.74.

-
- [211] M. Hamasaki *et al.*, “Autophagosomes form at ER-mitochondria contact sites,” *Nature*, vol. 495, no. 7441, pp. 389–393, Mar. 2013, doi: 10.1038/NATURE11910.
- [212] G. Szabadkai and R. Rizzuto, “Καλός και Αγαθός: how mitochondrial beauty translates into biological virtue,” *Curr Opin Cell Biol*, vol. 25, no. 4, pp. 477–482, 2013, doi: 10.1016/J.CEB.2013.03.006.
- [213] E. Area-Gomez and E. A. Schon, “On the Pathogenesis of Alzheimer’s Disease: The MAM Hypothesis,” *FASEB J*, vol. 31, no. 3, pp. 864–867, Mar. 2017, doi: 10.1096/FJ.201601309.
- [214] L. Sironi, L. M. Restelli, M. Tolnay, A. Neutzner, and S. Frank, “Dysregulated Interorganellar Crosstalk of Mitochondria in the Pathogenesis of Parkinson’s Disease,” *Cells*, vol. 9, no. 1, Jan. 2020, doi: 10.3390/CELLS9010233.
- [215] S. Aits and M. Jäättelä, “Lysosomal cell death at a glance,” *J Cell Sci*, vol. 126, no. Pt 9, pp. 1905–1912, May 2013, doi: 10.1242/JCS.091181.
- [216] Y. C. Wong, D. Ysselstein, and D. Krainc, “Mitochondria-lysosome contacts regulate mitochondrial fission via RAB7 GTP hydrolysis,” *Nature*, vol. 554, no. 7692, pp. 382–386, Feb. 2018, doi: 10.1038/NATURE25486.
- [217] D. Aston *et al.*, “High resolution structural evidence suggests the Sarcoplasmic Reticulum forms microdomains with Acidic Stores (lysosomes) in the heart,” *Sci Rep*, vol. 7, Jan. 2017, doi: 10.1038/SREP40620.
- [218] J. Fermie *et al.*, “Single organelle dynamics linked to 3D structure by correlative live-cell imaging and 3D electron microscopy,” *Traffic*, vol. 19, no. 5, pp. 354–369, May 2018, doi: 10.1111/TRA.12557.
- [219] A. M. Valm *et al.*, “Applying systems-level spectral imaging and analysis to reveal the organelle interactome,” *Nature*, vol. 546, no. 7656, pp. 162–167, Jun. 2017, doi: 10.1038/NATURE22369.
- [220] Y. Han, M. Li, F. Qiu, M. Zhang, and Y. H. Zhang, “Cell-permeable organic fluorescent probes for live-cell long-term super-resolution imaging reveal lysosome-mitochondrion interactions,” *Nat Commun*, vol. 8, no. 1, Dec. 2017, doi: 10.1038/S41467-017-01503-6.

-
- [221] Q. Chen *et al.*, “Super-Resolution Tracking of Mitochondrial Dynamics with An Iridium(III) Luminophore,” *Small*, vol. 14, no. 41, Oct. 2018, doi: 10.1002/SMLL.201802166.
- [222] A. H. Hutagalung and P. J. Novick, “Role of Rab GTPases in membrane traffic and cell physiology,” *Physiol Rev*, vol. 91, no. 1, pp. 119–149, Jan. 2011, doi: 10.1152/PHYSREV.00059.2009.
- [223] F. Burté, V. Carelli, P. F. Chinnery, and P. Yu-Wai-Man, “Disturbed mitochondrial dynamics and neurodegenerative disorders,” *Nat Rev Neurol*, vol. 11, no. 1, pp. 11–24, Jan. 2015, doi: 10.1038/NRNEURO.2014.228.
- [224] J. M. Mc Donald and D. Krainc, “Lysosomal Proteins as a Therapeutic Target in Neurodegeneration,” *Annu Rev Med*, vol. 68, pp. 445–458, Jan. 2017, doi: 10.1146/ANNUREV-MED-050715-104432.
- [225] N. Plotegher and M. R. Duchen, “Mitochondrial Dysfunction and Neurodegeneration in Lysosomal Storage Disorders,” *Trends Mol Med*, vol. 23, no. 2, pp. 116–134, Feb. 2017, doi: 10.1016/J.MOLMED.2016.12.003.
- [226] R. J. A. Wanders and H. R. Waterham, “Peroxisomal disorders: the single peroxisomal enzyme deficiencies,” *Biochim Biophys Acta*, vol. 1763, no. 12, pp. 1707–1720, Dec. 2006, doi: 10.1016/J.BBAMCR.2006.08.010.
- [227] C. Odendall and J. C. Kagan, “Peroxisomes and the antiviral responses of mammalian cells,” *Subcell Biochem*, vol. 69, pp. 67–75, May 2013, doi: 10.1007/978-94-007-6889-5_4.
- [228] M. Nordgren and M. Fransen, “Peroxisomal metabolism and oxidative stress,” *Biochimie*, vol. 98, no. 1, pp. 56–62, 2014, doi: 10.1016/J.BIOCHI.2013.07.026.
- [229] M. Schrader, S. Grille, H. Dariush Fahimi, and M. Islinger, “Peroxisome interactions and cross-talk with other subcellular compartments in animal cells,” *Subcell Biochem*, vol. 69, pp. 1–22, May 2013, doi: 10.1007/978-94-007-6889-5_1.
- [230] R. J. A. Wanders, “Peroxisomes in human health and disease: metabolic pathways, metabolite transport, interplay with other organelles and signal transduction,” *Subcell Biochem*, vol. 69, pp. 23–44, May 2013, doi: 10.1007/978-94-007-6889-5_2.
- [231] E. Dixit *et al.*, “Peroxisomes are signaling platforms for antiviral innate immunity,” *Cell*, vol. 141, no. 4, pp. 668–681, 2010, doi: 10.1016/J.CELL.2010.04.018.

-
- [232] J. C. Kagan, "Signaling organelles of the innate immune system," *Cell*, vol. 151, no. 6, pp. 1168–1178, Dec. 2012, doi: 10.1016/J.CELL.2012.11.011.
- [233] M. Fransen, M. Nordgren, B. Wang, and O. Apanasets, "Role of peroxisomes in ROS/RNS-metabolism: implications for human disease," *Biochim Biophys Acta*, vol. 1822, no. 9, pp. 1363–1373, Sep. 2012, doi: 10.1016/J.BBADIS.2011.12.001.
- [234] M. Schrader and H. D. Fahimi, "Growth and division of peroxisomes," *Int Rev Cytol*, vol. 255, pp. 237–290, 2006, doi: 10.1016/S0074-7696(06)55005-3.
- [235] M. Schrader, J. Costello, L. F. Godinho, and M. Islinger, "Peroxisome-mitochondria interplay and disease," *J Inherit Metab Dis*, vol. 38, no. 4, pp. 681–702, Jul. 2015, doi: 10.1007/S10545-015-9819-7.
- [236] V. D. Antonenkov and J. K. Hiltunen, "Transfer of metabolites across the peroxisomal membrane," *Biochim Biophys Acta*, vol. 1822, no. 9, pp. 1374–1386, Sep. 2012, doi: 10.1016/J.BBADIS.2011.12.011.
- [237] S. M. Horner, H. M. Liu, H. S. Park, J. Briley, and M. Gale, "Mitochondrial-associated endoplasmic reticulum membranes (MAM) form innate immune synapses and are targeted by hepatitis C virus," *Proc Natl Acad Sci U S A*, vol. 108, no. 35, pp. 14590–14595, Aug. 2011, doi: 10.1073/PNAS.1110133108.
- [238] J. Fan, X. Li, L. Issop, M. Culty, and V. Papadopoulos, "ACBD2/ECI2-Mediated Peroxisome-Mitochondria Interactions in Leydig Cell Steroid Biosynthesis," *Mol Endocrinol*, vol. 30, no. 7, pp. 763–782, Jul. 2016, doi: 10.1210/ME.2016-1008.
- [239] Palade George, "Subcellular Particles." The Ronal Press Company, New York, 1959.
- [240] I. Y. Benador *et al.*, "Mitochondria Bound to Lipid Droplets Have Unique Bioenergetics, Composition, and Dynamics that Support Lipid Droplet Expansion," *Cell Metab*, vol. 27, no. 4, pp. 869-885.e6, Apr. 2018, doi: 10.1016/J.CMET.2018.03.003.
- [241] A. Gemmink *et al.*, "Super-resolution microscopy localizes perilipin 5 at lipid droplet-mitochondria interaction sites and at lipid droplets juxtaposing to perilipin 2," *Biochim Biophys Acta Mol Cell Biol Lipids*, vol. 1863, no. 11, pp. 1423–1432, Nov. 2018, doi: 10.1016/J.BBALIP.2018.08.016.
- [242] J. Yu *et al.*, "Lipid droplet remodeling and interaction with mitochondria in mouse brown adipose tissue during cold treatment," *Biochim Biophys Acta*, vol. 1853, no. 5, pp. 918–928, May 2015, doi: 10.1016/J.BBAMCR.2015.01.020.

-
- [243] M. Boutant *et al.*, "Mfn2 is critical for brown adipose tissue thermogenic function," *EMBO J*, vol. 36, no. 11, pp. 1543–1558, Jun. 2017, doi: 10.15252/EMBJ.201694914.
- [244] P. A. Young *et al.*, "Long-chain acyl-CoA synthetase 1 interacts with key proteins that activate and direct fatty acids into niche hepatic pathways," *J Biol Chem*, vol. 293, no. 43, pp. 16724–16740, Oct. 2018, doi: 10.1074/JBC.RA118.004049.
- [245] M. Y. Lin and Z. H. Sheng, "Regulation of mitochondrial transport in neurons," *Exp Cell Res*, vol. 334, no. 1, pp. 35–44, May 2015, doi: 10.1016/J.YEXCR.2015.01.004.
- [246] A. F. MacAskill and J. T. Kittler, "Control of mitochondrial transport and localization in neurons," *Trends Cell Biol*, vol. 20, no. 2, pp. 102–112, Feb. 2010, doi: 10.1016/J.TCB.2009.11.002.
- [247] N. Hirokawa, R. Sato-Yoshitake, N. Kobayashi, K. K. Pfister, G. S. Bloom, and S. T. Brady, "Kinesin associates with anterogradely transported membranous organelles in vivo," *J Cell Biol*, vol. 114, no. 2, pp. 295–302, 1991, doi: 10.1083/JCB.114.2.295.
- [248] A. D. Pilling, D. Horiuchi, C. M. Lively, and W. M. Saxton, "Kinesin-1 and Dynein are the primary motors for fast transport of mitochondria in *Drosophila* motor axons," *Mol Biol Cell*, vol. 17, no. 4, pp. 2057–2068, Apr. 2006, doi: 10.1091/MBC.E05-06-0526.
- [249] O. S. Koutsopoulos *et al.*, "Human Mitons associate with mitochondria and induce microtubule-dependent remodeling of mitochondrial networks," *Biochim Biophys Acta*, vol. 1803, no. 5, pp. 564–574, May 2010, doi: 10.1016/J.BBAMCR.2010.03.006.
- [250] Q. Cai, C. Gerwin, and Z. H. Sheng, "Syntabulin-mediated anterograde transport of mitochondria along neuronal processes," *J Cell Biol*, vol. 170, no. 6, pp. 959–969, Sep. 2005, doi: 10.1083/JCB.200506042.
- [251] Q. Su, Q. Cai, C. Gerwin, C. L. Smith, and Z. H. Sheng, "Syntabulin is a microtubule-associated protein implicated in syntaxin transport in neurons," *Nat Cell Biol*, vol. 6, no. 10, pp. 941–953, Oct. 2004, doi: 10.1038/NCB1169.
- [252] T. Fujita *et al.*, "Axonal guidance protein FEZ1 associates with tubulin and kinesin motor protein to transport mitochondria in neurites of NGF-stimulated PC12 cells," *Biochem Biophys Res Commun*, vol. 361, no. 3, pp. 605–610, Sep. 2007, doi: 10.1016/J.BBRC.2007.07.050.

-
- [253] Y. Chen and Z. H. Sheng, "Kinesin-1-syntrophin coupling mediates activity-dependent regulation of axonal mitochondrial transport," *J Cell Biol*, vol. 202, no. 2, pp. 351–364, Jul. 2013, doi: 10.1083/JCB.201302040.
- [254] M. Saotome *et al.*, "Bidirectional Ca²⁺-dependent control of mitochondrial dynamics by the Miro GTPase," *Proc Natl Acad Sci U S A*, vol. 105, no. 52, pp. 20728–20733, Dec. 2008, doi: 10.1073/PNAS.0808953105.
- [255] L. Y. Shields *et al.*, "Dynamin-related protein 1 is required for normal mitochondrial bioenergetic and synaptic function in CA1 hippocampal neurons," *Cell Death Dis*, vol. 6, no. 4, Apr. 2015, doi: 10.1038/CDDIS.2015.94.
- [256] B. Oettinghaus *et al.*, "Synaptic dysfunction, memory deficits and hippocampal atrophy due to ablation of mitochondrial fission in adult forebrain neurons," *Cell Death Differ*, vol. 23, no. 1, pp. 18–28, Jan. 2016, doi: 10.1038/CDD.2015.39.
- [257] E. A. Schon and S. Przedborski, "Mitochondria: the next (neurode)generation," *Neuron*, vol. 70, no. 6, pp. 1033–1053, Jun. 2011, doi: 10.1016/J.NEURON.2011.06.003.
- [258] D. H. Cho, T. Nakamura, and S. A. Lipton, "Mitochondrial dynamics in cell death and neurodegeneration," *Cell Mol Life Sci*, vol. 67, no. 20, pp. 3435–3447, Oct. 2010, doi: 10.1007/S00018-010-0435-2.
- [259] A. Kathrin Lutz *et al.*, "Loss of parkin or PINK1 function increases Drp1-dependent mitochondrial fragmentation," *J Biol Chem*, vol. 284, no. 34, pp. 22938–22951, Aug. 2009, doi: 10.1074/JBC.M109.035774.
- [260] U. P. Shirendeb *et al.*, "Mutant huntingtin's interaction with mitochondrial protein Drp1 impairs mitochondrial biogenesis and causes defective axonal transport and synaptic degeneration in Huntington's disease," *Hum Mol Genet*, vol. 21, no. 2, pp. 406–420, Jan. 2012, doi: 10.1093/HMG/DDR475.
- [261] W. Song *et al.*, "Mutant huntingtin binds the mitochondrial fission GTPase dynamin-related protein-1 and increases its enzymatic activity," *Nat Med*, vol. 17, no. 3, pp. 377–383, Mar. 2011, doi: 10.1038/NM.2313.
- [262] X. Wang *et al.*, "Impaired balance of mitochondrial fission and fusion in Alzheimer's disease," *J Neurosci*, vol. 29, no. 28, pp. 9090–9103, Jul. 2009, doi: 10.1523/JNEUROSCI.1357-09.2009.

-
- [263] D. Twelves, K. S. M. Perkins, and C. Counsell, "Systematic review of incidence studies of Parkinson's disease," *Mov Disord*, vol. 18, no. 1, pp. 19–31, Jan. 2003, doi: 10.1002/MDS.10305.
- [264] W. Dauer and S. Przedborski, "Parkinson's disease: mechanisms and models," *Neuron*, vol. 39, no. 6, pp. 889–909, Sep. 2003, doi: 10.1016/S0896-6273(03)00568-3.
- [265] Q. Hu and G. Wang, "Mitochondrial dysfunction in Parkinson's disease," *Transl Neurodegener*, vol. 5, no. 1, Jul. 2016, doi: 10.1186/S40035-016-0060-6.
- [266] A. Bose and M. F. Beal, "Mitochondrial dysfunction in Parkinson's disease," *J Neurochem*, vol. 139 Suppl 1, pp. 216–231, Oct. 2016, doi: 10.1111/JNC.13731.
- [267] B. Wang, N. Abraham, G. Gao, and Q. Yang, "Dysregulation of autophagy and mitochondrial function in Parkinson's disease," *Transl Neurodegener*, vol. 5, no. 1, Oct. 2016, doi: 10.1186/S40035-016-0065-1.
- [268] M. C. Zanellati *et al.*, "Mitochondrial dysfunction in Parkinson disease: evidence in mutant PARK2 fibroblasts," *Front Genet*, vol. 6, no. MAR, 2015, doi: 10.3389/FGENE.2015.00078.
- [269] C. Alexander *et al.*, "OPA1, encoding a dynamin-related GTPase, is mutated in autosomal dominant optic atrophy linked to chromosome 3q28," *Nat Genet*, vol. 26, no. 2, pp. 211–215, Oct. 2000, doi: 10.1038/79944.
- [270] B. le Roux *et al.*, "OPA1: 516 unique variants and 831 patients registered in an updated centralized Variome database," *Orphanet J Rare Dis*, vol. 14, no. 1, Sep. 2019, doi: 10.1186/S13023-019-1187-1.
- [271] P. Amati-Bonneau *et al.*, "The association of autosomal dominant optic atrophy and moderate deafness may be due to the R445H mutation in the OPA1 gene," *Am J Ophthalmol*, vol. 136, no. 6, pp. 1170–1171, 2003, doi: 10.1016/S0002-9394(03)00665-2.
- [272] P. Amati-Bonneau *et al.*, "OPA1 mutations induce mitochondrial DNA instability and optic atrophy 'plus' phenotypes," *Brain*, vol. 131, no. Pt 2, pp. 338–351, Feb. 2008, doi: 10.1093/BRAIN/AWM298.
- [273] G. Hudson *et al.*, "Mutation of OPA1 causes dominant optic atrophy with external ophthalmoplegia, ataxia, deafness and multiple mitochondrial DNA deletions: a novel disorder of mtDNA maintenance," *Brain*, vol. 131, no. Pt 2, pp. 329–337, 2008, doi: 10.1093/BRAIN/AWM272.

-
- [274] M. Payne *et al.*, "Dominant optic atrophy, sensorineural hearing loss, ptosis, and ophthalmoplegia: a syndrome caused by a missense mutation in OPA1," *Am J Ophthalmol*, vol. 138, no. 5, pp. 749–755, Nov. 2004, doi: 10.1016/J.AJO.2004.06.011.
- [275] P. Yu-Wai-Man *et al.*, "Multi-system neurological disease is common in patients with OPA1 mutations," *Brain*, vol. 133, no. Pt 3, pp. 771–786, Mar. 2010, doi: 10.1093/BRAIN/AWQ007.
- [276] V. B. NJ, C. R. O. EC, C. JG, and T. IA, "Mitochondrial disorders and the eye," *Eye Brain*, vol. 3, p. 29, Sep. 2011, doi: 10.2147/EB.S16192.
- [277] G. Lenaers *et al.*, "Dominant optic atrophy: Culprit mitochondria in the optic nerve," *Prog Retin Eye Res*, vol. 83, Jul. 2021, doi: 10.1016/J.PRETEYERES.2020.100935.
- [278] C. Verny *et al.*, "Multiple sclerosis-like disorder in OPA1-related autosomal dominant optic atrophy," *Neurology*, vol. 70, no. 13 Pt 2, pp. 1152–1153, 2008, doi: 10.1212/01.WNL.0000289194.89359.A1.
- [279] R. Spiegel *et al.*, "Fatal infantile mitochondrial encephalomyopathy, hypertrophic cardiomyopathy and optic atrophy associated with a homozygous OPA1 mutation," *J Med Genet*, vol. 53, no. 2, pp. 127–131, 2016, doi: 10.1136/JMEDGENET-2015-103361.
- [280] V. Carelli *et al.*, "Syndromic parkinsonism and dementia associated with OPA1 missense mutations," *Ann Neurol*, vol. 78, no. 1, pp. 21–38, Jul. 2015, doi: 10.1002/ANA.24410.
- [281] D. S. Lynch *et al.*, "Nonsyndromic Parkinson disease in a family with autosomal dominant optic atrophy due to OPA1 mutations," *Neurol Genet*, vol. 3, no. 5, Oct. 2017, doi: 10.1212/NXG.0000000000000188.
- [282] A. Zerem *et al.*, "Metabolic stroke in a patient with bi-allelic OPA1 mutations," *Metab Brain Dis*, vol. 34, no. 4, pp. 1043–1048, Aug. 2019, doi: 10.1007/S11011-019-00415-2.
- [283] H. Inoue and T. Tanabe, "Transcriptional role of the nuclear factor kappa B site in the induction by lipopolysaccharide and suppression by dexamethasone of cyclooxygenase-2 in U937 cells," *Biochem Biophys Res Commun*, vol. 244, no. 1, pp. 143–148, Mar. 1998, doi: 10.1006/BBRC.1998.8222.
- [284] B. Delprat, T. Maurice, and C. Delettre, "Wolfram syndrome: MAMs' connection?," *Cell Death Dis*, vol. 9, no. 3, Mar. 2018, doi: 10.1038/S41419-018-0406-3.

-
- [285] C. la Morgia *et al.*, "Calcium mishandling in absence of primary mitochondrial dysfunction drives cellular pathology in Wolfram Syndrome," *Sci Rep*, vol. 10, no. 1, Dec. 2020, doi: 10.1038/S41598-020-61735-3.
- [286] A. Chaussenot *et al.*, "Mutation update and uncommon phenotypes in a French cohort of 96 patients with WFS1-related disorders," *Clin Genet*, vol. 87, no. 5, pp. 430–439, May 2015, doi: 10.1111/CGE.12437.
- [287] J. Grenier *et al.*, "WFS1 in Optic Neuropathies: Mutation Findings in Nonsyndromic Optic Atrophy and Assessment of Clinical Severity," *Ophthalmology*, vol. 123, no. 9, pp. 1989–1998, Sep. 2016, doi: 10.1016/J.OPHTHA.2016.05.036.
- [288] B. F. T. Hogewind *et al.*, "Autosomal dominant optic neuropathy and sensorineural hearing loss associated with a novel mutation of WFS1," *Mol Vis*, vol. 16, pp. 26–35, 2010, Accessed: Feb. 18, 2022. [Online]. Available: <https://pubmed.ncbi.nlm.nih.gov/20069065/>
- [289] N. D. Rendtorff *et al.*, "Identification of p.A684V missense mutation in the WFS1 gene as a frequent cause of autosomal dominant optic atrophy and hearing impairment," *Am J Med Genet A*, vol. 155A, no. 6, pp. 1298–1313, Jun. 2011, doi: 10.1002/AJMG.A.33970.
- [290] H. Eiberg *et al.*, "Autosomal dominant optic atrophy associated with hearing impairment and impaired glucose regulation caused by a missense mutation in the WFS1 gene," *J Med Genet*, vol. 43, no. 5, pp. 435–440, May 2006, doi: 10.1136/JMG.2005.034892.
- [291] R. Valéro, S. Bannwarth, S. Roman, V. Paquis-Flucklinger, and B. Vialettes, "Autosomal dominant transmission of diabetes and congenital hearing impairment secondary to a missense mutation in the WFS1 gene," *Diabet Med*, vol. 25, no. 6, pp. 657–661, Jun. 2008, doi: 10.1111/J.1464-5491.2008.02448.X.
- [292] I. N. Beshpalova *et al.*, "Mutations in the Wolfram syndrome 1 gene (WFS1) are a common cause of low frequency sensorineural hearing loss," *Hum Mol Genet*, vol. 10, no. 22, pp. 2501–2508, Oct. 2001, doi: 10.1093/HMG/10.22.2501.
- [293] T. L. Young *et al.*, "Non-syndromic progressive hearing loss DFNA38 is caused by heterozygous missense mutation in the Wolfram syndrome gene WFS1," *Hum Mol Genet*, vol. 10, no. 22, pp. 2509–2514, Oct. 2001, doi: 10.1093/HMG/10.22.2509.

-
- [294] S. da Cruz, I. Xenarios, J. Langridge, F. Vilbois, P. A. Parone, and J. C. Martinou, "Proteomic analysis of the mouse liver mitochondrial inner membrane," *J Biol Chem*, vol. 278, no. 42, pp. 41566–41571, Oct. 2003, doi: 10.1074/JBC.M304940200.
- [295] Y. Anikster, R. Kleta, A. Shaag, W. A. Gahl, and O. Elpeleg, "Type III 3-methylglutaconic aciduria (optic atrophy plus syndrome, or Costeff optic atrophy syndrome): identification of the OPA3 gene and its founder mutation in Iraqi Jews," *Am J Hum Genet*, vol. 69, no. 6, pp. 1218–1224, 2001, doi: 10.1086/324651.
- [296] H. Costeff, N. Gadoth, N. Apter, M. Prialni, and H. Savir, "A familial syndrome of infantile optic atrophy, movement disorder, and spastic paraplegia," *Neurology*, vol. 39, no. 4, pp. 595–597, 1989, doi: 10.1212/WNL.39.4.595.
- [297] X. Ayrygnac *et al.*, "OPA3--related autosomal dominant optic atrophy and cataract with ataxia and areflexia," *Eur Neurol*, vol. 68, no. 2, pp. 108–110, Aug. 2012, doi: 10.1159/000339310.
- [298] S. C. Bourne *et al.*, "Optic atrophy, cataracts, lipodystrophy/lipoatrophy, and peripheral neuropathy caused by a de novo OPA3 mutation," *Cold Spring Harb Mol Case Stud*, vol. 3, no. 1, p. a001156, Jan. 2017, doi: 10.1101/MCS.A001156.
- [299] T. Grau *et al.*, "A novel heterozygous OPA3 mutation located in the mitochondrial target sequence results in altered steady-state levels and fragmented mitochondrial network," *J Med Genet*, vol. 50, no. 12, pp. 848–858, 2013, doi: 10.1136/JMEDGENET-2013-101774.
- [300] A. Horga *et al.*, "Autosomal dominant optic atrophy and cataract 'plus' phenotype including axonal neuropathy," *Neurol Genet*, vol. 5, no. 2, Apr. 2019, doi: 10.1212/NXG.0000000000000322.
- [301] Y. Li, J. Li, X. Jia, X. Xiao, S. Li, and X. Guo, "Genetic and Clinical Analyses of DOA and LHON in 304 Chinese Patients with Suspected Childhood-Onset Hereditary Optic Neuropathy," *PLoS One*, vol. 12, no. 1, Jan. 2017, doi: 10.1371/JOURNAL.PONE.0170090.
- [302] M. Kazamel and C. J. Boes, "Charcot Marie Tooth disease (CMT): historical perspectives and evolution," *J Neurol*, vol. 262, no. 4, pp. 801–805, Apr. 2015, doi: 10.1007/S00415-014-7490-9.

-
- [303] P. J. Dyck and E. H. Lambert, "Lower motor and primary sensory neuron diseases with peroneal muscular atrophy. I. Neurologic, genetic, and electrophysiologic findings in hereditary polyneuropathies," *Arch Neurol*, vol. 18, no. 6, pp. 603–618, 1968, doi: 10.1001/ARCHNEUR.1968.00470360025002.
- [304] M. M. Reilly, M. E. Shy, F. Muntoni, and D. Pareyson, "168th ENMC International Workshop: outcome measures and clinical trials in Charcot-Marie-Tooth disease (CMT)," *Neuromuscul Disord*, vol. 20, no. 12, pp. 839–846, Dec. 2010, doi: 10.1016/J.NMD.2010.08.001.
- [305] A. S. D. Saporta, S. L. Sottile, L. J. Miller, S. M. E. Feely, C. E. Siskind, and M. E. Shy, "Charcot-Marie-Tooth disease subtypes and genetic testing strategies," *Ann Neurol*, vol. 69, no. 1, pp. 22–33, Jan. 2011, doi: 10.1002/ANA.22166.
- [306] S. Züchner *et al.*, "Mutations in the mitochondrial GTPase mitofusin 2 cause Charcot-Marie-Tooth neuropathy type 2A," *Nat Genet*, vol. 36, no. 5, pp. 449–451, May 2004, doi: 10.1038/NG1341.
- [307] S. Züchner *et al.*, "Axonal neuropathy with optic atrophy is caused by mutations in mitofusin 2," *Ann Neurol*, vol. 59, no. 2, pp. 276–281, Feb. 2006, doi: 10.1002/ANA.20797.
- [308] A. Niemann, M. Ruegg, V. la Padula, A. Schenone, and U. Suter, "Ganglioside-induced differentiation associated protein 1 is a regulator of the mitochondrial network: new implications for Charcot-Marie-Tooth disease," *J Cell Biol*, vol. 170, no. 7, pp. 1067–1078, Sep. 2005, doi: 10.1083/JCB.200507087.
- [309] L. Pedrola, A. Espert, X. Wu, R. Claramunt, M. E. Shy, and F. Palau, "GDAP1, the protein causing Charcot-Marie-Tooth disease type 4A, is expressed in neurons and is associated with mitochondria," *Hum Mol Genet*, vol. 14, no. 8, pp. 1087–1094, Apr. 2005, doi: 10.1093/HMG/DDI121.
- [310] S. A. Detmer and D. C. Chan, "Functions and dysfunctions of mitochondrial dynamics," *Nat Rev Mol Cell Biol*, vol. 8, no. 11, pp. 870–879, Nov. 2007, doi: 10.1038/NRM2275.
- [311] N. Huber, S. Guimaraes, M. Schrader, U. Suter, and A. Niemann, "Charcot-Marie-Tooth disease-associated mutants of GDAP1 dissociate its roles in peroxisomal and mitochondrial fission," *EMBO Rep*, vol. 14, no. 6, pp. 545–552, Jun. 2013, doi: 10.1038/EMBOR.2013.56.

-
- [312] M. Barneo-Muñoz *et al.*, “Lack of GDAP1 induces neuronal calcium and mitochondrial defects in a knockout mouse model of charcot-marie-tooth neuropathy,” *PLoS Genet*, vol. 11, no. 4, Apr. 2015, doi: 10.1371/JOURNAL.PGEN.1005115.
- [313] V. Askanas and W. K. Engel, “Sporadic inclusion-body myositis: conformational multifactorial ageing-related degenerative muscle disease associated with proteasomal and lysosomal inhibition, endoplasmic reticulum stress, and accumulation of amyloid- β 42 oligomers and phosphorylated tau,” *Presse medicale (Paris, France : 1983)*, vol. 40, no. 4 Pt 2, Apr. 2011, doi: 10.1016/J.LPM.2010.11.024.
- [314] V. E. Kimonis, E. Fulchiero, J. Vesa, and G. Watts, “VCP disease associated with myopathy, Paget disease of bone and frontotemporal dementia: review of a unique disorder,” *Biochim Biophys Acta*, vol. 1782, no. 12, pp. 744–748, Dec. 2008, doi: 10.1016/J.BBADIS.2008.09.003.
- [315] J. O. Johnson *et al.*, “Exome sequencing reveals VCP mutations as a cause of familial ALS,” *Neuron*, vol. 68, no. 5, pp. 857–864, Dec. 2010, doi: 10.1016/J.NEURON.2010.11.036.
- [316] G. D. J. Watts *et al.*, “Inclusion body myopathy associated with Paget disease of bone and frontotemporal dementia is caused by mutant valosin-containing protein,” *Nat Genet*, vol. 36, no. 4, pp. 377–381, Apr. 2004, doi: 10.1038/NG1332.
- [317] H. Niwa, C. A. Ewens, C. Tsang, H. O. Yeung, X. Zhang, and P. S. Freemont, “The role of the N-domain in the ATPase activity of the mammalian AAA ATPase p97/VCP,” *J Biol Chem*, vol. 287, no. 11, pp. 8561–8570, Mar. 2012, doi: 10.1074/JBC.M111.302778.
- [318] V. Fernández-Sáiz and A. Buchberger, “Imbalances in p97 co-factor interactions in human proteinopathy,” *EMBO Rep*, vol. 11, no. 6, pp. 479–485, Jun. 2010, doi: 10.1038/EMBOR.2010.49.
- [319] C. C. Weihl, A. Pestronk, and V. E. Kimonis, “Valosin-containing protein disease: inclusion body myopathy with Paget’s disease of the bone and fronto-temporal dementia,” *Neuromuscul Disord*, vol. 19, no. 5, pp. 308–315, May 2009, doi: 10.1016/J.NMD.2009.01.009.
- [320] A. K. Peyer *et al.*, “Novel valosin containing protein mutation in a Swiss family with hereditary inclusion body myopathy and dementia,” *Neuromuscul Disord*, vol. 23, no. 2, pp. 149–154, Feb. 2013, doi: 10.1016/J.NMD.2012.09.009.

-
- [321] I. R. A. Mackenzie, R. Rademakers, and M. Neumann, "TDP-43 and FUS in amyotrophic lateral sclerosis and frontotemporal dementia," *Lancet Neurol*, vol. 9, no. 10, pp. 995–1007, Oct. 2010, doi: 10.1016/S1474-4422(10)70195-2.
- [322] G. Bertani, "Lysogeny at mid-twentieth century: P1, P2, and other experimental systems," *J Bacteriol*, vol. 186, no. 3, pp. 595–600, Feb. 2004, doi: 10.1128/JB.186.3.595-600.2004.
- [323] K. Mullis, F. Faloona, S. Scharf, R. Saiki, G. Horn, and H. Erlich, "Specific enzymatic amplification of DNA in vitro: the polymerase chain reaction," *Cold Spring Harb Symp Quant Biol*, vol. 51 Pt 1, no. 1, pp. 263–273, 1986, doi: 10.1101/SQB.1986.051.01.032.
- [324] B. Moosavi, B. Mousavi, W. C. Yang, and G. F. Yang, "Yeast-based assays for detecting protein-protein/drug interactions and their inhibitors," *Eur J Cell Biol*, vol. 96, no. 6, pp. 529–541, Sep. 2017, doi: 10.1016/J.EJCB.2017.06.003.
- [325] B. I. Giasson, J. E. Duda, S. M. Quinn, B. Zhang, J. Q. Trojanowski, and V. M. Y. Lee, "Neuronal alpha-synucleinopathy with severe movement disorder in mice expressing A53T human alpha-synuclein," *Neuron*, vol. 34, no. 4, pp. 521–533, 2002, doi: 10.1016/S0896-6273(02)00682-7.
- [326] M. Sadelain, E. P. Papapetrou, and F. D. Bushman, "Safe harbours for the integration of new DNA in the human genome," *Nat Rev Cancer*, vol. 12, no. 1, pp. 51–58, Jan. 2011, doi: 10.1038/NRC3179.
- [327] M. Nagahama *et al.*, "UBXD1 is a VCP-interacting protein that is involved in ER-associated degradation," *Biochem Biophys Res Commun*, vol. 382, no. 2, pp. 303–308, May 2009, doi: 10.1016/J.BBRC.2009.03.012.
- [328] G. Civiletto *et al.*, "Opa1 overexpression ameliorates the phenotype of two mitochondrial disease mouse models," *Cell Metab*, vol. 21, no. 6, pp. 845–854, Jun. 2015, doi: 10.1016/J.CMET.2015.04.016.
- [329] S. Lamartina, E. Sporeno, E. Fattori, and C. Toniatti, "Characteristics of the adeno-associated virus preintegration site in human chromosome 19: open chromatin conformation and transcription-competent environment," *J Virol*, vol. 74, no. 16, pp. 7671–7677, Aug. 2000, doi: 10.1128/JVI.74.16.7671-7677.2000.
- [330] R. C. DeKelver *et al.*, "Functional genomics, proteomics, and regulatory DNA analysis in isogenic settings using zinc finger nuclease-driven transgenesis into a safe harbor

- locus in the human genome," *Genome Res*, vol. 20, no. 8, pp. 1133–1142, Aug. 2010, doi: 10.1101/GR.106773.110.
- [331] J. R. Masters, "HeLa cells 50 years on: the good, the bad and the ugly," *Nat Rev Cancer*, vol. 2, no. 4, pp. 315–319, 2002, doi: 10.1038/NRC775.
- [332] H. Xicoy, B. Wieringa, and G. J. M. Martens, "The SH-SY5Y cell line in Parkinson's disease research: a systematic review," *Mol Neurodegener*, vol. 12, no. 1, pp. 1–11, Jan. 2017, doi: 10.1186/S13024-017-0149-0.
- [333] A. Krishna *et al.*, "Systems genomics evaluation of the SH-SY5Y neuroblastoma cell line as a model for Parkinson's disease," *BMC Genomics*, vol. 15, no. 1, Dec. 2014, doi: 10.1186/1471-2164-15-1154.
- [334] H. Lee and Y. Yoon, "Mitochondrial Membrane Dynamics-Functional Positioning of OPA1," *Antioxidants (Basel)*, vol. 7, no. 12, Dec. 2018, doi: 10.3390/ANTIOX7120186.
- [335] G. Twig and O. S. Shirihai, "The interplay between mitochondrial dynamics and mitophagy," *Antioxid Redox Signal*, vol. 14, no. 10, pp. 1939–1951, May 2011, doi: 10.1089/ARS.2010.3779.
- [336] C. E. Rodger, T. G. McWilliams, and I. G. Ganley, "Mammalian mitophagy - from in vitro molecules to in vivo models," *FEBS J*, vol. 285, no. 7, pp. 1185–1202, Apr. 2018, doi: 10.1111/FEBS.14336.
- [337] E. Kara *et al.*, "A 6.4 Mb duplication of the α -synuclein locus causing frontotemporal dementia and Parkinsonism: phenotype-genotype correlations," *JAMA Neurol*, vol. 71, no. 9, pp. 1162–1171, Sep. 2014, doi: 10.1001/JAMANEUROL.2014.994.
- [338] P. Ibáñez *et al.*, "Causal relation between alpha-synuclein gene duplication and familial Parkinson's disease," *Lancet*, vol. 364, no. 9440, pp. 1169–1171, Sep. 2004, doi: 10.1016/S0140-6736(04)17104-3.
- [339] A. B. Singleton *et al.*, "alpha-Synuclein locus triplication causes Parkinson's disease," *Science*, vol. 302, no. 5646, p. 841, Oct. 2003, doi: 10.1126/SCIENCE.1090278.
- [340] H. Deng and L. Yuan, "Genetic variants and animal models in SNCA and Parkinson disease," *Ageing Res Rev*, vol. 15, no. 1, pp. 161–176, 2014, doi: 10.1016/J.ARR.2014.04.002.

-
- [341] C. Camilloni and M. Vendruscolo, "A relationship between the aggregation rates of α -synuclein variants and the β -sheet populations in their monomeric forms," *J Phys Chem B*, vol. 117, no. 37, pp. 10737–10741, Sep. 2013, doi: 10.1021/JP405614J.
- [342] G. A. P. de Oliveira and J. L. Silva, "Alpha-synuclein stepwise aggregation reveals features of an early onset mutation in Parkinson's disease," *Commun Biol*, vol. 2, no. 1, Dec. 2019, doi: 10.1038/S42003-019-0598-9.
- [343] K. J. Lin *et al.*, "The Overcrowded Crossroads: Mitochondria, Alpha-Synuclein, and the Endo-Lysosomal System Interaction in Parkinson's Disease," *Int J Mol Sci*, vol. 20, no. 21, Nov. 2019, doi: 10.3390/IJMS20215312.
- [344] A. L. Mahul-Mellier *et al.*, "The process of Lewy body formation, rather than simply α -synuclein fibrillization, is one of the major drivers of neurodegeneration," *Proc Natl Acad Sci U S A*, vol. 117, no. 9, pp. 4971–4982, Mar. 2020, doi: 10.1073/PNAS.1913904117/-/DCSUPPLEMENTAL.
- [345] J. S. Ju and C. C. Weihl, "Inclusion body myopathy, Paget's disease of the bone and fronto-temporal dementia: a disorder of autophagy," *Hum Mol Genet*, vol. 19, no. R1, Apr. 2010, doi: 10.1093/HMG/DDQ157.
- [346] H. Meyer and C. C. Weihl, "The VCP/p97 system at a glance: connecting cellular function to disease pathogenesis," *J Cell Sci*, vol. 127, no. Pt 18, pp. 3877–3883, 2014, doi: 10.1242/JCS.093831.
- [347] J. L. Brodsky, "Cleaning up: ER-associated degradation to the rescue," *Cell*, vol. 151, no. 6, pp. 1163–1167, Dec. 2012, doi: 10.1016/J.CELL.2012.11.012.
- [348] J. Boch, "TALEs of genome targeting," *Nat Biotechnol*, vol. 29, no. 2, pp. 135–136, Feb. 2011, doi: 10.1038/NBT.1767.

7. Review

Dysregulated Interorganellar Crosstalk of Mitochondria in the Pathogenesis of Parkinson's Disease

Lara Sironi ^{1,*}, Lisa Michelle Restelli ¹, Markus Tolnay ¹, Albert Neutzner ^{2,3} and Stephan Frank ^{1,*}

^{1.} Division of Neuropathology, Institute of Medical Genetics and Pathology, University Hospital Basel, Basel 4031, Switzerland; lisa.restelli@usb.ch (L.M.R.); markus.tolnay@usb.ch (M.T.)

^{2.} Department of Biomedicine, University Hospital Basel, University of Basel, Basel 4031, Switzerland; albert.neutzner@unibas.ch

^{3.} Department of Ophthalmology University Hospital Basel, University of Basel, Basel 4031, Switzerland

* Correspondence: lara.sironi@usb.ch (L.S.); stephan.frank@usb.ch (S.F.); Tel.: +41-61-265-2776 (L.S. & S.F.)

Received: 17 December 2019; Accepted: 16 January 2020; Published: date

Abstract: The pathogenesis of Parkinson's disease (PD), the second most common neurodegenerative disorder, is complex and involves the impairment of crucial intracellular physiological processes. Importantly, in addition to abnormal α -synuclein aggregation, the dysfunction of various mitochondria-dependent processes has been prominently implicated in PD pathogenesis. Besides the long-known loss of the organelles' bioenergetics function resulting in diminished ATP synthesis, more recent studies in the field have increasingly focused on compromised mitochondrial quality control as well as impaired biochemical processes specifically localized to ER-mitochondria interfaces (such as lipid biosynthesis and calcium homeostasis). In this review, we will discuss how dysregulated mitochondrial crosstalk with other organelles contributes to PD pathogenesis.

Keywords: α -syn; LRRK2; DJ-1; Parkin; PINK1; ATP13A2; VPS35; MAM; mitophagy; neurodegeneration

1. Introduction

Parkinson's disease (PD), the most common movement neurodegenerative disorder, is a complex multifactorial disease with an incidence range between 5 up to >35 per 100,000 population [1]. Clinically, it is characterized by motor symptoms such as bradykinesia, resting tremor, muscle rigidity, and postural instability, which may be accompanied by depression, sleep disorders, anosmia, and, with disease progression, dementia. The neuropathological hallmarks of the disease include a progressive loss of dopaminergic neurons in the substantia nigra (SN) pars compacta that project to the striatum, and the presence of α -synuclein (α -syn) positive neuronal inclusions known as Lewy bodies (LB) and Lewy neurites (LN) [2].

Familial and sporadic PD forms share common clinical, pathological, and biochemical characteristics. Although many aspects of PD pathogenesis remain elusive, dysregulation of various fundamental physiological processes has been implicated, including impairment of the ubiquitin-proteasome pathway, mitochondrial dysfunction, oxidative stress, and neuroinflammation.

Both environmental and genetic factors converge in the complex molecular pathophysiology of Parkinson's disease, with mitochondrial dysfunction playing a major role [3–6]. A discussion of PD-associated risk factors is not the focus of our review. Several lines of evidence obtained from studies of

familial forms of PD, patient tissue samples, and various in vitro/in vivo models point to a prominent involvement of dysregulated mitochondrial crosstalk with other organelles in addition to impaired mitochondrial quality control pathways. Here, we start from genes that have been linked to familial forms of PD to discuss the role of interorganellar crosstalk involving mitochondria (Table 1).

Table 1. Parkinson's disease (PD)-linked genes related to mitochondria interorganellar contacts.

HGNC ID	Gene Symbol	Alternative Designation	Chromosomal Location
Mitochondria-associated membranes (MAMs)			
HGNC:11138	SNCA	α -synuclein	4q22.1
HGNC:8607	PRKN	Parkin	6q26
HGNC:14581	PINK1	PTEN-induced putative kinase 1 (PINK1)	1p36.12
HGNC:16369	PARK7	DJ-1	1p36.23
HGNC:18618	LRRK2	Leucine-rich repeat kinase-2 (LRRK2)	12q12
Mitochondria-lysosome contact sites			
HGNC:13487	VPS35	Vacuolar sorting protein 35 (VPS35)	16q11.2
HGNC:30213	ATP13A2	ATPase 13A2	1p36.13
HGNC:18618	LRRK2	Leucine-rich repeat kinase-2 (LRRK2)	12q12

Overview of PD-linked genes role in interorganellar crosstalk involving mitochondria. HGNC IDs are in accordance with the *HUGO Gene Nomenclature Committee at the European Bioinformatics Institute* (HGNC) (<https://www.genenames.org>).

We specifically focus on how dysregulated communication of mitochondria with endoplasmic reticulum and lysosomes as well as compromised quality control at the mitochondrial level contribute to PD pathogenesis. For each interorganellar contact, we first provide a brief overview on their physiological organization and functions, and then describe how PD-linked genes affect these functions (Figure 1).

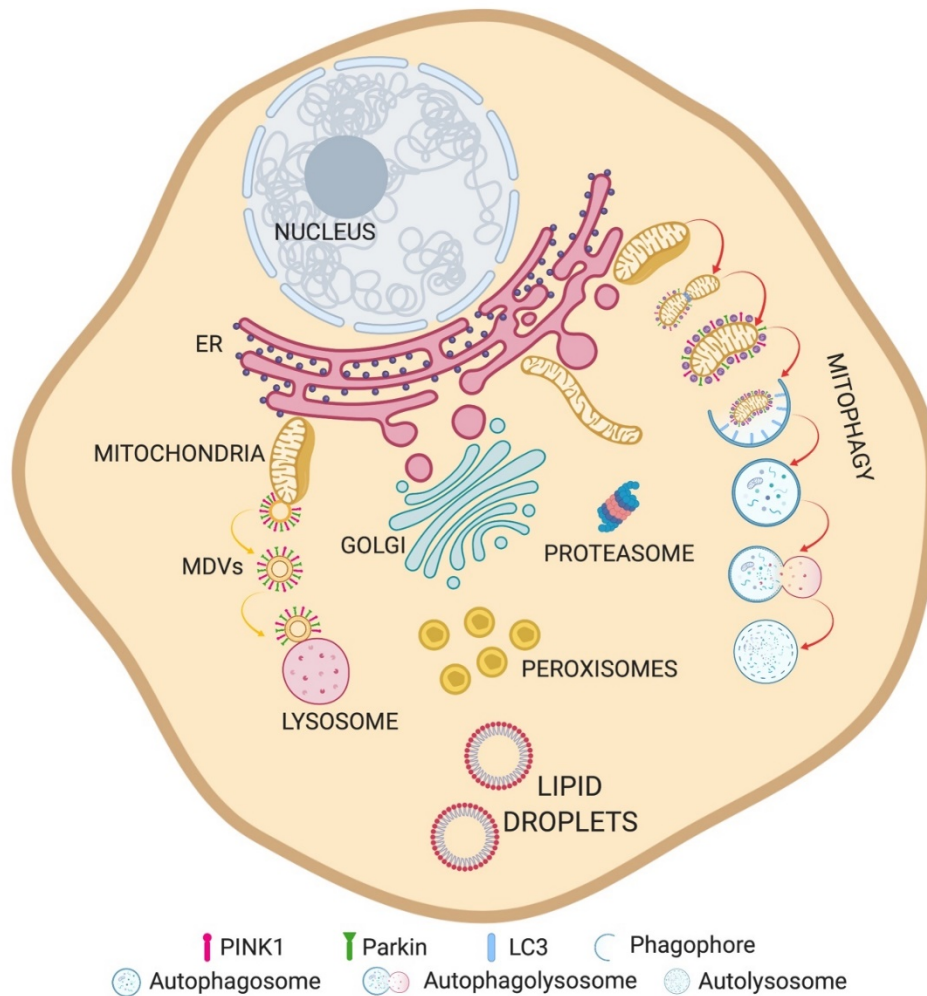


Figure 1. Overview of organelle crosstalks. Schematic representation of organelles and their relationships.

2. Mitochondria-Associated Membranes (MAMs)

The close apposition between ER and mitochondria was first described as an interorganellar contact by Bernhard in 1956 [7] and later by Copeland and Dalton, who, by electron microscopy, demonstrated the tight spatial relationship between these organelles in 1959 [8]. After performing fractionation studies, Jean Vance termed the biochemically distinct domains of the ER that are in close proximity to mitochondria MAMs (mitochondria-associated membranes), and showed that these specialized membrane contact sites contain the enzymatic activities involved in lipid transfer between ER and mitochondria for the biosynthesis of serine-containing phospholipids [9]. In electron microscopy studies, mitochondria were found to be in proximity to both smooth and rough ER tubules, with an interorganellar distance varying between 10 and 80 nm [8,10–12]. Different conditions, such as ER stress [13], metabolic state [12], and apoptotic stimuli [10] can affect the number, length, and/or width, as well as the protein composition [14] of these microdomains.

Reflecting their biochemical functions in lipid metabolism, MAMs are enriched in proteins such as phosphatidyl ethanolamine methyltransferase 2 (PEMT2), phosphatidylserine synthase 1 and 2 (PSS1/2) [15,16], and fatty acid CoA ligase 4 (FACL4). The latter, involved in triacylglycerol synthesis, is considered one of the most reliable MAM marker proteins [17].

Lipid synthesis, in particular the synthesis of triacylglycerol, phosphatidylcholine (PC), and phosphatidylethanolamine (PE), requires enzymatic activities associated with both ER and

mitochondria. Phosphatidylserine (PS) is synthesized from PA by PSS1 in MAMs and is converted to PE by PS decarboxylase in mitochondria. One of the enzymes implicated in the final steps of PC synthesis, PEMT2 [18], was found to be restricted to MAMs [16].

Another enzyme located at ER–mitochondrial contact sites is acyl-CoA/diacylglycerol acyltransferase 2 (DGAT2), which catalyzes triacylglycerol synthesis and promotes lipid droplet formation [19]. MAMs are also enriched in further lipid metabolism enzymes, such as acyl-CoA/cholesterol acyltransferase 1 (ACAT1/SOAT1), which catalyzes the production of cholesterol esters that are subsequently incorporated into lipid droplets.

Besides their role in lipid metabolism, MAMs are also critically involved in Ca^{2+} homeostasis [20–22], as reflected by the enrichment of the Ca^{2+} channel inositol-1,4,5-triphosphate (IP3) receptor (IP3R) at these contact sites [23,24]. IP3Rs: type 3 is strongly enriched at MAMs [25]. Thus, MAMs represent Ca^{2+} signaling hubs providing ER-to-mitochondria Ca^{2+} transfer to maintain cellular bioenergetics, mitochondrial dynamics and transport, and also to modulate cell death decisions [26–28].

The stimulation of Ca^{2+} release from the ER through IP3Rs forms microdomains with high Ca^{2+} concentrations, which are important for the Ca^{2+} uptake into the mitochondrial matrix [20,29]. Mitochondrial Ca^{2+} uptake involves its diffusion across voltage-dependent anion channels (VDACs) of the outer mitochondrial membrane (OMM) [30] and the subsequent uptake through the low-affinity mitochondrial calcium uniporter (MCU), juxtaposed at the inner mitochondrial membrane (IMM) [31,32]. Indeed, Ca^{2+} concentrations modulate the enzymatic activities of mitochondrial ATP synthase and of the dehydrogenases that provide reducing equivalents to the respiratory chain [26]; they also regulate protein folding capacity, as ER chaperones depend on Ca^{2+} [33]. Ca^{2+} homeostasis is facilitated by cytosolic Ca^{2+} re-uptake into the ER through the sarco/endoplasmic reticulum (SR/ER) Ca^{2+} ATPase pump (SERCA) [34]. While Ca^{2+} fluxes enhance upon increased energy demand [35], excessive Ca^{2+} transfer can initiate programmed cell death through mitochondrial Ca^{2+} overload and opening of the mitochondrial permeability transition pore, leading to pro-apoptotic mediator release from mitochondria with subsequent effector caspase activation [36].

IP3R interacts with the OMM protein voltage-dependent anion channel isoform 1 (VDAC1) through glucose-regulated protein 75 (GRP75), a member of the Hsp70 family of chaperones, forming an interorganellar tethering complex between ER and mitochondria [22]. However, loss of IP3R does not interfere with ER–mitochondria association, which argues against an indispensable role of this Ca^{2+} channel in ER–mitochondria tethering [9]. As discussed below, additional ER–mitochondrial tethers exist.

Close physical, bidirectional interactions between ER and the mitochondrial network also play an important role in mitochondrial fission. The mitochondrial adaptors syntaxin 17, Mff, MiD49, and MiD51 that are involved in the recruitment of the fission-promoting dynamin-related protein Drp1 localize to ER–mitochondria interfaces [37,38]. ER tubules wrap around mitochondria, mediating constriction of the organelles at sites where subsequent mitochondrial division will occur [39]. Recent reports indicate that ER-bound inverted formin 2 (IFN2) mediates actin polymerization to promote mitochondrial fission [40]. Moreover, ER–mitochondria contact sites are spatially linked to actively replicating mitochondrial nucleoids, thereby coordinating mitochondrial DNA (mtDNA) synthesis with mitochondrial division to enable proper distribution of nucleoids between daughter mitochondria [41].

In addition, MAMs are also involved in the regulation of mitochondrial retrograde and anterograde transport along microtubules. In this context, at resting cytosolic Ca^{2+} concentrations, mitochondria move at maximal velocity, while their motility is reduced at IP3R-dependent Ca^{2+} hotspot regions, so that mitochondria accumulate and enhance local Ca^{2+} buffering by Ca^{2+} uptake which represents an important feedback mechanism in Ca^{2+} signaling [27].

The protein composition of some tethering complexes at MAM level continues to be a matter of debate. While Mitofusin 2 (MFN2), localized both on the ER and OMM, has been implicated in regulating ER–mitochondria juxtaposition, the field is still divided on the question of whether it functions as tether [42–44] or tethering inhibitor [45–48] (Figure 2).

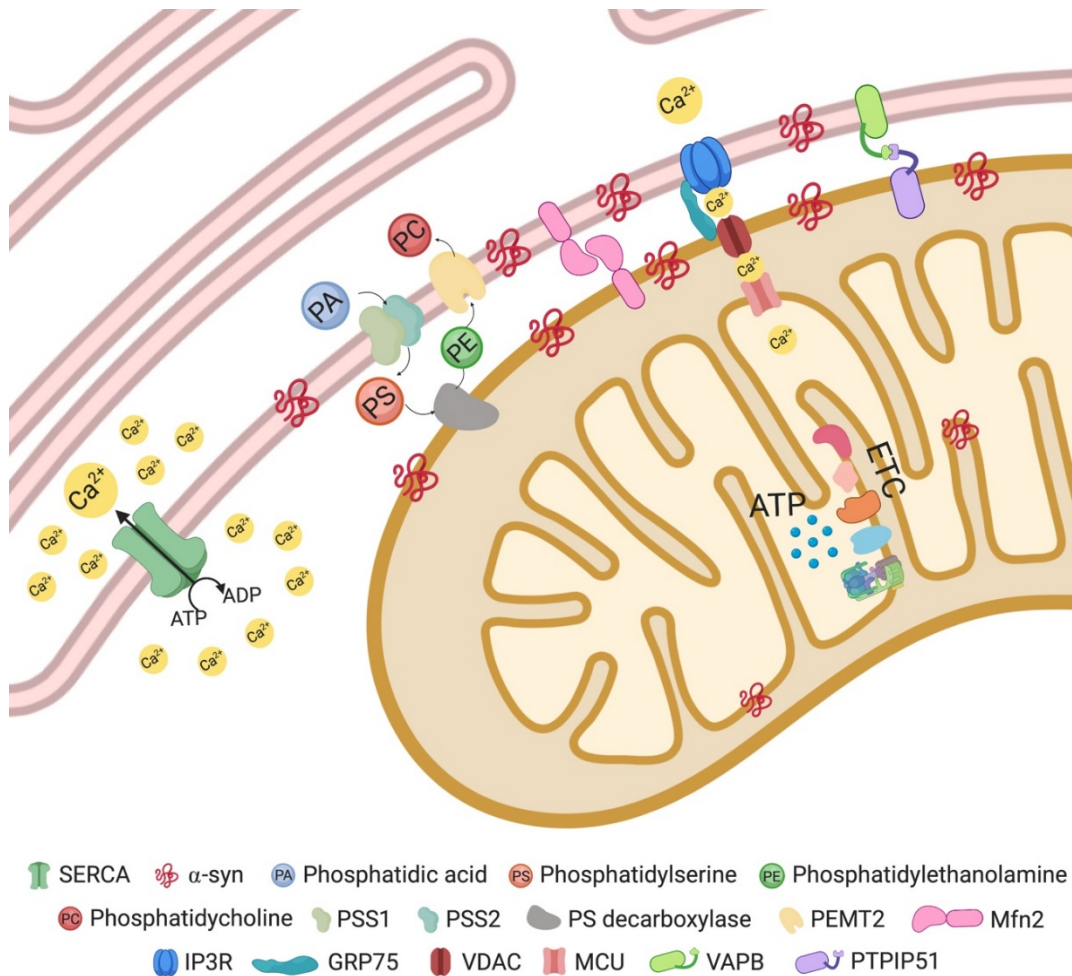


Figure 2. Mitochondria–ER contact site and main resident proteins (see text for details).

Various proteins localized at ER–mitochondria interface such as PACS-2 [49] and GRP75 [22] affect organelle proximity upon modulation of their expression. It still remains unclear how these proteins mediate the tethering between the two organelle membranes. A direct role in tethering has been highlighted for a complex formed by Vesicle-associated membrane protein-associated protein B (VAPB) enriched in MAMs, and the OMM protein tyrosine phosphatase-interacting protein 51 (PTPIP51) [50]. In various biochemical assays, VAPB and PTPIP51 were shown to interact, and modulation of their expression (by siRNA knockdown or overexpression) affects ER–mitochondrial Ca^{2+} exchange and modulates interorganellar contacts, as assayed by EM. Beyond its Ca^{2+} exchange function, this ER–mitochondria tethering complex was also proposed to play a role in autophagy regulation [51]. In addition, an interaction of the VAPB–PTPIP51 complex with two other proteins which localize at the ER–mitochondria interface, oxysterol-binding protein (OSBP)-related protein 5 (ORP5) and OSBP-related protein 8 (ORP8), was shown recently [52].

2.1. MAMs in Parkinson's Disease

MAMs serve crucial functions in various signaling pathways and metabolic processes, including mitochondrial bioenergetics and dynamics, Ca^{2+} homeostasis, and autophagy. While many of these functions are compromised in neurodegenerative disorders including Parkinson's disease (PD), it is still unclear whether MAM dysregulation is cause or consequence of the pathogenic processes leading to neurodegeneration. Nevertheless, it seems clear that MAM dysfunction can accelerate neuronal death. Both changes in the number of contacts between ER and mitochondria, and impairments of their functionality have been associated with PD [53–55].

Mutations in several PD-associated genes have been causally related to mitochondrial dysfunction. Even if our current knowledge about the role of PD-related proteins in ER–mitochondria crosstalk is still far from complete, the following sections highlight their roles in maintaining MAM structure and function.

2.1.1. α -Synuclein

SNCA was the first gene to be associated with familial cases of PD [56]. It encodes α -syn, a 14 kDa protein highly expressed in nervous tissues. On the cellular level, α -syn was found at presynaptic terminals where it is required for rapid and efficient clathrin-mediated synaptic vesicle endocytosis [57,58], reflecting a role in synaptic transmission. Beside its presence in the cytosol, a fraction of α -syn has been identified in mitochondria [59], where it is required for normal respiratory chain complex activity [60,61]. α -syn can influence Ca^{2+} exchange and the physical interaction between ER and mitochondria, as reported by different groups, with still-debated downstream effects [53,62,63].

α -syn presence has important implications for mitochondrial integrity: expression of either the α -syn disease mutation A53T at low levels, or of wild-type α -syn at high levels, result in fragmented mitochondria [64]. The mitochondrial fragmentation caused by α -syn mutations was reported to be independent of DRP1, as the function and recruitment of the fission protein to mitochondria was unaffected. It has been hypothesized that the increased mitochondrial fragmentation could be due to increased OPA1 cleavage, via an unknown mechanism [62].

Importantly, a portion of α -syn seems to be localized at MAMs [62], consistent with previous observations that the protein preferentially binds to lipid rafts [65] and to membrane domains rich in acidic phospholipids [66].

Pathogenic mutations of α -syn affect its binding to lipid membranes [67], as exemplified by the pathogenic A30P mutation, which decreases the amount of α -syn present in MAMs [65]. Decreased amounts of MAM-localized α -syn are also observed upon expression of the disease-causing mutation A53T [62], although in this case the ability of the mutant protein to bind to lipid membranes did not seem to be compromised [65]. It is known that this particular mutation makes the protein more prone to aggregation [68]. The reported net effect of both mutations (A53T, A30P) was a reduced amount of α -syn within MAMs and a concomitant increase of the mutant protein in the pure mitochondrial fraction, potentially leading to a decrease in mitochondrial membrane potential (MMP) [69] (Figure 3a).

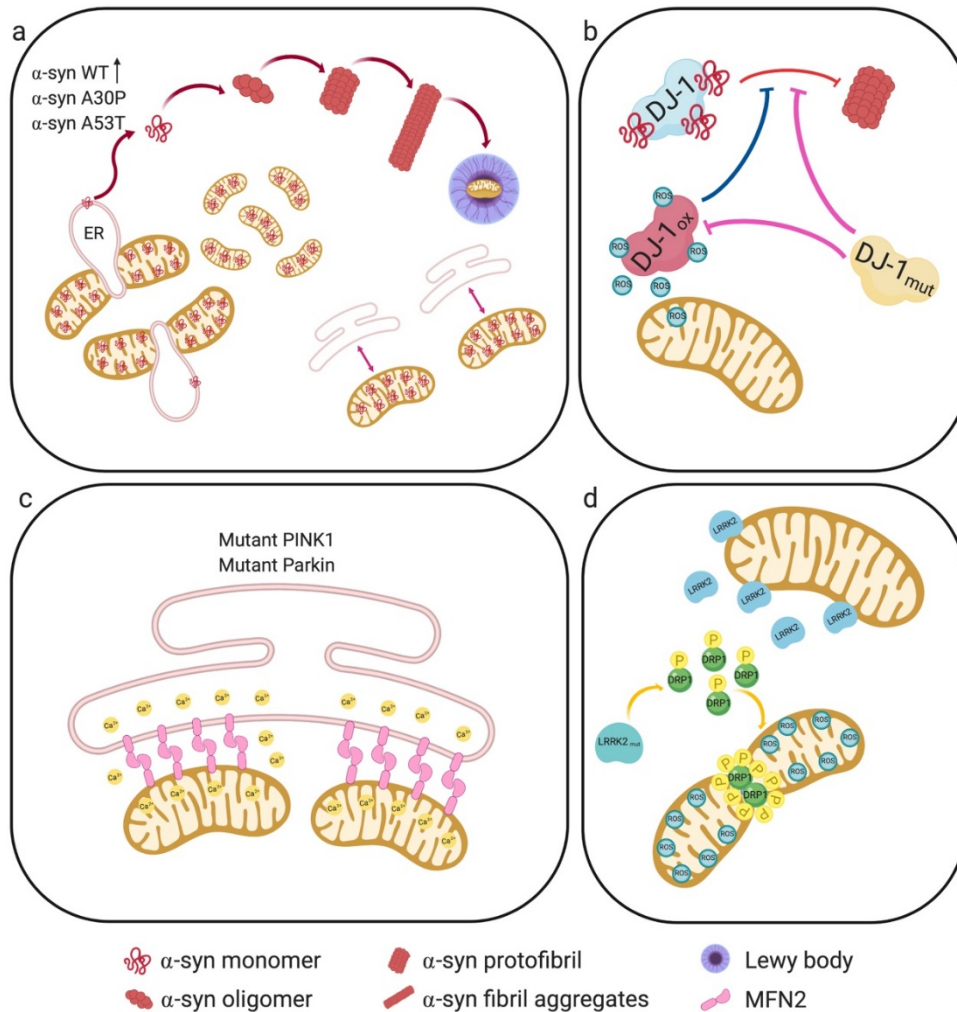


Figure 3. PD-associated genes and their roles in Mitochondria-associated membrane (MAM) structure and function. **(a)** Mutant α -syn results in DRP1-independent mitochondrial fragmentation, reduced MAM-associated mutant α -syn, with a concomitant increase in the pure mitochondrial fraction. This results in reduced ER–mitochondria apposition, leading to impaired interorganellar crosstalk. The A53T mutation makes the protein more prone to aggregation. **(b)** DJ-1 responds to oxidative stress, protecting cells against ROS. DJ-1 interacts with monomeric and oligomeric α -syn, preventing its oligomerization. Under oxidative stress conditions, oxidized DJ-1 is unable to interact with α -syn and to prevent its oligomerization. Likewise, DJ-1 mutations also abrogate its interaction with α -syn and no longer neutralize ROS. **(c)** Mutant PINK1 or Parkin increase ER–mitochondria juxtapposition, resulting in aberrant ER-to-mitochondria Ca^{2+} signaling. Furthermore, Parkin dysfunction could lead to increased levels of its substrate MFN2 at MAMs. **(d)** LRRK2 mutations increase its interaction with DRP1, and enhance DRP1 phosphorylation. This results in mitochondrial fragmentation, enhanced ROS, and decreased ATP levels.

This reduced MMP could promote OPA1 cleavage and consequently mitochondrial fragmentation [70]. In addition, decreased localization of both α -syn mutants at MAMs also reduced ER–mitochondria apposition, leading to impaired interorganellar crosstalk with compromised lipid synthesis; in fact, the conversion of PS into PE, a well-recognized biochemical MAM activity, was decreased upon mutant α -syn expression [62].

Although α -syn was shown to be a major component of Lewy bodies more than 20 years ago [71], subsequent proteomic studies revealed that LB consist of more than 300 proteins, of which around 90 were confirmed by immunohistochemistry [72]. Transmission electron microscopy (TEM) studies revealed that LB are composed of filamentous structures immunoreactive for α -syn [73]. More recently,

Shahmoradian and colleagues, using correlative light and electron microscopy (CLEM), demonstrated that the vast majority of LB and LN actually consist of a crowded environment of membrane fragments, dysmorphic mitochondria and vesicular structures resembling lysosomes and autophagosomes, combined with non-fibrillar α -syn [74]. It has been hypothesized that these observations could reflect cellular attempts to segregate damaged lipid-based elements into aggresome-like structures. Indeed, LB were previously found to be immunoreactive for several markers of aggresomes [75], which form in response to cytoplasmic accumulation of misfolded protein [76,77].

2.1.2. Parkin and PINK1

Aggregated proteins and damaged organelles are removed from the cytoplasm by autophagic mechanisms [78]. Mitophagy is a selective form of autophagy that mediates the removal of damaged mitochondria, thereby contributing to mitochondrial turnover [79]. Activation of this process is essential to protect neurons from pro-apoptotic proteins released by damaged mitochondria, which would otherwise trigger programmed cell death pathways in the cytosol [80].

Intriguingly, two PD-associated proteins, PTEN-induced putative kinase 1 (PINK1), a mitochondrially localized kinase, and Parkin, a cytosolic E3 ubiquitin ligase, are the two key players of this mitophagic quality control system. Mutations in PINK1 and Parkin are linked to early-onset familial PD [81], and extensive research efforts during the last decade have uncovered important aspects of the underlying pathogenic processes, some of which may also be shared with sporadic (idiopathic) PD.

Under basal conditions, PINK1 is imported into mitochondria through the translocase of the outer membrane (TOM) complex and then through the translocase of the inner membrane complex (TIM) into the matrix, where it is cleaved by the matrix processing peptidase and the inner membrane protease presenilin-associated rhomboid-like protease (PARL) [82–84]. Thereafter the cleaved product is released into the cytoplasm to be degraded by the proteasome via the N-end rule pathway [85]. However, in response to mitochondrial damage (loss of MMP or accumulation of misfolded proteins), PINK1 accumulates on the OMM. In addition to autophosphorylation, PINK1 phosphorylates Parkin, increasing its E3 ligase activity [86,87], and also phosphorylates pre-existing ubiquitin molecules at the mitochondrial surface [88]. Parkin is then thought to bind to phosphorylated ubiquitin, resulting in partial activation and tethering of Parkin to the OMM. The actions of PINK1 and Parkin contribute to amplification of ubiquitin phosphorylation, leading to conjugation of ubiquitin to several substrates [89]. The ubiquitinated cargo is then bound to specific autophagy receptor proteins that connect it to autophagosomes [90] which are formed at MAMs. In support of this model, upon stimulation of mitophagy, endogenous PINK1 was also found to be localized at MAMs.

Relevant to the ER-mitochondria interface, Parkin was also shown to ubiquitinate MFN2, VDACs and Miro [81]. BECN1/Beclin1 is required for the accomplishment of the mitophagic process, and silencing of this protein activates pro-apoptotic pathways [91]. Finally, autophagosomes fuse with lysosomes to complete the mitophagic process [92].

Fibroblasts from patients carrying mutated PINK1 or Parkin display increased ER-mitochondria juxtaposition, resulting in aberrant ER-to-mitochondria Ca^{2+} signaling [93,94]. Similar alterations were observed in mouse embryonic fibroblasts from Parkin knock-out mice and attributed to MFN2, which as a Parkin substrate is increased at the MAM fraction upon Parkin dysfunction [94] (Figure 3c).

Parkin and PINK1 null mice generally fail to recapitulate the degeneration of dopaminergic neurons in the SN [95–97]. Furthermore, loss of Parkin does not worsen the neurodegenerative phenotype of MitoPark mice [98]. Nevertheless, Parkin activity is critical for the survival of nigral dopaminergic neurons in Mutator mice (homozygous for a proofreading deficiency in DNA polymerase γ) which have accelerated mtDNA mutation rates [99].

Parkin was reported to co-regulate ER-mitochondria contact sites together with the transcription factor peroxisome proliferator-activated receptor γ coactivator 1 α (PGC-1 α), a key modulator of mitochondrial biogenesis [100]. Loss of Parkin function results in the accumulation of the zinc finger transcriptional repressor Parkin interacting substrate (PARIS), which suppresses PGC-1 α -dependent

transcription. Postmortem analysis of SN tissue of PD patients validated this finding, with dopaminergic neurons displaying reduced PGC-1 α levels [101].

Parkin has a Ser65 residue within its N-terminal ubiquitin-like (UBL) domain, similar to that of ubiquitin. This residue is phosphorylated by PINK1, resulting in an open and active conformation [102,103]. Characterization of primary cells derived from two unrelated, early-onset PD patients with homozygous Parkin Ser65Asn (ParkinS65N) mutation demonstrated that this mutant is inactive, suggesting that the loss of PINK1-dependent Parkin Ser65 phosphorylation and subsequent inactivation in humans is sufficient to cause PD [104].

PINK1-deficiency in *Drosophila*, mouse models and patient-derived cells resulted in mitochondrial complex I defects [105] and decreased mitochondrial membrane potential [106], associated with loss of Ser250 phosphorylation of the complex I subunit NADH ubiquinone oxidoreductase subunit A10 (NDUFA10).

2.1.3. DJ-1

The DJ-1 protein serves a broad variety of functions. It plays an essential role in sensing and reacting to oxidative stress, thereby protecting cells against reactive oxygen species (ROS) [107,108]. Within its active site, DJ-1 contains an essential cysteine residue that functions as an oxidative stress sensor. Beyond this function, DJ-1 neutralizes ROS [107,109]: mitochondria-localized DJ-1 is a component of the thioredoxin/apoptosis signal-regulating kinase 1 (Trx/Ask1) complex, which regulates the clearance of endogenous ROS through activation of the radical scavenging system [110]. Brains of PD patients contain high levels of oxidized DJ-1, which indicates an increased ROS scavenging activity [111,112].

In addition to oxidative stress, DJ-1 protects against other toxic agents by modulating PTEN activity and Akt signaling [113,114], either by interacting with the MAPK kinase cascade [115], the p53 pathway [114,116], or by stabilizing the antiapoptotic Bcl-XL protein [117]. Crystallography revealed that DJ-1 is a homodimer, which appears to be critical for its physiological function [118–120].

DJ-1 protein localizes at MAMs where it modulates ER–mitochondria interactions and consequently Ca²⁺ transfer between the two organelles, thereby maintaining mitochondrial function and structure. Depletion or lack of function of this protein causes alterations of mitochondrial morphology, decreases mitochondrial membrane potential, reduces ER-to-mitochondria Ca²⁺ transfer and impairs mitochondrial motility in neurites [55].

Whereas mutations in the gene encoding DJ-1 (PARK7) lead to familial early-onset PD, the exact mechanisms underlying its role in PD pathogenesis still remain elusive [121,122]. In *in vitro* systems as well as in living cells, DJ-1 interacts directly with monomeric and oligomeric α -syn [123]. The same study showed that familial DJ-1 mutations (L166P, M26I, L10P and P158 Δ) abrogated its interaction with α -syn, which could be due to the low expression levels of DJ-1 mutants, as they are more rapidly degraded than wild-type DJ-1 protein [120]. Furthermore, the above-mentioned DJ-1 mutants correlate with increased α -syn oligomerization, suggesting a loss of DJ-1 chaperone function [123]; (Figure 3b).

2.1.4. LRRK2

Leucine-rich repeat kinase-2 (LRRK2) is a large, multi-domain protein involved in a number of functions, such as GTP hydrolysis, kinase activity, and protein binding. Even though its cellular function is largely unknown, emerging evidence attributes to LRRK2 roles in autophagic regulation, microtubule dynamics, and mitochondrial function. In addition to being localized mainly to the cytoplasm, some LRRK2 also resides at mitochondria [124].

Autosomal dominant LRRK2 mutations are associated with both familial and sporadic PD [125,126]. Expression of mutant LRRK2 induces several negative effects at the mitochondrial level, such as increased fragmented mitochondria that produce more ROS and less ATP, leading to increased cell vulnerability to stressors. Skin biopsies from patients carrying the G2019S mutation, which results in an increased kinase activity of the protein, show reduced mitochondrial membrane potential, aberrant

organelle morphology, and decreased total intracellular ATP levels [127]. It still remains unclear how this increased kinase activity impairs cellular functions and promotes cell death [128].

LRRK2 interacts with a number of mitochondrial fission/fusion regulators, either in the cytosol or on mitochondrial membranes [129]. It was shown that LRRK2 associates with Drp1, the key mediator of mitochondrial fission. Neuronal expression of two LRRK2 mutants, G2019S and R1441C, led to increased interaction with DRP1 and higher phosphorylation levels of the fission protein, resulting in mitochondrial fragmentation and enhanced ROS levels [130,131] (Figure 3d).

LRRK2 also interacts and modulates the activities of the mitochondrial fusion regulators MFN1, MFN2, and OPA1. Indeed, PD patients carrying the G2019S mutation showed decreased levels of L-OPA1 [129]. Moreover, fibroblasts and neuroblastoma cells expressing the G2019S mutant display increased basal oxygen consumption and a decreased mitochondrial membrane potential, potentially due to a proton leak caused by upregulation of mitochondrial uncoupling proteins 2 and 4 (UCP2, UCP4) [132]. Thus, the effect of increased LRRK2 activity is decreased mitochondrial fusion with concomitantly increased fission of the organelles, suggesting that LRRK2 may be an important modulator of mitochondrial dynamics.

LRRK2 kinase activity also regulates ER–mitochondrial tethering by modulating the PERK-dependent ubiquitination pathway under ER stress conditions. In this context, LRRK2 interacts with the E3 ubiquitin ligases MARCH5, MULAN, and Parkin, thereby blocking PERK-mediated phosphorylation and activation of these E3 ubiquitin ligases. Kinase-active LRRK2 (G2019S) dissociates from ER ubiquitin ligases, allowing PERK to phosphorylate and thereby activate these enzymes towards MAM components, impinging on ER–mitochondrial tethering [133].

Another crucial aspect of mitochondrial dynamics in the context of neurodegeneration is mitochondrial trafficking, where mitochondrial locomotion is tightly controlled to preserve energy homeostasis. Before the initiation of the mitophagy cascade, mitochondrial motility halts, enabling the sequestration of damaged mitochondria. This arrest of depolarized mitochondria is achieved by removal of the Miro protein from the mitochondrial surface; this process is promoted by LRRK2, which forms a complex with Miro, targeting it for PINK1/Parkin-dependent degradation [134]. Interestingly, the LRRK2 mutant G2019S disrupts its interaction with Miro, slowing down Miro degradation and mitochondrial arrest, consequently delaying mitophagy [124].

3. Mitochondria–Lysosome Membrane Contact Sites

Lysosomes, together with mitochondria, are critical for the maintenance of cellular homeostasis, as reflected by the fact that dysfunction of both organelles is functionally and genetically linked to several human diseases [135–138]. Similar to mitochondria, lysosomes are highly dynamic organelles that are responsible for the turnover of cellular components, including proteins and lipids, via mature enzymes stored in the lysosomal lumen. In addition, these organelles also act as iron and calcium stores. Furthermore, they can mediate cell death signaling upon lysosomal membrane permeabilization [139].

Whereas numerous reports have demonstrated indirect functional interactions between mitochondria and lysosomes [140–147], studies focusing on lysosomal degradation of mitochondria either through mitophagy [81] or via fusion of mitochondrial-derived vesicles (MDVs) with lysosomes [148] showed a direct interaction between these organelles upon cellular stress [149]. The mitophagic process can occur via mitophagy receptors (Optineurin and NDP52) which are recruited in a PINK1/Parkin-dependent manner to ubiquitinated mitochondria, which are then targeted through LC3 to the autophagosome [150,151]. Alternatively, MDVs [148] are small vesicles that bud off from mitochondria and contain distinct subsets of OMM and mitochondrial matrix proteins. MDVs generated in a PINK1/Parkin-dependent manner are targeted to lysosomes, to selectively degrade a subset of mitochondrial proteins instead of entire mitochondria [152].

Mitochondria–lysosome contact sites have been imaged in various cell types under healthy conditions taking advantage of different techniques, such as 2D and 3D electron microscopy [153,154], correlative light electron microscopy (CLEM) [153], CLEM combined with focused ion beam scanning electron microscopy (FIB-SEM) [155], lattice light sheet spectral imaging [156], and structured

illumination microscopy [153,157,158]. The average distance between mitochondrial and lysosomal membranes is ~10 nm [153,154], and approximately 15% of lysosomes are in contact with mitochondria at any time point, with contact sites remaining stably tethered for an average of 60 s [154,157]. These contact sites do not represent autophagosome biogenesis events or mitophagy, given their negative staining for autophagosome markers [153]. Furthermore, knockout of five autophagy receptors (NDP52, OPTN, NBR1, TAX1BP1, and p62) did not prevent mitochondria–lysosome contact formation [158]. Moreover, mitochondria involved in these contacts were distinct from MDVs as they contained intermembrane space and mitochondrial matrix proteins, and were larger (over 500 nm) compared to MDVs (about 100 nm) [148,153].

The small GTPase Rab7 is a master regulator of lysosomal maturation, positioning, and network dynamics [159]. As evidence of the importance of lysosomal dynamics, mutations in Rab7 lead to peripheral neuropathy in humans [160–163]. Rab7 modulates mitochondrial–lysosome tethering and untethering through its ability to alternate between an active, lysosomal-localized GTP-binding state, and an inactive, cytosolic GDP-binding state. Lysosomal GTP-bound Rab7 promotes tethering via lysosomal membrane-bound Rab7 effector proteins [153]. Then Rab7 GTP hydrolysis mediates the untethering, involving the recruitment of cytosolic TBC1D15 (Rab7 GAP) to mitochondria via the OMM protein Fis1 [164], where it can interact with lysosomal GTP-bound Rab7 to promote GTP hydrolysis. GDP-bound Rab7 is no longer able to bind Rab7 effectors and loses its localization to the lysosomal membrane [165] leading to untethering of the two organelles. Contact sites between mitochondria and lysosomes are also able to modulate mitochondrial dynamics, as most mitochondrial fission events (>80%) are marked by LAMP1-positive vesicles but not early endosomes or peroxisomes [153].

3.1. VPS35

Vacuolar sorting protein 35 (VPS35) is a key component of the retromer complex, involved in intracellular protein trafficking. VPS35 mediates retrograde delivery of cargo from endosomes to Golgi, as well as recycling endosomal cargo to the cell surface [166,167].

The retromer can be divided into a cargo-selective complex (CSC) trimer composed of VPS26, VPS29 and VPS35, involved in binding and sorting protein cargo [168,169], and a sorting nexin (SNX) dimer, consisting of SNX1 or SNX2 and SNX5 or SNX6 in mammalian cells (SNX5 and SNX17 in yeast). These SNX proteins are members of the SNX-BAR family and function in retromer association with the endosomal membrane through a Bin-Amphiphysin-Rvs (BAR) and phox homology (PX) domain [166,168].

VPS35 has a role in the formation of MDVs, which shuttle cargo from mitochondria to either peroxisomes or lysosomes, being so involved in mitochondria quality control [148,170]. This component of the retromer was found to interact with DRP1 and implicated in mitochondrial DRP1 complex recycling and mitochondrial fission. Indeed, DRP1 complexes are present on the OMM where they remain with daughter mitochondria after fission [171]. These complexes probably become inhibitory for subsequent fission events, owing to the occupancy of fission sites or to the sequestration of DRP1 recruiting factors [172–177]. Through the interaction between VPS35 and DRP1, the retromer mediates DRP1 complex removal from mitochondria to lysosomes or peroxisomes via the formation of MDVs, diminishing their inhibitory effects on mitochondrial fission [178].

Remarkably, the VPS35 D620N mutation is associated with autosomal-dominant PD [179,180]. PD patient fibroblasts expressing this mutated protein showed fragmented and functionally impaired mitochondria. These alterations were accompanied by an increased VPS35–DRP1 interaction leading to an enhanced turnover of mitochondrial DRP1 complexes through MDVs and lysosomal degradation [178].

VPS35 can also impinge on mitochondrial dynamics by an MFN2-dependent mechanism. A proteomic study suggested that VPS35/retromer interacts with the OMM E3 ubiquitin ligase MUL1 (also known as mitochondrial-anchored protein ligase, MAPL) [181]. VPS35 promotes the degradation of MUL1, which would otherwise degrade MFN2. Accordingly, the PD-linked VPS35 D620N mutation increases MUL1-mediated MFN2 degradation [182] (Figure 4a).

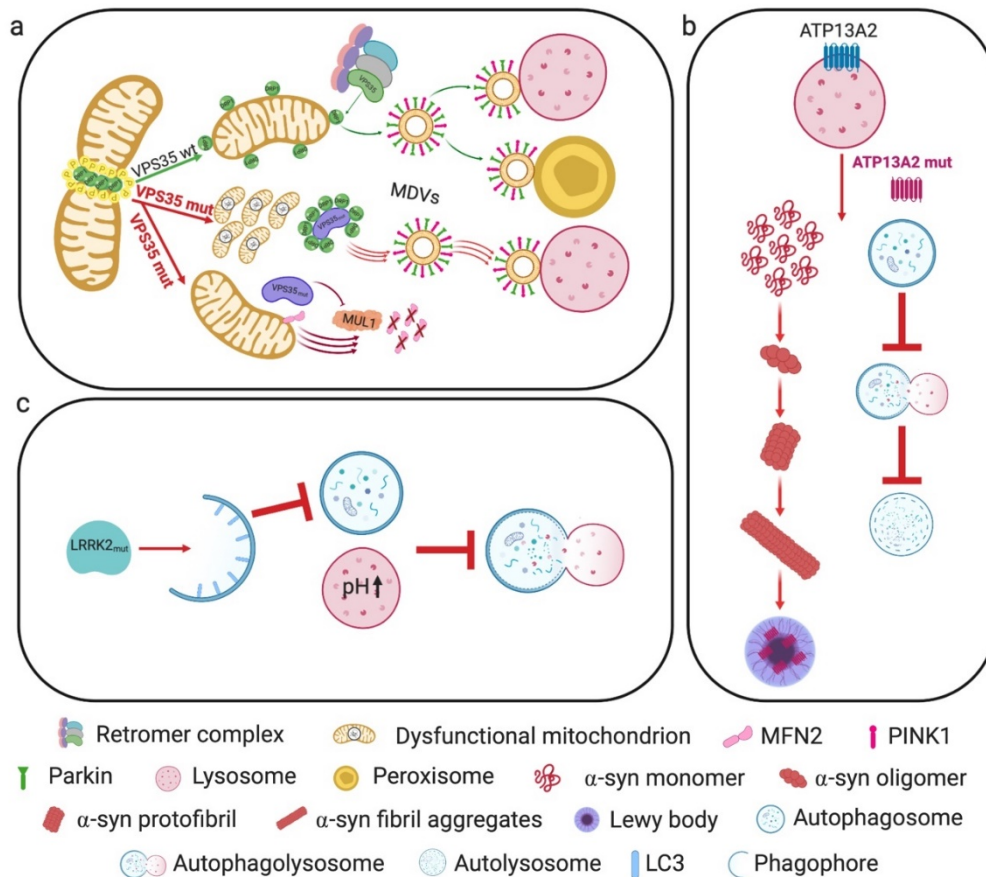


Figure 4. PD-associated genes and their roles in mitochondria-lysosome crosstalk. (a) VPS35 is a key component of the retromer complex involved in the removal of DRP1 complexes from mitochondria to lysosomes or peroxisomes through MDVs. Mutant VPS35 enhances turnover of mitochondrial DRP1 complexes through MDVs and lysosomal degradation, accompanied by fragmented and dysfunctional mitochondria. PD-linked VPS35 mutant also leads to increased MUL1-mediated MFN2 degradation. (b) ATP13A2 mutations impair the autophagic process, leading to the cytosolic accumulation of α -syn. Sporadic PD patients show decreased levels of this protein, which is also found in Lewy bodies. (c) Mutant LRRK2 protein impinges on autophagosome formation, alters lysosomal pH and lysosomal calcium dynamics, resulting in impaired autophagosome-lysosome fusion and lysosome-mediated degradation.

3.2. ATP13A2

The *PARK9* gene encodes the protein ATP13A2, a transmembrane lysosomal type 5 P-type ATPase [183], which has been linked to a neurodegenerative disorder known as Kufor-Rakeb syndrome (KRS), as well as to some juvenile and early-onset forms of PD [183–187]. Several studies focused on determining the cationic substrate of this transporter. While mammalian cell models supported Mn^{2+} -modulating activity of ATP13A2 [188–190], studies using KRS patient-derived cells revealed Zn^{2+} dyshomeostasis [191–193] causing abnormal mitochondrial and lysosomal metabolism, with dysfunctional energy production and reduced lysosomal proteolysis, respectively.

The analysis of fibroblasts from two patients with the L3292 and L6025 ATP13A2 mutations showed an impaired clearance of autophagic vacuoles, accompanied by impaired lysosomal acidification, cathepsin activity, and proteolytic capacity, while the delivery of substrates to lysosomes by either macroautophagy or chaperone-mediated autophagy (CMA) translocation did not seem to be affected [194]. α -syn can be degraded by lysosomal pathways, such as macroautophagy and CMA, as well as by the proteasome [195,196].

PD-linked mutations in ATP13A2 may result in insufficient clearance of α -syn through lysosomes, resulting in its accumulation in the cytosol. Furthermore, postmortem nigral tissue samples from sporadic PD patients exhibited decreased neuronal levels of ATP13A2, which appeared to be mostly trapped in Lewy bodies [194] (Figure 4b).

3.3. LRRK2

Beside its involvement at MAMs (described above), LRRK2 serves a critical role in the autophagic pathway at the lysosomal level. During autophagy, damaged organelles and aggregated proteins are engulfed within autophagosomes, subsequently delivered to the lysosome for degradation [197,198]. Local lysosomal release of calcium is required for autophagosome–lysosome fusion [199]. Any disruption affecting autophagosome formation, fusion of autophagosomes with amphisomes or lysosomes, hydrolytic degradation, or the re-formation of lysosomes can impair the autophagic process, resulting in accumulation of autophagy substrates and structures [197,198].

Lysosomal function and protein degradation are regulated by many factors, such as lysosomal pH [200], calcium release [199], and membrane trafficking [201]. Lysosomal dysfunction was shown to lead to α -syn accumulation [202], which could play a role in the formation of Lewy bodies, the pathological hallmark of PD. Furthermore, LRRK2 has been implicated in lysosomal pH regulation [203,204], which is critical for the activity of degradative enzymes and for the fusion of autophagosomes and lysosomes [205]. The authors of [206] investigated the role of LRRK2 in lysosome biology and the autophagy pathway in primary neurons by expressing human wild-type LRRK2 (hWT-LRRK2) and the human LRRK2-G2019S or LRRK2-R1441C mutations, and demonstrating that mutations in different enzymatic domains elicit different effects on LRRK2 enzymatic activity. Neurons expressing hWT-LRRK2 or LRRK2-G2019S displayed a decreased rate of autophagosome formation, which was dependent on LRRK2 kinase activity.

In contrast, neurons expressing LRRK2-R1441C displayed a significantly increased lysosomal pH and alterations in lysosomal calcium dynamics, resulting in impaired autophagosome–lysosome fusion and decreased lysosome-mediated degradation (Figure 4c). These latter effects occurred independently of LRRK2 kinase activity. It is interesting to note here that hWT-LRRK2 interacts with the α 1 subunit of the v-type H⁺ ATPase proton pump (vATPase α 1), responsible for the regulation of lysosomal pH. Conversely, LRRK2-R1441C loses this interaction, leading to dysregulated vATPase α 1 protein expression and cellular localization, and resulting in impaired autolysosome maturation [206].

4. Perspective

Over decades, research on PD pathogenesis has been dominated by a focus on mitochondrial bioenergetic defects, oxidative stress, and cell death mechanisms. With the discovery in 1997 that Lewy bodies are composed of misfolded/aggregated α -syn [72] and that mutations in the α -syn gene were linked to some inherited forms of the disease [57], the attention of the field has increasingly shifted towards the mechanisms of abnormal protein aggregation and spreading of α -syn pathology. The last years have further improved our understanding of the disease; in particular, the pathogenic importance of properly regulated interorganellar crosstalk was increasingly recognized. Relatively recent insights into dysregulated crosstalk of mitochondria with the endoplasmic reticulum and lysosomes may provide the foundation for a more unifying picture that could help to explain how mitochondrial dysfunction, bioenergetic defects, abnormal protein aggregation, and neuronal cell death converge in PD pathogenesis.

Clearly, our understanding of the complex molecular mechanisms underlying PD pathogenesis and progression is still far from complete, and crucial questions remain to be answered. Among these, it remains to be clarified what event(s) initiate(s) PD pathogenesis, how Lewy bodies form, which of the intracellular functions of α -syn are actually relevant for disease onset and progression, and what role the microbiome plays in modulating PD, to name but a few.

As research efforts in this field increasingly focus on interorganellar communication as opposed to single organelle biology [207], we expect that the picture of PD pathogenesis will become more defined in the near future.

Author Contributions: All authors were involved in manuscript writing and approved the submitted version.

Funding: The authors acknowledge funding by the Bangerter-Rhyner Foundation, the Mach-Gaensslen Foundation, and the Novartis Foundation for medical-biological Research (#18C194).

Conflicts of Interest: The authors declare no conflict of interest.

References

- Twelves, D.; Perkins, K.S.M.; Counsell, C. Systematic review of incidence studies of Parkinson's disease. *Mov. Disord.* **2003**, *18*, 19–31.
- Dauer, W.; Przedborski, S. Parkinson's disease: mechanisms and models. *Neuron* **2003**, *39*, 889–909.
- Hu, Q.; Wang, G. Mitochondrial dysfunction in Parkinson's disease. *Transl. Neurodegener.* **2016**, *5*, 14.
- Bose, A.; Beal, M.F. Mitochondrial dysfunction in Parkinson's disease. *J. Neurochem.* **2016**, *139 Suppl 1*, 216–231.
- Wang, B.; Abraham, N.; Gao, G.; Yang, Q. Dysregulation of autophagy and mitochondrial function in Parkinson's disease. *Transl. Neurodegener.* **2016**, *5*, 19.
- Zanellati, M.C.; Monti, V.; Barzaghi, C.; Reale, C.; Nardocci, N.; Albanese, A.; Valente, E.M.; Ghezzi, D.; Garavaglia, B. Mitochondrial dysfunction in Parkinson disease: evidence in mutant PARK2 fibroblasts. *Front. Genet.* **2015**, *6*, 78.
- Bernhard, W.; Rouiller, C. Close topographical relationship between mitochondria and ergastoplasm of liver cells in a definite phase of cellular activity. *J. Biophys. Biochem. Cytol.* **1956**, *2*, 73–78.
- Copeland, D.E.; Dalton, A.J. An association between mitochondria and the endoplasmic reticulum in cells of the pseudobranch gland of a teleost. *J. Biophys. Biochem. Cytol.* **1959**, *5*, 393–396.
- Vance, J.E. phospholipid synthesis in a membrane fraction associated with mitochondria. *J. Biol. Chem.* **1990**, *265*, 7248–7256.
- Csordás, G.; Renken, C.; Várnai, P.; Walter, L.; Weaver, D.; Buttle, K.F.; Balla, T.; Mannella, C.A.; Hajnóczky, G. Structural and functional features and significance of the physical linkage between ER and mitochondria. *J. Cell Biol.* **2006**, *174*, 915–921.
- Giacomello, M.; Pellegrini, L. The coming of age of the mitochondria-ER contact: a matter of thickness. *Cell Death Differ.* **2016**, *23*, 1417–1427.
- Sood, A.; Jeyaraju, D.V.; Prudent, J.; Caron, A.; Lemieux, P.; McBride, H.M.; Laplante, M.; Tóth, K.; Pellegrini, L. A Mitofusin-2-dependent inactivating cleavage of Opa1 links changes in mitochondria cristae and ER contacts in the postprandial liver. *Proc. Natl. Acad. Sci. U. S. A.* **2014**, *111*, 16017–16022.
- Bravo, R.; Vicencio, J.M.; Parra, V.; Troncoso, R.; Munoz, J.P.; Bui, M.; Quiroga, C.; Rodriguez, A.E.; Verdejo, H.E.; Ferreira, J.; et al. Increased ER-mitochondrial coupling promotes mitochondrial respiration and bioenergetics during early phases of ER stress. *J. Cell Sci.* **2011**, *124*, 2143–2152.
- Bravo-Sagua, R.; Parra, V.; Ortiz-Sandoval, C.; Navarro-Marquez, M.; Rodríguez, A.E.; Diaz-Valdivia, N.; Sanhueza, C.; Lopez-Crisosto, C.; Tahbaz, N.; Rothermel, B.A.; et al. Caveolin-1 impairs PKA-DRP1-mediated remodelling of ER-mitochondria communication during the early phase of ER stress. *Cell Death Differ.* **2019**, *26*, 1195–1212.
- Stone, S.J.; Vance, J.E. Phosphatidylserine synthase-1 and -2 are localized to mitochondria-associated membranes. *J. Biol. Chem.* **2000**, *275*, 34534–34540.
- Cui, Z.; Vance, J.E.; Chen, M.H.; Voelker, D.R.; Vance, D.E. Cloning and expression of a novel phosphatidylethanolamine N-methyltransferase. A specific biochemical and cytological marker for a unique membrane fraction in rat liver. *J. Biol. Chem.* **1993**, *268*, 16655–16663.
- Rusiñol, A.E.; Cui, Z.; Chen, M.H.; Vance, J.E. A unique mitochondria-associated membrane fraction from rat liver has a high capacity for lipid synthesis and contains pre-Golgi secretory proteins including nascent lipoproteins. *J. Biol. Chem.* **1994**, *269*, 27494–27502.
- Vance, D.E.; Walkey, C.J.; Cui, Z. Phosphatidylethanolamine N-methyltransferase from liver. *Biochim. Biophys. Acta* **1997**, *1348*, 142–150.

19. Stone, S.J.; Levin, M.C.; Zhou, P.; Han, J.; Walther, T.C.; Farese, R.V., Jr The endoplasmic reticulum enzyme DGAT2 is found in mitochondria-associated membranes and has a mitochondrial targeting signal that promotes its association with mitochondria. *J. Biol. Chem.* **2009**, *284*, 5352–5361.
20. Rizzuto, R.; Pinton, P.; Carrington, W.; Fay, F.S.; Fogarty, K.E.; Lifshitz, L.M.; Tuft, R.A.; Pozzan, T. Close contacts with the endoplasmic reticulum as determinants of mitochondrial Ca²⁺ responses. *Science* **1998**, *280*, 1763–1766.
21. Szabadkai, G.; Simoni, A.M.; Rizzuto, R. Mitochondrial Ca²⁺ uptake requires sustained Ca²⁺ release from the endoplasmic reticulum. *J. Biol. Chem.* **2003**, *278*, 15153–15161.
22. Szabadkai, G.; Bianchi, K.; Várnai, P.; De Stefani, D.; Wieckowski, M.R.; Cavagna, D.; Nagy, A.I.; Balla, T.; Rizzuto, R. Chaperone-mediated coupling of endoplasmic reticulum and mitochondrial Ca²⁺ channels. *J. Cell Biol.* **2006**, *175*, 901–911.
23. Mendes, C.C.P.; Gomes, D.A.; Thompson, M.; Souto, N.C.; Goes, T.S.; Goes, A.M.; Rodrigues, M.A.; Gomez, M.V.; Nathanson, M.H.; Leite, M.F. The type III inositol 1,4,5-trisphosphate receptor preferentially transmits apoptotic Ca²⁺ signals into mitochondria. *J. Biol. Chem.* **2005**, *280*, 40892–40900.
24. Rizzuto, R.; Pozzan, T. Microdomains of intracellular Ca²⁺: molecular determinants and functional consequences. *Physiol. Rev.* **2006**, *86*, 369–408.
25. Morciano, G.; Marchi, S.; Morganti, C.; Sbrano, L.; Bittremieux, M.; Kerkhofs, M.; Corricelli, M.; Danese, A.; Karkucinska-Wieckowska, A.; Wieckowski, M.R.; et al. Role of Mitochondria-Associated ER Membranes in Calcium Regulation in Cancer-Specific Settings. *Neoplasia* **2018**, *20*, 510–523.
26. Cárdenas, C.; Miller, R.A.; Smith, I.; Bui, T.; Molgó, J.; Müller, M.; Vais, H.; Cheung, K.-H.; Yang, J.; Parker, I.; et al. Essential regulation of cell bioenergetics by constitutive InsP₃ receptor Ca²⁺ transfer to mitochondria. *Cell* **2010**, *142*, 270–283.
27. Yi, M.; Weaver, D.; Hajnóczky, G. Control of mitochondrial motility and distribution by the calcium signal: a homeostatic circuit. *J. Cell Biol.* **2004**, *167*, 661–672.
28. Boehning, D.; Patterson, R.L.; Sedaghat, L.; Glebova, N.O.; Kurosaki, T.; Snyder, S.H. Cytochrome c binds to inositol(1,4,5) trisphosphate receptors, amplifying calcium-dependent apoptosis. *Nat. Cell Biol.* **2003**, *5*, 1051–1061.
29. Rizzuto, R.; Brini, M.; Murgia, M.; Pozzan, T. Microdomains with high Ca²⁺ close to IP₃-sensitive channels that are sensed by neighboring mitochondria. *Science* **1993**, *262*, 744–747.
30. Rapizzi, E.; Pinton, P.; Szabadkai, G.; Wieckowski, M.R.; Vandecasteele, G.; Baird, G.; Tuft, R.A.; Fogarty, K.E.; Rizzuto, R. Recombinant expression of the voltage-dependent anion channel enhances the transfer of Ca²⁺ microdomains to mitochondria. *J. Cell Biol.* **2002**, *159*, 613–624.
31. Baughman, J.M.; Perocchi, F.; Girgis, H.S.; Plovanich, M.; Belcher-Timme, C.A.; Sancak, Y.; Bao, X.R.; Strittmatter, L.; Goldberger, O.; Bogorad, R.L.; et al. Integrative genomics identifies MCU as an essential component of the mitochondrial calcium uniporter. *Nature* **2011**, *476*, 341–345.
32. De Stefani, D.; Raffaello, A.; Teardo, E.; Szabò, I.; Rizzuto, R. A forty-kilodalton protein of the inner membrane is the mitochondrial calcium uniporter. *Nature* **2011**, *476*, 336–340.
33. Simmen, T.; Lynes, E.M.; Gesson, K.; Thomas, G. Oxidative protein folding in the endoplasmic reticulum: tight links to the mitochondria-associated membrane (MAM). *Biochim. Biophys. Acta* **2010**, *1798*, 1465–1473.
34. Chemaly, E.R.; Troncone, L.; Lebeche, D. SERCA control of cell death and survival. *Cell Calcium* **2018**, *69*, 46–61.
35. Betz, C.; Stracka, D.; Prescianotto-Baschong, C.; Frieden, M.; Demaurex, N.; Hall, M.N. Feature Article: mTOR complex 2-Akt signaling at mitochondria-associated endoplasmic reticulum membranes (MAM) regulates mitochondrial physiology. *Proc. Natl. Acad. Sci. U. S. A.* **2013**, *110*, 12526–12534.
36. Vervliet, T.; Parys, J.B.; Bultynck, G. Bcl-2 proteins and calcium signaling: complexity beneath the surface. *Oncogene* **2016**, *35*, 5079–5092.
37. Arasaki, K.; Shimizu, H.; Mogari, H.; Nishida, N.; Hirota, N.; Furuno, A.; Kudo, Y.; Baba, M.; Baba, N.; Cheng, J.; et al. A role for the ancient SNARE syntaxin 17 in regulating mitochondrial division. *Dev. Cell* **2015**, *32*, 304–317.
38. Elgass, K.D.; Smith, E.A.; LeGros, M.A.; Larabell, C.A.; Ryan, M.T. Analysis of ER-mitochondria contacts using correlative fluorescence microscopy and soft X-ray tomography of mammalian cells. *J. Cell Sci.* **2015**, *128*, 2795–2804.

39. Dudley, M.W.; Howard, B.D.; Cho, A.K. The interaction of the beta-haloethyl benzylamines, xylamine, and DSP-4 with catecholaminergic neurons. *Annu. Rev. Pharmacol. Toxicol.* **1990**, *30*, 387–403.
40. Korobova, F.; Ramabhadran, V.; Higgs, H.N. An actin-dependent step in mitochondrial fission mediated by the ER-associated formin INF2. *Science* **2013**, *339*, 464–467.
41. Lewis, S.C.; Uchiyama, L.F.; Nunnari, J. ER-mitochondria contacts couple mtDNA synthesis with mitochondrial division in human cells. *Science* **2016**, *353*, aaf5549.
42. Alford, S.C.; Ding, Y.; Simmen, T.; Campbell, R.E. Dimerization-dependent green and yellow fluorescent proteins. *ACS Synth. Biol.* **2012**, *1*, 569–575.
43. Naon, D.; Zaninello, M.; Giacomello, M.; Varanita, T.; Grespi, F.; Lakshminarayanan, S.; Serafini, A.; Semenzato, M.; Herkenne, S.; Hernández-Alvarez, M.I.; et al. Critical reappraisal confirms that Mitofusin 2 is an endoplasmic reticulum-mitochondria tether. *Proc. Natl. Acad. Sci. U. S. A.* **2016**, *113*, 11249–11254.
44. Schneeberger, M.; Dietrich, M.O.; Sebastián, D.; Imbernón, M.; Castaño, C.; Garcia, A.; Esteban, Y.; Gonzalez-Franquesa, A.; Rodríguez, I.C.; Bortolozzi, A.; et al. Mitofusin 2 in POMC neurons connects ER stress with leptin resistance and energy imbalance. *Cell* **2013**, *155*, 172–187.
45. Cosson, P.; Marchetti, A.; Ravazzola, M.; Orci, L. Mitofusin-2 independent juxtaposition of endoplasmic reticulum and mitochondria: an ultrastructural study. *PLoS One* **2012**, *7*, e46293.
46. Filadi, R.; Greotti, E.; Turacchio, G.; Luini, A.; Pozzan, T.; Pizzo, P. Mitofusin 2 ablation increases endoplasmic reticulum-mitochondria coupling. *Proc. Natl. Acad. Sci. U. S. A.* **2015**, *112*, E2174–81.
47. Filadi, R.; Greotti, E.; Turacchio, G.; Luini, A.; Pozzan, T.; Pizzo, P. Presenilin 2 Modulates Endoplasmic Reticulum-Mitochondria Coupling by Tuning the Antagonistic Effect of Mitofusin 2. *Cell Rep.* **2016**, *15*, 2226–2238.
48. Leal, N.S.; Schreiner, B.; Pinho, C.M.; Filadi, R.; Wiehager, B.; Karlström, H.; Pizzo, P.; Ankarcrona, M. Mitofusin-2 knockdown increases ER-mitochondria contact and decreases amyloid β -peptide production. *J. Cell. Mol. Med.* **2016**, *20*, 1686–1695.
49. Simmen, T.; Aslan, J.E.; Blagoveshchenskaya, A.D.; Thomas, L.; Wan, L.; Xiang, Y.; Feliciangeli, S.F.; Hung, C.-H.; Crump, C.M.; Thomas, G. PACS-2 controls endoplasmic reticulum-mitochondria communication and Bid-mediated apoptosis. *EMBO J.* **2005**, *24*, 717–729.
50. De Vos, K.J.; Mórotz, G.M.; Stoica, R.; Tudor, E.L.; Lau, K.-F.; Ackerley, S.; Warley, A.; Shaw, C.E.; Miller, C.C.J. VAPB interacts with the mitochondrial protein PTPIP51 to regulate calcium homeostasis. *Hum. Mol. Genet.* **2012**, *21*, 1299–1311.
51. Niwa, M.; Fukuda, M. Clinical study on the control of dental plaque using a photo energy conversion toothbrush equipped with a TiO₂ semiconductor. *Shigaku* **1989**, *77*, 598–606.
52. Galmes, R.; Houcine, A.; van Vliet, A.R.; Agostinis, P.; Jackson, C.L.; Giordano, F. ORP5/ORP8 localize to endoplasmic reticulum-mitochondria contacts and are involved in mitochondrial function. *EMBO Rep.* **2016**, *17*, 800–810.
53. Calì, T.; Ottolini, D.; Negro, A.; Brini, M. α -Synuclein controls mitochondrial calcium homeostasis by enhancing endoplasmic reticulum-mitochondria interactions. *J. Biol. Chem.* **2012**, *287*, 17914–17929.
54. Calì, T.; Ottolini, D.; Negro, A.; Brini, M. Enhanced parkin levels favor ER-mitochondria crosstalk and guarantee Ca(2+) transfer to sustain cell bioenergetics. *Biochim. Biophys. Acta* **2013**, *1832*, 495–508.
55. Ottolini, D.; Calì, T.; Negro, A.; Brini, M. The Parkinson disease-related protein DJ-1 counteracts mitochondrial impairment induced by the tumour suppressor protein p53 by enhancing endoplasmic reticulum-mitochondria tethering. *Hum. Mol. Genet.* **2013**, *22*, 2152–2168.
56. Polymeropoulos, M.H.; Lavedan, C.; Leroy, E.; Ide, S.E.; Dehejia, A.; Dutra, A.; Pike, B.; Root, H.; Rubenstein, J.; Boyer, R.; et al. Mutation in the alpha-synuclein gene identified in families with Parkinson's disease. *Science* **1997**, *276*, 2045–2047.
57. Lee, S.-J.; Jeon, H.; Kandror, K.V. Alpha-synuclein is localized in a subpopulation of rat brain synaptic vesicles. *Acta Neurobiol. Exp.* **2008**, *68*, 509–515.
58. Vargas, K.J.; Makani, S.; Davis, T.; Westphal, C.H.; Castillo, P.E.; Chandra, S.S. Synucleins regulate the kinetics of synaptic vesicle endocytosis. *J. Neurosci.* **2014**, *34*, 9364–9376.
59. Li, W.-W.; Yang, R.; Guo, J.-C.; Ren, H.-M.; Zha, X.-L.; Cheng, J.-S.; Cai, D.-F. Localization of alpha-synuclein to mitochondria within midbrain of mice. *Neuroreport* **2007**, *18*, 1543–1546.

60. Ellis, C.E.; Murphy, E.J.; Mitchell, D.C.; Golovko, M.Y.; Scaglia, F.; Barceló-Coblijn, G.C.; Nussbaum, R.L. Mitochondrial lipid abnormality and electron transport chain impairment in mice lacking alpha-synuclein. *Mol. Cell. Biol.* **2005**, *25*, 10190–10201.
61. Devi, L.; Raghavendran, V.; Prabhu, B.M.; Avadhani, N.G.; Anandatheerthavarada, H.K. Mitochondrial import and accumulation of alpha-synuclein impair complex I in human dopaminergic neuronal cultures and Parkinson disease brain. *J. Biol. Chem.* **2008**, *283*, 9089–9100.
62. Guardia-Laguarta, C.; Area-Gomez, E.; Rüb, C.; Liu, Y.; Magrané, J.; Becker, D.; Voos, W.; Schon, E.A.; Przedborski, S. α -Synuclein is localized to mitochondria-associated ER membranes. *J. Neurosci.* **2014**, *34*, 249–259.
63. Paillusson, S.; Gomez-Suaga, P.; Stoica, R.; Little, D.; Gissen, P.; Devine, M.J.; Noble, W.; Hanger, D.P.; Miller, C.C.J. α -Synuclein binds to the ER-mitochondria tethering protein VAPB to disrupt Ca homeostasis and mitochondrial ATP production. *Acta Neuropathol.* **2017**, *134*, 129–149.
64. Pozo Devoto, V.M.; Dimopoulos, N.; Alloatti, M.; Pardi, M.B.; Saez, T.M.; Otero, M.G.; Cromberg, L.E.; Marín-Burgin, A.; Scassa, M.E.; Stokin, G.B.; et al. α Synuclein control of mitochondrial homeostasis in human-derived neurons is disrupted by mutations associated with Parkinson's disease. *Sci. Rep.* **2017**, *7*, 5042.
65. Fortin, D.L.; Troyer, M.D.; Nakamura, K.; Kubo, S.-I.; Anthony, M.D.; Edwards, R.H. Lipid rafts mediate the synaptic localization of alpha-synuclein. *J. Neurosci.* **2004**, *24*, 6715–6723.
66. Davidson, W.S.; Jonas, A.; Clayton, D.F.; George, J.M. Stabilization of alpha-synuclein secondary structure upon binding to synthetic membranes. *J. Biol. Chem.* **1998**, *273*, 9443–9449.
67. faculty
68. Narhi, L.; Wood, S.J.; Steavenson, S.; Jiang, Y.; Wu, G.M.; Anafi, D.; Kaufman, S.A.; Martin, F.; Sitney, K.; Denis, P.; et al. Both familial Parkinson's disease mutations accelerate alpha-synuclein aggregation. *J. Biol. Chem.* **1999**, *274*, 9843–9846.
69. Tanaka, Y.; Engelender, S.; Igarashi, S.; Rao, R.K.; Wanner, T.; Tanzi, R.E.; Sawa, A.; Dawson, V.; Dawson, T.M.; Ross, C.A. Inducible expression of mutant alpha-synuclein decreases proteasome activity and increases sensitivity to mitochondria-dependent apoptosis. *Hum. Mol. Genet.* **2001**, *10*, 919–926.
70. Duvezin-Caubet, S.; Jagasia, R.; Wagener, J.; Hofmann, S.; Trifunovic, A.; Hansson, A.; Chomyn, A.; Bauer, M.F.; Attardi, G.; Larsson, N.-G.; et al. Proteolytic processing of OPA1 links mitochondrial dysfunction to alterations in mitochondrial morphology. *J. Biol. Chem.* **2006**, *281*, 37972–37979.
71. Spillantini, M.G.; Schmidt, M.L.; Lee, V.M.; Trojanowski, J.Q.; Jakes, R.; Goedert, M. Alpha-synuclein in Lewy bodies. *Nature* **1997**, *388*, 839–840.
72. Wakabayashi, K.; Tanji, K.; Odagiri, S.; Miki, Y.; Mori, F.; Takahashi, H. The Lewy body in Parkinson's disease and related neurodegenerative disorders. *Mol. Neurobiol.* **2013**, *47*, 495–508.
73. Spillantini, M.G.; Crowther, R.A.; Jakes, R.; Hasegawa, M.; Goedert, M. alpha-Synuclein in filamentous inclusions of Lewy bodies from Parkinson's disease and dementia with lewy bodies. *Proc. Natl. Acad. Sci. U. S. A.* **1998**, *95*, 6469–6473.
74. Shahmoradian, S.H.; Lewis, A.J.; Genoud, C.; Hench, J.; Moors, T.E.; Navarro, P.P.; Castaño-Díez, D.; Schweighauser, G.; Graff-Meyer, A.; Goldie, K.N.; et al. Lewy pathology in Parkinson's disease consists of crowded organelles and lipid membranes. *Nat. Neurosci.* **2019**, *22*, 1099–1109.
75. McNaught, K.S.P.; Shashidharan, P.; Perl, D.P.; Jenner, P.; Olanow, C.W. Aggresome-related biogenesis of Lewy bodies. *Eur. J. Neurosci.* **2002**, *16*, 2136–2148.
76. Johnston, J.A.; Ward, C.L.; Kopito, R.R. Aggresomes: a cellular response to misfolded proteins. *J. Cell Biol.* **1998**, *143*, 1883–1898.
77. Olanow, C.W.; Perl, D.P.; DeMartino, G.N.; McNaught, K.S.P. Lewy-body formation is an aggresome-related process: a hypothesis. *Lancet Neurol.* **2004**, *3*, 496–503.
78. Harris, H.; Rubinsztein, D.C. Control of autophagy as a therapy for neurodegenerative disease. *Nat. Rev. Neurol.* **2011**, *8*, 108–117.
79. Pickles, S.; Vigié, P.; Youle, R.J. Mitophagy and Quality Control Mechanisms in Mitochondrial Maintenance. *Curr. Biol.* **2018**, *28*, R170–R185.
80. Palikaras, K.; Tavernarakis, N. Mitophagy in neurodegeneration and aging. *Front. Genet.* **2012**, *3*, 297.
81. Pickrell, A.M.; Youle, R.J. The roles of PINK1, parkin, and mitochondrial fidelity in Parkinson's disease. *Neuron* **2015**, *85*, 257–273.

82. Jin, S.M.; Lazarou, M.; Wang, C.; Kane, L.A.; Narendra, D.P.; Youle, R.J. Mitochondrial membrane potential regulates PINK1 import and proteolytic destabilization by PARL. *J. Cell Biol.* **2010**, *191*, 933–942.
83. Deas, E.; Plun-Favreau, H.; Gandhi, S.; Desmond, H.; Kjaer, S.; Loh, S.H.Y.; Renton, A.E.M.; Harvey, R.J.; Whitworth, A.J.; Martins, L.M.; et al. PINK1 cleavage at position A103 by the mitochondrial protease PARL. *Hum. Mol. Genet.* **2011**, *20*, 867–879.
84. Meissner, C.; Lorenz, H.; Weihofen, A.; Selkoe, D.J.; Lemberg, M.K. The mitochondrial intramembrane protease PARL cleaves human Pink1 to regulate Pink1 trafficking. *J. Neurochem.* **2011**, *117*, 856–867.
85. Yamano, K.; Youle, R.J. PINK1 is degraded through the N-end rule pathway. *Autophagy* **2013**, *9*, 1758–1769.
86. Kondapalli, C.; Kazlauskaitė, A.; Zhang, N.; Woodroof, H.I.; Campbell, D.G.; Gourlay, R.; Burchell, L.; Walden, H.; Macartney, T.J.; Deak, M.; et al. PINK1 is activated by mitochondrial membrane potential depolarization and stimulates Parkin E3 ligase activity by phosphorylating Serine 65. *Open Biol.* **2012**, *2*, 120080.
87. Shiba-Fukushima, K.; Imai, Y.; Yoshida, S.; Ishihama, Y.; Kanao, T.; Sato, S.; Hattori, N. PINK1-mediated phosphorylation of the Parkin ubiquitin-like domain primes mitochondrial translocation of Parkin and regulates mitophagy. *Sci. Rep.* **2012**, *2*, 1002.
88. Kane, L.A.; Lazarou, M.; Fogel, A.I.; Li, Y.; Yamano, K.; Sarraf, S.A.; Banerjee, S.; Youle, R.J. PINK1 phosphorylates ubiquitin to activate Parkin E3 ubiquitin ligase activity. *J. Cell Biol.* **2014**, *205*, 143–153.
89. Okatsu, K.; Koyano, F.; Kimura, M.; Kosako, H.; Saeki, Y.; Tanaka, K.; Matsuda, N. Phosphorylated ubiquitin chain is the genuine Parkin receptor. *J. Cell Biol.* **2015**, *209*, 111–128.
90. Stolz, A.; Ernst, A.; Dikic, I. Cargo recognition and trafficking in selective autophagy. *Nat. Cell Biol.* **2014**, *16*, 495–501.
91. Gelmetti, V.; De Rosa, P.; Torosantucci, L.; Marini, E.S.; Romagnoli, A.; Di Rienzo, M.; Arena, G.; Vignone, D.; Fimia, G.M.; Valente, E.M. PINK1 and BECN1 relocalize at mitochondria-associated membranes during mitophagy and promote ER-mitochondria tethering and autophagosome formation. *Autophagy* **2017**, *13*, 654–669.
92. Jin, S.M.; Youle, R.J. PINK1- and Parkin-mediated mitophagy at a glance. *J. Cell Sci.* **2012**, *125*, 795–799.
93. Celardo, I.; Costa, A.C.; Lehmann, S.; Jones, C.; Wood, N.; Mencacci, N.E.; Mallucci, G.R.; Loh, S.H.Y.; Martins, L.M. Mitofusin-mediated ER stress triggers neurodegeneration in pink1/parkin models of Parkinson's disease. *Cell Death Dis.* **2016**, *7*, e2271.
94. Gautier, C.A.; Erpapazoglou, Z.; Mouton-Liger, F.; Muriel, M.P.; Cormier, F.; Bigou, S.; Duffaure, S.; Girard, M.; Foret, B.; Iannielli, A.; et al. The endoplasmic reticulum-mitochondria interface is perturbed in PARK2 knockout mice and patients with PARK2 mutations. *Hum. Mol. Genet.* **2016**, *25*, 2972–2984.
95. Goldberg, M.S.; Fleming, S.M.; Palacino, J.J.; Cepeda, C.; Lam, H.A.; Bhatnagar, A.; Meloni, E.G.; Wu, N.; Ackerson, L.C.; Klapstein, G.J.; et al. Parkin-deficient mice exhibit nigrostriatal deficits but not loss of dopaminergic neurons. *J. Biol. Chem.* **2003**, *278*, 43628–43635.
96. Gautier, C.A.; Kitada, T.; Shen, J. Loss of PINK1 causes mitochondrial functional defects and increased sensitivity to oxidative stress. *Proc. Natl. Acad. Sci. U. S. A.* **2008**, *105*, 11364–11369.
97. Perez, F.A.; Palmiter, R.D. Parkin-deficient mice are not a robust model of parkinsonism. *Proc. Natl. Acad. Sci. U. S. A.* **2005**, *102*, 2174–2179.
98. Sterky, F.H.; Lee, S.; Wibom, R.; Olson, L.; Larsson, N.-G. Impaired mitochondrial transport and Parkin-independent degeneration of respiratory chain-deficient dopamine neurons in vivo. *Proc. Natl. Acad. Sci. U. S. A.* **2011**, *108*, 12937–12942.
99. Pickrell, A.M.; Huang, C.-H.; Kennedy, S.R.; Ordureau, A.; Sideris, D.P.; Hoekstra, J.G.; Harper, J.W.; Youle, R.J. Endogenous Parkin Preserves Dopaminergic Substantia Nigral Neurons following Mitochondrial DNA Mutagenic Stress. *Neuron* **2015**, *87*, 371–381.
100. Zheng, L.; Bernard-Marissal, N.; Moullan, N.; D'Amico, D.; Auwerx, J.; Moore, D.J.; Knott, G.; Aebischer, P.; Schneider, B.L. Parkin functionally interacts with PGC-1 α to preserve mitochondria and protect dopaminergic neurons. *Hum. Mol. Genet.* **2017**, *26*, 582–598.
101. Shin, J.-H.; Ko, H.S.; Kang, H.; Lee, Y.; Lee, Y.-I.; Pletinkova, O.; Troconso, J.C.; Dawson, V.L.; Dawson, T.M. PARIS(ZNF746) repression of PGC-1 α contributes to neurodegeneration in Parkinson's disease. *Cell* **2011**, *144*, 689–702.

102. Trempe, J.-F.; Sauv , V.; Grenier, K.; Seirafi, M.; Tang, M.Y.; M nade, M.; Al-Abdul-Wahid, S.; Krett, J.; Wong, K.; Kozlov, G.; et al. Structure of parkin reveals mechanisms for ubiquitin ligase activation. *Science* **2013**, *340*, 1451–1455.
103. Aguirre, J.D.; Dunkerley, K.M.; Mercier, P.; Shaw, G.S. Structure of phosphorylated UBL domain and insights into PINK1-orchestrated parkin activation. *Proc. Natl. Acad. Sci. U. S. A.* **2017**, *114*, 298–303.
104. McWilliams, T.G.; Barini, E.; Pohjolan-Pirhonen, R.; Brooks, S.P.; Singh, F.; Burel, S.; Balk, K.; Kumar, A.; Montava-Garriga, L.; Prescott, A.R.; et al. Phosphorylation of Parkin at serine 65 is essential for its activation. *Open Biol.* **2018**, *8*.
105. Morais, V.A.; Verstreken, P.; Roethig, A.; Smet, J.; Snellinx, A.; Vanbrabant, M.; Haddad, D.; Frezza, C.; Mandemakers, W.; Vogt-Weisenhorn, D.; et al. Parkinson’s disease mutations in PINK1 result in decreased Complex I activity and deficient synaptic function. *EMBO Mol. Med.* **2009**, *1*, 99–111.
106. Morais, V.A.; Haddad, D.; Craessaerts, K.; De Bock, P.-J.; Swerts, J.; Vilain, S.; Aerts, L.; Overbergh, L.; Gr newald, A.; Seibler, P.; et al. PINK1 loss-of-function mutations affect mitochondrial complex I activity via NdufA10 ubiquinone uncoupling. *Science* **2014**, *344*, 203–207.
107. Taira, T.; Saito, Y.; Niki, T.; Iguchi-Arigo, S.M.M.; Takahashi, K.; Ariga, H. DJ-1 has a role in antioxidative stress to prevent cell death. *EMBO Rep.* **2004**, *5*, 213–218.
108. Inden, M.; Kitamura, Y.; Takahashi, K.; Takata, K.; Ito, N.; Niwa, R.; Funayama, R.; Nishimura, K.; Taniguchi, T.; Honda, T.; et al. Protection against dopaminergic neurodegeneration in Parkinson’s disease-model animals by a modulator of the oxidized form of DJ-1, a wild-type of familial Parkinson’s disease-linked PARK7. *J. Pharmacol. Sci.* **2011**, *117*, 189–203.
109. Cookson, M.R. Pathways to Parkinsonism. *Neuron* **2003**, *37*, 7–10.
110. Andres-Mateos, E.; Perier, C.; Zhang, L.; Blanchard-Fillion, B.; Greco, T.M.; Thomas, B.; Ko, H.S.; Sasaki, M.; Ischiropoulos, H.; Przedborski, S.; et al. DJ-1 gene deletion reveals that DJ-1 is an atypical peroxiredoxin-like peroxidase. *Proc. Natl. Acad. Sci. U. S. A.* **2007**, *104*, 14807–14812.
111. Choi, J.; Sullards, M.C.; Olzmann, J.A.; Rees, H.D.; Weintraub, S.T.; Bostwick, D.E.; Gearing, M.; Levey, A.I.; Chin, L.-S.; Li, L. Oxidative damage of DJ-1 is linked to sporadic Parkinson and Alzheimer diseases. *J. Biol. Chem.* **2006**, *281*, 10816–10824.
112. Bandopadhyay, R.; Kingsbury, A.E.; Cookson, M.R.; Reid, A.R.; Evans, I.M.; Hope, A.D.; Pittman, A.M.; Lashley, T.; Canet-Aviles, R.; Miller, D.W.; et al. The expression of DJ-1 (PARK7) in normal human CNS and idiopathic Parkinson’s disease. *Brain* **2004**, *127*, 420–430.
113. Kim, R.H.; Peters, M.; Jang, Y.; Shi, W.; Pintilie, M.; Fletcher, G.C.; DeLuca, C.; Liepa, J.; Zhou, L.; Snow, B.; et al. DJ-1, a novel regulator of the tumor suppressor PTEN. *Cancer Cell* **2005**, *7*, 263–273.
114. Giaime, E.; Sunyach, C.; Druon, C.; Scarzello, S.; Robert, G.; Grosso, S.; Auberger, P.; Goldberg, M.S.; Shen, J.; Heutink, P.; et al. Loss of function of DJ-1 triggered by Parkinson’s disease-associated mutation is due to proteolytic resistance to caspase-6. *Cell Death Differ.* **2010**, *17*, 158–169.
115. Gu, L.; Cui, T.; Fan, C.; Zhao, H.; Zhao, C.; Lu, L.; Yang, H. Involvement of ERK1/2 signaling pathway in DJ-1-induced neuroprotection against oxidative stress. *Biochem. Biophys. Res. Commun.* **2009**, *383*, 469–474.
116. Bretau, S.; Allen, C.; Ingham, P.W.; Bandmann, O. p53-dependent neuronal cell death in a DJ-1-deficient zebrafish model of Parkinson’s disease. *J. Neurochem.* **2007**, *100*, 1626–1635.
117. Ren, H.; Fu, K.; Wang, D.; Mu, C.; Wang, G. Oxidized DJ-1 interacts with the mitochondrial protein BCL-XL. *J. Biol. Chem.* **2011**, *286*, 35308–35317.
118. Wilson, M.A.; Collins, J.L.; Hod, Y.; Ringe, D.; Petsko, G.A. The 1.1-Å resolution crystal structure of DJ-1, the protein mutated in autosomal recessive early onset Parkinson’s disease. *Proc. Natl. Acad. Sci. U. S. A.* **2003**, *100*, 9256–9261.
119. G rner, K.; Holtorf, E.; Waak, J.; Pham, T.-T.; Vogt-Weisenhorn, D.M.; Wurst, W.; Haass, C.; Kahle, P.J. Structural determinants of the C-terminal helix-kink-helix motif essential for protein stability and survival promoting activity of DJ-1. *J. Biol. Chem.* **2007**, *282*, 13680–13691.
120. Repici, M.; Straatman, K.R.; Balduccio, N.; Enguita, F.J.; Outeiro, T.F.; Giorgini, F. Parkinson’s disease-associated mutations in DJ-1 modulate its dimerization in living cells. *J. Mol. Med.* **2013**, *91*, 599–611.
121. Bonifati, V.; Rizzu, P.; Squitieri, F.; Krieger, E.; Vanacore, N.; van Swieten, J.C.; Brice, A.; van Duijn, C.M.; Oostra, B.; Meco, G.; et al. DJ-1 (PARK7), a novel gene for autosomal recessive, early onset parkinsonism. *Neurol. Sci.* **2003**, *24*, 159–160.

122. van Duijn, C.M.; Dekker, M.C.; Bonifati, V.; Galjaard, R.J.; Houwing-Duistermaat, J.J.; Snijders, P.J.; Testers, L.; Breedveld, G.J.; Horstink, M.; Sandkuijl, L.A.; et al. Park7, a novel locus for autosomal recessive early-onset parkinsonism, on chromosome 1p36. *Am. J. Hum. Genet.* **2001**, *69*, 629–634.
123. Zondler, L.; Miller-Fleming, L.; Repici, M.; Gonçalves, S.; Tenreiro, S.; Rosado-Ramos, R.; Betzer, C.; Straatman, K.R.; Jensen, P.H.; Giorgini, F.; et al. DJ-1 interactions with α -synuclein attenuate aggregation and cellular toxicity in models of Parkinson's disease. *Cell Death Dis.* **2014**, *5*, e1350.
124. Ammal Kaidery, N.; Thomas, B. Current perspective of mitochondrial biology in Parkinson's disease. *Neurochem. Int.* **2018**, *117*, 91–113.
125. Healy, D.G.; Falchi, M.; O'Sullivan, S.S.; Bonifati, V.; Durr, A.; Bressman, S.; Brice, A.; Aasly, J.; Zabetian, C.P.; Goldwurm, S.; et al. Phenotype, genotype, and worldwide genetic penetrance of LRRK2-associated Parkinson's disease: a case-control study. *Lancet Neurol.* **2008**, *7*, 583–590.
126. Martin, I.; Kim, J.W.; Dawson, V.L.; Dawson, T.M. LRRK2 pathobiology in Parkinson's disease. *J. Neurochem.* **2014**, *131*, 554–565.
127. Mortiboys, H.; Johansen, K.K.; Aasly, J.O.; Bandmann, O. Mitochondrial impairment in patients with Parkinson disease with the G2019S mutation in LRRK2. *Neurology* **2010**, *75*, 2017–2020.
128. Smith, W.W.; Pei, Z.; Jiang, H.; Dawson, V.L.; Dawson, T.M.; Ross, C.A. Kinase activity of mutant LRRK2 mediates neuronal toxicity. *Nat. Neurosci.* **2006**, *9*, 1231–1233.
129. Stafa, K.; Tsika, E.; Moser, R.; Musso, A.; Glauser, L.; Jones, A.; Biskup, S.; Xiong, Y.; Bandopadhyay, R.; Dawson, V.L.; et al. Functional interaction of Parkinson's disease-associated LRRK2 with members of the dynamin GTPase superfamily. *Hum. Mol. Genet.* **2014**, *23*, 2055–2077.
130. Wang, X.; Yan, M.H.; Fujioka, H.; Liu, J.; Wilson-Delfosse, A.; Chen, S.G.; Perry, G.; Casadesus, G.; Zhu, X. LRRK2 regulates mitochondrial dynamics and function through direct interaction with DLP1. *Hum. Mol. Genet.* **2012**, *21*, 1931–1944.
131. Niu, J.; Yu, M.; Wang, C.; Xu, Z. Leucine-rich repeat kinase 2 disturbs mitochondrial dynamics via Dynamin-like protein. *J. Neurochem.* **2012**, *122*, 650–658.
132. Papkovskaia, T.D.; Chau, K.-Y.; Inesta-Vaquera, F.; Papkovsky, D.B.; Healy, D.G.; Nishio, K.; Staddon, J.; Duchen, M.R.; Hardy, J.; Schapira, A.H.V.; et al. G2019S leucine-rich repeat kinase 2 causes uncoupling protein-mediated mitochondrial depolarization. *Hum. Mol. Genet.* **2012**, *21*, 4201–4213.
133. Toyofuku, T.; Okamoto, Y.; Ishikawa, T.; Sasawatari, S.; Kumanogoh, A. LRRK2 regulates endoplasmic reticulum-mitochondrial tethering through the PERK-mediated ubiquitination pathway. *EMBO J.* **2019**, e100875.
134. Wang, X.; Winter, D.; Ashrafi, G.; Schlehe, J.; Wong, Y.L.; Selkoe, D.; Rice, S.; Steen, J.; LaVoie, M.J.; Schwarz, T.L. PINK1 and Parkin target Miro for phosphorylation and degradation to arrest mitochondrial motility. *Cell* **2011**, *147*, 893–906.
135. Hutagalung, A.H.; Novick, P.J. Role of Rab GTPases in membrane traffic and cell physiology. *Physiol. Rev.* **2011**, *91*, 119–149.
136. Burté, F.; Carelli, V.; Chinnery, P.F.; Yu-Wai-Man, P. Disturbed mitochondrial dynamics and neurodegenerative disorders. *Nat. Rev. Neurol.* **2015**, *11*, 11–24.
137. Mc Donald, J.M.; Krainc, D. Lysosomal Proteins as a Therapeutic Target in Neurodegeneration. *Annu. Rev. Med.* **2017**, *68*, 445–458.
138. Plotegher, N.; Duchen, M.R. Mitochondrial Dysfunction and Neurodegeneration in Lysosomal Storage Disorders. *Trends Mol. Med.* **2017**, *23*, 116–134.
139. Aits, S.; Jäättelä, M. Lysosomal cell death at a glance. *J. Cell Sci.* **2013**, *126*, 1905–1912.
140. Demers-Lamarche, J.; Guillebaud, G.; Tlili, M.; Todkar, K.; Bélanger, N.; Grondin, M.; Nguyen, A.P.; Michel, J.; Germain, M. Loss of Mitochondrial Function Impairs Lysosomes. *J. Biol. Chem.* **2016**, *291*, 10263–10276.
141. Brahimi-Horn, M.C.; Lacas-Gervais, S.; Adaixo, R.; Ilc, K.; Rouleau, M.; Notte, A.; Dieu, M.; Michiels, C.; Voeltzel, T.; Maguer-Satta, V.; et al. Local mitochondrial-endolysosomal microfusion cleaves voltage-dependent anion channel 1 to promote survival in hypoxia. *Mol. Cell. Biol.* **2015**, *35*, 1491–1505.
142. Baixauli, F.; Acín-Pérez, R.; Villarroya-Beltrí, C.; Mazzeo, C.; Nuñez-Andrade, N.; Gabandé-Rodríguez, E.; Ledesma, M.D.; Blázquez, A.; Martín, M.A.; Falcón-Pérez, J.M.; et al. Mitochondrial Respiration Controls Lysosomal Function during Inflammatory T Cell Responses. *Cell Metab.* **2015**, *22*, 485–498.

143. Fernández-Mosquera, L.; Diogo, C.V.; Yambire, K.F.; Santos, G.L.; Luna Sánchez, M.; Bénit, P.; Rustin, P.; Lopez, L.C.; Milosevic, I.; Raimundo, N. Acute and chronic mitochondrial respiratory chain deficiency differentially regulate lysosomal biogenesis. *Sci. Rep.* **2017**, *7*, 45076.
144. Burbulla, L.F.; Song, P.; Mazzulli, J.R.; Zampese, E.; Wong, Y.C.; Jeon, S.; Santos, D.P.; Blanz, J.; Obermaier, C.D.; Strojny, C.; et al. Dopamine oxidation mediates mitochondrial and lysosomal dysfunction in Parkinson's disease. *Science* **2017**, *357*, 1255–1261.
145. Monteleon, C.L.; Agnihotri, T.; Dahal, A.; Liu, M.; Rebecca, V.W.; Beatty, G.L.; Amaravadi, R.K.; Ridky, T.W. Lysosomes Support the Degradation, Signaling, and Mitochondrial Metabolism Necessary for Human Epidermal Differentiation. *J. Invest. Dermatol.* **2018**, *138*, 1945–1954.
146. Yamano, K.; Wang, C.; Sarraf, S.A.; Münch, C.; Kikuchi, R.; Noda, N.N.; Hizukuri, Y.; Kanemaki, M.T.; Harper, W.; Tanaka, K.; et al. Endosomal Rab cycles regulate Parkin-mediated mitophagy. *Elife* **2018**, *7*.
147. Hsu, F.; Spann, S.; Ferguson, C.; Hyman, A.A.; Parton, R.G.; Zerial, M. Rab5 and Alsln regulate stress-activated cytoprotective signaling on mitochondria. *Elife* **2018**, *7*.
148. Sugiura, A.; McLelland, G.-L.; Fon, E.A.; McBride, H.M. A new pathway for mitochondrial quality control: mitochondrial-derived vesicles. *EMBO J.* **2014**, *33*, 2142–2156.
149. Hamacher-Brady, A.; Choe, S.C.; Krijnse-Locker, J.; Brady, N.R. Intramitochondrial recruitment of endolysosomes mediates Smac degradation and constitutes a novel intrinsic apoptosis antagonizing function of XIAP E3 ligase. *Cell Death Differ.* **2014**, *21*, 1862–1876.
150. Wong, Y.C.; Holzbaur, E.L.F. Optineurin is an autophagy receptor for damaged mitochondria in parkin-mediated mitophagy that is disrupted by an ALS-linked mutation. *Proc. Natl. Acad. Sci. U. S. A.* **2014**, *111*, E4439–48.
151. Lazarou, M.; Sliter, D.A.; Kane, L.A.; Sarraf, S.A.; Wang, C.; Burman, J.L.; Sideris, D.P.; Fogel, A.I.; Youle, R.J. The ubiquitin kinase PINK1 recruits autophagy receptors to induce mitophagy. *Nature* **2015**, *524*, 309–314.
152. McLelland, G.-L.; Soubannier, V.; Chen, C.X.; McBride, H.M.; Fon, E.A. Parkin and PINK1 function in a vesicular trafficking pathway regulating mitochondrial quality control. *EMBO J.* **2014**, *33*, 282–295.
153. Wong, Y.C.; Ysselstein, D.; Krainc, D. Mitochondria-lysosome contacts regulate mitochondrial fission via RAB7 GTP hydrolysis. *Nature* **2018**, *554*, 382–386.
154. Aston, D.; Capel, R.A.; Ford, K.L.; Christian, H.C.; Mirams, G.R.; Rog-Zielinska, E.A.; Kohl, P.; Galione, A.; Burton, R.A.B.; Terrar, D.A. High resolution structural evidence suggests the Sarcoplasmic Reticulum forms microdomains with Acidic Stores (lysosomes) in the heart. *Sci. Rep.* **2017**, *7*, 40620.
155. Fermie, J.; Liv, N.; Ten Brink, C.; van Donselaar, E.G.; Müller, W.H.; Schieber, N.L.; Schwab, Y.; Gerritsen, H.C.; Klumperman, J. Single organelle dynamics linked to 3D structure by correlative live-cell imaging and 3D electron microscopy. *Traffic* **2018**, *19*, 354–369.
156. Valm, A.M.; Cohen, S.; Legant, W.R.; Melunis, J.; Hershberg, U.; Wait, E.; Cohen, A.R.; Davidson, M.W.; Betzig, E.; Lippincott-Schwartz, J. Applying systems-level spectral imaging and analysis to reveal the organelle interactome. *Nature* **2017**, *546*, 162–167.
157. Han, Y.; Li, M.; Qiu, F.; Zhang, M.; Zhang, Y.-H. Cell-permeable organic fluorescent probes for live-cell long-term super-resolution imaging reveal lysosome-mitochondrion interactions. *Nat. Commun.* **2017**, *8*, 1307.
158. Chen, Q.; Jin, C.; Shao, X.; Guan, R.; Tian, Z.; Wang, C.; Liu, F.; Ling, P.; Guan, J.-L.; Ji, L.; et al. Super-Resolution Tracking of Mitochondrial Dynamics with An Iridium(III) Luminophore. *Small* **2018**, *14*, e1802166.
159. Zhen, Y.; Stenmark, H. Cellular functions of Rab GTPases at a glance. *J. Cell Sci.* **2015**, *128*, 3171–3176.
160. Houlden, H.; King, R.H.M.; Muddle, J.R.; Warner, T.T.; Reilly, M.M.; Orrell, R.W.; Ginsberg, L. A novel RAB7 mutation associated with ulcero-mutilating neuropathy. *Ann. Neurol.* **2004**, *56*, 586–590.
161. Meggouh, F.; Bienfait, H.M.E.; Weterman, M.A.J.; de Visser, M.; Baas, F. Charcot-Marie-Tooth disease due to a de novo mutation of the RAB7 gene. *Neurology* **2006**, *67*, 1476–1478.
162. Verhoeven, K.; De Jonghe, P.; Coen, K.; Verpoorten, N.; Auer-Grumbach, M.; Kwon, J.M.; FitzPatrick, D.; Schmedding, E.; De Vriendt, E.; Jacobs, A.; et al. Mutations in the small GTP-ase late endosomal protein RAB7 cause Charcot-Marie-Tooth type 2B neuropathy. *Am. J. Hum. Genet.* **2003**, *72*, 722–727.
163. Wang, X.; Han, C.; Liu, W.; Wang, P.; Zhang, X. A novel RAB7 mutation in a Chinese family with Charcot-Marie-Tooth type 2B disease. *Gene* **2014**, *534*, 431–434.
164. Onoue, K.; Jofuku, A.; Ban-Ishihara, R.; Ishihara, T.; Maeda, M.; Koshiba, T.; Itoh, T.; Fukuda, M.; Otera, H.; Oka, T.; et al. Fis1 acts as a mitochondrial recruitment factor for TBC1D15 that is involved in regulation of mitochondrial morphology. *J. Cell Sci.* **2013**, *126*, 176–185.

-
165. Langemeyer, L.; Fröhlich, F.; Ungermann, C. Rab GTPase Function in Endosome and Lysosome Biogenesis. *Trends Cell Biol.* **2018**, *28*, 957–970.
166. Bonifacino, J.S.; Hurley, J.H. Retromer. *Curr. Opin. Cell Biol.* **2008**, *20*, 427–436.
167. Burd, C.; Cullen, P.J. Retromer: a master conductor of endosome sorting. *Cold Spring Harb. Perspect. Biol.* **2014**, *6*.
168. Seaman, M.N.J. The retromer complex - endosomal protein recycling and beyond. *J. Cell Sci.* **2012**, *125*, 4693–4702.
169. Hierro, A.; Rojas, A.L.; Rojas, R.; Murthy, N.; Effantin, G.; Kajava, A.V.; Steven, A.C.; Bonifacino, J.S.; Hurley, J.H. Functional architecture of the retromer cargo-recognition complex. *Nature* **2007**, *449*, 1063–1067.
170. Soubannier, V.; McLelland, G.-L.; Zunino, R.; Braschi, E.; Rippstein, P.; Fon, E.A.; McBride, H.M. A vesicular transport pathway shuttles cargo from mitochondria to lysosomes. *Curr. Biol.* **2012**, *22*, 135–141.
171. Chan, D.C. Mitochondrial fusion and fission in mammals. *Annu. Rev. Cell Dev. Biol.* **2006**, *22*, 79–99.
172. Merrill, R.A.; Dagda, R.K.; Dickey, A.S.; Cribbs, J.T.; Green, S.H.; Usachev, Y.M.; Strack, S. Mechanism of neuroprotective mitochondrial remodeling by PKA/AKAP1. *PLoS Biol.* **2011**, *9*, e1000612.
173. Zhu, P.-P.; Patterson, A.; Stadler, J.; Seeburg, D.P.; Sheng, M.; Blackstone, C. Intra- and intermolecular domain interactions of the C-terminal GTPase effector domain of the multimeric dynamin-like GTPase Drp1. *J. Biol. Chem.* **2004**, *279*, 35967–35974.
174. Zhao, J.; Liu, T.; Jin, S.; Wang, X.; Qu, M.; Uhlén, P.; Tomilin, N.; Shupliakov, O.; Lendahl, U.; Nistér, M. Human MIEF1 recruits Drp1 to mitochondrial outer membranes and promotes mitochondrial fusion rather than fission. *EMBO J.* **2011**, *30*, 2762–2778.
175. Liu, T.; Yu, R.; Jin, S.-B.; Han, L.; Lendahl, U.; Zhao, J.; Nistér, M. The mitochondrial elongation factors MIEF1 and MIEF2 exert partially distinct functions in mitochondrial dynamics. *Exp. Cell Res.* **2013**, *319*, 2893–2904.
176. Lackner, L.L.; Nunnari, J.M. The molecular mechanism and cellular functions of mitochondrial division. *Biochim. Biophys. Acta* **2009**, *1792*, 1138–1144.
177. Zunino, R.; Braschi, E.; Xu, L.; McBride, H.M. Translocation of SenP5 from the nucleoli to the mitochondria modulates DRP1-dependent fission during mitosis. *J. Biol. Chem.* **2009**, *284*, 17783–17795.
178. Wang, W.; Wang, X.; Fujioka, H.; Hoppel, C.; Whone, A.L.; Caldwell, M.A.; Cullen, P.J.; Liu, J.; Zhu, X. Parkinson's disease-associated mutant VPS35 causes mitochondrial dysfunction by recycling DLP1 complexes. *Nat. Med.* **2016**, *22*, 54–63.
179. Sharma, M.; Ioannidis, J.P.A.; Aasly, J.O.; Annesi, G.; Brice, A.; Bertram, L.; Bozi, M.; Barcikowska, M.; Crosiers, D.; Clarke, C.E.; et al. A multi-centre clinico-genetic analysis of the VPS35 gene in Parkinson disease indicates reduced penetrance for disease-associated variants. *J. Med. Genet.* **2012**, *49*, 721–726.
180. Vilariño-Güell, C.; Wider, C.; Ross, O.A.; Dachsel, J.C.; Kachergus, J.M.; Lincoln, S.J.; Soto-Ortolaza, A.I.; Cobb, S.A.; Wilhoite, G.J.; Bacon, J.A.; et al. VPS35 mutations in Parkinson disease. *Am. J. Hum. Genet.* **2011**, *89*, 162–167.
181. Braschi, E.; Goyon, V.; Zunino, R.; Mohanty, A.; Xu, L.; McBride, H.M. Vps35 mediates vesicle transport between the mitochondria and peroxisomes. *Curr. Biol.* **2010**, *20*, 1310–1315.
182. Tang, F.-L.; Liu, W.; Hu, J.-X.; Erion, J.R.; Ye, J.; Mei, L.; Xiong, W.-C. VPS35 Deficiency or Mutation Causes Dopaminergic Neuronal Loss by Impairing Mitochondrial Fusion and Function. *Cell Rep.* **2015**, *12*, 1631–1643.
183. Ramirez, A.; Heimbach, A.; Gründemann, J.; Stiller, B.; Hampshire, D.; Cid, L.P.; Goebel, I.; Mubaidin, A.F.; Wriekat, A.-L.; Roeper, J.; et al. Hereditary parkinsonism with dementia is caused by mutations in ATP13A2, encoding a lysosomal type 5 P-type ATPase. *Nat. Genet.* **2006**, *38*, 1184–1191.
184. Najim al-Din, A.S.; Wriekat, A.; Mubaidin, A.; Dasouki, M.; Hiari, M. Pallido-pyramidal degeneration, supranuclear upgaze paresis and dementia: Kufor-Rakeb syndrome. *Acta Neurol. Scand.* **1994**, *89*, 347–352.
185. Di Fonzo, A.; Chien, H.F.; Socal, M.; Giraudo, S.; Tassorelli, C.; Iliceto, G.; Fabbrini, G.; Marconi, R.; Fincati, E.; Abbruzzese, G.; et al. ATP13A2 missense mutations in juvenile parkinsonism and young onset Parkinson disease. *Neurology* **2007**, *68*, 1557–1562.
186. Park, J.-S.; Mehta, P.; Cooper, A.A.; Veivers, D.; Heimbach, A.; Stiller, B.; Kubisch, C.; Fung, V.S.; Krainc, D.; Mackay-Sim, A.; et al. Pathogenic effects of novel mutations in the P-type ATPase ATP13A2 (PARK9) causing Kufor-Rakeb syndrome, a form of early-onset parkinsonism. *Hum. Mutat.* **2011**, *32*, 956–964.
187. Eiberg, H.; Hansen, L.; Korbo, L.; Nielsen, I.M.; Svenstrup, K.; Bech, S.; Pinborg, L.H.; Friberg, L.; Hjermind, L.E.; Olsen, O.R.; et al. Novel mutation in ATP13A2 widens the spectrum of Kufor-Rakeb syndrome (PARK9). *Clin. Genet.* **2012**, *82*, 256–263.

188. Gitler, A.D.; Chesi, A.; Geddie, M.L.; Strathearn, K.E.; Hamamichi, S.; Hill, K.J.; Caldwell, K.A.; Caldwell, G.A.; Cooper, A.A.; Rochet, J.-C.; et al. Alpha-synuclein is part of a diverse and highly conserved interaction network that includes PARK9 and manganese toxicity. *Nat. Genet.* 2009, 41, 308–315.
189. Covy, J.P.; Waxman, E.A.; Giasson, B.I. Characterization of cellular protective effects of ATP13A2/PARK9 expression and alterations resulting from pathogenic mutants. *J. Neurosci. Res.* 2012, 90, 2306–2316.
190. Tan, J.; Zhang, T.; Jiang, L.; Chi, J.; Hu, D.; Pan, Q.; Wang, D.; Zhang, Z. Regulation of intracellular manganese homeostasis by Kufor-Rakeb syndrome-associated ATP13A2 protein. *J. Biol. Chem.* 2011, 286, 29654–29662.
191. Kong, S.M.Y.; Chan, B.K.K.; Park, J.-S.; Hill, K.J.; Aitken, J.B.; Cottle, L.; Farghaian, H.; Cole, A.R.; Lay, P.A.; Sue, C.M.; et al. Parkinson's disease-linked human PARK9/ATP13A2 maintains zinc homeostasis and promotes α -Synuclein externalization via exosomes. *Hum. Mol. Genet.* 2014, 23, 2816–2833.
192. Tsunemi, T.; Krainc, D. Zn^{2+} dyshomeostasis caused by loss of ATP13A2/PARK9 leads to lysosomal dysfunction and alpha-synuclein accumulation. *Hum. Mol. Genet.* 2014, 23, 2791–2801.
193. Park, J.-S.; Koentjoro, B.; Veivers, D.; Mackay-Sim, A.; Sue, C.M. Parkinson's disease-associated human ATP13A2 (PARK9) deficiency causes zinc dyshomeostasis and mitochondrial dysfunction. *Hum. Mol. Genet.* 2014, 23, 2802–2815.
194. Dehay, B.; Ramirez, A.; Martinez-Vicente, M.; Perier, C.; Canon, M.-H.; Doudnikoff, E.; Vital, A.; Vila, M.; Klein, C.; Bezdard, E. Loss of P-type ATPase ATP13A2/PARK9 function induces general lysosomal deficiency and leads to Parkinson disease neurodegeneration. *Proc. Natl. Acad. Sci. U. S. A.* 2012, 109, 9611–9616.
195. Webb, J.L.; Ravikumar, B.; Atkins, J.; Skepper, J.N.; Rubinsztein, D.C. Alpha-Synuclein is degraded by both autophagy and the proteasome. *J. Biol. Chem.* 2003, 278, 25009–25013.
196. Cuervo, A.M.; Stefanis, L.; Fredenburg, R.; Lansbury, P.T.; Sulzer, D. Impaired degradation of mutant alpha-synuclein by chaperone-mediated autophagy. *Science* 2004, 305, 1292–1295.
197. Yang, Z.; Klionsky, D.J. Eaten alive: a history of macroautophagy. *Nat. Cell Biol.* 2010, 12, 814–822.
198. Codogno, P.; Mehrpour, M.; Proikas-Cezanne, T. Canonical and non-canonical autophagy: variations on a common theme of self-eating? *Nat. Rev. Mol. Cell Biol.* 2011, 13, 7–12.
199. Pryor, P.R.; Mullock, B.M.; Bright, N.A.; Gray, S.R.; Luzio, J.P. The role of intraorganellar Ca^{2+} in late endosome-lysosome heterotypic fusion and in the reformation of lysosomes from hybrid organelles. *J. Cell Biol.* 2000, 149, 1053–1062.
200. Klionsky, D.J.; Elazar, Z.; Seglen, P.O.; Rubinsztein, D.C. Does bafilomycin A1 block the fusion of autophagosomes with lysosomes? *Autophagy* 2008, 4, 849–850.
201. Korolchuk, V.I.; Saiki, S.; Lichtenberg, M.; Siddiqi, F.H.; Roberts, E.A.; Imarisio, S.; Jahreiss, L.; Sarkar, S.; Futter, M.; Menzies, F.M.; et al. Lysosomal positioning coordinates cellular nutrient responses. *Nat. Cell Biol.* 2011, 13, 453–460.
202. Miura, E.; Hasegawa, T.; Konno, M.; Suzuki, M.; Sugeno, N.; Fujikake, N.; Geisler, S.; Tabuchi, M.; Oshima, R.; Kikuchi, A.; et al. VPS35 dysfunction impairs lysosomal degradation of α -synuclein and exacerbates neurotoxicity in a Drosophila model of Parkinson's disease. *Neurobiol. Dis.* 2014, 71, 1–13.
203. Gómez-Suaga, P.; Churchill, G.C.; Patel, S.; Hilfiker, S. A link between LRRK2, autophagy and NAADP-mediated endolysosomal calcium signalling. *Biochem. Soc. Trans.* 2012, 40, 1140–1146.
204. Tong, Y.; Giaime, E.; Yamaguchi, H.; Ichimura, T.; Liu, Y.; Si, H.; Cai, H.; Bonventre, J.V.; Shen, J. Loss of leucine-rich repeat kinase 2 causes age-dependent bi-phasic alterations of the autophagy pathway. *Mol. Neurodegener.* 2012, 7, 2.
205. Manzoni, C.; Mamais, A.; Roosen, D.A.; Dihanich, S.; Soutar, M.P.M.; Plun-Favreau, H.; Bandopadhyay, R.; Hardy, J.; Tooze, S.A.; Cookson, M.R.; et al. mTOR independent regulation of macroautophagy by Leucine Rich Repeat Kinase 2 via Beclin-1. *Sci. Rep.* 2016, 6, 35106.
206. Wallings, R.; Connor-Robson, N.; Wade-Martins, R. LRRK2 interacts with the vacuolar-type H^{+} -ATPase pump $\alpha 1$ subunit to regulate lysosomal function. *Hum. Mol. Genet.* 2019, 28, 2696–2710.
207. Nguyen, M.; Wong, Y.C.; Ysselstein, D.; Severino, A.; Krainc, D. Synaptic, Mitochondrial, and Lysosomal Dysfunction in Parkinson's Disease. *Trends Neurosci.* 2019, 42, 140–149.



© 2020 by the authors. Submitted for possible open access publication under the terms and conditions of the Creative Commons Attribution (CC BY) license (<http://creativecommons.org/licenses/by/4.0/>).

8. Acknowledgements

This thesis and all the work behind it would not have been possible without the help and support of many people, close and far away, who always believed in me throughout these long years.

I would like to express my gratitude to my boss Prof. Stephan Frank for giving me the chance to work in his laboratory at the Institute of Pathology. Thank you for your patient guidance, mentoring and cooperation.

I'm also grateful to Dr. Lisa Restelli: thank you for introducing me not only to the "enchanted" world of mitochondria, but also to the "crazy pathology" environment.

Many thanks to the members of my thesis committee, Prof. Christoph Handschin and Prof. Frank Edlich for accepting to be part of my PhD committee.

My most heartfelt thanks go to Prof. Albert Neutzner, the "Master of cloning". Thank you for your support, patience and willingness to discuss, and to remember me to never give up, even in the darkest moments. Thank you for always recalling me to "have fun" whenever I was starting a new experiment.

Many thanks go to all the current and former members of the Neutzner Lab: Claudia, Corina, Melanie, Jessica, Sarah, Suba, Bart and Chantal. Thank you for letting me feel part of the group.

I would also like to thank all the research people of the Pathology Institute that I met in these past five years, with a special thanks to Ilaria and Mara.

A huge thanks go to the very first friend I found in Basel, Nicole. Thank you for introducing me to the city, to the barbecues and drinks along the Rhine, and for "forcing" me to swim in the Rhine. And thank you for sharing the burden of my crazy PhD.

I also want to thank Stephy, my first swiss friend. Thank you for all our coffee breaks, our trash movie/mario kart nights (together with Dave), and our chats combined with glasses (or better bottles) of wine.

A big thanks go to my beloved friend, Noemi. Thank you not only for the scientific knowledge I acquired working with you, but also for all the support, even if we were far away.

I want to thank my girls Martina, Bianca, Eleonora and Stefania: thank you for always being there every time I was coming back home, for coming visit me in Basel, for our chats, gossips, dinners and party nights.

To my dearest friend Aurora, the only one who came twice here in Switzerland for me. Thank you Borina mia for all our voice massages (even if you were replying months later) and late-night phone calls.

I want to thank a lot Gaia and Stefano: when I thought I was completely alone, I found genuine friends.

A special mention goes to Stephanie, my weekend lab fellow: thank you my dear for sharing with me multiple working weekends.

A special thanks go to the Radiology volleyball people: thank you for all the good matches on sand and indoor. I always arrived back home tired as hell but happy.

My deepest gratitude goes to my Mum, my Dad and my Brother: thank you very much for supporting me since the beginning of this journey, and not just providing good Italian food. Thank you for teaching me how to live in this world with the proper kindness towards myself and the others

Last but not least, there is one more person I should thank, and that is me, for not giving up when I was alone, when no experiment was working, when it didn't seem worthy to go on. It was most probably worthy to hold on and arrive here.

*"Happiness can be found, even in the darkest of times,
if one only remembers to turn on the light."*

Albus Dumbledore

Harry Potter and the Prisoner of Azkaban

